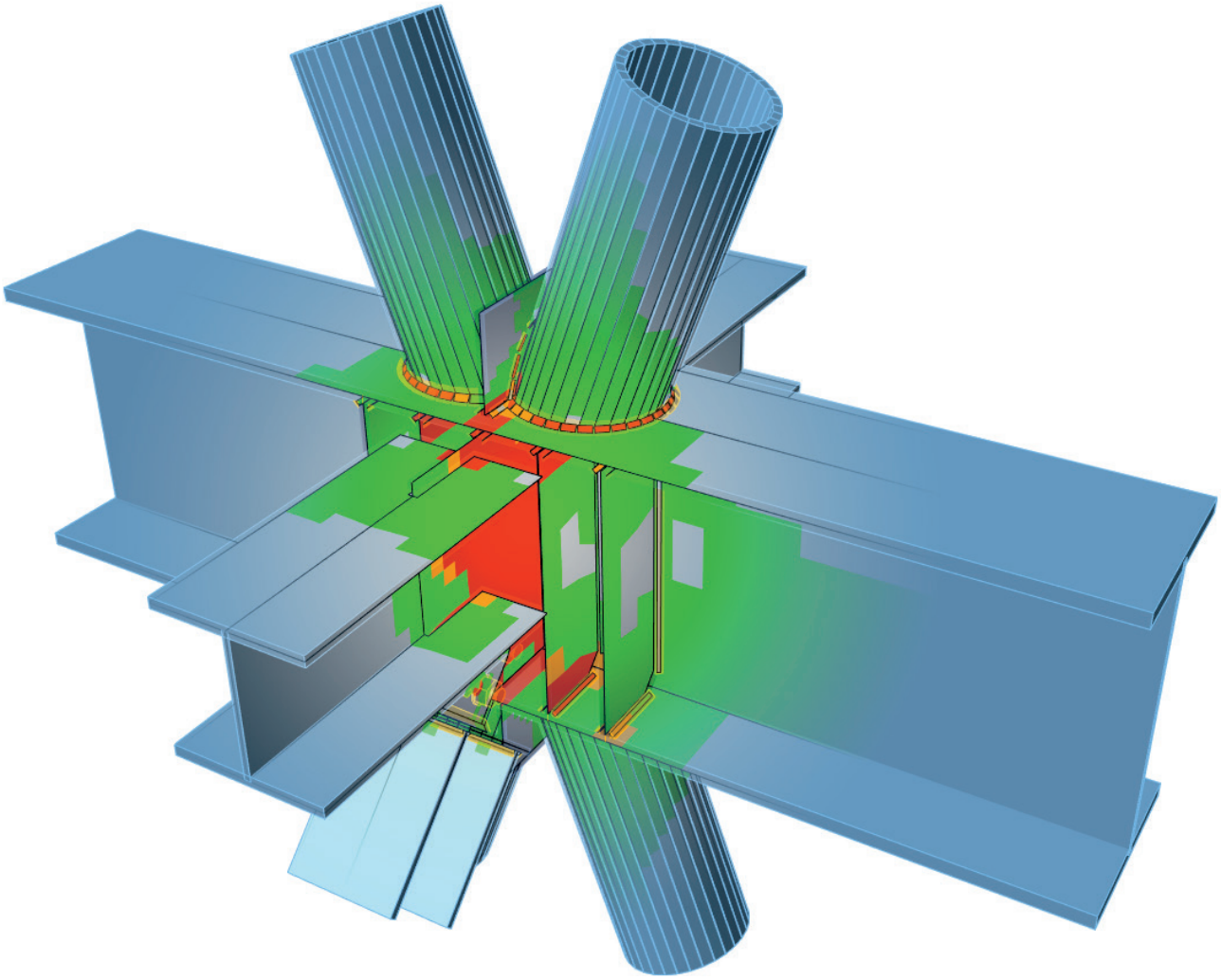

COMPONENT–BASED FINITE ELEMENT DESIGN OF STEEL CONNECTIONS

Frantisek Wald et al.

Prof Frantisek Wald

Professor and Head of the Department of Steel and Timber Structures at the Czech Technical University in Prague. During his rich professional career, he has participated in ten European projects in connection design and several other projects focused on component method, column bases, steel and concrete connections, fire design and the advanced finite element analysis.
He has been working in ECCS TC 10 Structural joints in WG8 and Project team for preparation of EN 1993-1-8:2025.
He is also a member of CEN Working Groups for new generation of EN 1993-1-2 and EN 1993-1-14.

Prof Wald received two awards for the development of Component-based Finite Element Method (CBFEM) – the CKAIT Pavel Juchelka Czech Award and the ECCS Charles Massonet European Award.

Component-based finite element design of steel connections

Wald F., Šabatka L., Bajer M.,

Jehlička P., Kabeláč J., Kožich M., Kuříková M., Vild M.

Component-based finite element design
of steel connections
Wald F., Šabatka L., Bajer M.,
Jehlička P., Kabeláč J., Kožich M., Kuříková M., Vild M.

Published by the Czech Technical University in Prague
Prepared by Faculties of Civil Engineering of the Brno University of Technology and Czech Technical University in Prague
ISBN 978-80-01-06702-4 print
ISBN 978-80-01-06703-1 online

LIST OF CONTENTS

Terms and symbols

The symbols are introduced in relevant chapters. The terminology and symbols follow the rules applied in EN1993-1-8:2006. The major general variables are described below.

Terms

Connection

Connection is a location at which two or more elements meet. For design purposes, it represents the location where the relevant internal forces and moments are transferred.

Initial stiffness

The secant rotational stiffness at the initial part of the moment-rotational curve at 2/3 of the joint bending resistance.

Joint

Joint represents a zone where two or more members are interconnected. A beam-to-column joint consists usually of a column web panel and either one connection (single-sided joint configuration) or two connections (double-sided joint configuration).

Node

Node is defined as a point within which axes of two or more inter-connected members intersect.

Rotational capacity

The angle through which the joint can rotate for a given resistance level without failing.

Rotational stiffness

The moment required to produce unit rotation in a joint.

Symbols

The following symbols are used:

a is the length of base plate;

a_w is the effective throat thickness of fillet weld;

b is the width of base plate;

b_b is the width of the beam;

b_c is the width of the column;

b_i is the overall out-of-plane width of RHS member i (i = 0, 1, 2 or 3);

b_{eff} is the effective width for a brace member to chord connection;

$b_{e,ov}$ is the effective width for an overlapping brace to overlapped brace connection;

$b_{e,p}$ is the effective width for punching shear;

b_p is the width of a plate;

c is the effective width of the flexible base plate;

d is the nominal bolt diameter, the diameter of the pin or the diameter of the fastener;

d_0 is the hole diameter for a bolt, a rivet or a pin;

d_c is the clear depth of the column web;

d_i is the overall diameter of CHS member i (i = 0, 1, 2 or 3);

d_m is the mean of the across points and across flats dimensions of the bolt head or the nut, whichever is smaller;

d_w is the depth of the web of an I or H section chord member;

e is the eccentricity of a joint;

e_1 is the end distance from the center of a fastener hole to the adjacent end of any part, measured in the direction of load transfer;

e_2 is the edge distance from the center of a fastener hole to the adjacent edge of any part, measured at right angles to the direction of load transfer;

e_3 is the distance from the axis of a slotted hole to the adjacent end or edge of any part;

e_4 is the distance from the center of the end radius of a slotted hole to the adjacent end or edge of any part;

f_{cd} is the design value of compressive cylinder strength of concrete $f_{cd} = f_{ck} / \gamma_c$;

f_{ck} is the characteristic value of concrete compressive cylinder strength;

f_u is the material ultimate strength;

f_{ub} is the ultimate strength of the bolt;

f_y is the material yield stress;

f_{yb} is the yield stress of the bolt;

g is the gap between the brace members in a K or N joint (negative values of g represent an overlap q); the gap g is measured along the length of the connecting face of the chord, between the toes of the adjacent brace members;

h_b is the depth of the beam;

h_c is the depth of the column;

h_i is the overall in-plane depth of the cross-section of member i (i = 0, 1, 2 or 3);

i is an integer subscript used to designate a member of a joint, i = 0 denoting a chord and i = 1, 2 or 3 the brace members. In joints with two brace members, i = 1 normally denotes the compression brace and i = 2 the tension brace;

k_{eq} is the equivalent stiffness coefficient;

k_i is the stiffness coefficient of component i;

ℓ_{eff} is the effective length (of fillet weld or T stub);

n is the number of the friction surfaces or the number of fastener holes on the shear face;

p_1 is the spacing between centers of fasteners in a line in the direction of load transfer;

$p_{1,0}$ is the spacing between centers of fasteners in an outer line in the direction of load transfer;

$p_{1,i}$ is the spacing between centers of fasteners in an inner line in the direction of load transfer;

p_2 is the spacing measured perpendicular to the load transfer direction between adjacent lines of fasteners;

r is the root radius of an I or H section or the corner radius of a rectangular hollow section;

s_s is the length of stiff bearing;

t_a is the thickness of the angle cleat;

t_f is the flange thickness of an I or H section;

t_i is the wall thickness of member i (i = 0, 1, 2 or 3);

t_p is the thickness of the end plate or base plate;

t_w is the thickness of the web or bracket;

z is the lever arm;

A is the gross cross-section area of bolt;

A_i is the cross-sectional area of member i (i = 0, 1, 2 or 3);

A_{vc} is the shear area of the column;

A_s is the tensile stress area of the bolt or of the anchor bolt;

$A_{v,eff}$ is the effective shear area;

$B_{p,Rd}$ is the design punching shear resistance of the bolt head and the nut;

E is Young's modulus of steel;

$F_{t,Ed}$ is the design tensile force per bolt for the ultimate limit state;

$F_{t,Rd}$ is the design tension resistance per bolt;

$F_{T,Rd}$ is the tension resistance of an equivalent T-stub flange;

$F_{v,Rd}$ is the design shear resistance per bolt;

$F_{b,Rd}$ is the design bearing resistance per bolt;

$F_{v,Ed}$ is the design shear force per bolt for the ultimate limit state;

L is the system length of a member;

$M_{ip,i,Rd}$ is the design value of the resistance of the joint, expressed in terms of the in-plane internal moment in member i (i = 0, 1, 2 or 3);

$M_{ip,i,Ed}$ is the design value of the in-plane internal moment in member i (i = 0, 1, 2 or 3);

$M_{j,Rd}$ is the design moment resistance of a joint;

$M_{pl,Rd}$ is the design plastic moment resistance of a cross-section;

$N_{i,Rd}$ is the design value of the resistance of the joint, expressed in terms of the internal axial force in member i (i = 0, 1, 2 or 3);

$N_{i,Ed}$ is the design value of the internal axial force in member i (i = 0, 1, 2 or 3);

$N_{j,Rd}$ is the axial design resistance of the joint;

S_j is the rotational stiffness of a joint;

$S_{j,ini}$ is the initial rotational stiffness of a joint;

$V_{wp,Rd}$ is the plastic shear resistance of a column web panel;

$W_{e\ell,i}$ is the elastic section modulus of member i (i = 0, 1, 2 or 3);

$W_{p\ell,i}$ is the plastic section modulus of member i (i = 0, 1, 2 or 3);

α is the reduction factor of bearing resistance;

α_b is the factor for bearing resistance;

α_{cr} is the critical buckling factor;

$\alpha_{ult,k}$ is the load amplifier;

β_{Lw} is the reduction factor for long welds;

ε is the material yield strain;

φ is the rotation of a joint;

φ_{Cd} is the design rotation capacity of a joint;

θ_i is the included angle between brace member i and the chord (i = 1, 2 or 3);

φ is the angle between the planes in a multiplanar joint.

n is the stiffness reduction factor;

λ_{ov} is the overlap ratio, expressed as a percentage ($\lambda_{ov} = (q/p)$ x 100%);

λ_p is the plate slenderness;

ρ is the reduction buckling factor;

$\sigma_{0,Ed}$ is the maximum compressive stress in the chord at a joint;

$\sigma_{p,Ed}$ is the value of $\sigma_{0,Ed}$ excluding the stress due to the components parallel to the chord axis of the axial forces in the braces at that joint;

$\sigma_{\perp}$ is the normal stress perpendicular to the throat section;

$\tau_{\perp}$ is the shear stress (in the plane of the throat section) perpendicular to the axis of the weld;

$\tau_{\parallel}$ is the shear stress (in the plane of the throat section) parallel to the axis of the weld.

1 INTRODUCTION

Four decades ago, Finite Element Analysis (FEA) of structural connection was treated by some researchers as a non-scientific matter. Two decades later, it was already a widely accepted addition or even necessarily an extension of experimental and theoretical work. Today computational analysis, in particular computational mechanics and fluid dynamics, is commonly used as an indispensable design tool and a catalyst for many relevant research fields. The recommendation for design by advanced modeling in structural steel is already hidden but ready to be used in Chapter 5 and Annex C of EN 1993-1-5:2006. Development of modern general-purpose software and decreasing cost of computational resources facilitate this trend. As the computational tools become more readily available and easier to use, even to relatively inexperienced engineers, more skepticism and scrutiny should be employed when judging one's computational analysis. The FEA of structural connection is the next, fast approaching step in structural steel design.

The only way to prove the correctness of simulated results is through a methodical verification and validation (V&V) process. Without V&V the finite element analysis is meaningless and cannot be used for making any decisions. To help with this process is prepared the presented monography.

The work was developed under the R&D project MERLION III supported by Technology Agency of the Czech Republic, project No. TH02020301. The review of the text was prepared by A. Uhlíř, M. Strejček, and J. Šabatka.

In Prague, 28 February 2020
František Wald

2 CONNECTION DESIGN

2.1 Design models

The structural steel connections are designed by experimental, curve fitting, analytical and numerical models. The tests with connections are a simple and economical solution for a prediction of their behavior. Designed tables for standardized connections were prepared by interpolation and even extrapolation based on tests. In the nineties of the last century, databases of tests, see e.g. (Chen and Abdalla, 1995), were collected and published. Over three thousand tests are described, and the collection is a valuable resource for learning about the behavior of typical joints, although some necessary data is missing. Curve fitting models are known since 1930. Mathematical formulas expressing the influence of geometrical and material parameters are reproducing the behavior of similar connections well but are not appointing the significant parameters for design and, in particular, the resistance. Today, modeling is applied even for connections in seismic design. The analytical modeling of components of connections is well developed for connectors, bolts, welds, anchor bolts etc. Analytical models of connections need good engineering assumption of internal forces and proper selection of components, which affects the resistance and stiffness.

The complexity of finite element analyses was deeply studied in the last twenty years. Later, the procedures to reach proper results in research-oriented finite element models were commonly accepted together with the firm limits for the application of design FE models. The behavior of well-described and published components loaded by elevated temperature, as tying forces, moment normal interaction and torsion, and of the new less described components, such as backing channel, was developed based on numerical experiments validated on experiments. The fast development of the computer-assisted design of steel and composite structures in the field of complex structures, such as plated structures in bridges, excavators and wind towers, glass structures, and cold-formed structures, clarified the design procedures of models and its application in civil engineering.

2.2 Component method

The latest version of analytical models for connections of steel and steel and concrete structures predicts not only the most important design resistance but also the initial stiffness and the deformation capacity, which allows design of ductile structures. This model, prepared for selected types of configurations, is known as Component method (CM). CM builds upon standard procedures evaluating the internal forces in selected geometries of connections and their checking. Zoetemeijer (1985) was the first who equipped the model for resistance with prediction of stiffness and deformation capacity for end plate connections. The formulation and calculation

of the elastic stiffness were improved in the work of Steenhius (1994). For most beam-to-column joint configurations, description of components behavior by Jaspart (Jaspart, 2002) and by for column bases Wald et al. (2008) were prepared under European network COST C1. Method is currently implemented in the current European structural standard for steel and composite connections; see EN 1993-1-8:2005 and EN 1994-1-1:2010 and applied in the majority of software for structural steel design used in Europe. The component model was generalized by da Silva (2008). Currently, the model is applied for the design of joints at elevated temperatures during fire, see e.g. (Block et al. 2013), for 3D modeling of connections in space structures, for joints in timber structures, for prediction of behavior under cyclic loading during earthquake etc.

The procedure starts with a decomposition of a joint to components followed by their description in terms of normal/shear force deformation behavior. After that, components are grouped to examine joint moment–rotational behavior and classification/representation in a spring/shear model and application in global analyses. The advantage of the component model is an integration of current experimental and analytical knowledge of connection components behavior: bolts, welds, end plates, flanges, anchor bolts, and base plates. This provides a very accurate prediction of behavior in elastic and ultimate level of loading. Verification of the model is possible using simplified calculation. Disadvantage of component model is that experimental evaluation of internal forces distribution is done only for a limited number of joint configurations. Also, in temporary scientific papers and background materials, description of typical components is either not present or has low validity.

There are no generally accepted standardized procedures for determination of rotation capacity compared to well-accepted methods for determination of initial stiffness and resistance of many types of structural joints. The criteria are selected in EN 1993-1-8:2005 to help the engineers. The estimation of the rotation capacity is important in many applications, namely in connections exposed to seismic; see (Grecea et al. 2004). The deformation capacity of components has been studied from the end of last century; see (Foley and Vinnakota, 1995). Faella et al. (2000) carried out tests on T-stubs and derived deformation capacity by analytical expressions. Kuhlmann and Kuhnemund (2000) performed tests on the column web subjected to transverse compression at different levels of axial compression force in the column. Da Silva et al. (2002) predicted deformation capacity at different levels of axial force in the connected beam. Based on the test results combined with FE analysis, deformation capacities are established for the basic components by analytical models by Beg at al. (2004), where components are represented by non-linear springs, and appropriately combined in order to determine the rotation capacity of the joint for end-plate connections with an extended or flush end-plate and welded connections. For these connections, the most important components that may significantly contribute to the rotation capacity were recognized as the column web in compression, column web in tension, column web

in shear, column flange in bending, and end-plate in bending. Components related to the column web are relevant only when there are no stiffeners in the column that resist compression, tension or shear forces. The presence of a stiffener eliminates the corresponding component, and therefore its contribution to the rotation capacity of the joint can be neglected. End plates and column flanges are important only for end plate connections, where the components act as a T-stub, where also the deformation capacity of the bolts in tension is included. The questions and limits of deformation capacity of connections of high strength steel were studied by Girao et al. (2004). In all works, the connector's behavior was combined with FEA analyses of plates to check the steel limiting strain, which was first prepared by Sherbourne and Bahaari (1994) and (1996).

Models of hollow section connections based on knowledge from the nineties are described in Ch. 7 of EN 1993-1-8:2005 by curve fitting procedures. The latest version brings the world standard IIW XV-1439-13 ISO/FDIS 14346 (2012). The transfer to a higher level of analytical modeling by component method was finished by mechanical transferring of reduction factors to the effective widths and the predefined lever arms; see (Jaspart and Weinand 2015).

The CM is not developed for hand calculation. The analyses of all components in connection and its assembly is focused on preparation of design tables or tools.

2.3 Finite element models

Finite element analyses (FEA) for connections are used from the 70s of last century as research-oriented procedures. Their ability to express real behavior of connections is making it a valid alternative to testing – standard but expensive source of knowledge of connection behavior. Material model for FEM uses true strain stress-strain diagram, which is calculated from experimental results of coupon tests taking into account the contraction of the sample during the inelastic stage of testing. Today computational analysis, in particular computational mechanics and fluid dynamics, is commonly used as an indispensable design tool and a catalyst for many relevant research fields. The recommendation for design by advanced modeling in structural steel is ready to be used in Chapter 5 and Annex C of EN 1993-1-5:2006. The design strain is recommended to be limited to 5%, see Cl. C.8(1) EN 1993-1-5:2006. Implementation of safety into advanced design models under ultimate limit state design is summarised in Cl. C.9(2) of EN 1993-1-5:2006. Standard procedure with partial safety factors for material/connections may be applied. More advanced and accurate solution, which takes into consideration accuracy of a model and material separately, gives more accurate and economical solution to structural connections.

The complexity of FE modeling of the structural steel connections was deeply studied since the eighties; see (Krishnamurthy, 1978). Later the procedures to reach proper results in scientific oriented FE models and the strong limits for application of design FE models were commonly accepted; see (Bursi and Jaspart, 1997) and (Virdi K. S. et al. 1999).

2.4 Validation and verification

In publications dealing with computational mechanics, the authors express a need for Validation and Verification (V&V) studies, which could be used by software developers and users; see (Kwasniewski, 2010). However, there are different opinions on how such reference material should be developed, how complex problems should be considered, theoretical or with practical meaning, and if benchmark questions should refer only to analytical and numerical solutions or should also include experimental data. These inquiries are related to the differences between validation and verification. In the formal procedure called System Response Quantity (SRQ), see prEN1993-1-14:2020, validation compares the numerical solution with the experimental data, whereas verification compares computational solutions with highly accurate (analytical or numerical) benchmark solutions. According to AIAA Guide (1998), code verification can be conducted through tests of agreement between a computational solution and four types of benchmark solutions: analytical, highly accurate numerical solutions, and manufactured solutions (Oberkampf and Trucano, 2008). In contrast to numerical solutions used in the validation stage, the numerical solutions applied for verification can represent mathematical models with little physical importance. The verification on the analyst's side is based on the test of agreement with the known correct results, if such are available. Most of commercial codes, such as ANSYS, ABAQUS (SIMULIA, 2011), and MIDAS, support lists of well-documented benchmark cases (tests). For example, ABAQUS in three manuals provides a wide variety of benchmark tests (including 93 NAFEMS benchmarks) from simple one-element tests to complex engineering problems and experiments (validation benchmarks). These example problems, containing input files, are advantageous for a user not only as material for verification but also as a great help in individual modeling, see (Wald et al. 2014). Nevertheless, there is still lack of benchmark studies for some specific research areas, such as connection design.

The experimental data, which can be used for validation, should be treated separately and differently compared to benchmark solutions applied for verification. The reasons for that are unavoidable errors and uncertainties associated with the results of experimental measurements. An error of measurement (calculation) can be defined as the result of measurement (calculation) minus the value of the measured (accurate solution); see (ISO, 1993). As the accurate solution is usually unknown (eventually known for simplified cases), the user can only deal with estimates of errors. Uncertainty can be thought of as a parameter associated with the result of measurement (solution) that characterizes the dispersion of the values that could be reasonably attributed to the measured.

Experimental validation in structural connection design through comparison between numerical results and experimental data obtained using the beam tests with simple connections loaded in shear and cruciform tests for moment resistant connections loaded by bending moments

are especially tricky and have their limitations. Complex connection tests may be compared to the simplest ones, but are the comparison is limited due to inevitable uncertainties characterizing the specimen behavior. The limitations of experimental validation increase the importance of verification, which is supposed to deliver evidence that mathematical models are adequately implemented and that the numerical solution is correct with respect to the mathematical model.

2.5 Benchmark cases

Even though examples of experimental studies and examples of calculations following the structural Eurocode procedures are also useful and can be helpful for other users, here the term benchmark studies refer to computer simulations (numerical analysis). A well-developed benchmark example should satisfy the following requirements. The problem considered should be relatively simple, easy to understand. In authors' opinion, for more complex problem, less reliable solution can be provided. For complex problems, for example with actual material properties of steel or concrete, only numerical solutions can be obtained. Comparison among the numerical solutions obtained with the help of different software shows quite often unexpected discrepancy among the results as well. Even if the results are similar, this should not be considered as strong evidence of the solution's reliability. Two different numerical solutions can only be compared based on a solution sensitivity analysis.

Seeking simplicity, we should accept that a considered case may show little practical meaning. It is supposed to be used for verification of computational models not to solve an engineering problem. Critical is the material model considered. If the material models developed for actual structural materials are used, for example based on EC, with all required nonlinearities, only approximate solutions are possible and can substantially vary for different software. It is difficult to find a good balance between simplicity and a practical meaning of the chosen benchmark case. To solve this difficulty, it is recommended to use in benchmark studies a hierarchical approach where a set of problems is considered, starting from simple cases with analytical solutions. Then more complex problems, closer to the practice, are investigated numerically. Such approach gives more confidence towards obtained solutions.

As a part of benchmark study, the complete input data must be provided in the way easy to follow. All assumptions, such as material properties, boundary conditions, temperature distribution, loading conditions, and large/small deformations and displacements, must be clearly identified. For experimental examples, all measurements and a detailed description of the test procedure should be provided. For numerical benchmark examples, mesh density study should also be conducted. It should be shown that the provided results are within the range of asymptotic convergence. If possible, the recommended solution should be given as the estimate of the asymptotic solution based on solutions for at least two succeeding mesh densities. For finite

element calculations, the complete procedures such as Grid Convergence Index (GCI), based on Richardson extrapolation, are recommended (Roache, 1998). During the development of benchmark studies, it also should be considered to check alternative numerical models. e. g. using different codes or solid vs. shell finite elements (if possible). Such approach increases the validity of the solution.

2.6 Numerical experiments

Parametric study is a desired element of experimental work and an indispensable element of a numerical analysis. The cost needed to perform multiple experiments related to structural connections is usually small, but a probabilistic distribution of the system response is rarely available. However, in the case of simulated benchmark problems, computational cost of running multiple instances of a simple numerical experiment with varying input parameters is competitive.

The variance of a system response depends on the variance in the input parameters but also on the range at which it is tested. Nonlinearity of the response has to be considered as well when designing the benchmark tests. The numerical experiments should be performed out in the range where a reasonable variation in an input parameter causes a reasonable change in the system's response. Designing a benchmark test producing either a non-sensitive or overly sensitive response is undesirable. The sensitivity study for a system with multiple variable input parameters and multiple responses should be performed by regression analysis or variance-based methods.

Actually, selection of the System Response Quantity (SRQ), see (Kwasniewski, 2010), is important for both verification and validation. However, in both cases, it is subject to different limitations. In verification, SRQ means a quantity which describes the response of the structure and is selected for comparison with the value obtained from the benchmark solution. A user is less limited here than in the case of validation, where the experimental data is always limited by the number of gauges and other instrumentation. The selection of the SRQ should reflect the main objective of the analysis, and for structures in fires, it usually refers to quantities describing heat transfer or mechanical response. For heat transfer problems, temperatures obtained at the specific time instance at selected locations seem to be an optimal choice. For mechanical structural response, we can choose between local and global (integral) quantities. Engineers are usually interested in stresses and internal forces, which are local quantities. They are subject to larger uncertainties, especially in the case of validation. More appropriate are global quantities such as deflection, which reflects deformation of the whole, or a large part of structure and its boundary condition.

2.7 Experimental validation

As the experimental data is stochastic by nature and is always subject to some variation, it should be actually defined by a probability distribution. For complete comparison, the numerical results should also be presented in an analogous probabilistic manner using a probability distribution, generated by repeated calculations with some selected input data varying following prescribed distributions, so-called probability simulations. Such extensive calculations can be conducted automatically with the help of specialized optimization packages (e.g., LS-OPT®, HyperStudy® or ModeFrontier®), which are more often included in nowadays commercial computational systems.

For many authors working on principles of validation and verification (Kwasniewski, 2010), the term calibration has a negative meaning and describes a practice which should be avoided in numerical modeling. Calibration here means unjustified modification of the input data applied to a numerical model in order to shift the numerical results closer to the experimental data. An example of erroneous calibration is shown in Fig. 2.1, where at the beginning, it is assumed that the numerical model well reflects the experiment. However, due to some uncertainties associated with the experiment, the first numerical prediction differs from the first experimental result. Frequently in such cases, the discrepancy between the experiment and the numerical simulation is attributable to some by the analyst unidentified input parameter and not to a limitation of the software, and then, through hiding one error by introducing another, the calibration process itself is erroneous. Calibration, applied for example through variation of material input data, shifts the result closer to the experimental response but, at the same time, changes the whole numerical model whose probability is now moved away from the experimental one. Due to the calibration, the new numerical model may easily show poorer predictive capability. This fact is principally revealed for modified input data, e.g. loading conditions.

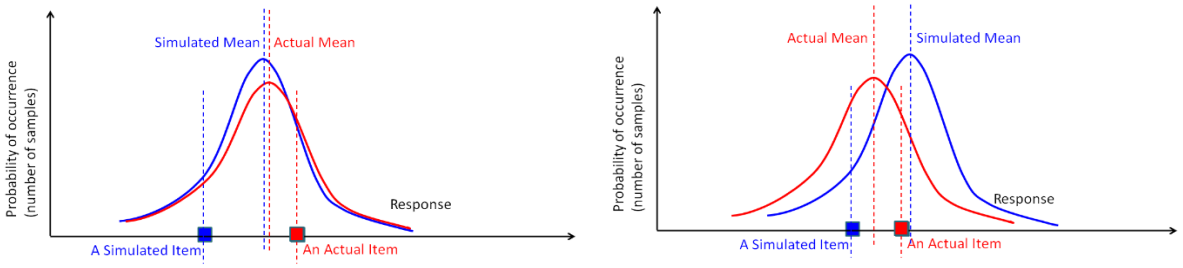

Fig. 2.1: Example of calibration meaning unjustified shifting the numerical results closer to the experimental data (Kwasniewski, 2010)

There is a situation when the calibration process actually makes sense. If a full stochastic description of experimental data is known and probabilistic analysis was performed for the simulation, and there is a difference between means of measured and simulated responses, then

calibration of physical models may be needed. The adjustment of the model introduces a change in the response that brings the entire spectrum of results closer to the experimental set of data. The calibration defined that way is much more complex process than just tweaking of the models and must be confirmed on different simulated events.

3 COMPONENT-BASED FINITE ELEMENT METHOD

3.1 Material model

The most common material diagrams used in finite element modeling of structural steel are the ideal plastic, elastic model with strain hardening, and the true stress-strain diagram, see Fig. 3.1.1. The true stress-strain diagram is calculated from the material properties of mild steels at ambient temperature obtained in tensile tests. The true stress and strain may be obtained as follows:

$$\sigma_{true} = \sigma\,(1 + \varepsilon) \qquad (3.1.1)$$

$$\varepsilon_{true} = \ln(1 + \varepsilon) \qquad (3.1.2)$$

where σ_{true} is true stress, ε_{true} true strain, σ nominal stress, and ε nominal strain. The elastoplastic material with strain hardening is modeled according to EN 1993-1-5:2006. The material behavior is based on von Mises yield criterion. It is assumed to be elastic before reaching the yield strength, f_y. The ultimate limit state criteria for regions not susceptible to buckling is reaching a limiting value of the principal membrane strain. The value of 5 % is recommended.

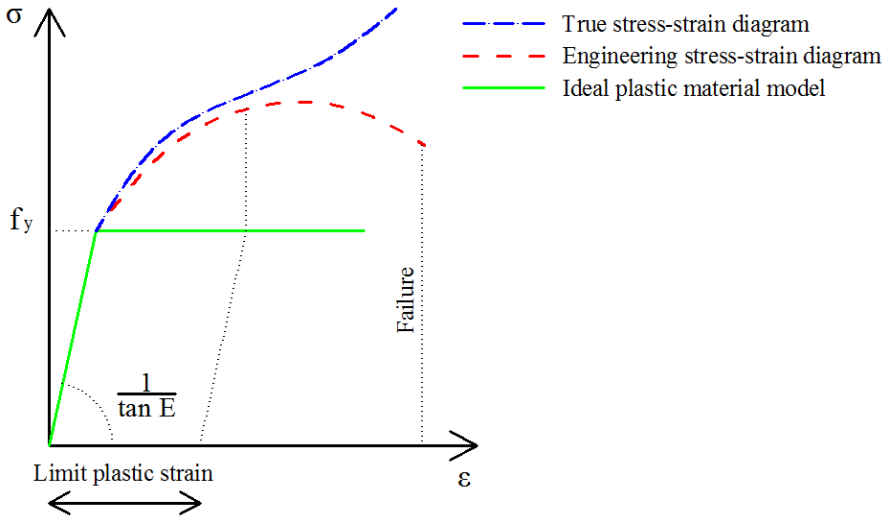

Fig. 3.1.1 Material diagrams of steel in numerical models

The limit value of plastic strain is often discussed. In fact, ultimate load has low sensitivity to the limit value of plastic strain when ideal plastic model is used. It is demonstrated in the following example of a beam-to-column joint. An open section beam IPE 180 is connected to an open section column HEB 300 and loaded by bending moment, as shown in Fig. 3.1.2. The influence of the limit value of plastic strain on the resistance of the beam is shown in Fig. 3.1.3. The limit plastic strain is changing from 2 % to 8 %, but the change in moment resistance is less than 4 %.

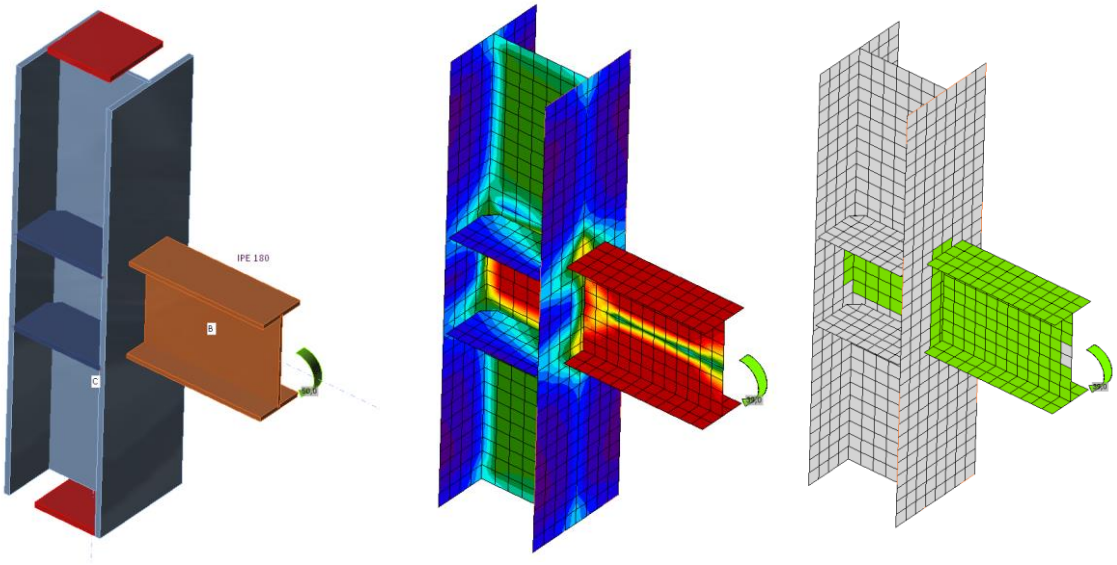

a) loads b) stresses c) strains

Fig. 3.1.2 Example of prediction of ultimate limit state of a beam to column joint

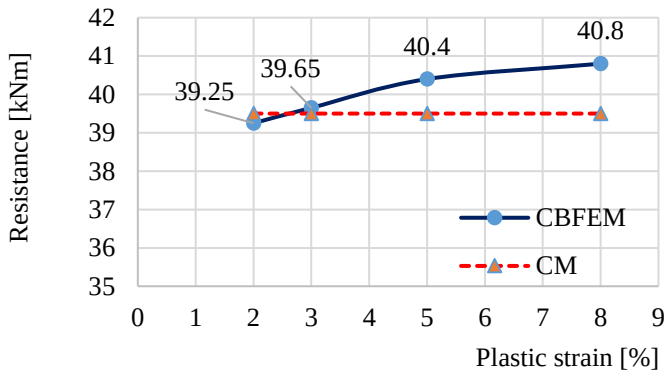

Fig. 3.1.3 Influence of the limit value of plastic strain on the moment resistance

3.2 Plate model and mesh convergence

3.2.1 Plate model

Shell elements are recommended for modeling of plates in design FEA of structural connection. 4-node quadrangle shell elements with nodes at its corners are applied. Six degrees of freedom are considered in every node: 3 translations (u_x, u_y, u_z) and 3 rotations (φ_x, φ_y, φ_z). Deformations of the element are divided into membrane and flexural components.

The formulation of membrane behavior is based on the work of Ibrahimbegovic (1990). Rotations perpendicular to the plane of the element are considered. Complete 3D formulation of the element is provided. The out-of-plane shear deformations are considered in the formulation of the flexural behavior of element based on Mindlin hypothesis. The MITC4 elements are applied, see Dvorkin (1984). The shell is divided into five integration points along the height of the plate, and plastic behavior is analyzed in each point. It is called Gaus–Lobatto integration. The nonlinear elastic-plastic stage of material is analyzed in each layer based on the known strains.

3.2.2 Mesh convergence

There are some criteria for the mesh generation in the connection model. The connection check should be independent of the element size. Mesh generation on a separate plate is problem-free. The attention should be paid to complex geometries such as stiffened panels, T-stubs, and base plates. The sensitivity analysis considering mesh discretization should be performed for complicated geometries.

All plates of a beam cross-section have common size of elements. Size of generated finite elements is limited. Minimal element size is set to 10 mm and maximal element size to 50 mm. Meshes on flanges and webs are independent of each other. Default number of finite elements is set to 8 elements per cross-section height, as shown in Fig. 3.2.1.

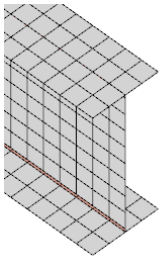

Fig. 3.2.1 Mesh on beam with constrains between web and flange plate

The mesh of end plates is separate and independent of other connection parts. Default finite element size is set to 16 elements per cross-section height, as shown in Fig. 3.2.2.

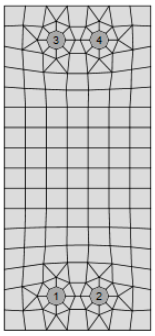

Fig. 3.2.2 Mesh on end plate, with 7 elements along its width

Following example of a beam-to-column joint shows the influence of mesh size on moment resistance. An open section beam IPE 220 is connected to an open section column HEA 200 and loaded by bending moment, as shown in Fig. 3.2.3. The critical component is column panel in shear. The number of finite elements along the cross-section height is changing from 4 to 40, and the results are compared; see Fig. 3.2.4. Dashed lines are representing 5%, 10%, and 15% difference. It is recommended to subdivide the cross-section height into 8 elements.

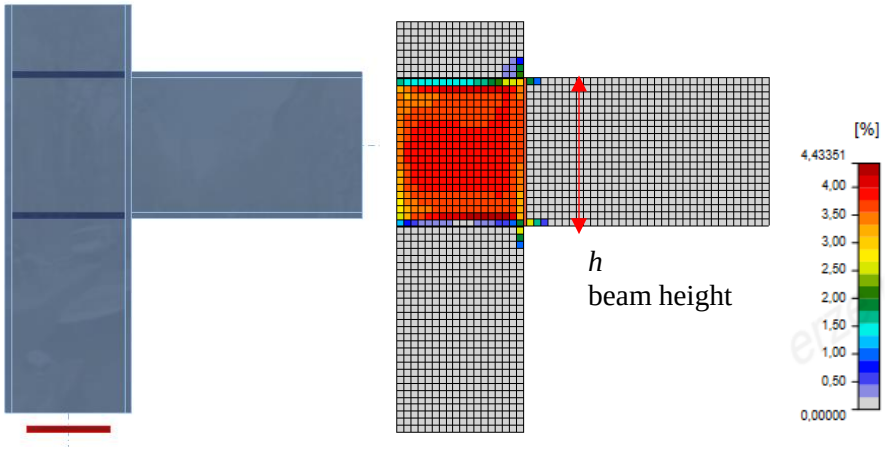

Fig. 3.2.3 Beam to column joint model and plastic strains at ultimate limit state

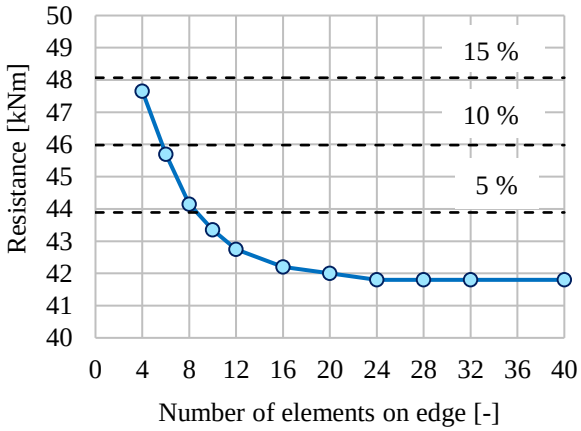

Fig. 3.2.4 Influence of number of elements on the moment resistance

Mesh sensitivity study of a slender compressed stiffener of column web panel is presented. The geometry of the example is taken from Chapter 6.3. The number of elements along the width of the stiffener is changed from 4 to 20. The first buckling mode and the influence of a number of elements on the buckling resistance and critical load are shown in Fig. 3.2.5. The differences by 5% and 10% are displayed. It is recommended to use 8 elements along the stiffener width.

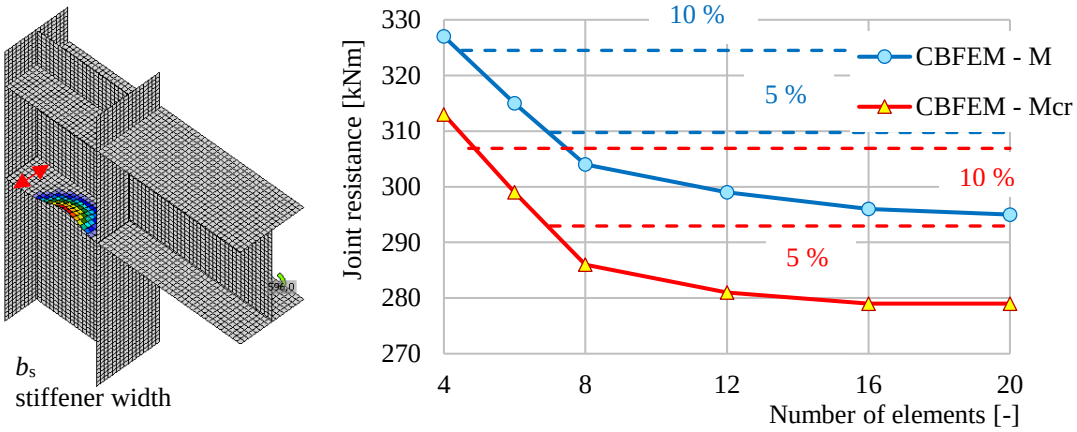

Fig. 3.2.5 First buckling mode and influence of number of elements along the stiffener on the moment resistance

Mesh sensitivity study of T-stub in tension is presented. The geometry of the T-stub is described in Chapter 5.1. Half of the flange width is subdivided into 8 to 40 elements, and the minimal element size is set to 1 mm. The influence of the number of elements on the T-stub resistance is shown in Fig. 3.2.6. The dashed lines are representing the 5 %, 10 %, and 15 % difference. It is recommended to use 16 elements on the half of the flange width.

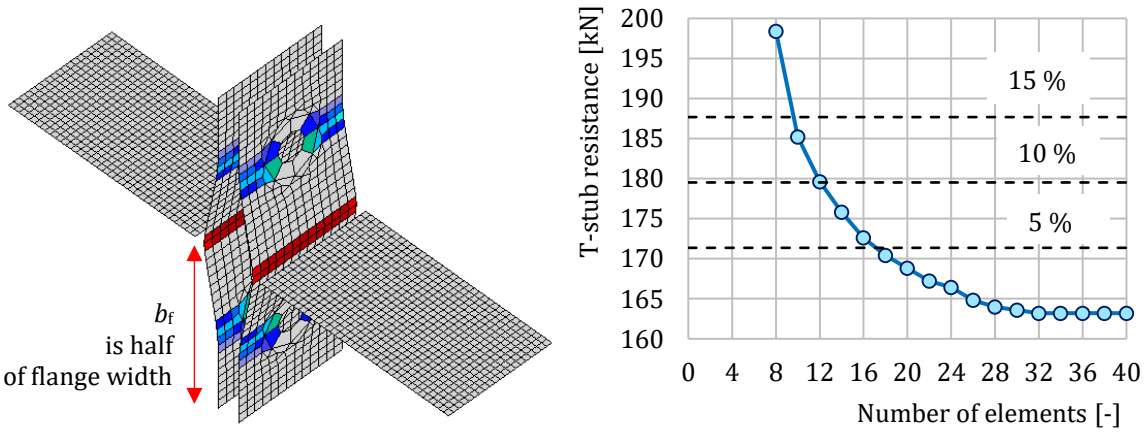

Fig. 3.2.6 Influence of number of elements on the T-stub resistance

Mesh sensitivity study of uniplanar transverse plate circular hollow section T joint in compresion is presented. The geometry of the T joint is described in Chapter 7.3. The number of elements along surface of the biggest circular hollow member is changed from 16 to 128. The influence of the number of elements on the joint resistance is shown in Fig. 3.2.7. The dashed lines

are representing the 5 % and 15 % difference. It is recommended to use 64 elements along the surface of the circular hollow member.

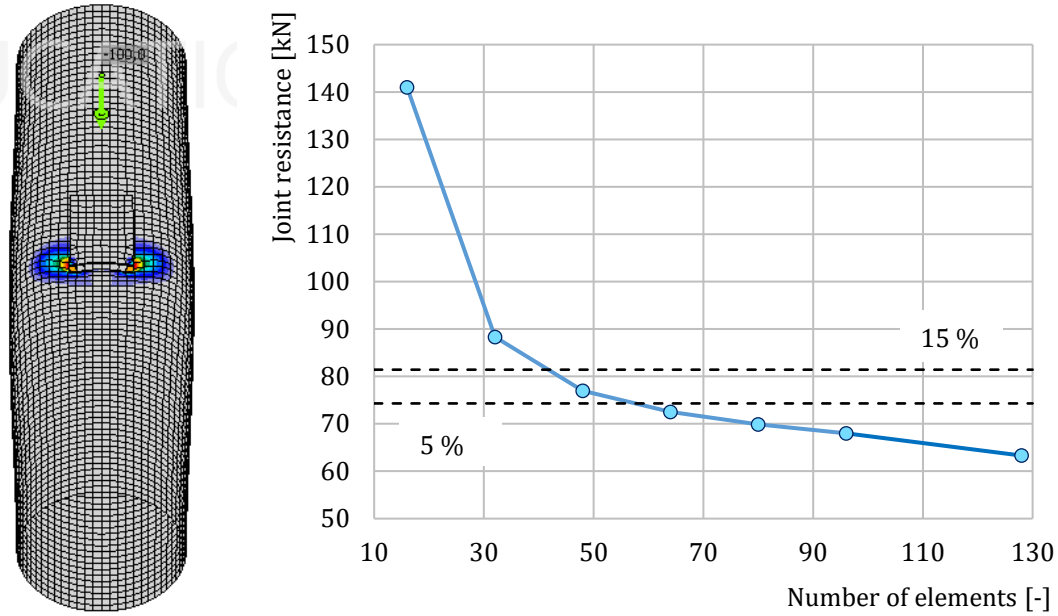

Fig. 3.2.7 Influence of number of elements on the joint resistance of CHS member

Mesh sensitivity study of uniplanar square hollow section X joint in compresion is presented in Fig. 3.2.8. The geometry of the joint is described in Chapter 7.2. The number of elements on the biggest web of hollow member is changed from 4 to 24. The influence of the number of elements on the joint resistance is shown. The dashed lines are representing the 5 % and 15 % difference. It is recommended to use 16 elements on the biggest web of rectangular hollow member.

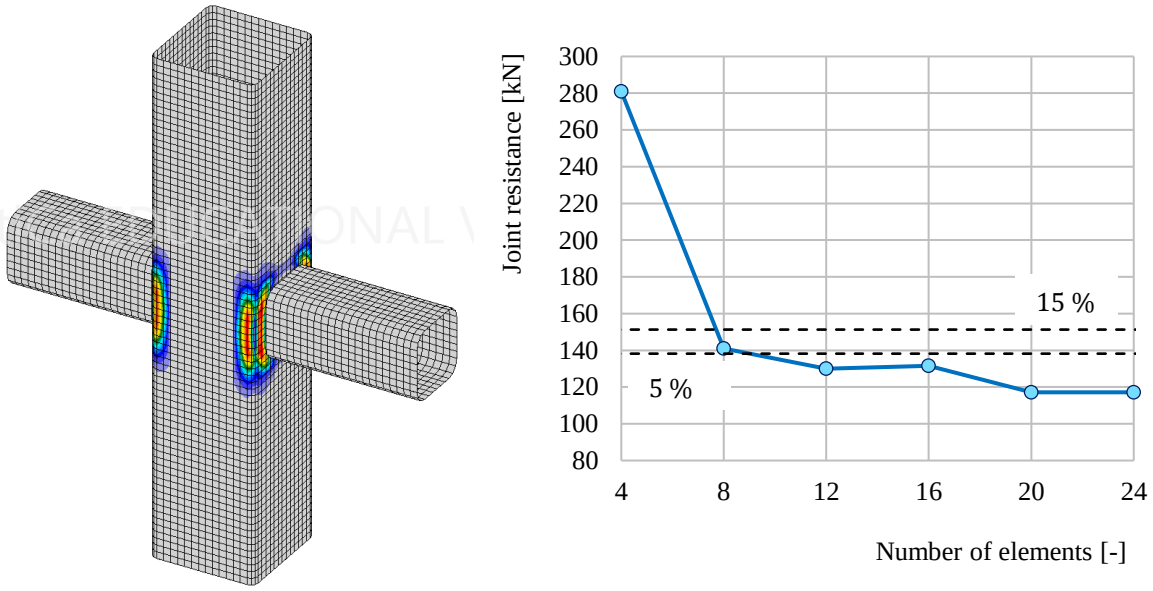

Fig. 3.2.8 Influence of number of elements on the joint resistance of rectangular hollow member

3.3 Contacts

The standard penalty method is recommended for modeling a contact between plates. If penetration of a node into an opposite contact surface is detected, penalty stiffness is added between the node and the opposite plate. The penalty stiffness is controlled by a heuristic algorithm during nonlinear iteration to get better convergence. The solver automatically detects the point of penetration and solves the distribution of contact force between the penetrated node and nodes on the opposite plate. It allows creating the contact between different meshes, as shown in Fig. 3.3.1. The advantage of the penalty method is the automatic assembly of the model. The contact between the plates has a significant impact on the redistribution of forces in connection.

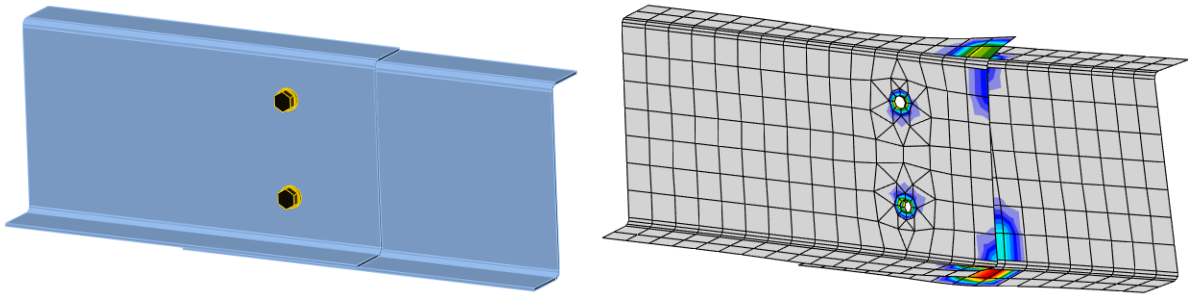

Fig. 3.3.1 Example of contact stress of two overlapped Z sections for bolted connections of purlins

3.4 Welds

Several options for treating welds in numerical models exist. Large deformations make the mechanical analysis more complex, and it is possible to use different mesh descriptions, different kinetic and kinematic variables, and constitutive models. The different types of geometric 2D and 3D models and thereby finite elements with their applicability for different accuracy levels are generally used. Most often used material model is the common rate-independent plasticity model based on von Mises yield criterion. Two approaches that are used for welds are described.

3.4.1 Direct connection of plates

The first option of weld model between plates is direct merge of meshes, as shown in Fig. 3.4.1. The load is transmitted through force-deformation constrains based on Lagrangian formulation to the opposite plate. The connection is called multi point constraint (MPC) and relates the finite element nodes of one plate edge to another plate. The finite element nodes are not connected directly. The advantage of this approach is the ability to connect meshes with different densities. The constraint allows to model midline surface of the connected plates with the offset, which respects the real plate thickness. This type of connection is used for full penetration butt welds.

3.4.2 Weld with plastic redistribution of stress

The load distribution in weld is derived from the MPC, so the stresses are calculated in the throat section. This is important for stress distribution in a plate under the weld and for modeling of T-stubs. This model does not respect the stiffness of the weld, and the stress distribution is conservative. Stress peaks, which appear at the ends of plate edges, in corners and rounding, govern the resistance along the whole length of the weld. To express the weld behavior, an improved weld model is applied. A special elastoplastic element is added between the plates. The element respects the weld throat thickness, position, and orientation. The equivalent weld solid is inserted with the corresponding weld dimensions, as shown in Fig. 3.4.2. The nonlinear material analysis is applied, and elastoplastic behavior in equivalent weld solid is considered. The stress peaks are redistributed along the weld length.

The aim of design weld models is not to capture reality perfectly. Residual stresses or weld shrinkage are neglected. The design weld models are verified for their resistance according to relevant codes. An appropriate design weld model is selected for each code. The resistances of the regular welds, welds to unstiffened flange, long welds, and multi-oriented weld groups were investigated to select parameters of the design weld element. The plastic strain in steel plates is normalized to 5 % to confirm with the maximum plastic strain of plates.

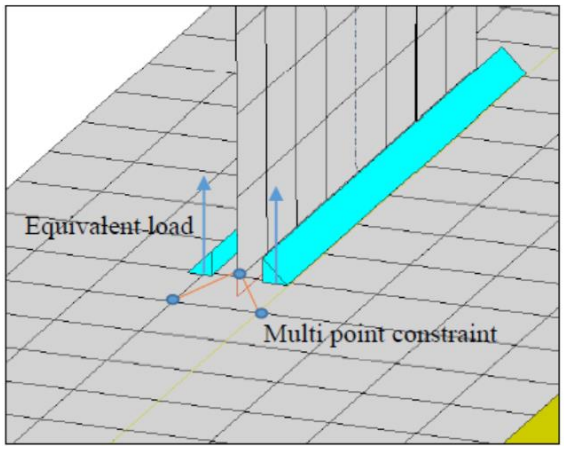

Fig. 3.4.1 Constraint between mesh nodes

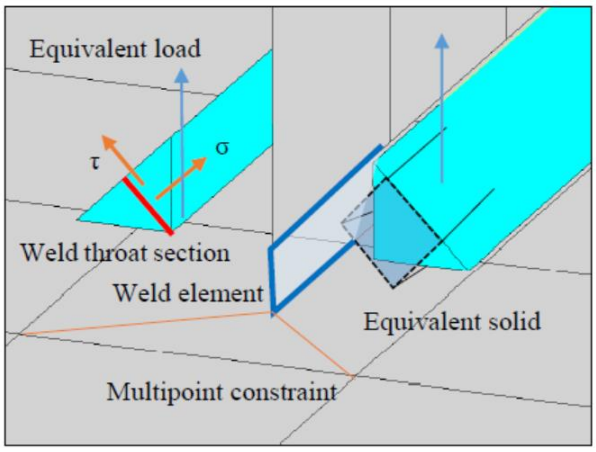

Fig. 3.4.2 Constraint between weld element and mesh nodes

3.4.3 Weld deformation capacity

The weld deformation capacity is determined to comply with resistance of welds to unstiffened flange, see cl. 4.10 in EN 1993-1-8:2006 and long welds, see cl. 4.11 in EN 1993-1-8:2008 and cl. J.2.2b AISC 360-16 etc. The deformation capacity was compared to sets of experiments from literature for longitudinal welds (Kleiner, 2018) and transverse welds (Ng et al, 2002). From the following figures, it can be seen that the weld model with plastic redistribution of stress is very conservative for longitudinal welds and at lower boundary for transverse welds.

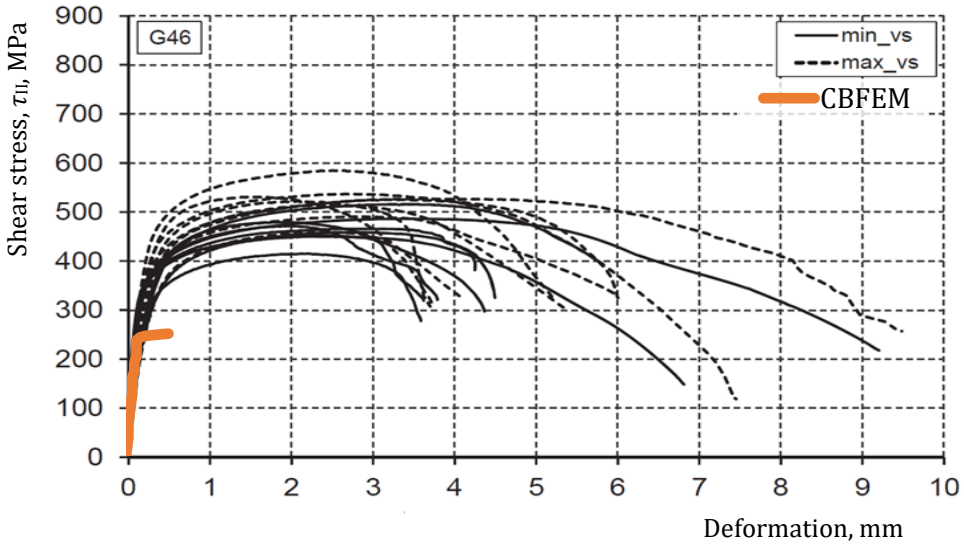

Fig. 3.4.3 Longitudinal welds, stress–deformation diagrams of real tests from (Kleiner, 2018) compared to model of weld with plastic stress redistribution

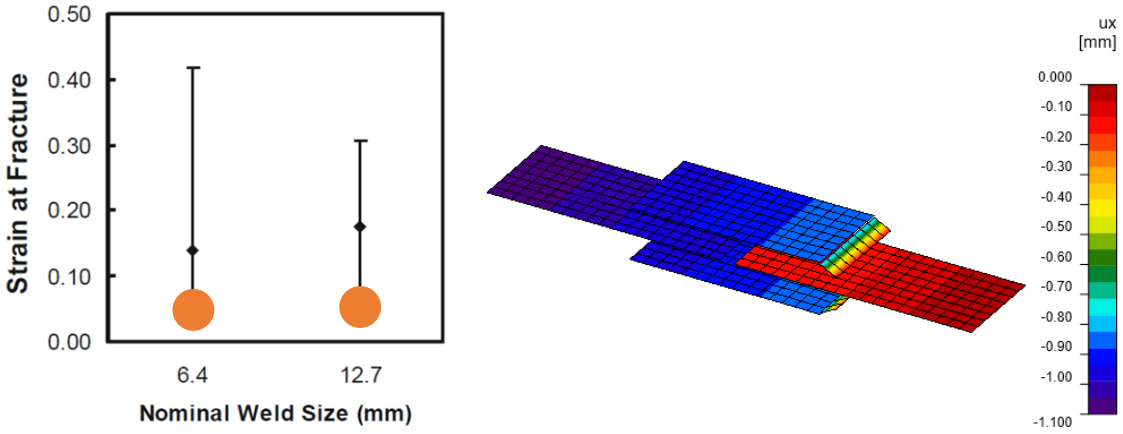

Fig. 3.4.3 Transverse welds, strain at fracture, e.g. deformation divided by weld leg size, for tests of lapped splice joints in (Ng et al., 2002) compared to the model of weld with plastic stress redistribution.

3.5 Bolts

In CBFEM, the component bolt in tension and shear is modeled by a dependent nonlinear spring. The deformation stiffness of the shell element modeling the plates distributes the forces between the bolts and simulates the adequate bearing of the plate.

3.5.1 Tension

The spring of a bolt in tension is described by its initial deformation stiffness, design resistance, initialization of yielding, and deformation capacity. The initial stiffness is derived analytically as

$$k = \frac{EA_\mathrm{s}}{L_\mathrm{b}} \tag{3.5.1}$$

where E is Young's modulus, A_s the tensile stress area of a bolt, and L_b the bolt elongation length.

The model corresponds well to experimental data, see (Gödrich et al. 2014). For the initialization of yielding and the deformation capacity, it is assumed that the plastic deformation occurs in the threaded part of the bolt shank only. The load-deformation diagram of the bolt is shown in Fig. 3.5.1 and is derived for

$$F_\mathrm{t,el} = \frac{F_\mathrm{t,Rd}}{c_1 \cdot c_2 - c_1 + 1} \tag{3.5.2}$$

$$k_\mathrm{t} = c_1 \cdot k;\ c_1 = \frac{R_\mathrm{m} - R_\mathrm{e}}{\frac{1}{4} \cdot AE - R_\mathrm{e}} \tag{3.5.3}$$

$$u_\mathrm{el} = \frac{F_\mathrm{t,el}}{k} \tag{3.5.4}$$

$$u_\mathrm{t,Rd} = c_2 \cdot u_\mathrm{el};\ c_2 = \frac{A \cdot E}{4 \cdot R_\mathrm{e}} \tag{3.5.5}$$

where k is the linear stiffness of bolt, k_t the stiffness of bolt at the plastic branch, $F_\mathrm{t,el}$ the limit force for linear behavior, A the percentage elongation after a fracture of a bolt, $F_\mathrm{t,Rd}$ the limit bolt resistance, and $u_\mathrm{t,Rd}$ the limit deformation of a bolt. The design values according to ISO 898:2009 are summarised in Tab. 3.5.1.

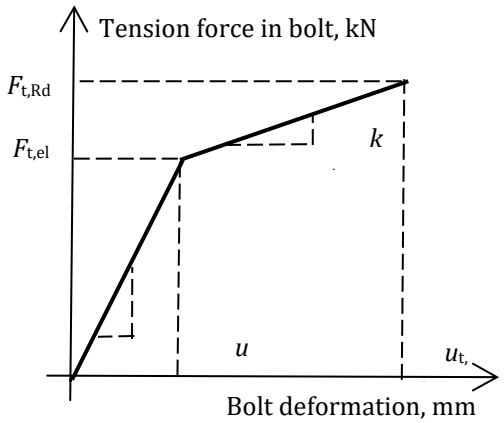

Fig. 3.5.1 Load–deformation diagram of a bolt in tension

Table 3.5.1 Bolt parameters in tension, based on ISO 898:2009

Grade	R_m	$R_e = R_{p02}$	A	E	c_1	c_2
	[MPa]	[MPa]	[%]	[MPa]	[-]	[-]
4.8	420	340	14	2,1E+05	0,011	21,6
5.6	500	300	20	2,1E+05	0,020	35,0
5.8	520	420	10	2,1E+05	0,021	12,5
6.8	600	480	8	2,1E+05	0,032	8,8
8.8	830	660	12	2,1E+05	0,030	9,5
10.9	1040	940	9	2,1E+05	0,026	5,0

3.5.2 Shear

The initial stiffness and the design resistance of a bolt in shear are modeled in CBFEM according to Cl. 3.6 and 6.3.2 in EN 1993-1-8:2006. The spring representing the bolt in shear has bi-linear force deformation behavior. Deformation capacity is considered according to (Wald et al. 2002) as

$$\delta_{pl} = 3\ \delta_{el} \tag{3.5.6}$$

Initialization of yielding is expected, see Fig. 3.5.2, at

$$F_{v,el} = 2/3\ F_{v,Rd} \tag{3.5.7}$$

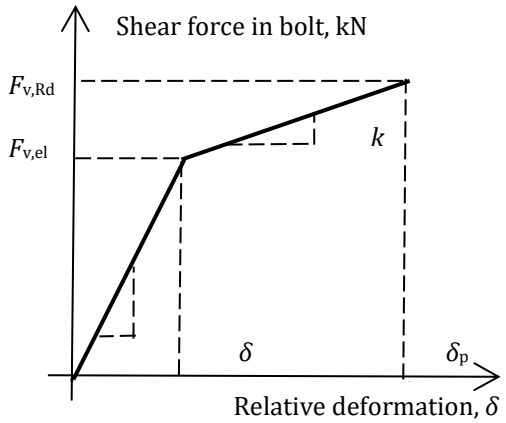

Fig. 3.5.2 Force–deformation diagram of the bolt in shear

3.6 Interaction of shear and tension in a bolt

A combination of shear and tension in a bolt is expressed in EN 1993-1-8:2005, Tab. 3.4 by a bilinear relation and checked as

$$\max\left\{\frac{F_{t,\mathrm{Ed}}}{F_{\mathrm{t,Rd}}}, \frac{F_{\mathrm{v,Ed}}}{F_{\mathrm{v,Rd}}} + \frac{F_{\mathrm{t,Ed}}}{1{,}4\,F_{\mathrm{t,Rd}}}\right\} \leq 1{,}0 \qquad (3.6.1)$$

where $F_{\mathrm{v,Ed}}$ is the acting bolt shear force, $F_{\mathrm{t,Ed}}$ is the acting bolt tensile force, $F_{\mathrm{v.Rd}}$ is the bolt shear resistance, and $F_{\mathrm{t.Rd}}$ is the bolt tensile resistance. A condition limiting the bolt resistance is shown in Fig. 3.6.1.

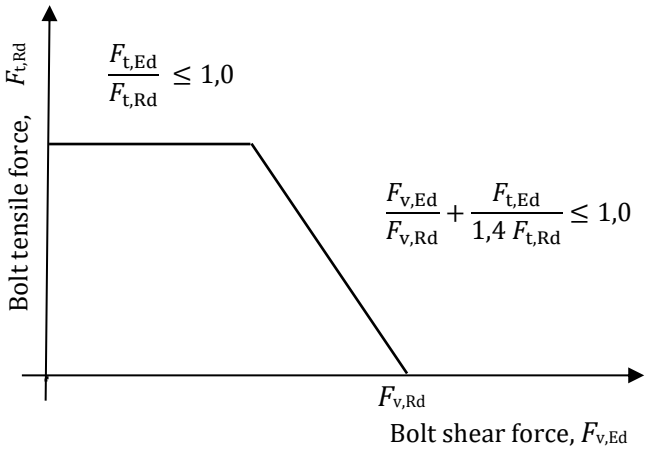

Fig. 3.6.1 Limit condition of interaction of shear and tension in a bolt

The tensile and shear behaviors of the bolt in a numerical model are represented by a bilinear spring model, see previous Chapter 3.5. The nonlinear spring has special behavior in the interaction of the shear and tension. The shear and tension forces are presented as nonlinear functions of shear and tension deformations composed from ruled surfaces; see Fig. 3.6.2 and 3.6.3, where δ_{s} is the bolt shear deformation, δ_{t} is the bolt deformation in tension, δ_{el} is the elastic limit of the bolt deformation, δ_{Rd} is the bolt deformation at its resistance, F_{el} is the bolt force at the elastic limit of deformation, and F_{Rd} is the bolt resistance. The functions respect the limit condition of interaction, which is shown above. It is clear that the bolt can be in three states: a linear behavior, a plastic state in tension, and a plastic state in interaction of the tension and the shear.

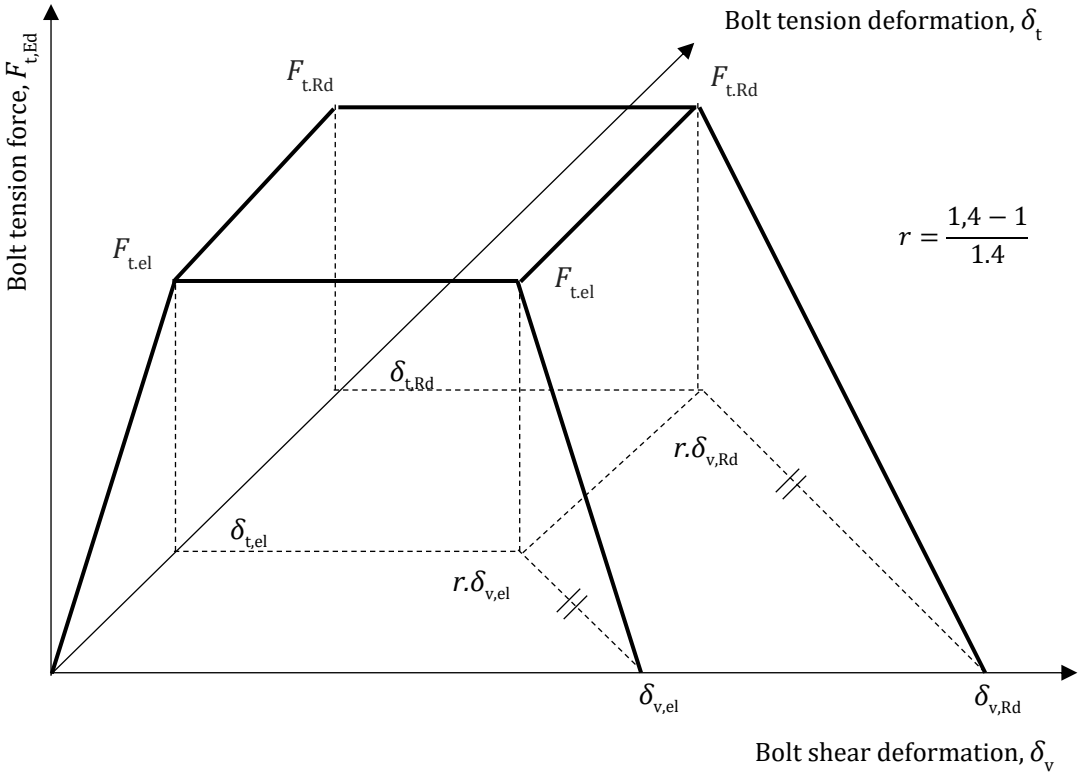

Fig. 3.6.2 Bolt tension force as a function of deformation in shear and tension

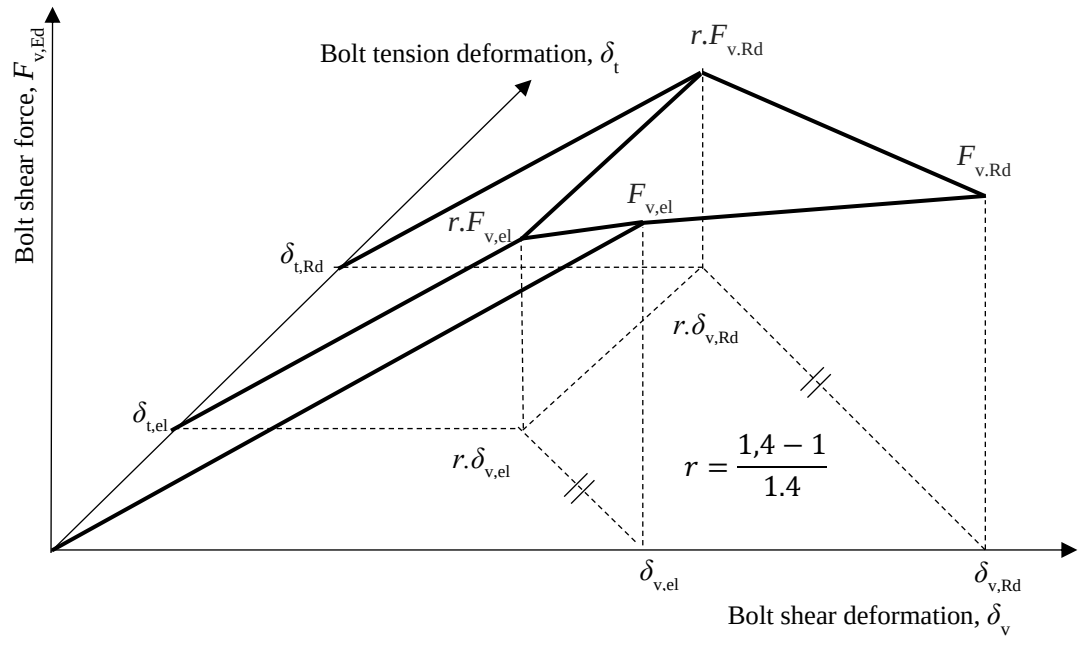

Fig. 3.6.3 Bolt shear force as a function of deformation in shear and tension

3.7 Preloaded bolts

In connection with preloaded bolts, the shear force is transferred by friction between both surfaces. Compared to regular bolts, the friction is controlled by the preloaded force. The final resistance is assured by bolt shearing and bolt and plate bearing after the slippage of a bolt in a hole. In EN 1993-1-8:2005, the resistances of preloaded bolts classes 8.8 and 10.9 are summarized in Chapter 3.9. The bolts are expected to be preloaded to 70 % of their strength, f_{ub}, see eq. 3.7.1 (eq. 3.6 in EN 1993-1-8:2005) and the bolt preloading force is

$$F_{p,C} = 0{,}7 f_{ub} A_s \tag{3.7.1}$$

where f_{ub} is the bolt strength and A_s is the bolt area effective in tension. It is expected that the bolt deforms by 80 % and the plate by 20 %. If the external tensile force $F_{t.Ed}$ is applied to joint in the direction of a bolt, the slip resistance will be reduced

$$F_{s,Rd} = k_s \mu \frac{F_{p,C} - 0{,}8F_{t,Ed}}{\gamma_{M3}} \tag{3.7.2}$$

where k_s is the bolt hole size factor and μ the slip factor.

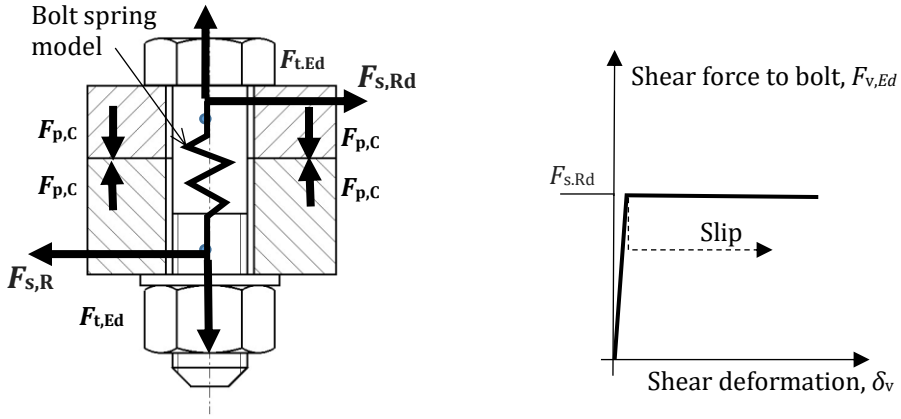

Fig. 3.7.1 Shear characteristic of the preloaded bolt

In numerical design model, the component preloaded bolt is simulated either as nonlinear spring using the preloading force and deformation or by restrains between surfaces, which are representing the friction, with a spring, which is including a preloading force in a bolt. For the bolt component represented by the preloading force and its slip deformation, the model is similar to a conventional, snug-tight bolt model. The shear characteristic is shown in Fig. 3.7.1. The initial linear shear stiffness is determined from the stiffness of the cylinder under the head of the bolt, and it is practically rigid. The shear force limit includes the external tensile load to the bolt in accordance with EN 1993-1-8:2005. The advantage of this simplified model is its computational stability and low demands of the FE model and the consistency of results with Cl. 3.6.2.2 in EN 1993-1-8:2005. The model does not respect the actual distribution of contact pressures between the plates and the history of preloading.

3.8 Anchor bolt

3.8.1 Description

The anchor bolt is modeled with similar procedures as structural bolts. The bolt is fixed on one side to the concrete block. Its length L_b is taken according to EN 1993-1-8:2005 as a sum of washer thickness t_w, base plate thickness t_{bp}, grout thickness t_g, and free length embedded in concrete, which is expected as $8d$, where d is bolt diameter. The stiffness in tension is calculated as $k = E\,A_s/L_b$. The load-deformation diagram of the anchor bolt is shown in Fig. 3.8.1. The used design values according to ISO 898:2009 are summarised in Tab. 3.5.1 and in eq. (3.5.1) to (3.5.4).

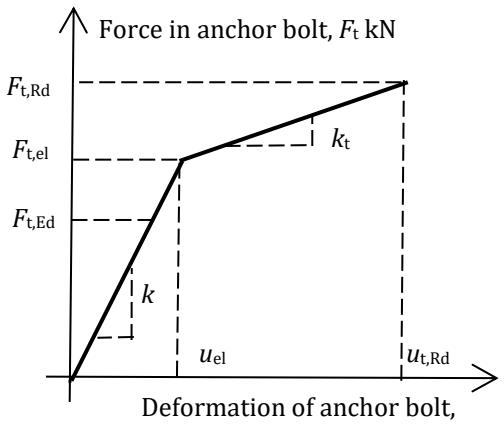

Fig. 3.8.1 Load–deformation diagram of the anchor bolt

The stiffness of the anchor bolt in shear is taken as the stiffness of the structural bolt in shear. The anchor bolt resistance is evaluated according to EN 1992-4:2018. Steel failure mode is determined according to Cl. 6.2.6.12 in EN 1993-1-8:2005.

3.8.2 Anchor bolts with stand-off

Anchors with stand-off can be checked as a construction stage before the column base is grouted or as a permanent state. Anchor with stand-off is designed as a bar element loaded by shear force, bending moment, and compressive or tensile force. The anchor is fixed on both sides; one side is $0.5\times d$ below the concrete level, the other side is in the middle of the thickness of the plate. The buckling length is conservatively assumed as twice the length of the bar element. Plastic section modulus is used. The forces in anchor with stand-off are determined using finite element analysis. Bending moment is dependent on the stiffness ratio of anchors and base plate.

3.9 Concrete block

3.9.1 Design model

In component-based finite element method (CBFEM), it is convenient to simplify the concrete block as 2D contact elements. The connection between the concrete and the base plate resists in compression only. Compression is transferred via Winkler-Pasternak subsoil model, which represents deformations of the concrete block. Tension force between the base plate and concrete block is carried by anchor bolts. Shear force is transferred by friction between a base plate and a concrete block, by shear lug, or by bending of anchor bolts. The resistance of bolts in shear is assessed analytically. Friction is modeled as a full single-point constraint in the plane of the base plate-concrete contact. At the shear lug model, the shear load is assumed to act in the mid-plane of the base plate, and it is resisted by concrete bearing stress at the whole area of the shear lug embedded in concrete. The bearing strength is based on a uniform bearing stress acting over the area of the shear lug. The area of the shear lug in grout layer is assumed as ineffective. There is a lever arm between the point of shear load application (base plate mid-plane) and the center of resistance (mid-depth of the shear lug embedded in concrete). This causes additional bending moment that needs to be resisted by the bearing resistance of concrete and tension in anchors.

3.9.2 Resistance

The resistance of concrete in 3D compression is determined based on EN 1993-1-8:2005 by calculating the design bearing strength of concrete in the joint f_{jd} under the effective area A_{eff} of the base plate. The design bearing strength of the joint f_{jd} is evaluated according to Cl. 6.2.5 in EN 1993-1-8:2005 and Cl. 6.7 in EN 1992-1-1:2005. The grout quality and thickness is introduced by the joint coefficient β_{jd}. For grout quality equal or better than the quality of the concrete block is expected β_{jd} = 1,0. The effective area A_{CM} under the base plate is estimated to be of the shape of the column cross-section increased by additional bearing width c

$$c = t\sqrt{\frac{f_y}{3\,f_j\,\gamma_{M0}}} \qquad (3.9.1)$$

where t is the thickness of the base plate, f_y is the base plate yield strength, γ_c is the partial safety factor for concrete, and γ_{M0} is the partial safety factor for steel.

The effective area is calculated by iteration until the difference between additional bearing widths of a current and a previous iteration $|c_i - c_{i-1}|$ is less than 1 mm.

The area where the concrete is in compression is taken from the results of FEA. This area in compression A_{FEM} allows determining the position of a neutral axis. The intersection of the area in compression A_{FEM} and the effective area A_{CM} creates the effective area in compression A_{eff}, which allows assessing the resistance for a generally loaded column base of any column shape with any

stiffeners. The average stress σ on the effective area A_{eff} is determined as the compression force divided by the effective area. Check of the component is in stresses $\sigma \leq f_{jd}$.

This procedure of assessing the resistance of the concrete in compression is independent of the mesh of the base plate, as can be seen in Fig. 3.9.1 and 3.9.2. The geometry of the model used for comparison is described in detail in Chapter 8.1.3. Two cases are investigated: loading by pure compression 1 200 kN, see Fig. 3.9.1, and loading by a combination of compressive force 1 200 kN and bending moment 90 kNm; see Fig. 3.9.2.

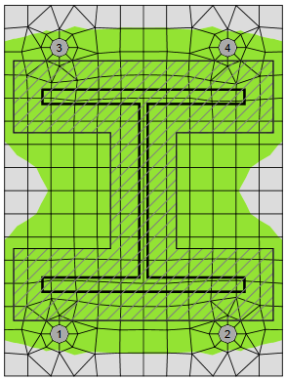

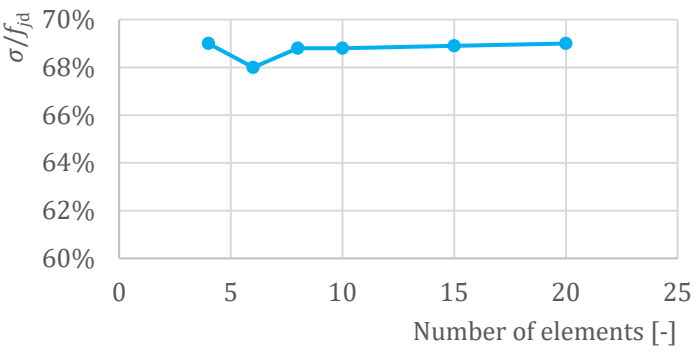

No. of elements	A_{eff} [m²]	σ [MPa]	f_{jd} [MPa]
4	0,06	18,5	26,8
6	0,06	18,2	26,8
8	0,06	18,5	26,8
10	0,06	18,4	26,8
15	0,06	18,5	26,8
20	0,06	18,5	26,8

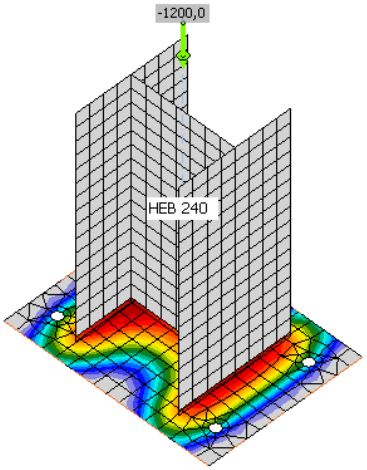

Fig. 3.9.1 Influence of number of elements on prediction
of resistance of concrete in compression in case of pure compression

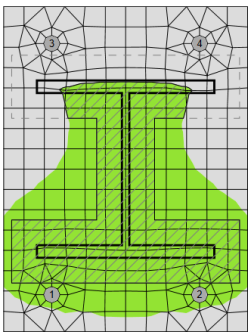

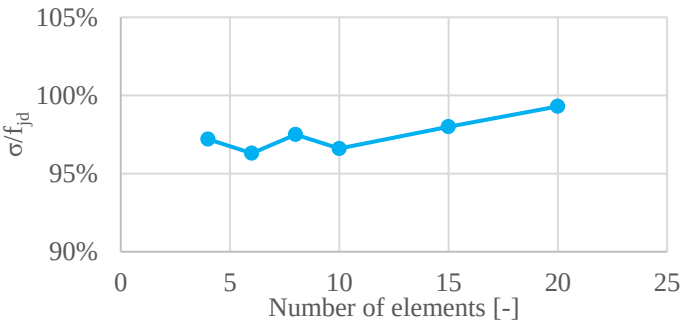

No. of elements	A_{eff} [m²]	σ [MPa]	f_{jd} [MPa]
4	0,05	26,0	26,8
6	0,04	25,8	26,8
8	0,04	26,1	26,8
10	0,05	25,9	26,8
15	0,04	26,3	26,8
20	0,04	26,6	26,8

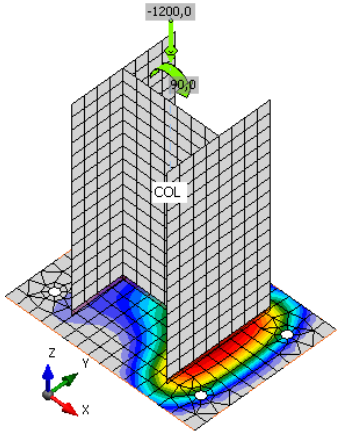

Fig. 3.9.2 Influence of number of elements on prediction
of resistance of concrete in compression in case of compression and bending

3.9.3 Deformation stiffness

The stiffness of the concrete block may be predicted for the design of column bases as an elastic hemisphere. A Winkler-Pasternak subsoil model is commonly used for a simplified calculation of foundations. The stiffness of subsoil is determined using modulus of elasticity of concrete and effective height of subsoil as

$$k = \frac{E_c}{(\alpha_1 + \upsilon)\cdot\sqrt{\frac{A_{eff}}{A_{ref}}}}\cdot\left(\frac{1}{\frac{h}{\alpha_2\cdot d}+\alpha_3}+\alpha_4\right) \qquad (3.9.2)$$

where k is stiffness in compression, E_c is modulus of elasticity, n is Poisson coefficient of concrete foundation, A_{eff} is effective area, A_{ref} is reference area, d is base plate width, h is column base height, and α_i are coefficients. The following values for coefficient were used based on the results of research-oriented finite element models with concrete modeled by solid elements:

A_{ref} = 1 m²; α_1 = 1,65; α_2 = 0,5; α_3 = 0,3; α_4 =1,0.

3.10 Local buckling of compressed plates

In research FEA models, the slender plates in compression taking into account plate geometrical imperfections, residual stresses, and large deformation during analyses may be designed according to EN 1993-1-5:2006. This should be précised according to the different plate/joint configuration. The FEA procedure naturally offers the prediction of the buckling load of the joint. The design procedure for class 4 cross-sections according to reduced stress method is described in Annex B of EN 1993-1-5:2006. It allows predicting the post-buckling resistance of the joints. Critical buckling modes are determined by materially linear and geometrically nonlinear analysis. In the first step, the minimum load amplifier for the design loads to reach the characteristic value of the resistance of the most critical point coefficient $\alpha_{ult,k}$ is obtained. Ultimate limit state is reached at 5 % plastic strain. The critical buckling factor α_{cr} is determined by linear buckling analysis and stands for the load amplifier to reach the elastic critical load under complex stress field. Examples of critical buckling mode in steel joints are shown in Fig. 3.10.1.

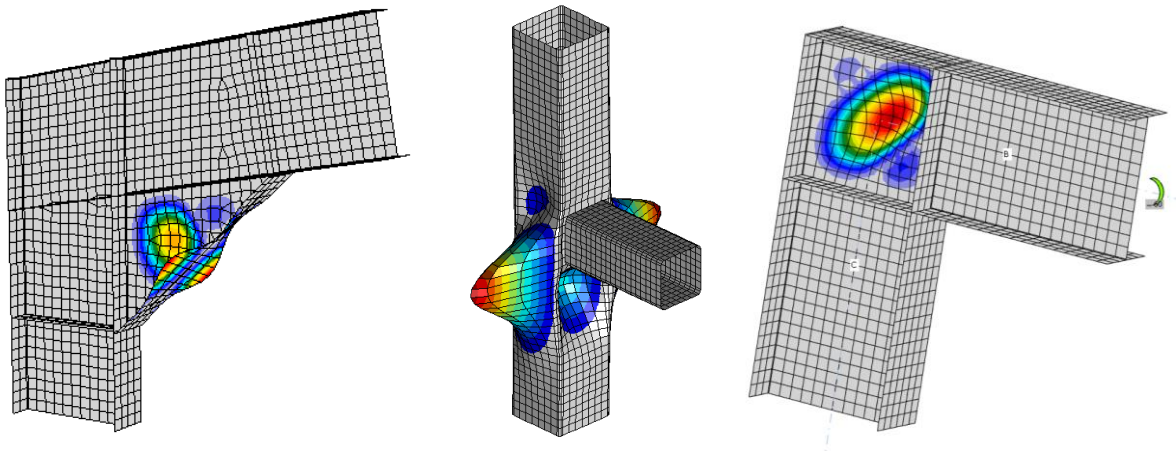

Fig. 3.10.1 Examples of first buckling mode in CBFEM models

The load amplifiers are related to the non-dimensional plate slenderness, which is determined as follows

$$\overline{\lambda} = \sqrt{\frac{\alpha_{ult}}{\alpha_{cr}}} \qquad (3.10.1)$$

Reduction buckling factor ρ is calculated according to EN 1993-1-5:2006 Annex B. Conservatively, the lowest value from longitudinal, transverse, and shear stress is taken. Fig. 3.10.2 shows the relation between plate slenderness and reduction buckling factor.

The verification of the plate is based on von Mises yield criterion and reduced stress method. Buckling resistance is assessed as

$$\frac{\alpha_{ult}\rho}{\gamma_{M1}} \geq 1 \qquad (3.10.2)$$

where γ_{M1} is partial safety factor. Based on the distribution of strains calculated in MNA and the critical buckling factor in LBA is assessed the buckling resistance without using second order calculation and applying imperfections. It is recommended to check the buckling resistance for critical buckling factor smaller than 3.0. Otherwise is the resistance governed by reaching 5 % plastic strain for plates with smaller slenderness. The procedure is summarised in the diagram, see Fig. 3.10.3.

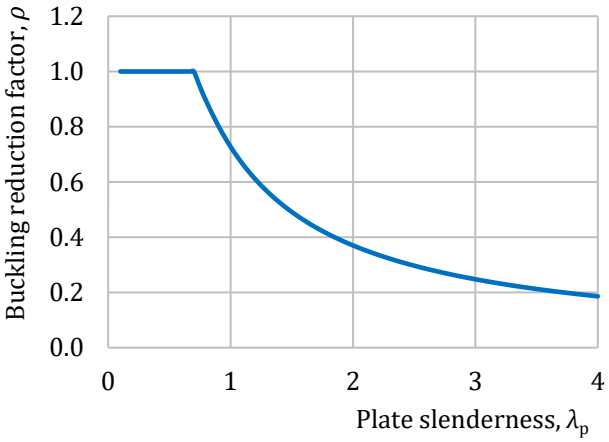

Fig. 3.10.2 Buckling reduction factor ρ according to EN 1993-1-5:2006 Annex B

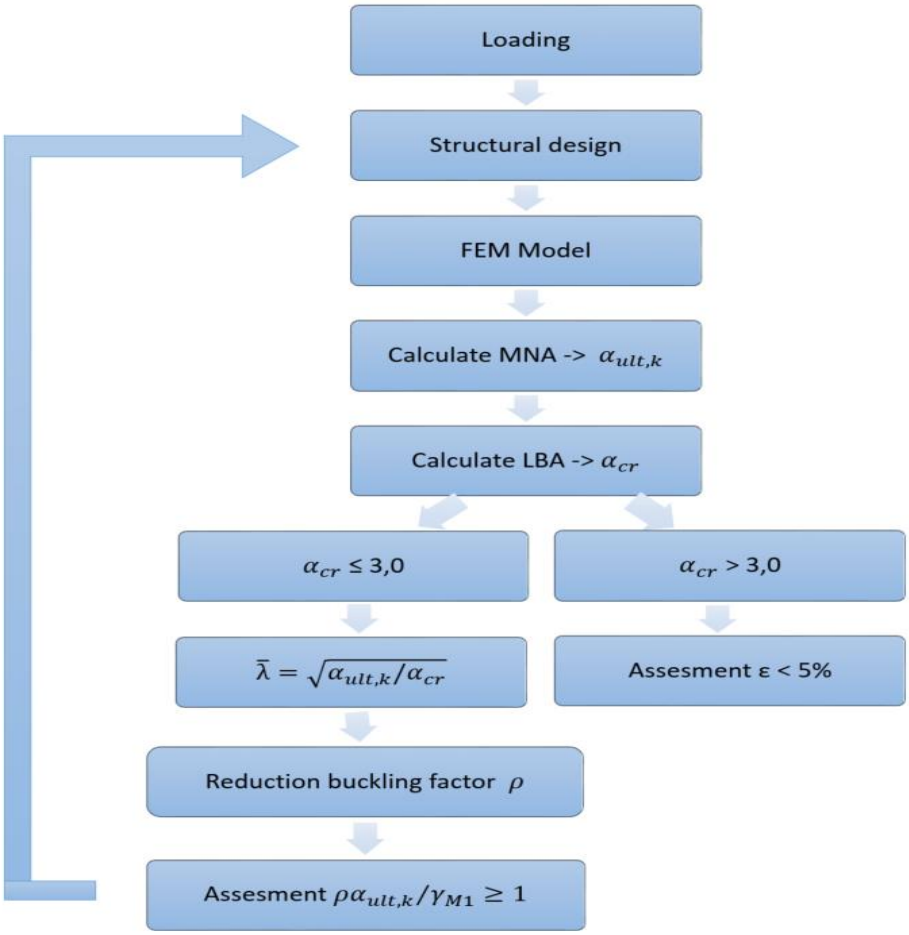

Fig. 3.10.3 The design procedure according to EN 1993-1-5:2006 Annex B

3.11 Moment-rotation relation

The joint is generally three dimensional. The moment–rotation curve for connection in a joint is evaluated for each element, which is attached to the joint. The calculation of the moment–rotation relation by the FEA model is different compared to the stress/strain analysis of a joint. The moment rotation is analyzed for connection of the connected member separately in the planes where the connections are loaded.

The modeling of the moment rotational curve may be documented on the behavior of a well-designed portal frame eaves moment bolted connection developed based on US best practice and applied in good European practice represented by British and German design books. The composition of the connection geometry of the bolted connection is demonstrated in Fig. 3.11.1. The rafter of cross-section IPE 400 column is connected to column HEA 320 by the full depth end plate of thickness 25 mm by 12 bolts M24 8.8. The haunch is 700 mm long and 300 mm high with flange dimensions 15×150 mm. The stiffeners are designed from plate thickness 20 mm. The material of all plates is steel grade S355. The results of CBFEM analyses show in Fig. 3.11.2 the development of plastic zones in connection, from first yielding under the bolt in tension, through the development of full plasticity in the column web panel in shear, till reaching the 5 % strain in column web panel. After reaching this strain, the plastic zones propagate rapidly in the column web panel in shear, and for small steps in bending moment, the rotation of the joint rises significantly, see Fig. 3.11.3.

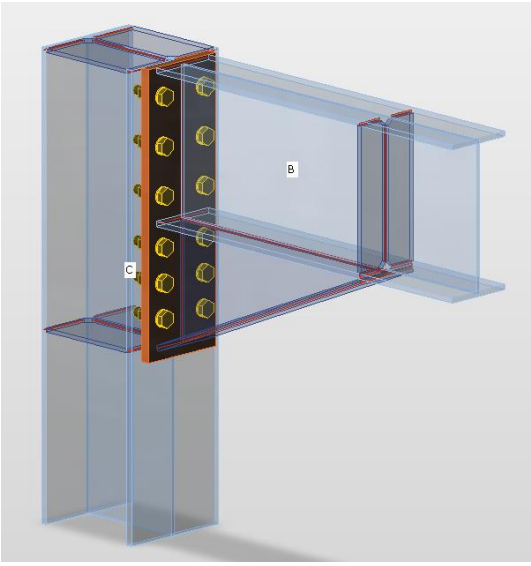

Fig. 3.11.1 Composition portal frame eaves moment bolted connection

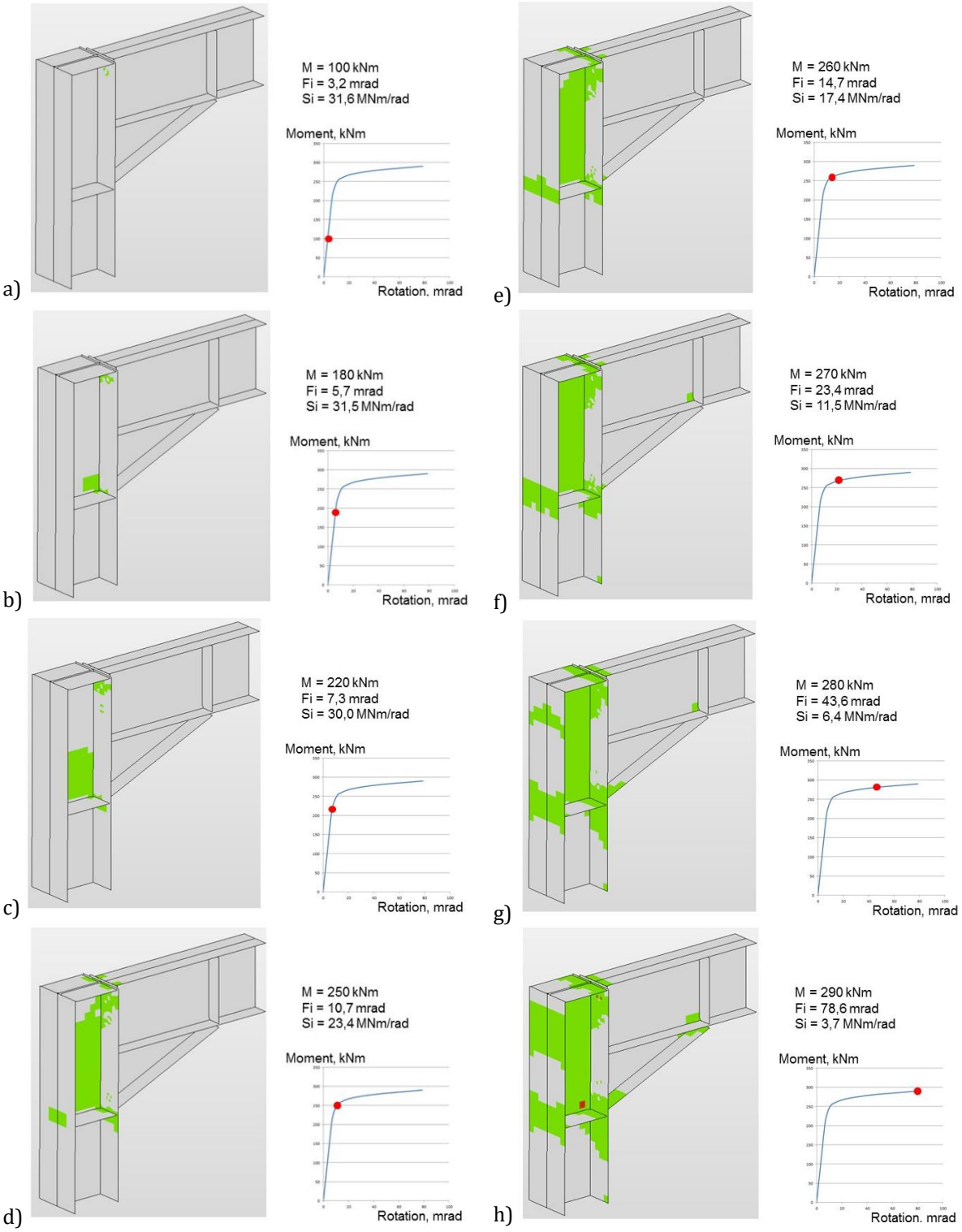

Fig. 3.11.2 Development of plastic zones in connection by CBFEM analyses, from first yielding under the tensile bolt a), through development of full plasticity in the column web panel loaded in shear e)–f), till reaching the 5 % strain in panel h)

As is commonly known in well-designed connections, the plastification starts early, see Fig. 3.11.2a. The column web panel in shear brings the deformation capacity of a connection and guides the nonlinear part of behavior; see Fig. 3.11.2e–f. Fig. 3.11.3 demonstrates the fast development of yielding in the column web panel after reaching the 5 % strain.

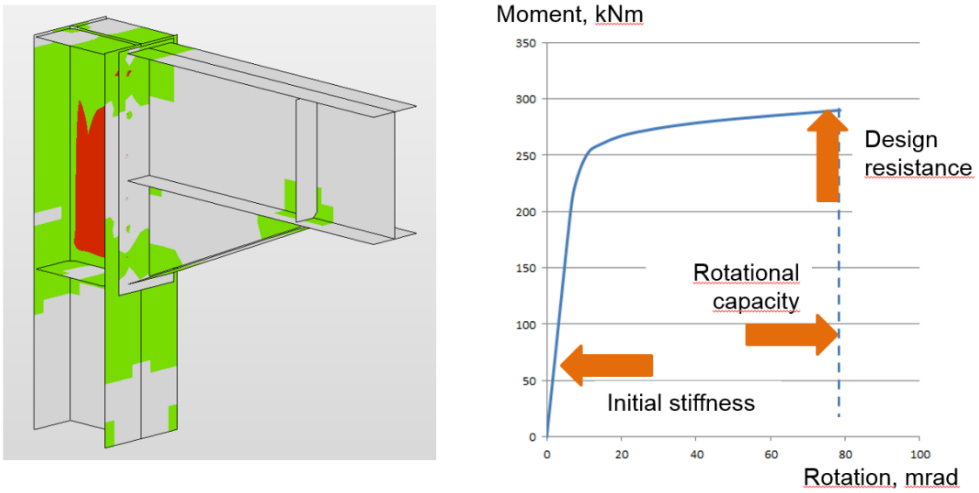

Fig. 3.11.3 After reaching the 5 % strain in the column web panel in shear, the plastic zones propagate rapidly

3.12 Bending stiffness

The bending/deformation stiffness of structural joints has only an indirect influence on the resistance of the structure. Generally, it is expected that its underestimation is a safe assumption. The prediction models by component method (CM) show mostly higher values compared to experiments. It is given by stiffness of experimental set-ups but also by an assumption of modulus of elasticity of streel as 210 000 MPa. In reality, the experimental value is 206 000 MPa as a maximum. The calculation by the FEA model is different compared to the stress/strain analysis of a joint. The joint is three dimensional. The bending/deformation stiffness for connection of a member is influenced by the shear deformation in the joint and the connection deformation of the particular member in the selected plane of the member. For joints connecting more members, the bending stiffnesses of the connections are analyzed separately in the plains, where they are loaded.

For the evaluation of the bending stiffness of a particular connection, it is assumed that members are supported at the ends, and only the analyzed member *i* has a free end, see Fig. 3.12.1. The analyzed member *i* is loaded by a bending moment in plane *yz* coming from the global analyses. To learn the secant rotational stiffness $S_{j,i,yz}$ for rotation $\phi_{i,yz}$ the bending moment $M_{j,Ed,i,yz}$ is applied in a selected plane *yz*. The secant rotational stiffness $S_{j,s,i,yz}$ is derived from the formula:

$$S_{j,s,i,yz} = M_{j,Ed,i,yz} / \phi_{i,yz} \qquad (3.12.1)$$

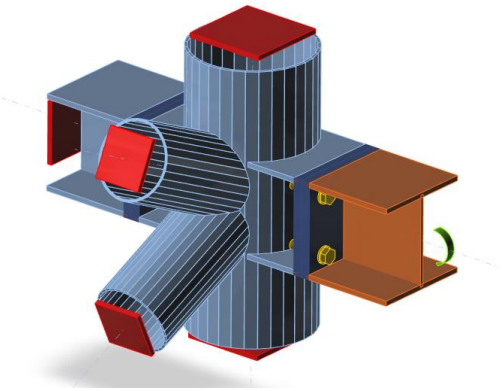

3.12.1 FEA model for analysis of stiffness of selected connected member

The total rotation $\phi_{j,i,yz}$ of the end section of analyzed member *i* in plane *yz* is derived on a model with one free/observed member. All the other members are fixed. The calculated value is influenced by the deformation of all members in the joint. The effects of member deformation are removed by analyzing the substitute model of the joint, which is composed of members with appropriate cross-sections, as shown in Fig. 3.12.2. By loading this substitute model by bending moment $M_{i,yz}$ the rotation $\phi_{j,ei,yz}$ is obtained, which represents the stiffness of the particular

connected member only. In the substitute model, the node is expected to be rigid. The rotation caused only by the construction of the connection is derived as:

$$\phi_{j,i,yz} = \phi_{j,ti,yz} - \phi_{j,ei,yz} \quad (3.12.2)$$

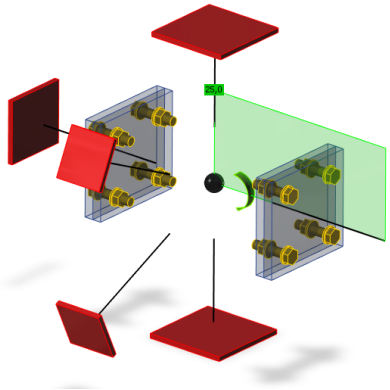

Fig. 3.12.2 The substitute 1D model to eliminate the bending flexibility if the connected elements

The secant stiffness of connection $\phi_{j,i,yz}$ is derived during its loading. The initial stiffness $\phi_{j,ini}$ is defined as elastic stiffness and is expected to be linear till 2/3 $M_{j,Rd}$, see Cl. 6.3.1 in EN 1993-1-8:2005. The calculation of the initial bending stiffness by the FEA model is taken as a secant stiffness loaded till 2/3 $M_{j,Rd}$ from the acting bending moment till 2/3 $M_{2/3Rd,i,yz}$ and corresponding rotation in connection $\phi_{2/3Rd,i,yz}$ as:

$$S_{j,ini,i,zy} \cong S_{j,s,2/3Rd,i,zy} = M_{2/3Rd,i,yz} \,/\, \phi_{2/3Rd,i,yz} \quad (3.12.3)$$

For the connection presented in Fig. 3.12.1, the values of the bending resistance $M_{j,Rd,i,yz}$ and initial stiffness $\phi_{j.ini,i,yz}$ are summarized in Fig. 3.12.3.

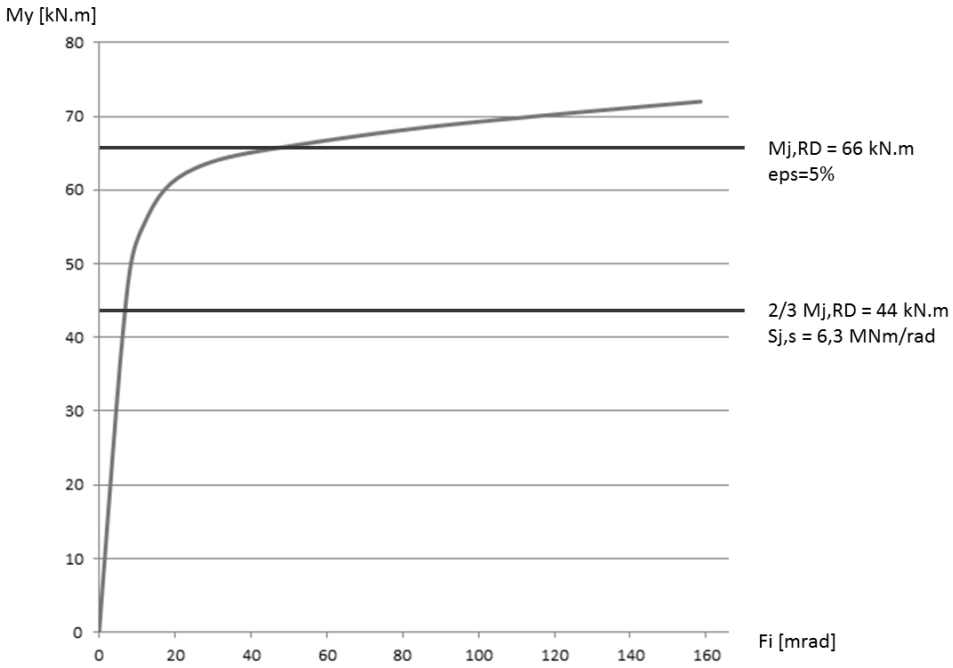

Fig. 3.12.3 Moment/rotation diagram of connection in joint for one connected member

The bending resistance $M_{j,Rd,i,yz}$ of connection is in CBFEM evaluated by strain 5 % in plates/sections or resistance of connectors, e.g. bolts, welds. Fig. 3.12.4 shows the strain in the joint exposed to moments in the plane of the strong axis of the connected open I section beam in Fig. 3.12.1 from M_y = 25 kNm to 72 kNm. The maximal reached strain ε_{max} ranges from 0,2 % till 22,7 %.

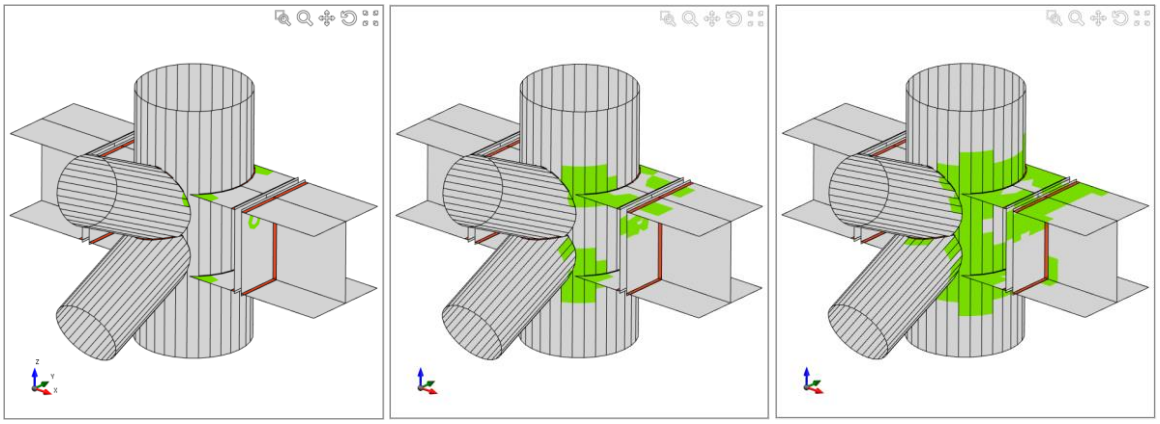

M_y = 25 kNm with ε_{max} = 0,2 % | M_y =40 kNm with ε_{max} = 0,4 % | M_y =55 kNm with ε_{max} = 0,7 %

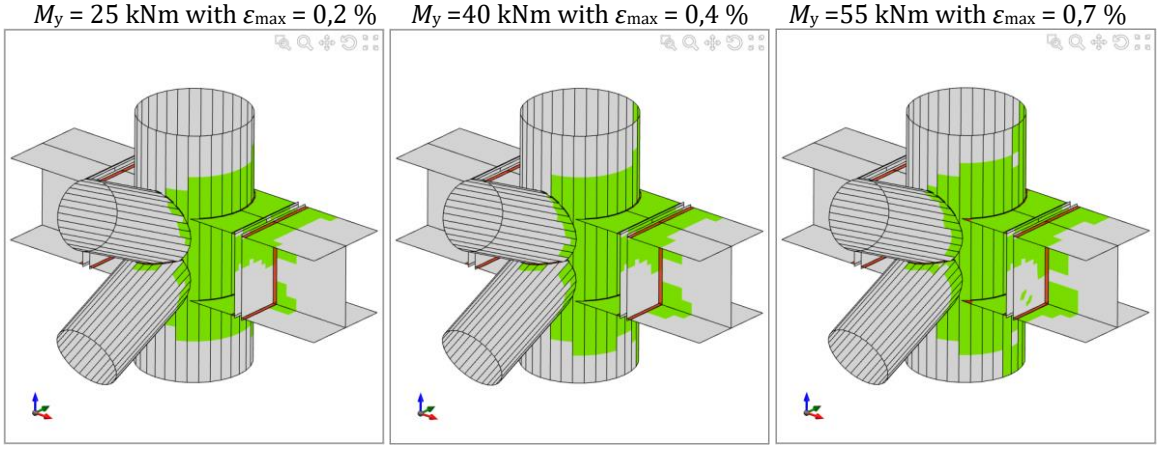

M_y =60 kNm with ε_{max} = 1,3 % | M_y = 63 kNm with ε_{max} = 2,5 % | M_y =65 kNm with ε_{max} = 4,6 %

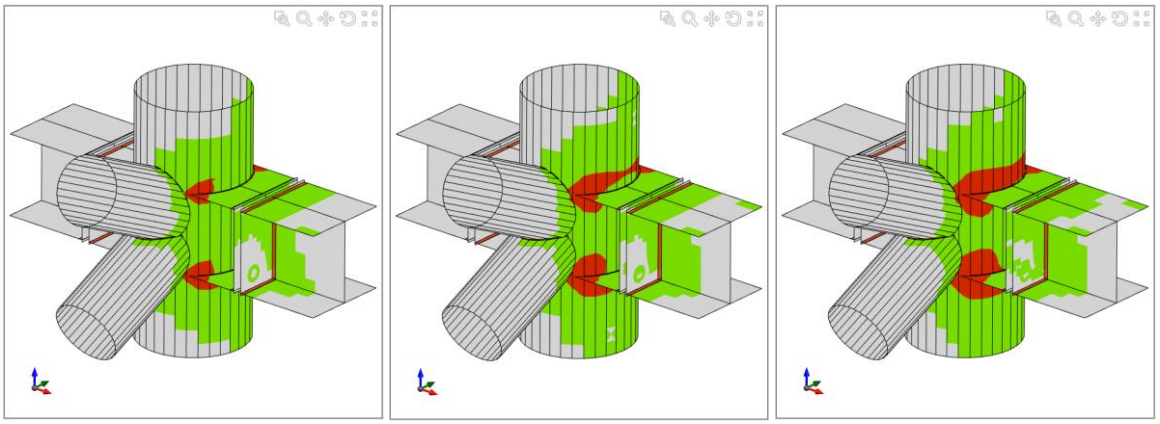

M_y =68 kNm with ε_{max} = 10,8 % | M_y =70 kNm with ε_{max} = 16,4 % | M_y =72 kNm with ε_{max} = 22,7 %

Fig. 3.12.4 The maximal strains ε_{max} in joint during its loading by bending moment M_y in the plane of the strong axis of the connected open I section beam

3.13 Deformation capacity

The deformation capacity/ductility δ_{Cd} belongs, together with resistance and stiffness, to the three basic parameters describing the behavior of connections. In moment resistant connections, the ductility is achieved by a sufficient rotation capacity φ_{Cd}. The deformation/rotation capacity is calculated for each connection in the joint separately. The prediction of deformation capacity δ_{Cd} of connections is currently studied by component method (CM) but is not offered as a standardized procedure. Compared to well-accepted methods for determination of the initial stiffness and resistance of many types of structural joints, there are no generally accepted standardized procedures for the determination of the rotation capacity. The deemed to satisfy criteria are selected to help the engineers in Cl 6.4.2 of EN 1993-1-8:2005.

A beam-to-column joint in which the design moment resistance of the joint $M_{j,Rd}$ is governed by the design resistance of the column web panel in shear, may be assumed to have adequate rotation capacity for global plastic analysis, provided that:

$$d/t_w \leq 69\,\varepsilon \qquad (3.13.1)$$

where d the column web panel width, t_w is the web thickness, and $\varepsilon \leq \sqrt{235/f_y}$ is the steel yield strength ratio.

In Cl 6.4.2(2), the plastic distribution between the bolt rows for joints with a bolted end plate connection is limited provided that the design moment resistance of the joint is governed by the design resistance of the column flange or the beam end plate in bending or the thickness t of either the column flange or the beam end plate or tension flange cleat satisfies:

$$t \leq 0{,}36\, d \sqrt{f_{ub}/f_y} \qquad (3.13.2)$$

where d and $f_{u.b}$ are the diameter and ultimate strength of a bolt and f_y is the yield strength of the relevant plate.

The rotation capacity φ_{Cd} of a welded beam-to-column connection may be assumed to be not less than the value given by the following expression provided that its column web is stiffened in compression but unstiffened in tension, and its design moment resistance is not governed by the design shear resistance of the column web panel, see 6.4.2(1):

$$\varphi_{Cd} = 0{,}025\, h_c / h_b \ldots \qquad (3.13.3)$$

where h_b is the depth of the beam and h_c is the depth of the column. An unstiffened welded beam-to-column joint designed in conformity with the provisions of this section may be assumed to have a rotation capacity φ_{Cd} of at least 0,015 radians.

The estimation of the rotation capacity is important for connections exposed to earthquake; see (Gioncu and Mazzolani, 2002) and (Grecea 2004), and extreme loading; see (Sherbourne AN, Bahaari, 1994 and 1996). The deformation capacity of components has been studied from the end

of the last century (Foley and Vinnakota, 1995). Faella et al. (2000) carried out tests on T-stubs and derived the analytical expressions for the deformation capacity. Kuhlmann and Kuhnemund (2000) performed tests on the column web subjected to transverse compression at different levels of axial compression force in the column. Da Silva et al. (2002) predicted deformation capacity at different levels of axial force in the connected beam. Based on the test results combined with FE analysis, deformation capacities are established for the basic components by analytical models by Beg et al. (2004). In this work, components are represented by non-linear springs, and appropriately combined in order to determine the rotation capacity of the joint for the end plate connections, with an extended or flush end plate, and welded connections. For these connections, the most important components that may significantly contribute to the rotation capacity column were recognized as the web in compression, column web in tension, column web in shear, column flange in bending, and end plate in bending. Components related to the column web are relevant only when there are no stiffeners in the column that resist compression, tension or shear forces. The presence of a stiffener eliminates the corresponding component, and its contribution to the rotation capacity of the joint can be therefore neglected. End plates and column flanges are important only for end plate connections, where the components act as a T-stub, where also the deformation capacity of the bolts in tension is included. The questions and limits of deformation capacity of connections of high strength steel were studied by Girao et al. (2004).

3.14 Joint model in global analyses

The recommendation about the joint modeling is summarized in EN 1993-1-8:2005 in Ch. 5. Ch. 5.1 helps to select a joint model for a global analysis according to its bending stiffness as nominally pinned, rigid or semi-rigid. Cl. 5.1.5 covers a global analysis of lattice girders from hollow sections. The distribution of axial forces in a lattice girder may be determined on the assumption that the members are connected by pinned joints. The eccentricity of members is discussed. Ch. 5.3 covers the modeling of beam-to-column joints. The influence of the column web panel in shear is discussed. The transfer of a web panel stiffness to a central point and a simplified model are included. Questions of the application of advanced models using FEA in global analyses are summarized in the chapter below.

Joints of members are in 2D FEA used for global analyses and modeled as massless points when analyzing a steel frame or a girder structure, see Fig. 3.14.1. Equilibrium equations are assembled in joints, and after solving the whole structure, internal forces on ends of beams are determined. In fact, the joint is loaded by those forces. The resultant of the forces from all members in the joint is zero – the whole joint is in equilibrium. The real shape of the joint is not known in the structural model. For better visualization of CBFEM model, the end forces on 1D members are applied as loads on segment ends. Six components of the internal forces from the theoretical node are transferred to the outer end of segment – the values of forces are kept, but the moments are modified by the actions of the forces on corresponding arms. Inner ends of the segments are not connected.

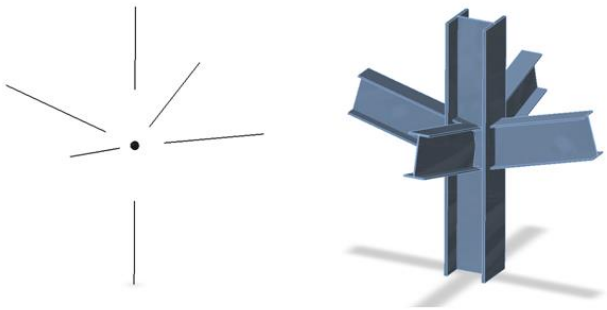

Fig. 3.14.1 Theoretical (massless) joint and the real shape of the joint without modified member ends

Each node of a 3D FEM model is in equilibrium. The equilibrium requirement is correct, but the input of data may be treated more sophisticatedly. One member of a joint is treated as bearing and the others as connected. If only a connection of the connected member is checked, it is not

necessary to keep the equilibrium during the loading. Two modes of the load input are shown in Fig. 3.14.2.

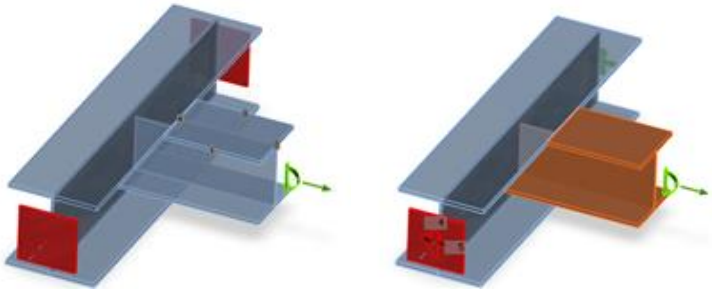

Fig. 3.14.2 Simplified and advanced model of supports in CBFEM model of the joint

End forces of the frame analysis model are transferred to the outer ends of the member segments. Eccentricities of the members caused by the joint design are respected during the transfer. The analysis model created by CBFEM corresponds to the real joint very precisely. On the other hand, the analysis of the internal forces is performed on the idealized 3D FEM model where the individual beams are modeled using centerlines, and the joints are modeled using immaterial nodes, as shown in Fig.3.14.3.

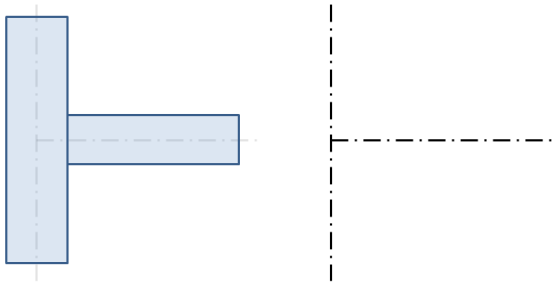

a) Real shape of joint b) Theoretical shape in 3D FEM model

Fig. 3.14.3 Joint of vertical column and horizontal beam

The internal forces are analyzed using 1D members in 3D model. Fig. 3.14.4 shows an example of courses of the internal forces.

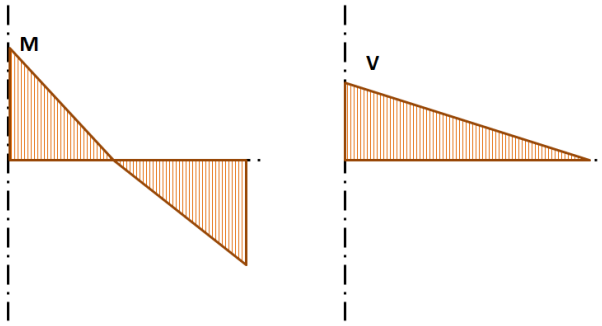

a) Bending moment *M* b) Shear force *V*

Fig. 3.14.4 Internal forces on horizontal beam; *M* and *V* are the end forces of the joint

The effects caused by a member on a joint are important to design the joint with its connections. The effects are illustrated in Fig. 3.14.5.

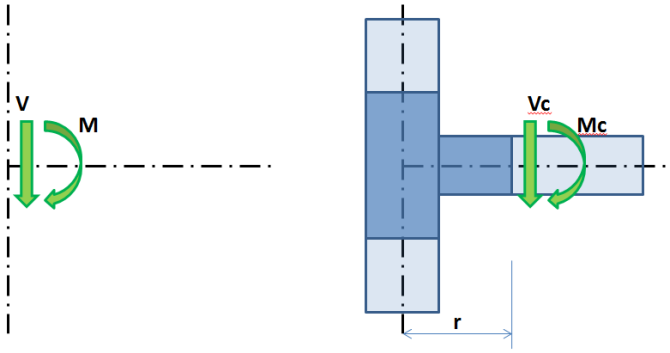

a) 1D member model b) CBFEM model – dark color

Fig. 3.14.5 Load effects of member on the joint

A bending moment M_{Ed} and a shear force V_{Ed} act in a theoretical joint. The point of the theoretical joint does not exist in CBFEM model; thus the load cannot be applied here. The model is loaded by actions M and V which are transferred to the end of a segment in a distance r

$$M_{Ed,c} = M_{Ed} - V_{Ed} \,.\, r \qquad (3.14.1)$$

$$V_{Ed.c} = V_{Ed} \qquad (3.14.2)$$

In the CBFEM model, the end section of the segment is loaded by the moment $M_{Ed,c}$ and the shear force $V_{Ed.c}$.

When designing the joint, its real position relative to the theoretical point of the joint should be determined and respected. The internal forces in the position of the real joint are often different from the internal forces in the theoretical point of the joint. Thanks to the precise CBFEM model, the design is performed on reduced forces, see moment $M_{Ed,r}$ in Fig. 3.14.6.

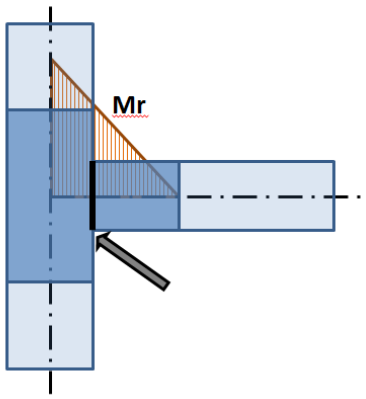

Fig. 3.14.6 Course of bending moment in CBFEM model,
the arrow points to the real position of the connection

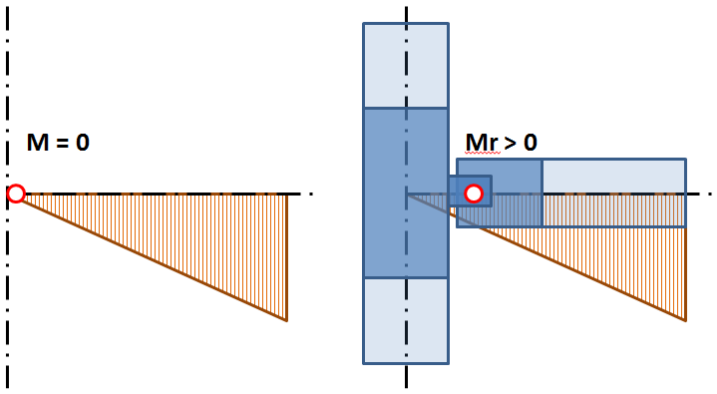

a) 1D members model b) CBFEM model

Fig. 3.14.7 Position of the hinge in theoretical 3D FEM model and in the real structure.

Fig. 3.14.7 illustrates that the position of a hinge in the theoretical 1D model differs from the real position in the structure. The theoretical model does not correspond to reality. When applying the calculated internal forces, a significant bending moment is applied to the shifted joint, and the designed joint is either overloaded or cannot be designed. The solution is simple – both models must correspond. Either the hinge in the 1D member model must be defined in the proper position, or the courses of the internal forces must be shifted to get the zero moment in the real position of the hinge.

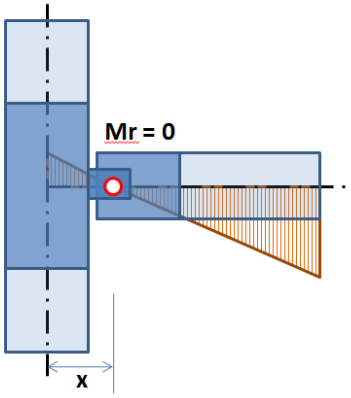

Fig. 3.14.8 Position of the hinge in theoretical 3D FEM model and in the real structure.

4 WELDED CONNECTION

4.1 Fillet weld in lap joint

4.1.1 Description

The object of this chapter is verification of component-based finite element method (CBFEM) of a fillet weld in a lap joint with component method (CM). Two plates are connected in three configurations, namely with a transverse weld, with a longitudinal weld, and a combination of transverse and longitudinal welds. The length and throat thickness of the weld are the changing parameters in the study. The study covers long welds whose resistance is reduced due to stress concentration. The joint is loaded by a normal force.

4.1.2 Analytical model

The fillet weld is the only component examined in the study. The welds are designed to be the weakest component in the joint. The weld is designed according to EN 1993-1-8:2005. The design resistance of the fillet weld is determined using the Directional method given in section 4.5.3.2 in EN 1993-1-8:2005. The available calculation methods for checking the strength of fillet welds are based upon simplifying assumption that stresses are uniformly distributed within a throat section of a fillet weld. Uniform distribution of stress is assumed in a throat section of a weld, leading to the normal stresses and shear stresses shown in Fig. 4.1.1, as follows:

$\sigma_\perp$ is the normal stress perpendicular to the throat section;

$\sigma_\parallel$ is the normal stress parallel to the axis of the weld in its cross-section;

$\tau_\perp$ is the shear stress (in the plane of the throat section) perpendicular to the axis of the weld;

$\tau_\parallel$ is the shear stress (in the plane of the throat section) parallel to the axis of the weld.

The normal stress $\sigma_\parallel$ parallel to the axis is not considered when verifying the design resistance of a weld.

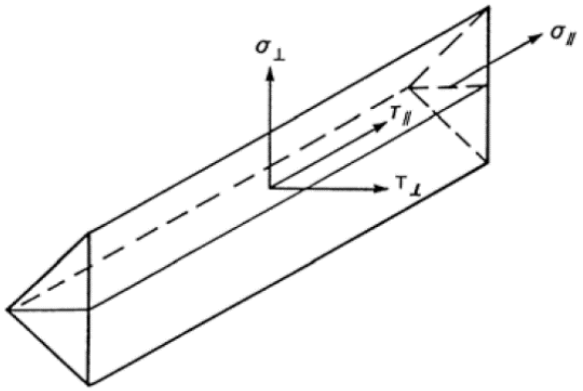

Fig. 4.1.1 Stresses in a throat section of a fillet weld

The design resistance of the fillet weld will be sufficient if the following are both satisfied:

$$\sqrt{\sigma_{\perp}^2 + 3\left(\tau_{\perp}^2 + \tau_{\parallel}^2\right)} \leq \frac{f_{\mathrm{u}}}{\beta_{\mathrm{w}}\gamma_{\mathrm{M2}}} \tag{4.1.1}$$

$$\sigma_{\perp} \leq \frac{0{,}9f_{\mathrm{u}}}{\gamma_{\mathrm{M2}}} \tag{4.1.2}$$

In lap joints longer than 150 a, the reduction factor β_{Lw1} is given by:

$$\beta_{\mathrm{Lw,1}} = 1{,}2 - \frac{0{,}2L_{\mathrm{j}}}{150a} \qquad \text{but} \qquad \beta_{\mathrm{Lw,1}} \leq 1{,}0 \tag{4.1.3}$$

Overview of the considered examples and the material properties is given in Tab. 4.1.1. The weld configurations T is for transverse, P for parallel weld, and TP for a combination of both; see the geometry in Fig. 4.1.2. The sensitivity of two parameters, weld length and effective throat thickness, was investigated.

Tab. 4.1.1 Overview of examples

Example	Material					Weld a		Plate 1		Plate 2	
	f_{y}	f_{u}	E	γ_{M0}	γ_{M2}	a_{a}	L_{a}	b_1	t_1	b_2	t_2
	[MPa]	[MPa]	[GPa]	[-]	[-]	[mm]	[mm]	[mm]	[mm]	[mm]	[mm]
T100	235	360	210	1	1,25	3	100	100	10	320	10
T110	235	360	210	1	1,25	3	110	110	10	320	10
T120	235	360	210	1	1,25	3	120	120	10	320	10
T130	235	360	210	1	1,25	3	130	130	10	320	10
T140	235	360	210	1	1,25	3	140	140	10	320	10
T150	235	360	210	1	1,25	3	150	150	10	320	10
T200	235	360	210	1	1,25	3	200	200	10	320	10
T250	235	360	210	1	1,25	3	250	250	10	320	10
T300	235	360	210	1	1,25	3	300	300	10	320	10
T3	235	360	210	1	1,25	3	120	120	20	200	20
T4	235	360	210	1	1,25	4	120	120	20	200	20
T5	235	360	210	1	1,25	5	120	120	20	200	20
T6	235	360	210	1	1,25	6	120	120	20	200	20
T7	235	360	210	1	1,25	7	120	120	20	200	20
T8	235	360	210	1	1,25	8	120	120	20	200	20
T9	235	360	210	1	1,25	9	120	120	20	200	20
T10	235	360	210	1	1,25	10	120	120	20	200	20

Example	Material					Weld b		Plate 1		Plate 2	
	f_y	f_u	E	γ_{M0}	γ_{M2}	a_a	L_a	b_1	t_1	b_2	t_2
	[MPa]	[MPa]	[GPa]	[-]	[-]	[mm]	[mm]	[mm]	[mm]	[mm]	[mm]
P150	235	360	210	1	1,25	3	150	200	20	300	20
P200	235	360	210	1	1,25	3	200	200	20	300	20
P250	235	360	210	1	1,25	3	250	200	20	300	20
P300	235	360	210	1	1,25	3	300	200	20	300	20
P350	235	360	210	1	1,25	3	350	200	20	300	20
P400	235	360	210	1	1,25	3	400	200	20	300	20
P450	235	360	210	1	1,25	3	450	200	20	300	20
P500	235	360	210	1	1,25	3	500	200	20	300	20
P550	235	360	210	1	1,25	3	550	200	20	300	20
P600	235	360	210	1	1,25	3	600	200	20	300	20
P700	235	360	210	1	1,25	3	700	200	20	300	20
P800	235	360	210	1	1,25	3	800	200	20	300	20
P3	235	360	210	1	1,25	3	140	200	20	300	20
P4	235	360	210	1	1,25	4	140	200	20	300	20
P5	235	360	210	1	1,25	5	140	200	20	300	20
P6	235	360	210	1	1,25	6	140	200	20	300	20
P7	235	360	210	1	1,25	7	140	200	20	300	20
P8	235	360	210	1	1,25	8	140	200	20	300	20
P9	235	360	210	1	1,25	9	140	200	20	300	20
P10	235	360	210	1	1,25	10	140	200	20	300	20

Example	Material					Weld a		Weld b		Plate 1		Plate 2	
	f_y	f_u	E	γ_{M0}	γ_{M2}	a_a	L_a	a_b	L_b	b_1	t_1	b_2	t_2
	[MPa]	[MPa]	[GPa]	[-]	[-]	[mm]	[mm]	[mm]	[mm]	[mm]	[mm]	[mm]	[mm]
TPa100	235	360	210	1	1,25	3	100	3	100	100	20	400	20
TPa150	235	360	210	1	1,25	3	150	3	100	150	20	400	20
TPa200	235	360	210	1	1,25	3	200	3	100	200	20	400	20
TPa250	235	360	210	1	1,25	3	250	3	100	250	20	400	20
TPa300	235	360	210	1	1,25	3	300	3	100	300	20	400	20
TPa3	235	360	210	1	1,25	3	100	4	100	100	20	200	20
TPa4	235	360	210	1	1,25	4	100	4	100	100	20	200	20
TPa5	235	360	210	1	1,25	5	100	4	100	100	20	200	20
TPa6	235	360	210	1	1,25	6	100	4	100	100	20	200	20
TPa7	235	360	210	1	1,25	7	100	4	100	100	20	200	20

Example	Material					Weld a		Weld b		Plate 1		Plate 2	
	f_y	f_u	E	γ_{M0}	γ_{M2}	a_a	L_a	a_b	L_b	b_1	t_1	b_2	t_2
	[MPa]	[MPa]	[GPa]	[-]	[-]	[mm]	[mm]	[mm]	[mm]	[mm]	[mm]	[mm]	[mm]
TPb80	235	360	210	1	1,25	3	120	3	80	120	20	300	20
TPb100	235	360	210	1	1,25	3	120	3	100	120	20	300	20
TPb120	235	360	210	1	1,25	3	120	3	120	120	20	300	20
TPb140	235	360	210	1	1,25	3	120	3	140	120	20	300	20
TPb160	235	360	210	1	1,25	3	120	3	160	120	20	300	20
TPb180	235	360	210	1	1,25	3	120	3	180	120	20	300	20
TPb200	235	360	210	1	1,25	3	120	3	200	120	20	300	20
TPb3	235	360	210	1	1,25	3	160	3	100	160	20	200	20
TPb4	235	360	210	1	1,25	3	160	4	100	160	20	200	20
TPb5	235	360	210	1	1,25	3	160	5	100	160	20	200	20
TPb6	235	360	210	1	1,25	3	160	6	100	160	20	200	20
TPb7	235	360	210	1	1,25	3	160	7	100	160	20	200	20
TPb8	235	360	210	1	1,25	3	160	8	100	160	20	200	20

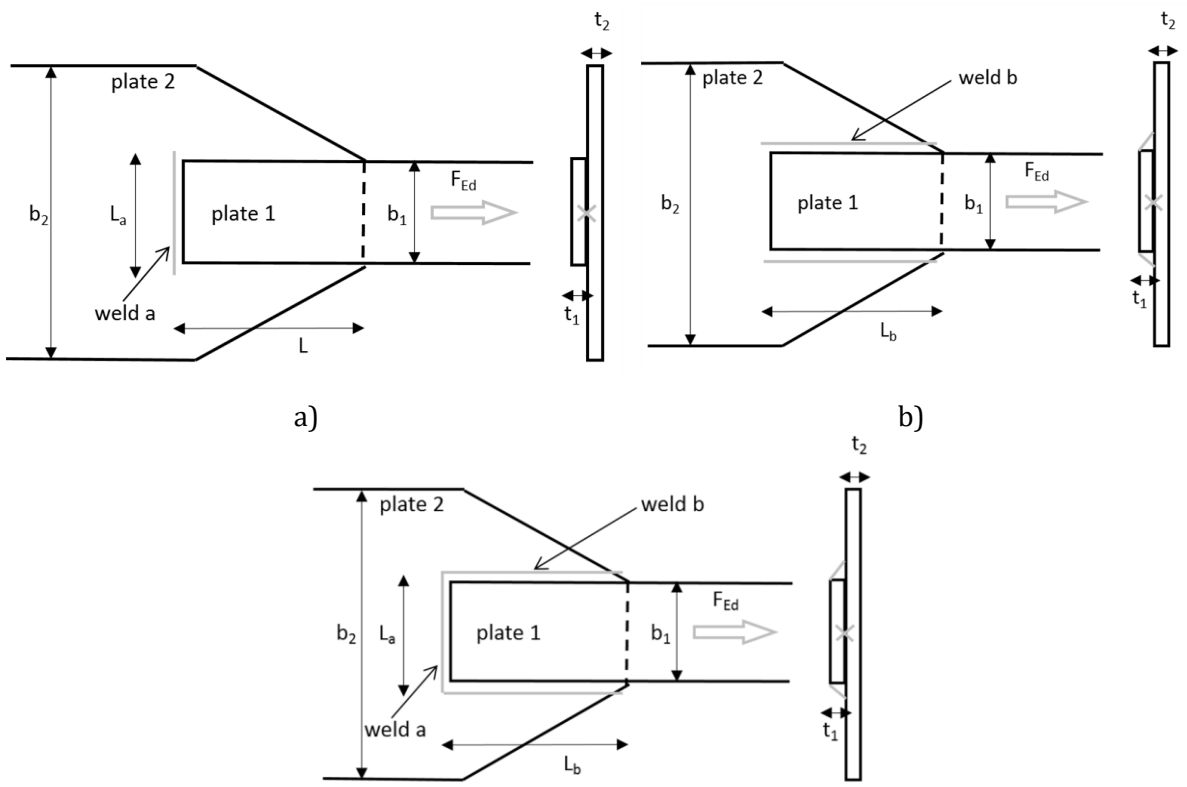

Fig, 4.1.2 Joint geometry with dimensions

a) Transverse weld b) Parallel weld c) Combination of transverse and parallel weld

4.1.3 Numerical model

The weld component in CBFEM is described in Chapter 3.4. Nonlinear elastic-plastic material is used for welds in this study. The limiting plastic strain is reached in the longer part of the weld, and stress peaks are redistributed.

4.1.4 Verification of resistance

Design weld resistance calculated by CBFEM is compared with the results of CM. The results are presented in Tab. 4.1.2. The study is performed for two parameters, length of the weld and effective throat thickness, in three weld configurations: for the transverse weld, parallel welds, and a combination of transverse and parallel welds.

Tab. 4.1.2 Comparison of CBFEM and CM

Example	Design resistance		
	CM	CBFEM	Diff.
	[kN]	[kN]	[%]
T100	76	76	0
T110	84	84	0
T120	91	91	0
T130	99	99	0
T140	106	106	0
T150	114	114	0
T200	152	152	0
T250	190	191	1
T300	229	229	0
T3	91	93	2
T4	122	124	2
T5	152	155	2
T6	183	186	2
T7	213	217	2
T8	244	247	1
T9	274	278	1
T10	305	309	1

	Example	Design resistance		
		CM	CBFEM	Diff.
		[kN]	[kN]	[%]
Long weld	P150	187	183	-2
	P200	249	244	-2
	P250	311	305	-2
	P300	374	363	-3
	P350	436	422	-3
	P400	498	480	-4
	P450	561	539	-4
	P500	609	574	-6
	P550	655	598	-10
	P600	698	631	-10
	P3	174	172	-1
	P4	232	230	-1
	P5	290	288	-1
	P6	349	344	-2
	P7	407	401	-2
	P8	465	460	-1
	P9	523	518	-1
	P10	581	574	-1

Example	Design resistance		
	CM	CBFEM	Diff.
	[kN]	[kN]	[%]
TPa100	201	200	0
TPa150	239	239	0
TPa200	277	278	0
TPa250	316	316	0
TPa300	354	355	0
TPa3	242	242	0
TPa4	267	268	0
TPa5	293	293	0
TPa6	319	317	-1
TPa7	344	336	-2

Example	Design resistance		
	CM	CBFEM	Diff.
	[kN]	[kN]	[%]
TPb80	191	190	-1
TPb100	216	215	0
TPb120	241	239	-1
TPb140	266	263	-1
TPb160	291	286	-2
TPb180	316	310	-2
TPb200	341	333	-2
TPb3	246	246	0
TPb4	288	288	0
TPb5	330	328	-1
TPb6	371	368	-1
TPb7	413	406	-2
TPb8	454	443	-3

Results of CBFEM and CM are compared, and a sensitivity study is presented. The influence of weld length and effective throat thickness on the design resistance of the transverse weld, parallel welds, and a combination of both welds is shown in Fig. 4.1.3, 4.1.4, and 4.1.5, respectively. The sensitivity study shows good agreement for all weld configurations.

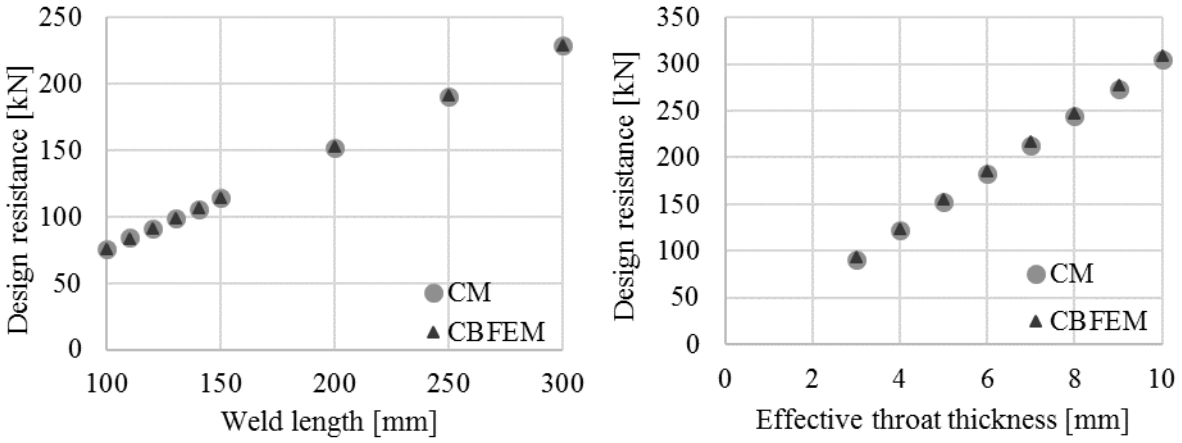

a) b)

Fig. 4.1.3 Parametric study of transverse weld a) Weld length b) Effective throat thickness

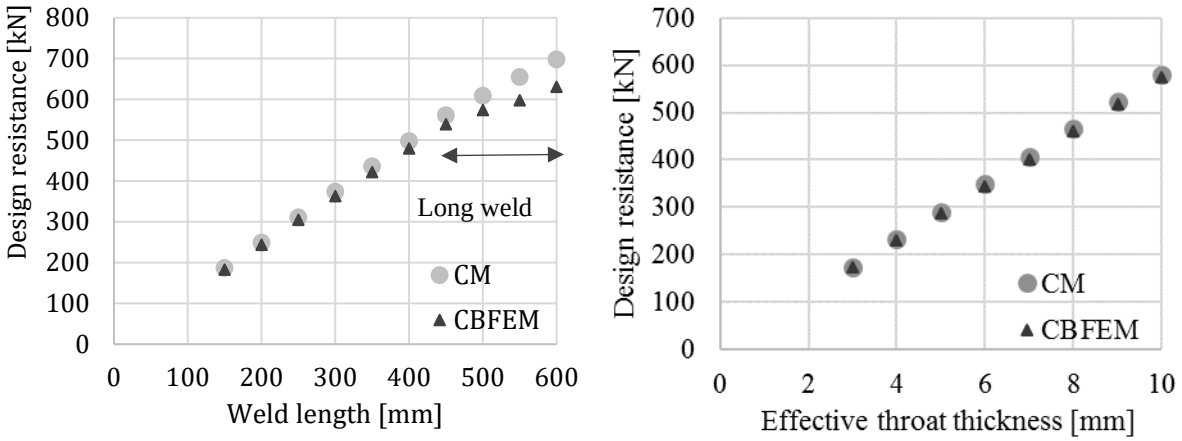

a) b)

Fig. 4.1.4 Parametric study of parallel weld a) Weld length b) Effective throat thickness

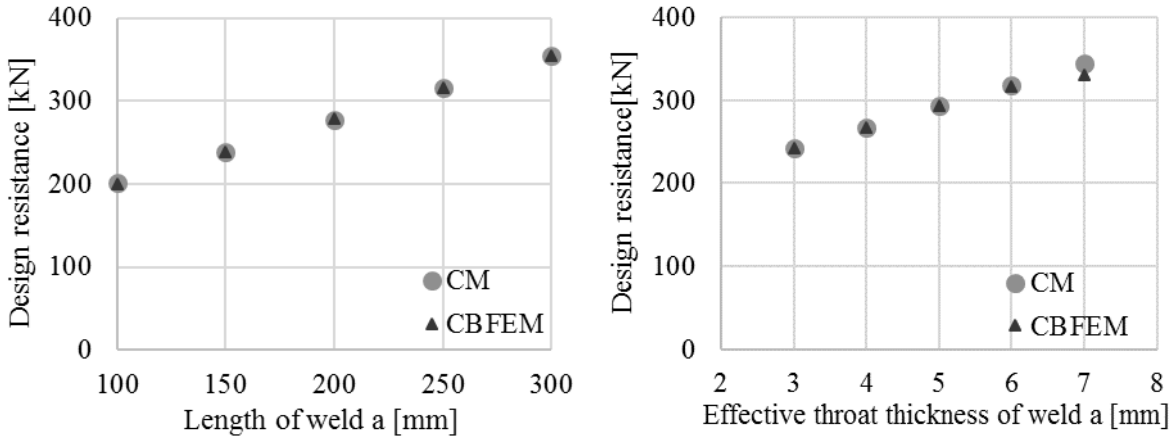

a) b)

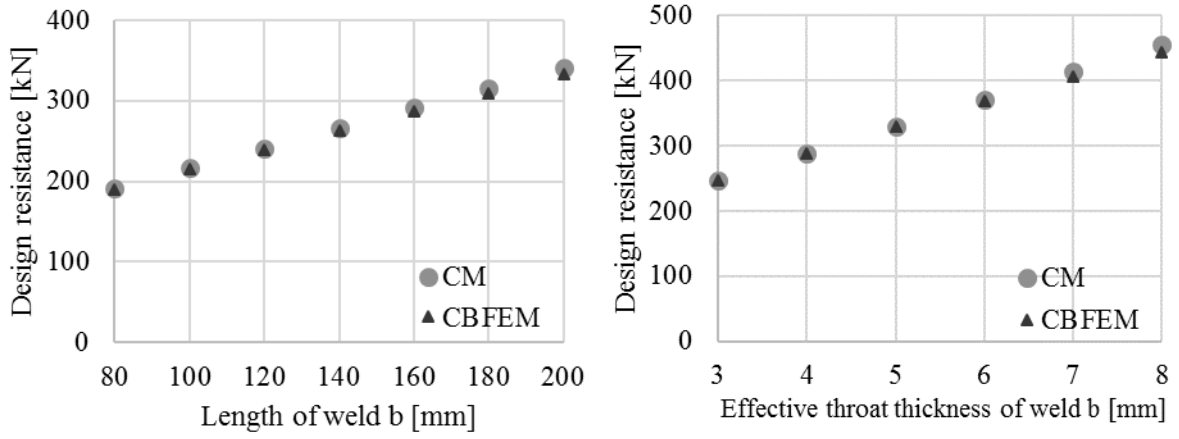

c) d)

Fig. 4.1.5 Parametric study of a combination of transverse and parallel weld a) Length of weld *a* b) Effective throat thickness of weld *a* c) Length of weld *b* d) Effective throat thickness of weld *b*

To illustrate the accuracy of the CBFEM model, the results of the sensitivity study are summarized in a diagram comparing CBFEM and CM design resistance; see Fig. 4.1.6. The results show that the difference between the two calculation methods is in all cases below 10 %.

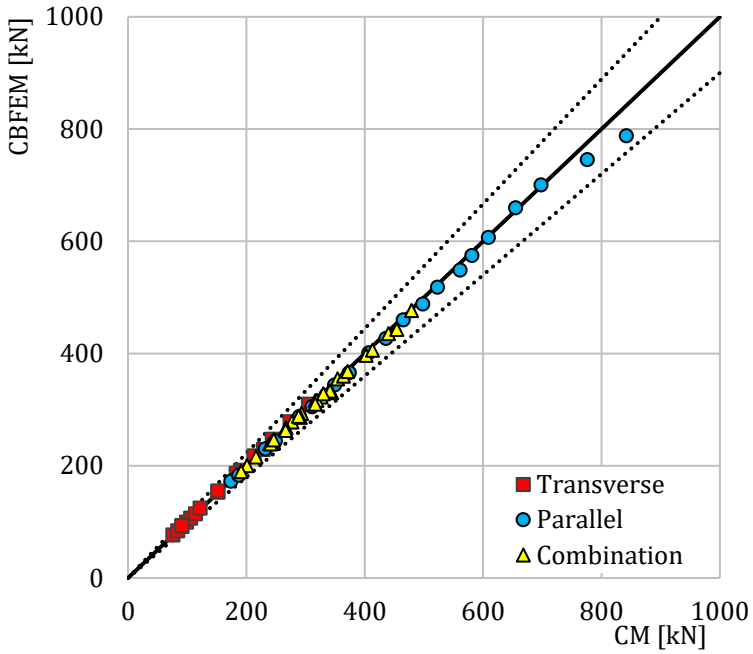

Fig. 4.1.6 Verification of CBFEM to CM

4.1.5 Benchmark example

Inputs

Plate 1

- Thickness t_1 = 20 mm
- Width b_1 = 200 mm
- Steel S235

Plate 2

- Thickness t_2 = 20 mm
- Width b_2 = 300 mm
- Offset e_z = −20 mm
- Steel S235

Weld, parallel fillet welds see Fig. 4.1.7.

- Throat thickness a_b = 3 mm
- Weld length L_b = 150 mm

Output

- Design resistance in tension F_{Rd} = 183 kN

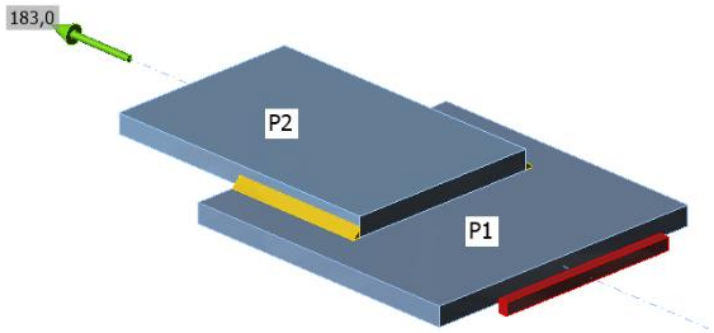

Fig. 4.1.7 Benchmark example for the welded lap joint with parallel fillet welds

4.2 Fillet weld in angle plate joint

4.2.1 Description

In this chapter, the model of the fillet weld in angle plate joint calculated by component-based finite element method (CBFEM) is verified on component method (CM). An angle is welded to a plate and loaded by normal force. The angle size and the length of the weld are studied in a sensitivity study.

4.2.2 Analytical model

The fillet weld is the only component examined in the study. The welds are designed according to Chapter 4 in EN 1993-1-8:2005 to be the weakest component in the joint. The design resistance of the fillet weld is described in section 4.1. Overview of considered examples and material is given in Tab. 4.2.1. The geometry of the joints with dimensions is shown in Fig. 4.2.1.

Tab. 4.2.1 Examples overview

Example	Material					Weld a		Weld b		Angle	Plate	
	f_y	f_u	E	γ_{M0}	γ_{M2}	a_a	L_a	a_b	L_b	section	b_p	t_p
	[MPa]	[MPa]	[GPa]	[-]	[-]	[mm]	[mm]	[mm]	[mm]	[-]	[mm]	[mm]
50×L80×10	235	360	210	1	1,25	3	50	3	50	80×10	240	10
100×L80×10	235	360	210	1	1,25	3	100	3	100	80×10	240	10
150×L80×10	235	360	210	1	1,25	3	150	3	150	80×10	240	10
200×L80×10	235	360	210	1	1,25	3	200	3	200	80×10	240	10
100×L160×16	235	360	210	1	1,25	5	100	3	100	160×16	400	16
170×L160×16	235	360	210	1	1,25	5	170	3	170	160×16	400	16
240×L160×16	235	360	210	1	1,25	5	240	3	240	160×16	400	16
310×L160×16	235	360	210	1	1,25	5	310	3	310	160×16	400	16
380×L160×16	235	360	210	1	1,25	5	380	3	380	160×16	400	16
450×L160×16	235	360	210	1	1,25	5	450	3	450	160×16	400	16

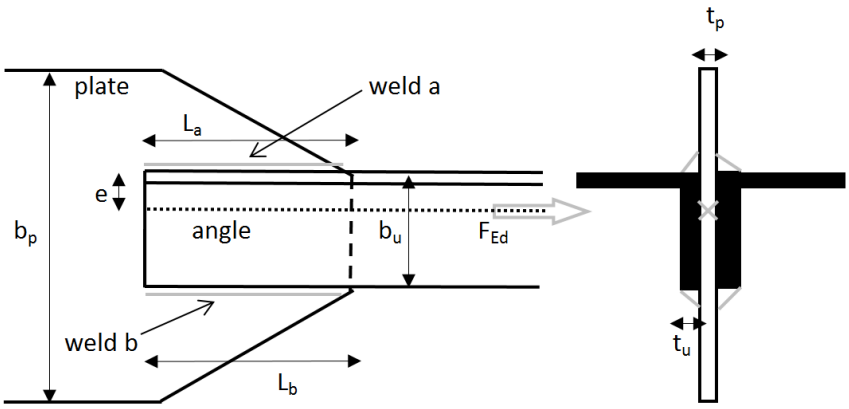

Fig. 4.2.1 Joint geometry with dimensions

4.2.3 Numerical model

The model of the weld in CBFEM is described in section 3.4. The weld model has an elastic-plastic material diagram, and stress peaks are redistributed along the weld length.

4.2.4 Verification of resistance

The weld design resistances calculated by CBFEM are compared with the results of CM; see Tab. 4.2.2. Two parameters are studied: the length of the weld and the angle section.

Tab. 4.2.2 Comparison of CBFEM and CM

Example	Design resistance		
	CM	CBFEM	diff.
	[kN]	[kN]	[%]
50×L80×10	124	120	-3
100×L80×10	249	235	-6
150×L80×10	374	350	-7
200×L80×10	498	457	-9

Example	Design resistance		
	CM	CBFEM	diff.
	[kN]	[kN]	[%]
100×L160×16	332	328	-1
170×L160×16	565	555	-2
240×L160×16	798	773	-3
310×L160×16	1030	988	-4
380×L160×16	1263	1206	-5
450×L160×16	1496	1419	-5

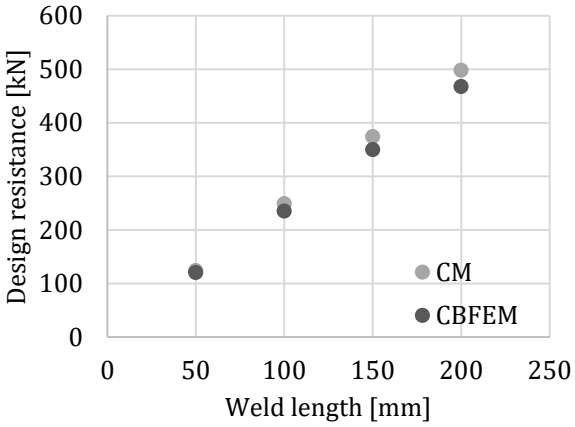

a) Angle cleat 80×10

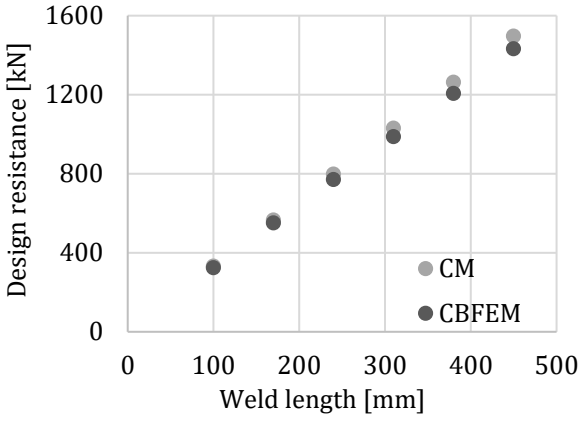

b) Angle cleat 160×16

Fig. 4.2.2 Sensitivity study of weld length

Results of CBFEM and CM are compared, and the sensitivity study is presented. The influence of weld length on the design resistance of a welded angle joint is shown in Fig. 4.2.2. The study shows good agreement for all weld configurations. To illustrate the accuracy of the CBFEM model, the results of the study are summarized in a diagram comparing design resistances by CBFEM and CM; see Fig. 4.2.3. The results show that the difference between the two calculation methods is in all cases less than 10 %.

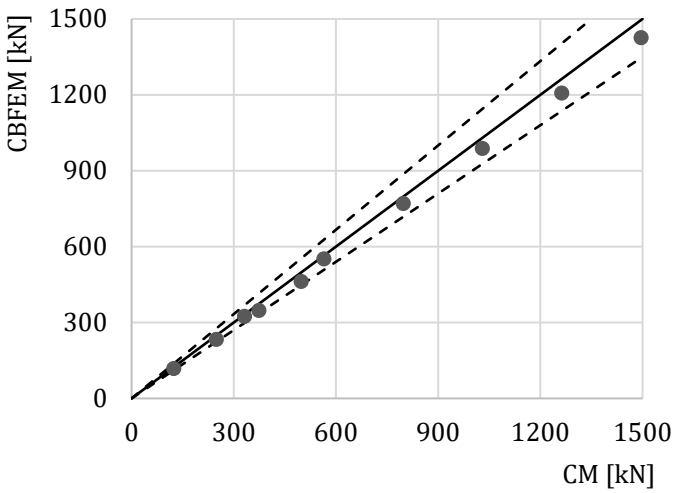

Fig. 4.2.3 Verification of CBFEM to CM

4.2.5 Benchmark example

Inputs

Angle

- Cross-section 2×L80×10
- Distance between angles 10 mm

Plate

- Thickness t_p = 10 mm
- Width b_p = 240 mm

Weld, parallel fillet welds, see Fig. 4.2.4

- Throat thickness a_w = 3 mm
- Weld length L_w = 200 mm

Outputs

- Design resistance in tension F_{Rd} = 457 kN

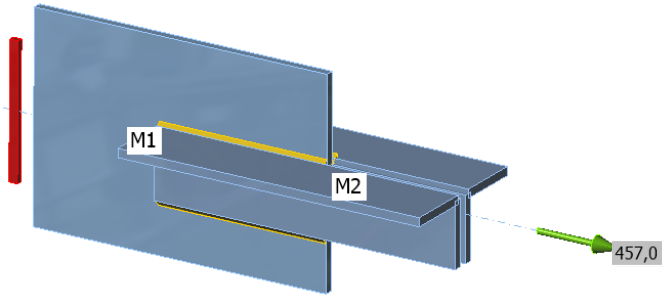

Fig. 4.2.4 Benchmark example of the welded angle plate joint with parallel fillet welds

4.3 Fillet weld in fin plate joint

4.3.1 Description

In this chapter, component-based finite element method (CBFEM) of a fillet weld in a fin plate joint is verified with component method (CM). A fin plate is welded to open section column HEB. The height of the fin plate is changed from 150 to 300 mm. The plate/weld is loaded by normal and shear force and bending moment.

4.3.2 Analytical model

The fillet weld is the only component examined in the study. The welds are designed to be the weakest component in the joint according to Chapter 4 in EN 1993-1-8:2005. The design resistance of the fillet weld is described in section 4.1. Overview of considered examples and material is given in Tab. 4.3.1. Three load cases are considered: normal force *N*, shear force *V*, and bending moment *M*. Geometry of the joint with dimensions is shown in Fig. 4.3.1.

Tab. 4.3.1 Examples overview

Example	Material					Weld	Fin plate			Column
	f_y	f_u	E	γ_{M0}	γ_{M2}	a_w	h_p	t_p	e	Section
	[MPa]	[MPa]	[GPa]	[-]	[-]	[mm]	[mm]	[mm]	[mm]	
N150	235	360	210	1	1,25	3	150	10	200	HEB400
N175	235	360	210	1	1,25	3	175	10	200	HEB400
N200	235	360	210	1	1,25	3	200	10	200	HEB400
N225	235	360	210	1	1,25	3	225	10	200	HEB400
N250	235	360	210	1	1,25	3	250	10	200	HEB400
N275	235	360	210	1	1,25	3	275	10	200	HEB400
N300	235	360	210	1	1,25	3	300	10	200	HEB400
V150	235	360	210	1	1,25	3	150	15	100	HEB200
V175	235	360	210	1	1,25	3	175	15	100	HEB200
V200	235	360	210	1	1,25	3	200	15	100	HEB200
V225	235	360	210	1	1,25	3	225	15	100	HEB200
V250	235	360	210	1	1,25	3	250	15	100	HEB200
V275	235	360	210	1	1,25	3	275	15	100	HEB200
V300	235	360	210	1	1,25	3	300	15	100	HEB200
M150	235	360	210	1	1,25	3	150	15	200	HEB400
M175	235	360	210	1	1,25	3	175	15	200	HEB400
M200	235	360	210	1	1,25	3	200	15	200	HEB400
M225	235	360	210	1	1,25	3	225	15	200	HEB400
M250	235	360	210	1	1,25	3	250	15	200	HEB400
M275	235	360	210	1	1,25	3	275	15	200	HEB400
M300	235	360	210	1	1,25	3	300	15	200	HEB400

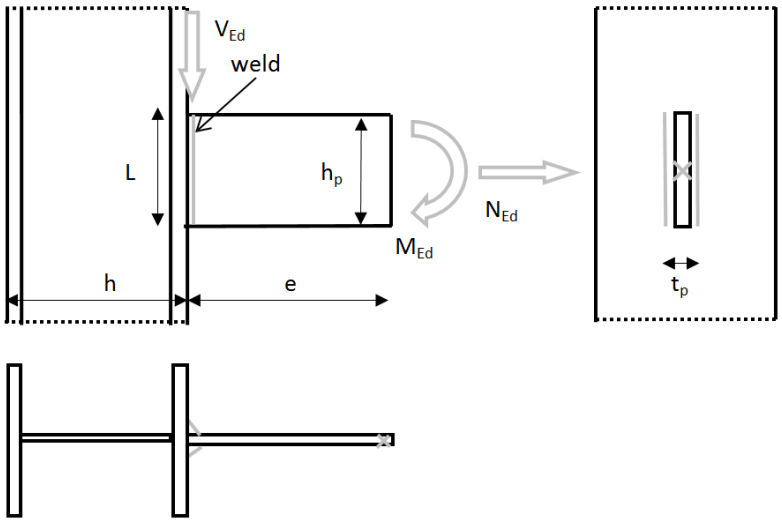

Fig. 4.3.1 Joint geometry with dimensions

4.3.3 Numerical model

The model of the weld in CBFEM is described in section 3.4. The weld model has an elastic-plastic material diagram, and stress peaks are redistributed along the weld length.

4.3.4 Verification of resistance

Design resistance calculated by CBFEM is compared with the results of CM. The comparison is presented in Tab. 4.3.2. The study is performed for one parameter: length of the weld, i.e. height of the fin plate, and three load cases: normal and shear force and bending moment. The shear force is applied in a weld plane to neglect the effect of an additional bending. The bending moment is applied at the end of the fin plate. The influence of the weld length on the design resistance of the fin plate joints loaded by the normal and shear force are shown in Fig. 4.3.2. The relation between the weld length and the bending moment resistance of the joint is shown in Fig. 4.3.3.

Tab. 4.3.2 Comparison of CBFEM and CM

Example	Design resistance			Example	Design resistance			Example	Design resistance		
	CM	CBFEM	diff.		CM	CBFEM	diff.		CM	CBFEM	diff.
	[kN]	[kN]	[%]		[kN]	[kN]	[%]		[kN]	[kN]	[%]
N150	229	227	-1	V150	187	184	-1	M150	8,5	8,4	-1
N175	267	264	-1	V175	218	216	-1	M175	11,6	11,5	-1
N200	305	301	-1	V200	249	247	-1	M200	15,2	15,0	-1
N225	343	338	-1	V225	280	278	-1	M225	19,3	19,0	-2
N250	381	375	-2	V250	310	309	0	M250	23,8	23,4	-2
N275	419	412	-2	V275	342	341	0	M275	28,8	28,4	-1
N300	457	449	-2	V300	374	372	-1	M300	34,3	33,8	-2

The results of CBFEM and CM are compared, and the sensitivity study is presented. The influence of weld length on the design resistance in a fin plate joint loaded by normal force is shown in Fig. 4.3.2, by shear force in Fig. 4.3.3, and by bending moment in Fig. 4.3.4. The study shows good agreement for all applied load cases.

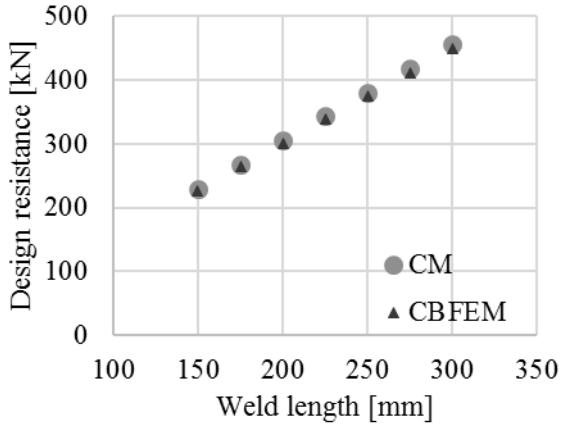

Fig. 4.3.2 Parametric study of fin plate joint loaded by normal force

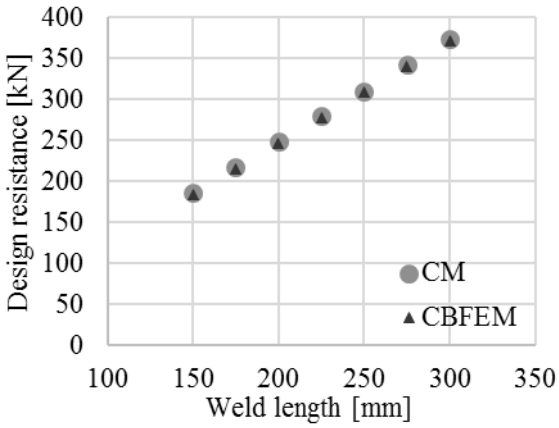

Fig. 4.3.3 Parametric study of fin plate joint loaded by shear force

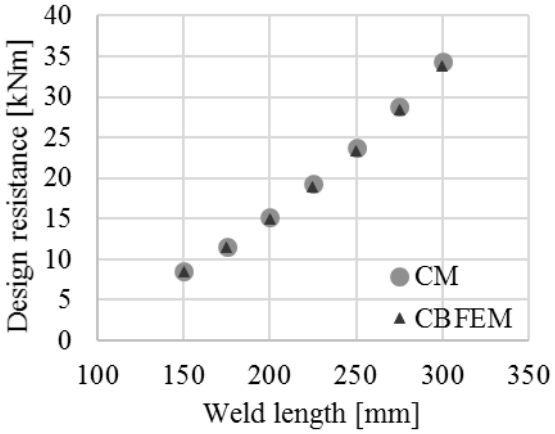

Fig. 4.3.4 Parametric study of fin plate joint loaded by bending moment

To illustrate the accuracy of the CBFEM model, the results of the parametric studies are summarized in a diagram comparing the design resistancesof CBFEM and CM; see Fig. 4.3.5. The results show that the difference between the two calculation methods is in all cases less than 10 %.

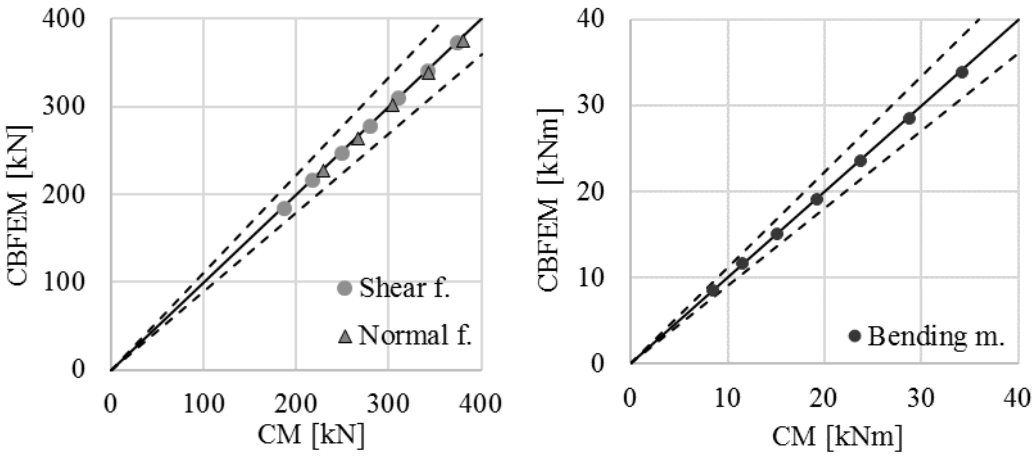

Fig. 4.3.5 Verification of CBFEM to CM

4.3.5 Benchmark example

Inputs

Column

- Steel S235
- HEB 400

Fin plate

- Thickness t_p = 15 mm
- Height h_p = 175 mm

Weld, double fillet weld see Fig. 4.3.6

- Throat thickness a_w = 3 mm

Outputs

- Design resistance in poor bending M_{Rd} = 11,5 kNm

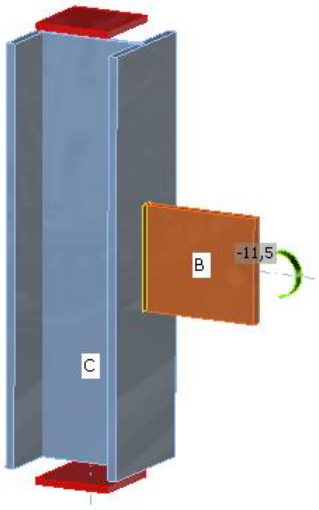

Fig. 4.3.6 Benchmark example for the welded fin plate joint

4.4 Fillet weld in beam to column joint

4.4.1 Description

The objective of this chapter is verification of component-based finite element method (CBFEM) for a fillet weld in a stiffened beam-to-column joint with component method (CM). An open section beam IPE is connected to open section column HEB 400. The stiffeners are inside column opposite to beam flanges. The beam section is the changing parameter. Three load cases are considered: the beam is loaded in tension, shear, and bending.

4.4.2 Analytical model

The fillet weld is the only component examined in the study. The welds are designed according to Chapter 4 in EN 1993-1-8:2005 to be the weakest component in the joint. The design resistance of the fillet weld is described in section 4.1. Overview of considered examples and material is given in the Tab. 4.4.1. Geometry of the joint with dimensions is shown in Fig. 4.4.1.

Tab. 4.4.1 Examples overview

Example	Material					Weld	Beam		Column
	f_y	f_u	E	γ_{M0}	γ_{M2}	a_w	Section	e	Section
	[MPa]	[MPa]	[GPa]	[-]	[-]	[mm]		[mm]	
IPE160	235	360	210	1	1,25	3	IPE160	200	HEB400
IPE180	235	360	210	1	1,25	3	IPE180	200	HEB400
IPE200	235	360	210	1	1,25	3	IPE200	200	HEB400
IPE220	235	360	210	1	1,25	3	IPE220	200	HEB400
IPE240	235	360	210	1	1,25	3	IPE240	200	HEB400
IPE270	235	360	210	1	1,25	3	IPE270	200	HEB400
IPE300	235	360	210	1	1,25	3	IPE300	200	HEB400
IPE330	235	360	210	1	1,25	3	IPE330	200	HEB400
IPE360	235	360	210	1	1,25	3	IPE360	200	HEB400
IPE400	235	360	210	1	1,25	3	IPE400	200	HEB400

4.4.3 Numerical model

The model of weld in CBFEM is described in section 3.4. Nonlinear elastic-plastic material is used for welds in this study. The plastic branch is reached in a part of the weld, and stress peaks are redistributed along the weld length.

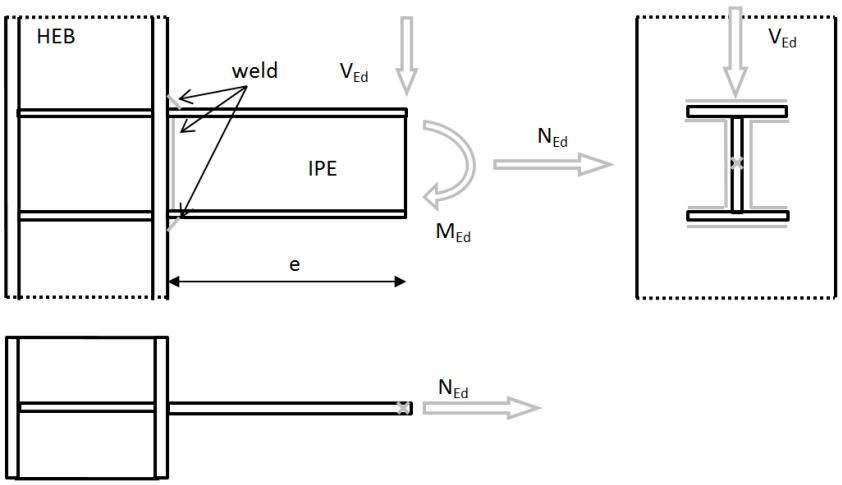

Fig. 4.4.1 Joint geometry with dimensions

4.4.4 Verification of resistance

Design resistance calculated by CBFEM Idea StatiCa software is compared with the results of CM. The weld design resistances are compared; see Tab. 4.4.2. The study is performed for one parameter beam section and three load cases: normal force N_{Ed}, shear force V_{Ed}, and bending moment M_{Ed}.

Tab. 4.4.2 Comparison of CBFEM and CM

Normal force N_{Ed}				Shear force V_{Ed}				Bending moment M_{Ed}			
Example	CM [kN]	CBFEM [kN]	Diff. [%]	Example	CM [kN]	CBFEM [kN]	Diff. [%]	Example	CM [kN]	CBFEM [kN]	Diff. [%]
IPE160	455	441	3	IPE160	105	108	-2	IPE160	26	26	0
IPE180	511	508	1	IPE180	127	130	0	IPE180	33	33	0
IPE200	567	578	-2	IPE200	151	152	-1	IPE200	40	41	-2
IPE220	625	645	-3	IPE220	175	178	0	IPE220	49	50	-2
IPE240	684	707	-3	IPE240	200	203	1	IPE240	59	60	-2
IPE270	774	797	-3	IPE270	239	244	2	IPE270	75	76	-1
IPE300	863	883	-2	IPE300	278	289	5	IPE300	93	94	-1
IPE330	937	949	-1	IPE330	315	336	6	IPE330	110	110	0
IPE360	1008	1008	0	IPE360	350	391	10	IPE360	129	126	2
IPE400	1097	1082	1	IPE400	399	461	10	IPE400	155	148	5

Results of CBFEM and CM are compared, and a sensitivity study is presented. The influence of beam cross-section on the design resistance of a welded beam-to-column joint loaded in tension is shown in Fig. 4.4.2, in shear in Fig. 4.4.3, and in bending in Fig. 4.4.4. The study shows good agreement for all applied load cases.

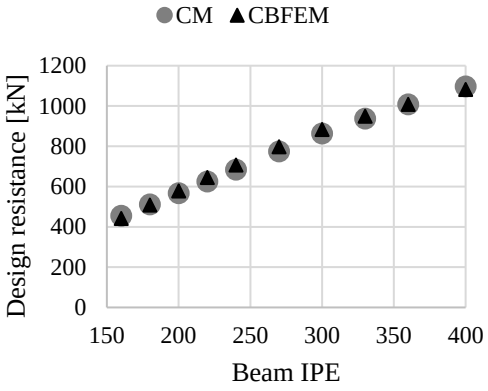

Fig. 4.4.2 Sensitivity study of beam-to-column joint loaded by normal force

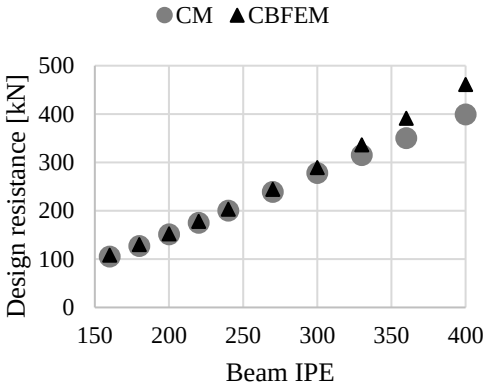

Fig. 4.4.3 Sensitivity study of beam-to-column joint loaded by shear force

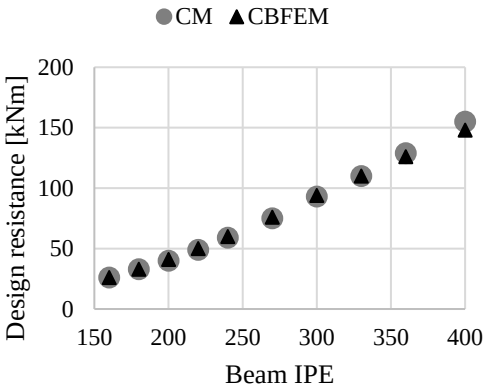

Fig. 4.4.4 Sensitivity study of beam-to-column joint loaded by bending moment

To illustrate the accuracy of the CBFEM model, the results of the sensitivity study are summarized in a diagram comparing design resistances of CBFEM and CM; see Fig. 4.4.5. The results show that the difference between the two calculation methods is in all cases less than 10%.

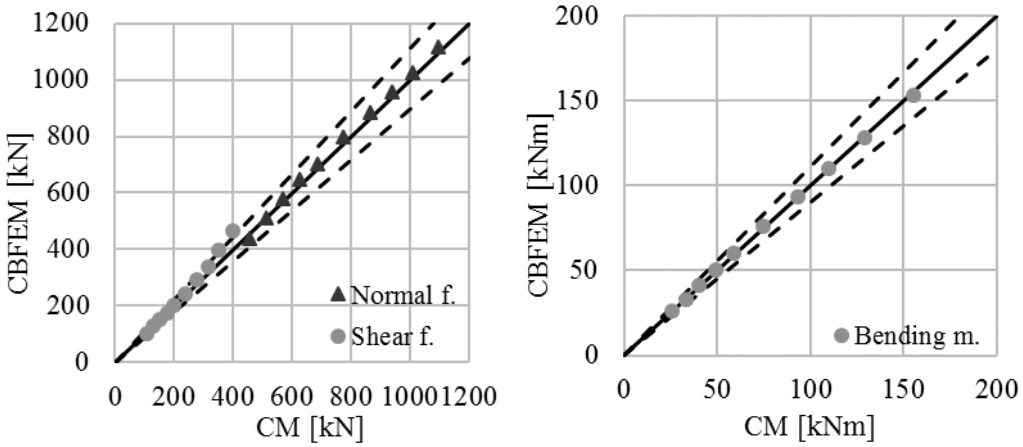

Fig. 4.4.5 Verification of CBFEM to CM

4.4.5 Benchmark example

Inputs

Column

- Steel S235
- HEB 400

Beam

- Steel S235
- IPE 270
- Length L = 200 mm
- Force eccentricity to weld x = 400 mm, see Fig. 4.4.6

Column stiffeners

- Thickness t_s = 10 mm
- Width b_s = 140 mm
- Related to beam flange, position upper and lower

Weld

- Throat thickness a_w = 3 mm

Outputs:

- Design resistance in shear V_{Rd} = 244 kN

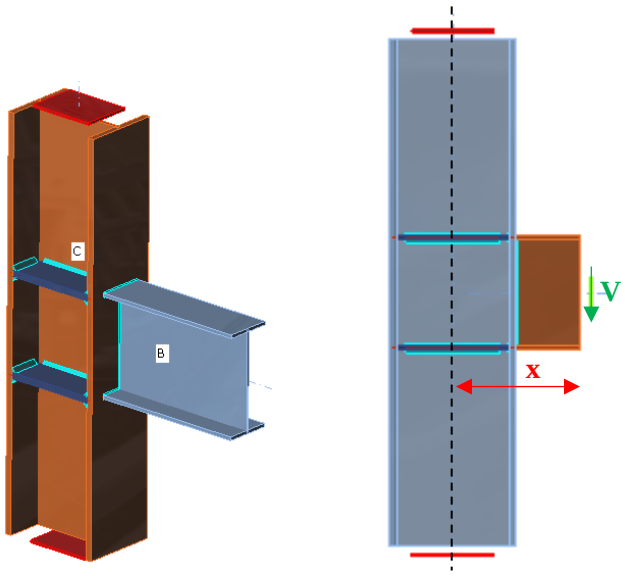

Fig. 4.4.6 Benchmark example of the welded beam to column joint with force eccentricity

4.5 Connection to unstiffened flanges

4.5.1. Description

In this chapter, component-based finite element method (CBFEM) of a fillet weld connecting a plate to an unstiffened column is verified on component method (CM). The steel plate is connected to the open and box section columns and loaded in tension.

4.5.2. Analytical model

The fillet weld is the only component examined in the study. The welds are designed according to Chapter 4 in EN 1993-1-8:2005 to be the weakest component in the joint. The design resistance of the fillet weld is described in section 4.1. The force applied perpendicular to a flexible plate, which is welded to an unstiffened section, is limited. The stresses are concentrated in an effective width while the weld resistance around the unstiffened parts is neglected, as shown in Fig. 4.5.1. For an unstiffened I or H section the effective width is obtained according to:

$$b_{\text{eff}} = t_{\text{w}} + 2s + 7kt_{\text{f}} \tag{4.5.1}$$

$$k = \frac{t_{\text{f}} f_{\text{y,f}}}{t_{\text{p}} f_{\text{y,p}}} \tag{4.5.2}$$

The dimension s is for a rolled section $s = r$ and for a welded section $s = \sqrt{2}\, a$. For a box or channel section, the effective width should be obtained from:

$$b_{\text{eff}} = 2t_{\text{w}} + 5t_{\text{f}} \qquad \text{but} \qquad b_{\text{eff}} \leq 2t_{\text{w}} + 5kt_{\text{f}} \tag{4.5.3}$$

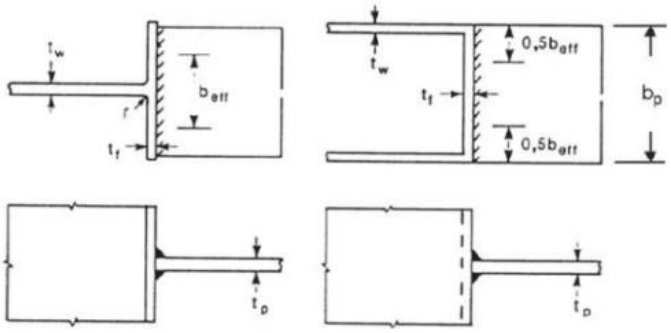

Fig. 4.5.1 Effective width of an unstiffened joint (Fig. 4.8 in EN 1993-1-8:2005)

4.5.3. Numerical model

The model of weld in CBFEM is described in section 3.4. The plastic branch is reached in a part of the weld, and stress peaks are redistributed along the weld length.

4.5.4. Verification of resistance

Design resistance calculated by CBFEM is compared with the results of CM. The weld design resistance is compared only. Overview of considered examples and material is given in Tab. 4.5.1. Geometry of joints with dimensions is shown in Fig. 4.5.2.

Tab. 4.5.1 Examples overview

Column	Material					Weld	Plate	
Section	f_y	f_u	E	γ_{M0}	γ_{M2}	a_w	b_p	t_p
	[MPa]	[MPa]	[GPa]	[-]	[-]	[mm]	[mm]	[mm]
HEB160	235	360	210	1	1,25	3	160	15
HEB180	235	360	210	1	1,25	3	180	16
HEB200	235	360	210	1	1,25	3	200	17
HEB220	235	360	210	1	1,25	3	220	18
HEB240	235	360	210	1	1,25	3	240	19
HEB260	235	360	210	1	1,25	3	260	19

Column	Material					Weld	Flexible plate		Column		
	f_y	f_u	E	γ_{M0}	γ_{M2}	a_w	b_p	t_p	b_f	t_f	t_w
	[MPa]	[MPa]	[GPa]	[-]	[-]	[mm]	[mm]	[mm]	[mm]	[mm]	[mm]
K200/5	235	360	210	1	1,25	3	190	5	200	5	5
K200/6	235	360	210	1	1,25	3	190	6	200	6	6
K200/7	235	360	210	1	1,25	3	190	7	200	7	7
K200/8	235	360	210	1	1,25	3	190	8	200	8	8
K200/10	235	360	210	1	1,25	3	190	10	200	10	10

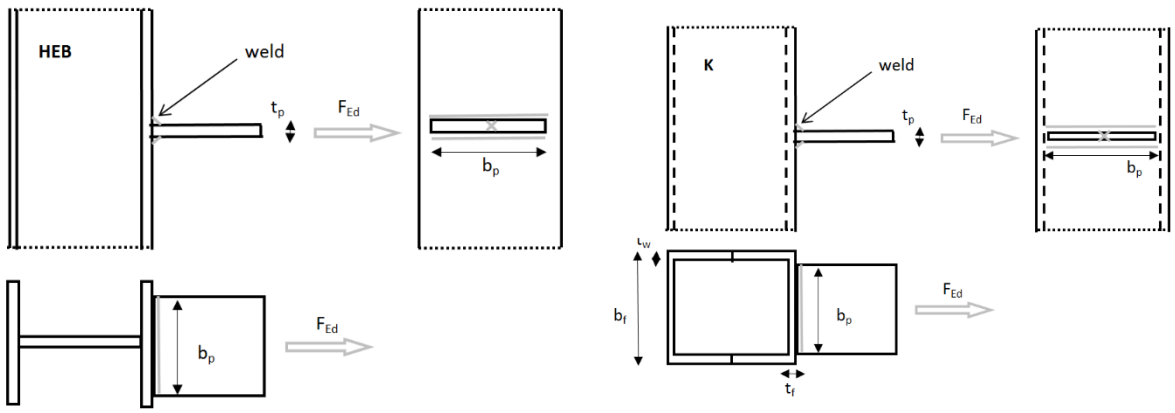

a) Flexible plate to open section b) Flexible plate to box section

Fig. 4.5.2 Joint geometry and dimensions

The results are presented in Tab. 4.5.2. The study is performed for two parameters: flange width of the HEB section and web thickness of the box section. The flexible plate is loaded in

tension. The influence of the flange width of HEB section on design resistance of a joint is shown in Fig. 4.5.3. The relation between the web thickness of box section on design resistance of a joint is shown in Fig. 4.5.4.

Tab. 4.5.2 Comparison of CBFEM and CM

Example	Design resistance		
	CM	CBFEM	Diff.
	[kN]	[kN]	[%]
HEB160	178	161	-10
HEB180	189	177	-7
HEB200	210	192	-10
HEB220	221	207	-7
HEB240	242	223	-9
HEB260	260	234	-11

Example	Design resistance		
	CM	CBFEM	Diff.
	[kN]	[kN]	[%]
K200/5	53	50	-6
K200/6	64	71	9
K200/7	74	76	2
K200/8	85	83	-2
K200/10	106	101	-5

Results of CBFEM and CM are compared in a sensitivity study. The influence of the flange width of HEB section on design resistance of a joint is studied in Fig. 4.5.3. The influence of the web thickness of box section on design resistance of a joint is presented in Fig. 4.5.4. The parametric studies show very good agreement of the results for all weld configurations.

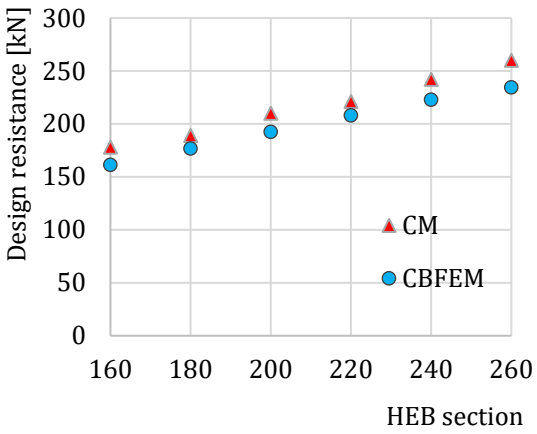

Fig. 4.5.3 Flange width of the HEB section

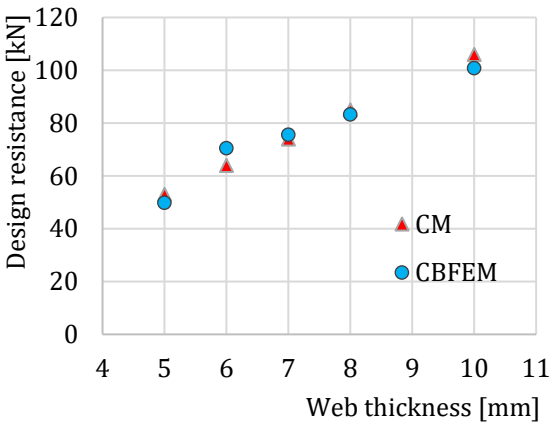

Fig. 4.5.4 Web thickness of the box section

The results of the sensitivity study are summarized in a diagram comparing design resistances of CBFEM and CM; see Fig. 4.5.5 illustrating the accuracy of the CBFEM model.

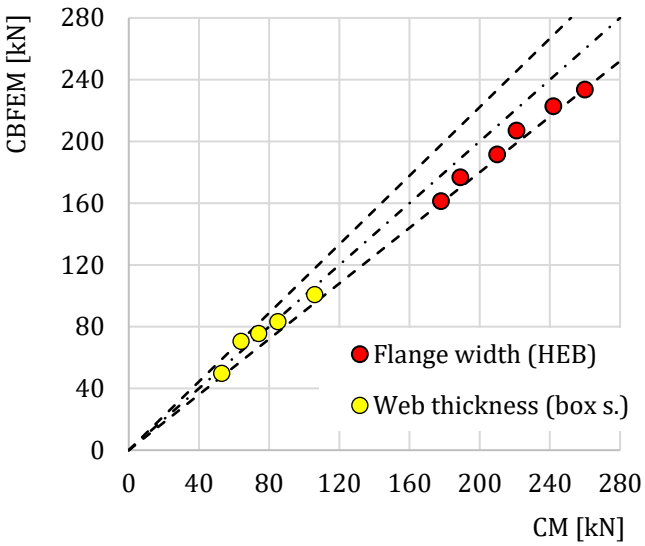

Fig. 4.5.5 Verification of CBFEM to CM

The influence of the plate thickness on the design resistance of the weld is shown in Fig. 4.5.6. The column cross-section is HEB 180 with a flange thickness of 14 mm. A weld connecting a plate thicker than the column flange has the same resistance for CM and CBFEM. On the other hand, the weld connecting the plate to column flange of the same or smaller thickness has in numerical models design resistance smaller by 20%. The plate thickness is not taken into account in numerical models with shell elements, which causes the difference.

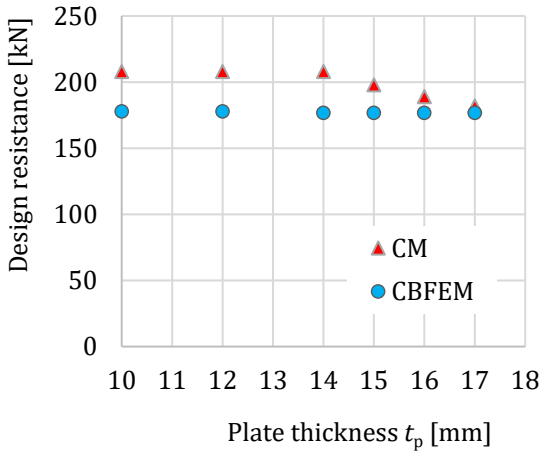

Fig. 4.5.6 Influence of plate thickness on the resistance of joint with unstiffened column HEB 180

4.5.5. Benchmark example

Inputs

Column

- Steel S235
- RHS 200/200/5

Flexible plate

- Steel S235
- Thickness t_p = 5 mm
- Width b_p = 190 mm

Weld, double fillet welds see Fig. 4.5.7

- Throat thickness a_w = 3 mm

Outputs

- Design resistance in tension N_{Rd} = 50 kN

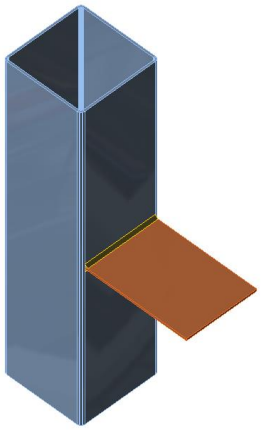

Fig. 4.5.7 Benchmark example for the welded connection of plate to unstiffened column

5 BOLTED CONNECTION

5.1 T-stub in tension

5.1.1. Description

The objective of this chapter is verification of component-based finite element method (CBFEM) of T-stubs connected with two bolts loaded in tension with component method (CM) and research FEM model (RM) created in Midas FEA software; see (Gödrich et al. 2019).

5.1.2. Analytical model

Welded T-stub and bolt in tension are components examined in the study. Both components are designed according to EN 1993-1-8:2005. The welds are designed not to be the weakest component. Effective lengths for circular and noncircular failures are considered according to EN 1993-1-8:2005 cl. 6.2.6. Only tension loads are considered. Three modes of collapse according to EN 1993-1-8:2005 cl. 6.2.4.1 are considered: 1. mode with full yielding of the flange, 2. mode with two yield lines by web and rupture of the bolts, and 3. mode for rupture of the bolts; see Fig. 5.1.1. Bolts are designed according to cl. 3.6.1 in EN 1993-1-8:2005. Design resistance considers punching shear resistance and rupture of the bolt.

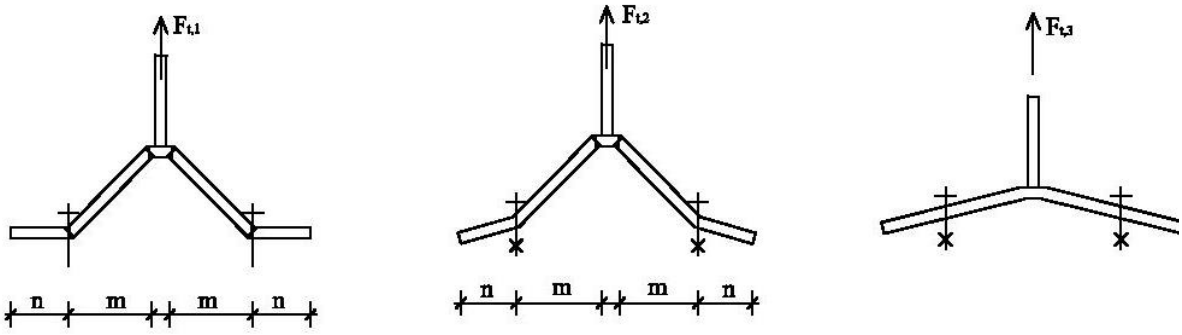

1. Mode 2. Mode 3. Mode

Fig. 5.1.1 Collapse modes of T-stub

5.1.3. Design numerical model

T-stub is modeled by 4-nodes shell elements as described in Chapter 3 and summarised further. Every node has 6 degrees of freedom. Deformations of the element consist of membrane and flexural contributions. Nonlinear elastic-plastic material status is investigated in each layer of integration point. Assessment is based on the maximum strain given according to EN 1993-1-5:2006 by value of 5 %. Bolts are divided into three sub-components. The first is the bolt shank, which is modeled as a nonlinear spring and caries tension only. The second sub-

component transmits tensile force into the flanges. The third sub-component solves shear transmission.

5.1.4. Research numerical model

In cases where the CBFEM gives higher resistance, initial stiffness, or deformation capacity, research FEM model (RM) from brick elements validated on experiments (Gödrich et al. 2013) is used to verify the CBFEM model. RM is created in Midas FEA software of hexahedral and octahedral solid elements, see Fig. 5.1.2 Mesh sensitivity study was provided to reach proper results in adequate time. Numerical model of the bolts is based on the model by (Wu et al. 2012). The nominal diameter is considered in the shank, and the effective core diameter is considered in the threaded part. Washers are coupled with the head and nut. Deformation caused by stripping of the threads in thread–nut contact area is modeled using interface elements. Interface elements are unable to transfer tensile stresses. Contact elements allowing the transmission of pressure and friction are used between washers and flanges of the T-stub. One-quarter of the sample was modeled using the symmetry.

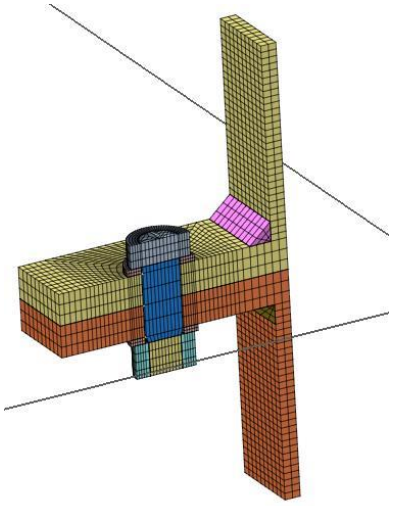

Fig. 5.1.2 Research FEM model

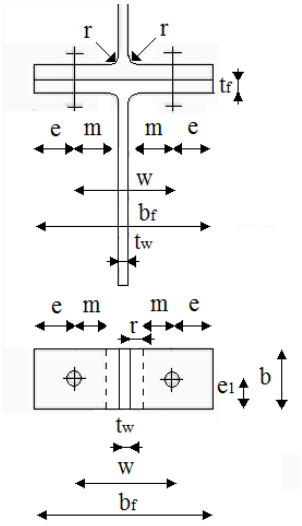

Fig. 5.1.3 Geometry of the T stubs

5.1.5. Range of validity

CBFEM was verified for the selected typical T-stub geometries. The minimal thickness of the flange is 8 mm. Maximal distance of the bolts to bolt diameter is limited by $p/d_b \leq 20$. The distance of the bolt line to the web is limited to $m/d_b \leq 5$. Overview of the considered samples with steel plates of S235: f_y = 235 MPa, f_u = 360 MPa, $E = E_{bolt}$ = 210 GPa is shown in the Tab. 5.1.1 and in Fig. 5.1.3.

Tab. 5.1.1 Overview of the considered samples of T stubs

Sample	T-stub										Bolts	
	t_f	t_w	b_f	a_w	b	w	e_1	m	e	n	Diam.	Mat.
	[mm]	[mm]	[mm]	[mm]	[mm]	[mm]	[mm]	[mm]	[mm]	[mm]		
tf10	10	20	300	10	100	165	50	61,19	67,5	67,5	M24	8.8
tf12	12	20	300	10	100	165	50	61,19	67,5	67,5	M24	8.8
tf15	15	20	300	10	100	165	50	61,19	67,5	67,5	M24	8.8
tf20	20	20	300	10	100	165	50	61,19	67,5	67,5	M24	8.8
tf25	25	20	300	13,5	100	165	50	57,23	67,5	67,5	M24	8.8
tf30	30	20	300	13,5	100	165	50	57,23	67,5	67,5	M24	8.8
tf35	35	20	300	13,5	100	165	50	57,23	67,5	67,5	M24	8.8
tf40	40	20	300	13,5	100	165	50	57,23	67,5	67,5	M24	8.8
tf45	45	20	300	13,5	100	165	50	57,23	67,5	67,5	M24	8.8
tf50	50	20	300	13,5	100	165	50	57,23	67,5	67,5	M24	8.8
M16 8.8	25	20	300	10	100	165	50	61,19	67,5	67,5	M16	8.8
M20 8.8	25	20	300	10	100	165	50	61,19	67,5	67,5	M20	8.8
M24 8.8	25	20	300	10	100	165	50	61,19	67,5	67,5	M24	8.8
M27 8.8	25	20	300	10	100	165	50	61,19	67,5	67,5	M27	8.8
M24 4.8	25	20	300	10	100	165	50	61,19	67,5	67,5	M24	4.8
M24 5.8	25	20	300	10	100	165	50	61,19	67,5	67,5	M24	5.8
M24 6.8	25	20	300	10	100	165	50	61,19	67,5	67,5	M24	6.8
M24 10.9	25	20	300	10	100	165	50	61,19	67,5	67,5	M24	10.9
w110	20	20	300	7	100	110	50	37,08	95	46,35	M24	8.8
w150	20	20	300	7	100	150	50	57,08	75	71,35	M24	8.8
w200	20	20	300	7	100	200	50	82,08	50	50	M24	8.8
w240	20	20	300	7	100	240	50	102,1	30	30	M24	8.8
b100	20	20	300	7	100	110	50	37,08	95	46,35	M24	10.9
b250	20	20	300	7	250	110	125	37,08	95	46,35	M24	10.9
b300	20	20	300	7	300	110	150	37,08	95	46,35	M24	10.9
b400	20	20	300	7	400	110	200	37,08	95	46,35	M24	10.9

5.1.6. Global behavior

Comparison of the global behavior of the T-stub described by force–deformation diagrams for all design procedures was prepared. Attention was focused on the main characteristics: initial stiffness, design resistance, and deformation capacity. Sample tf20 was chosen to present as a reference; see Fig. 5.1.4 and Tab. 5.1.2. CM generally gives higher initial stiffness compared to CBFEM and RM. In all cases, RM gives the highest design resistance, as shown in chapter 6. Deformation capacity is also compared. Deformation capacity of T-stub was calculated according

to (Beg et al. 2004). RM does not consider cracking of the material, so the prediction of deformation capacity is limited.

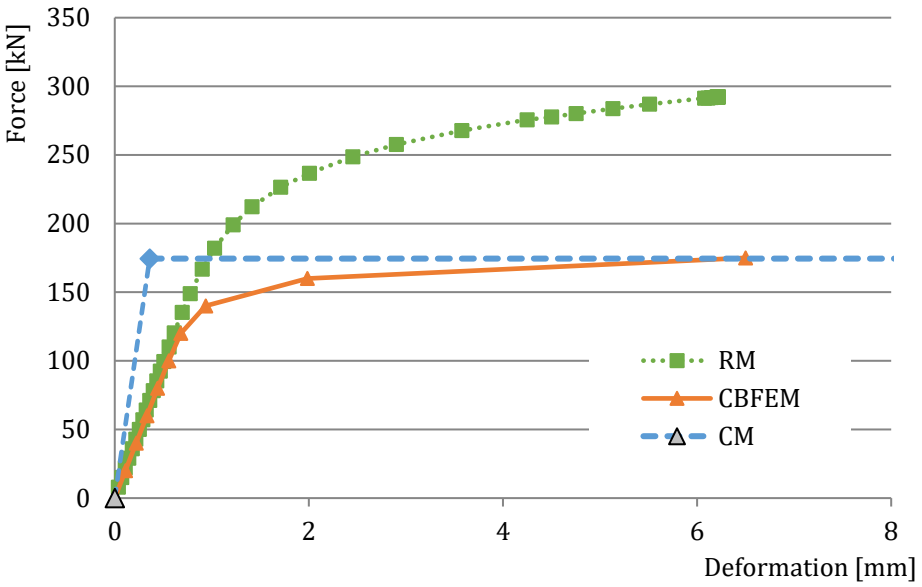

Fig. 5.1.4 Force–deformation diagram

Tab. 5.1.2 Global behavior overview

		CM	CBFEM	RM	CM/CBFEM	RM/CBFEM
Initial stiffness	[kN/m]	484727	181818	197400	2,67	1,09
Design resistance	[kNm]	174	165	268,8	1,05	1,63
Deformation capacity	[mm]	24,5	6,5	-	3,77	-

5.1.7. Verification of resistance

Design resistances calculated by CBFEM were compared with the results of CM and RM in the next step. The comparison was focused on the deformation capacity and determination of the collapse mode too. All results are ordered in Tab. 5.1.3. The study was performed for five parameters: thickness of the flange, bolt size, bolt material, bolt space, and T-stub width.

Tab. 5.1.3 Global behavior overview

Sample	CM			CBFEM			RM		
	Design res.	Collapse mode	Initial stiffness	Design res.	Collapse mode	Initial stiffness	Design res.	Collapse mode	Initial stiffness
	[kN]		[kN/mm]	[kN]		[kN/mm]	[kN]		[kN/mm]
Parameter: Thickness of the flange									
tf10	44	1	80,0	63	1	39,4	115	1	53,6
tf12	63	1	134,6	78	1	58,8	144	1	80,9
tf15	98	1	246,6	105	1	97,1	199,7	1	120,5
tf20	174	1	484,7	165	1	181,8	268,8	2	197,4
tf25	279	2	789,3	238	1	285,7	310,3	2	297,8
tf30	305	2	922,6	288	2	392,2	328,7	2	363
tf35	335	2	968,8	320	2	485,4	347,3	2	416,8
tf40	371	2	961,3	344	2	573,8	370,7	2	464,4
tf45	407	3	927,3	385	2	654,2	400	2	510,6
tf50	407	3	882,4	412	3	736,8	407	3	553,8
Parameter: bolt size									
M16 8.8	152	2	486,6	150	2	-	-	-	-
M20 8.8	205	2	612,7	200	2	-	-	-	-
M24 8.8	270	2	710,2	238	1	-	-	-	-
M27 8.8	278	1	782,4	250	1	-	-	-	-
Parameter: bolt material									
M24 4.8	164	2	710,2	163	2	-	-	-	-
M24 5.8	190	2	710,2	186	2	-	-	-	-
M24 6.8	217	2	693,6	210	2	-	-	-	-
M24 10.9	273	1	677,8	253	1	-	-	-	-
Parameter: bolt space									
w110	282	2	1129,7	262	1	465,1	344	2	432,5
w150	188	1	562,4	184	1	229,0	281	2	228,0
w200	129	1	237,8	133	1	111,9	222	2	112,7
w240	107	1	131,9	109	1	66,1	162,7	2	64,9
Parameter: T-stub width									
b100	314	1	1129,7	285	1	463,0	407	2	432,2
b250	423	2	1443,5	448	2	534,4	480,5	2	640,0
b300	433	2	1443,5	466	2	534,4	486	2	686,0
b400	433	2	1443,5	492	2	538,5	494	2	721,5

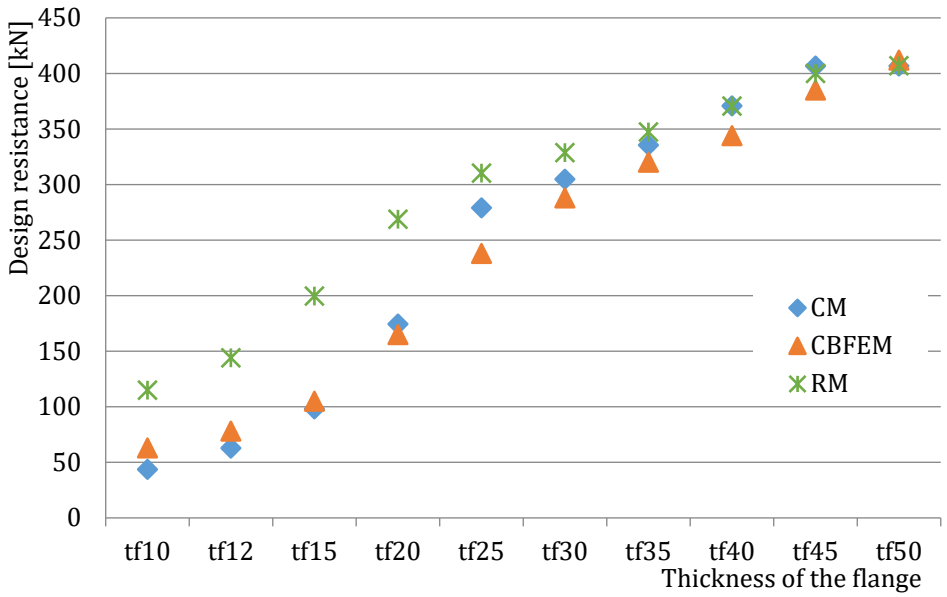

Fig. 5.1.5 Sensitivity study of flange thickness

The sensitivity study of thickness of the flange shows higher resistance according to CBFEM compared to CM for samples with flange thicknesses up to 20 mm. RM gives even higher resistance for these samples; see Fig. 5.1.5. Higher resistance of both numerical models is explained by neglecting membrane effect in CM. In case of the bolt diameter and bolt material (see Fig. 5.1.6 and Fig. 5.1.7, respectively), the results of CBFEM correspond to these of CM. Due to a good agreement of both methods, the results of RM are not required.

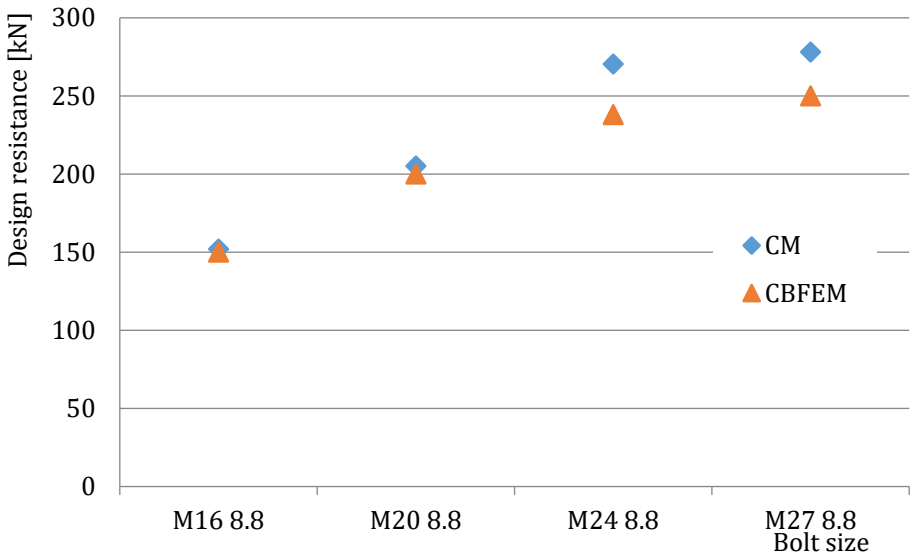

Fig. 5.1.6 Sensitivity study of the bolt size

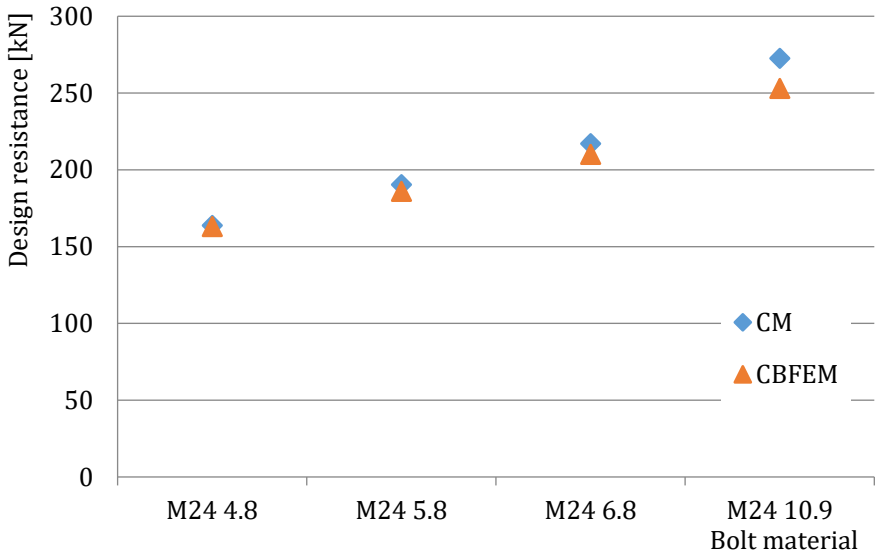

Fig. 5.1.7 Sensitivity study of the bolt material

In the case of the bolt distances, the results of CBFEM and CM show generally good agreement; see Fig. 5.1.8. With an increase in bolt spacing, CBFEM gives slightly higher resistance compared to CM. For that reason, the results of RM are also shown. RM gives the highest resistance in all cases.

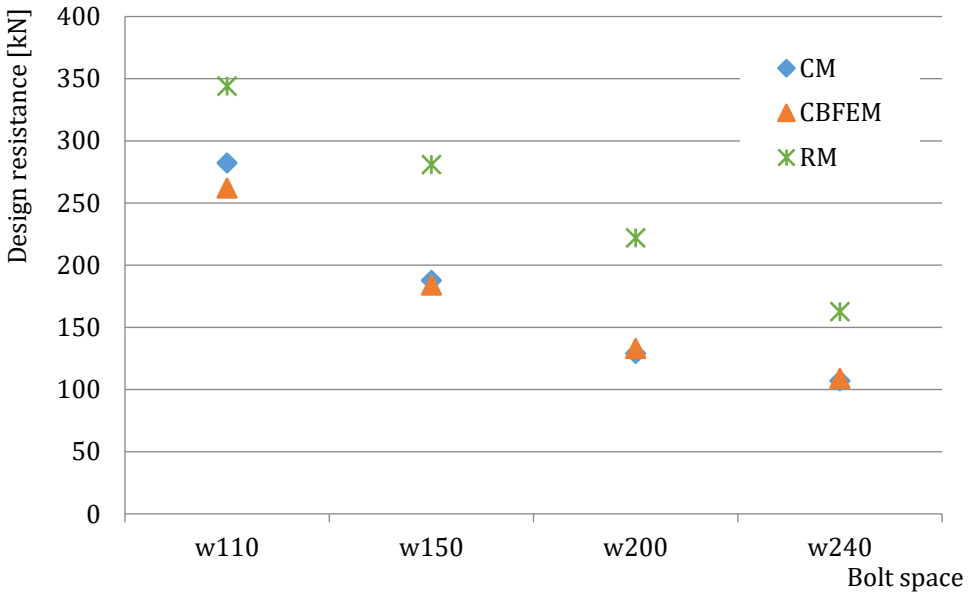

Fig. 5.1.8 Sensitivity study of the bolt distance

In the study of T-stub width, CBFEM shows higher resistance compared to CM with an increase in width. Results of RM were prepared, which again provide the highest resistance in all cases; see Fig. 5.1.9.

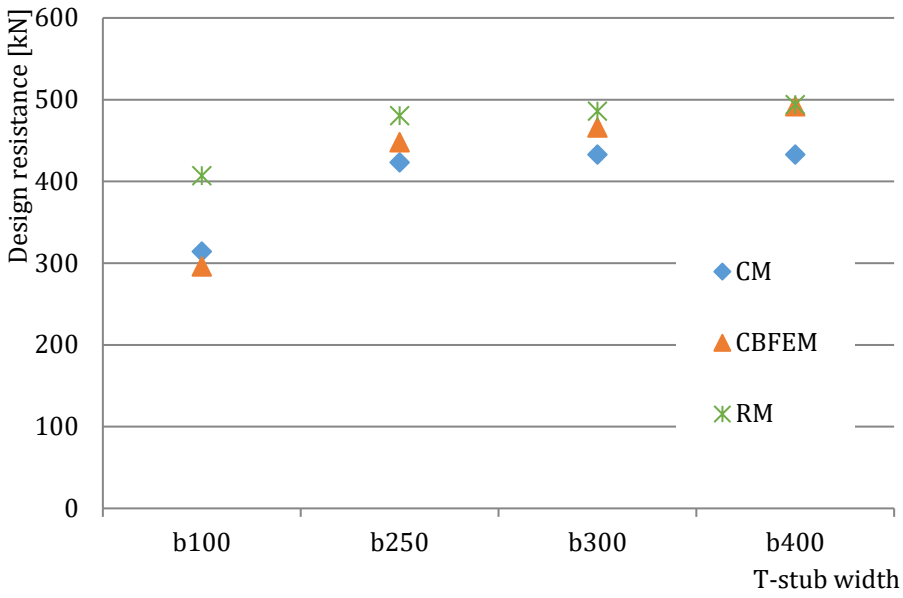

Fig. 5.1.9 Sensitivity study of T-stub width

To show the prediction of the CBFEM model, the results of the studies were summarized in graph comparing resistances by CBFEM and CM; see Fig. 5.1.10. The results show that the difference between the two calculation methods is mostly up to 10 %. In cases with CBFEM/CM > 1,1, accuracy of CBFEM was verified by the results of RM, which gives the highest resistance in all selected cases.

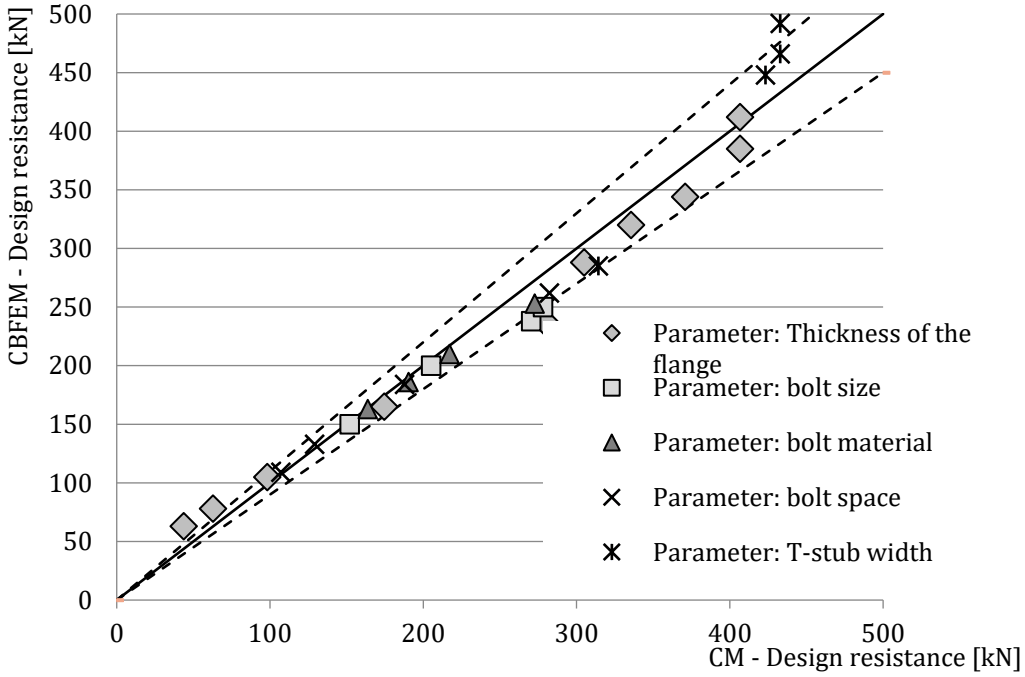

Fig. 5.1.10 Summary of verification of CBFEM to CM

5.1.8. Benchmark example

Inputs

T-stub, see Fig. 5.1.11

- Steel S235
- Flange thickness t_f = 20 mm
- Web thickness t_w = 20 mm
- Flange width b_f = 300 mm
- Length b = 100 mm
- Double fillet weld a_w = 10 mm

Bolts

- 2 × M24 8.8
- Distance of the bolts w = 165 mm

Outputs

- Design resistance in tension $F_{T,Rd}$ = 165 kN
- Collapse mode – full yielding of the flange with maximal strain 5 %
- Utilization of the bolts 86,0 %
- Utilization of the welds 45,1 %

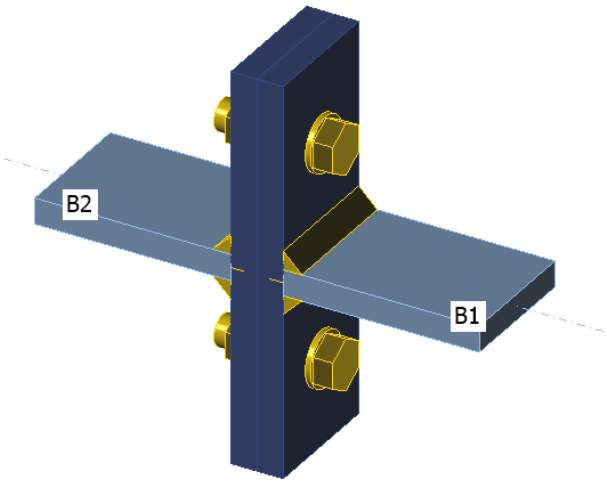

Fig. 5.1.11 Benchmark example for the T-stub

5.2 Splices in shear

5.2.1. Description

This study is focused on the verification of component-based finite element method (CBFEM) for the resistance of the symmetrical double splice bolted connection to an analytical model (AM).

5.2.2. Analytical model

The bolt resistance in shear and the plate resistance in bearing are designed according to Tab. 3.4 in chapter 3.6.1 in EN 1993-1-8:2005. For long connection, reduction factor according to cl. 3.8 is considered. Design resistance of connected members with reductions for fastener holes is taken into account according to cl 3.10.

5.2.3. Verification of resistance

Design resistances calculated by CBFEM were compared with results of analytical model (AM). Results are summarised in Tab. 5.2.1. The parameters are bolt material, splice thickness, bolt diameter, and bolt distances, see Figs. 5.2.1 to 5.2.4.

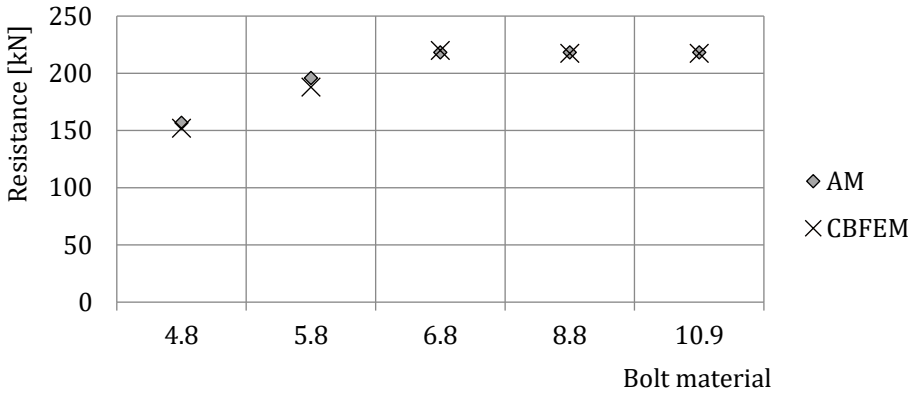

Fig. 5.2.1 Sensitivity study for the bolt material

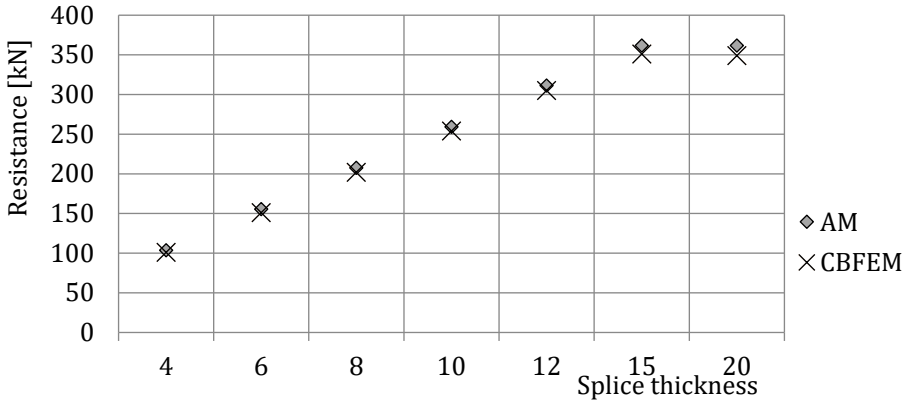

Fig. 5.2.2 Sensitivity study for the splice thickness

Tab. 5.2.1 Sensitivity study of resistance

Parameter		Analytical Model (AM)		CBFEM		AM/ CBFEM
		Resist. kN	Critical component	Resist. kN	Critical component	
Bolt material		Joint description: splice 150/10mm, bolts 2×M20 in distances p =70, e_1=50, plates 2×150/6mm, steel S235				
4.8		157	Bolt in shear	152	Bolt in shear	1,03
5.8		196	Bolt in shear	188	Bolt in shear	1,04
6.8		218	Bearing	214	Bearing	1,01
8.8		218	Bearing	218	Bearing	1,00
10.9		218	Bearing	218	Bearing	1,00
Splice thickness		Joint description: splice height 200mm, bolts 3×M16 8,8 in distances p = 55mm e_1 = 40mm, plates 2×200/10 mm, steel S235				
4		104	Bearing	104	Bearing	1,00
6		156	Bearing	156	Bearing	1,00
8		208	Bearing	207	Bearing	1,00
10		259	Bearing	258	Bearing	1,00
12		311	Bearing	309	Bearing	1,00
15		362	Bolt in shear	350	Interaction of tension and shear in bolt	1,03
20		362	Bolt in shear	349	Interaction of tension and shear in bolt	1,04
Diam.	Distances	Joint description: splice 120/10mm, bolts 2×MX 8,8, plates 2×120/6 mm, steel S235				
M16	p = 55, e_1 = 40	171	Bearing	170	Bearing	1,00
M20	p = 70, e_1= 50	218	Bearing	219	Bearing	1,00
M24	p = 80, e_1 = 60	244	Splice in tension	241	Splice in tension	1,01
M27	p = 90, e_1 = 70	233	Splice in tension	236	Splice in tension	0,99
M30	p = 100, e_1 = 75	226	Splice in tension	231	Splice in tension	0,98
Bolt spacing		Joint description: Splice 200/6 mm, bolts 3×M16 8,8, plates 2×200/3mm, steel S235				
p = 40, e_1 = 25		98	Bearing	95	Bearing	1,03
p = 55, e_1 = 40		156	Bearing	152	Bearing	1,02
p = 70, e_1 = 55		207	Bearing	205	Bearing	1,01

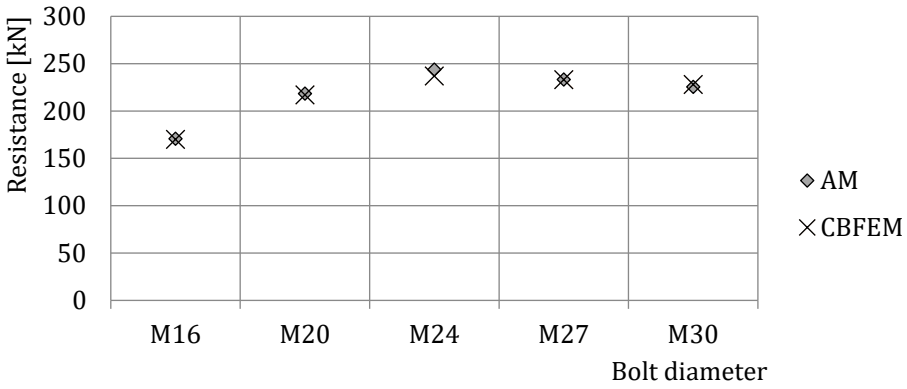

Fig. 5.2.3 Sensitivity study for the bolt diameter

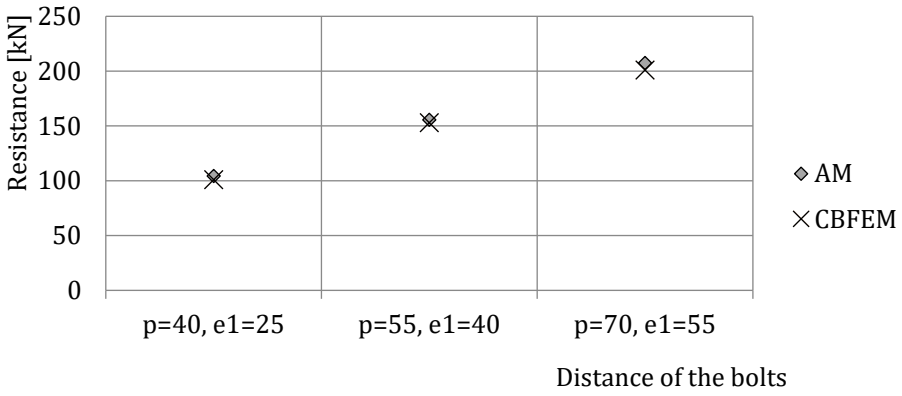

Fig. 5.2.4 Sensitivity study for the distance of bolts

The results of sensitivity studies are summarized in the graph in Fig. 5.2.5. The results show that the differences between the two calculation methods are below 5 %. The analytical model gives generally higher resistance.

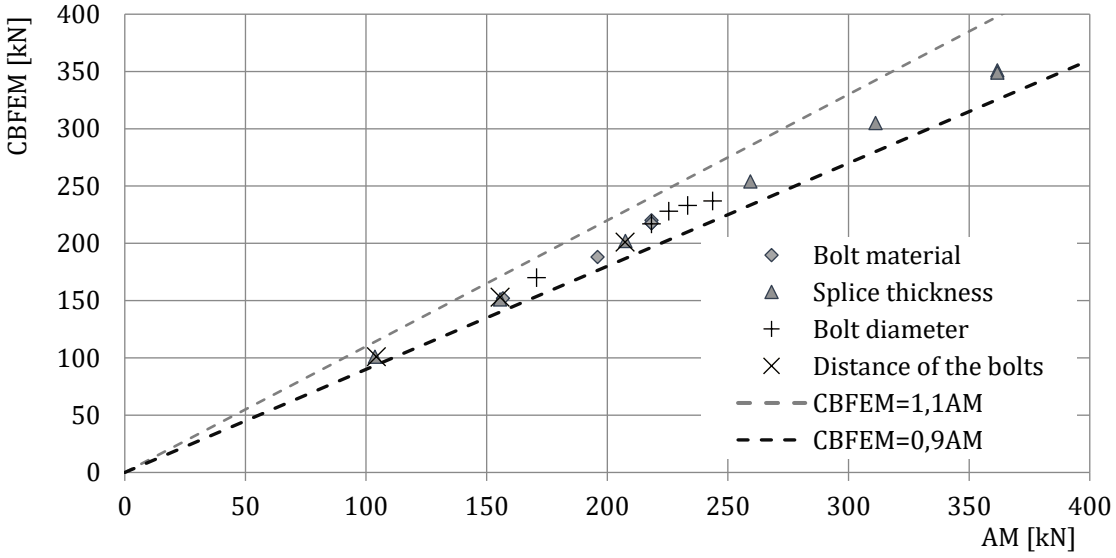

Fig. 5.2.5 Verification of CBFEM to AM for the symmetrical double splice connection

5.2.4. Benchmark example

Inputs

Connected member

- Steel S235
- Splice 200/10 mm

Connectors

Bolts

- 3 × M16 8.8
- Distances e_1 = 40 mm, p = 55 mm

2 x splice

- Steel S235
- Plate 380×200×10

Outputs

- Design resistance F_{Rd} = 258 kN
- Critical is bearing of the connected splice

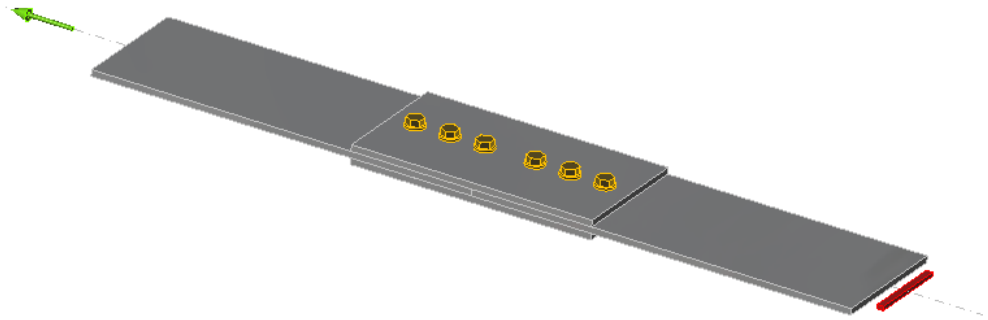

Fig. 5.2.6 Benchmark example of the bolted splices in shear

5.3 End plate minor axis connection

5.3.1 Description

Component-based finite element method (CBFEM) model of the beam to column joint is verified on Component method (CM). The extended end plate with three bolt rows is connected to column web and loaded by bending moment; see Fig. 5.3.1.

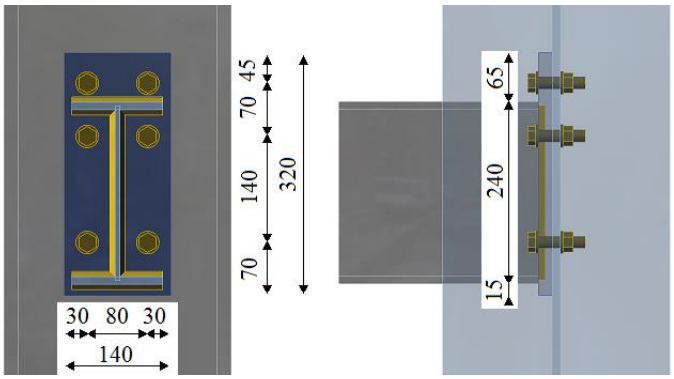

Fig. 5.3.1 Joint geometry

5.3.2 Analytical model

Three components, which are guiding the behavior, are the end plate in bending, the beam flange in tension and in compression, and the column web in bending. The end plate and the beam flange in tension and in compression are designed according to EN 1993-1-8:2005. The behavior of the column web in bending is predicted according to (Steenhuis et al. 1998). The results of experiments of the beam to column minor axis joints, e.g. (Lima et al. 2009), show good prediction of this type of joint loaded in-plane of a connected beam.

5.3.3 Numerical model

Assessment is based on the maximum strain given according to EN 1993-1-5:2006 by the value of 5 %. Detailed information about CBFEM model is summarized in Chapter 3.

5.3.4 Verification of resistance

The sensitivity study of the joint resistance was prepared for column cross-sections. Joint geometry is shown in Fig. 5.3.1. In Tab. 5.3.1 and in Fig. 5.3.2, the results of calculations in case of enlarging end plate P18 relatively with the column section are summarized.

Tab. 5.3.1 Results of prediction of the of end plate minor axis connection for different rafters

Column HEB	200	240	280	300	320	340	360	400	450	500	600	700	800	900	1000
CM	40	35	31	32	33	34	36	38	38	39	42	48	49	52	54
CBFEM	34	32	31	32	32	34	35	39	38	38	40	44	44	47	48
CM/CBFEM	1,14	1,06	0,97	1,0	1,00	1,00	1,03	0,95	1,00	1,00	1,05	1,09	1,11	1,11	1,13

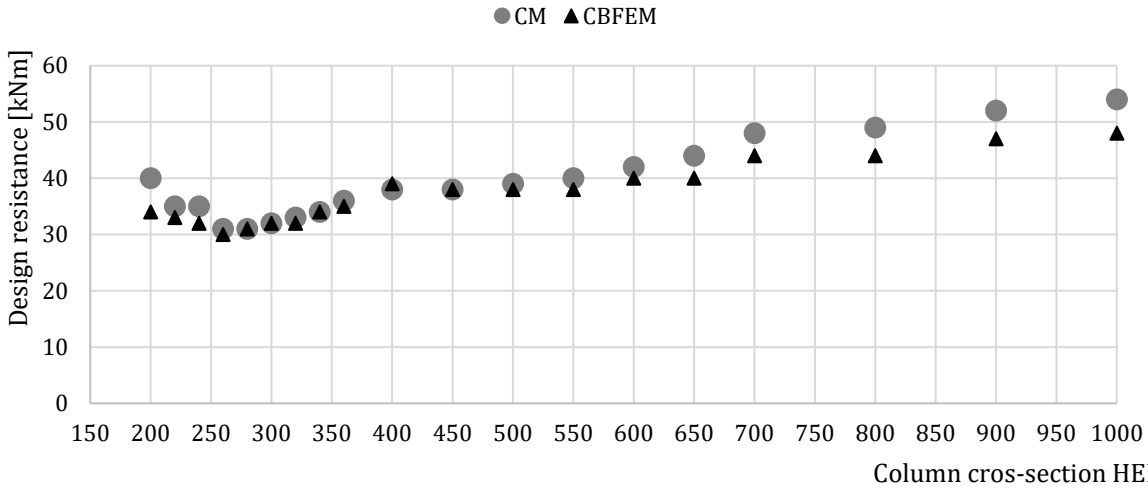

Fig. 5.3.2 Comparison resistance of end plate minor axis connection predicted by CBFEM and CM

5.3.5 Global behavior

Global behavior is presented on force-deformation curve. Beam IPE 240 is connected to column HEB 300 with six bolts M16 8.8. End plate geometry is shown in Fig. 5.3.1 and in Tab. 5.3.1. Comparison of both methods results is presented in Fig. 5.3.3 and in Tab.5.3.2. Both methods predict similar design resistance. CBFEM generally gives lower initial stiffness compared to CM.

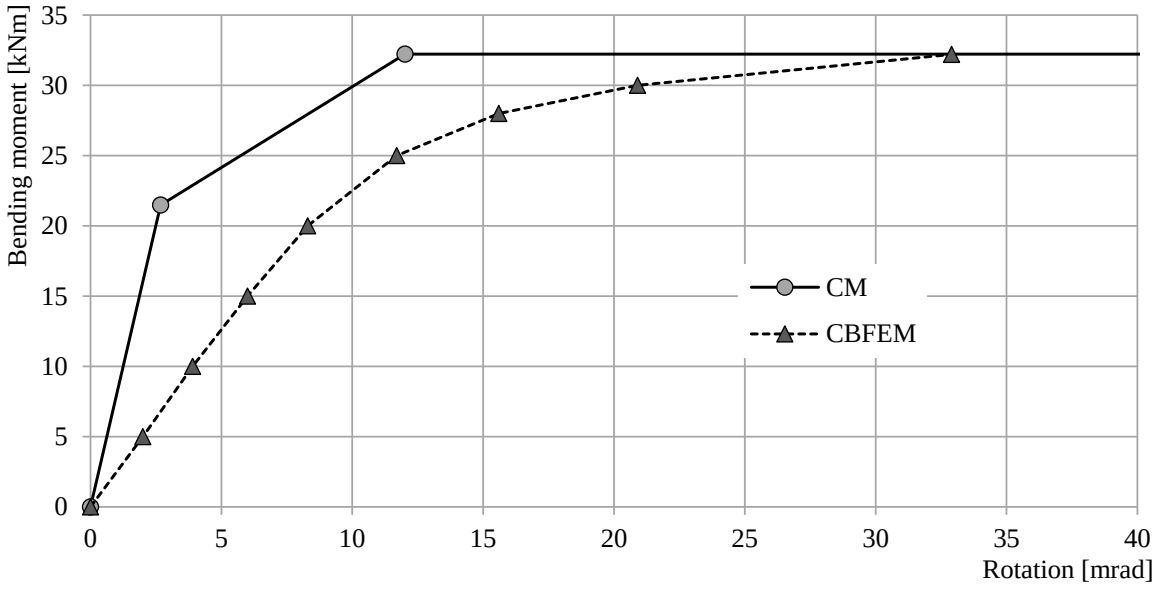

Fig. 5.3.3 Prediction of behavior of end plate minor axis connection on moment rotational curve

Tab. 5.3.2 Main characteristics for global behavior

		CM	CBFEM	CM/CBFEM
Initial stiffness	[kNm/rad]	8013	2300	3,48
Design resistance	[kNm]	32	32	1,00
Deformation capacity	[mrad]	-	34	-

The results of studies are summarized in the graph comparing resistances by CBFEM and component method; see Fig. 5.3.4. The results show that the difference between methods is up to 14 %. CBFEM predicts in all cases lower resistance compared to CM, which is based on simplification in (Steenhuis et al. 1998). Similar results may be observed in work by (Wang and Wang, 2012).

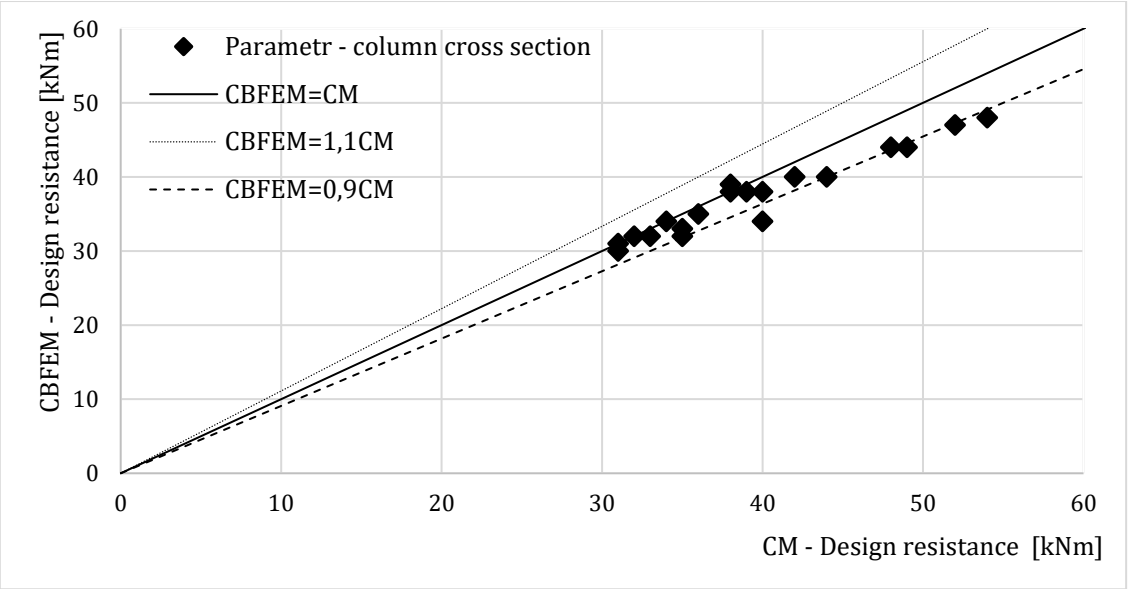

Fig. 5.3.4 Summary of verification of CBFEM to CM for the end plate minor axis connection

5.3.6 Benchmark example

The benchmark case is prepared for the end plate minor axis connection according to Fig. 5.3.1 with modified geometry as summarized below.

Inputs

- Steel S235
- Column HEB 300
- Beam IPE 240
- Bolts 6×M16 8.8
- Welds thickness 5 mm
- End-plate thickness t_p = 18 mm

Outputs

- Design resistance in bending M_{Rd} = 32,4 kNm
- Governing component – column web in bending

5.4 Generally loaded end plate

5.4.1 Description

Component-based finite element method (CBFEM) of the generally loaded end plate joint is verified with component method (CM). The end plate joints of hollow section beams were loaded with a combination of bending moments and shear forces to both axes.

5.4.2 Experimental investigation

Experimental investigation of three samples of end plate joints was performed. End plates were welded on two RHS 250×150×16 beams of different lengths, 2000 mm and 1000 mm. The beams and plates were designed from steel grade S355, with measured values of $f_{y,m}$ = 410 MPa and $f_{u,m}$ = 582 MPa. The end plates P10 – 400 × 300 were connected by M20 8.8 bolts, with the vertical distances 35 – 230 – 100 – 35 mm and horizontal ones 30 – 240 – 30 mm. The beam with connection 500 mm from its center was loaded in its center through P20 by a hydraulic jack; see Fig. 5.4.1. The configuration creates shear forces and bending moments in the connection. The results of the contact imprints on paper placed between the end plates are included on right side of the figure; see (Wald et al. 2016). The inclination of the specimens varied from 0°; 30° till 45°. The test set-up with 0° inclination is documented in Fig. 5.4.2.

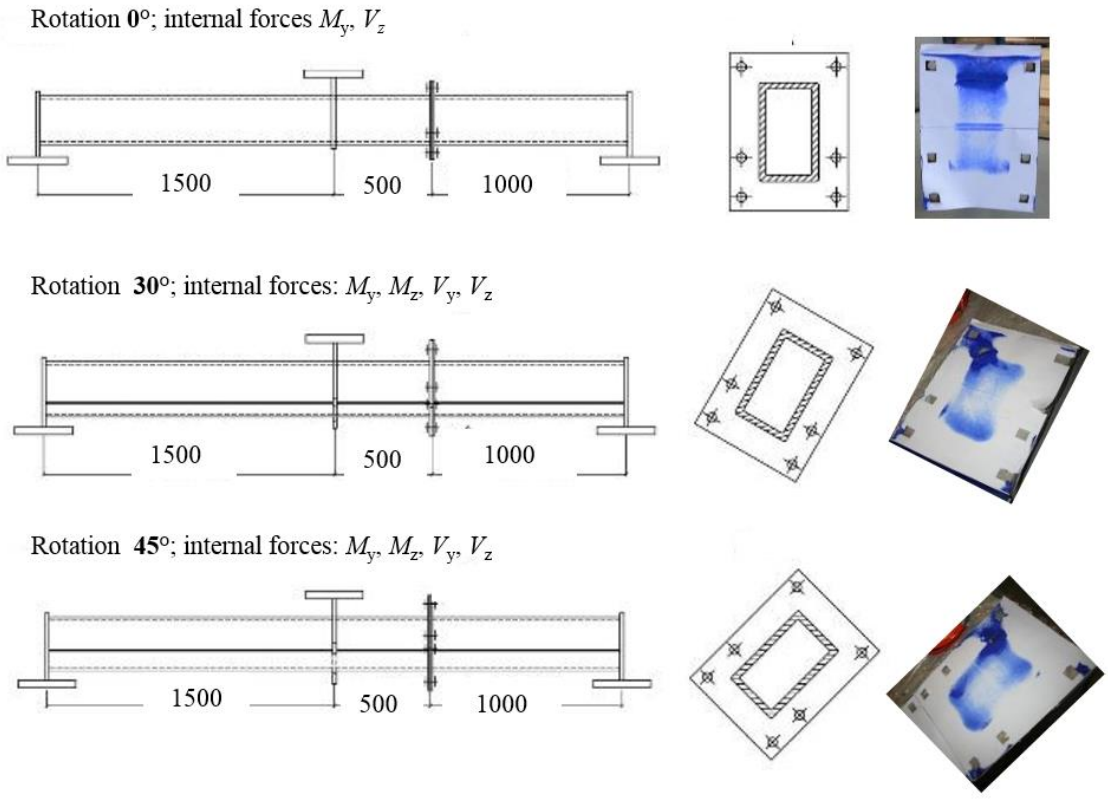

Fig. 5.4.1 Position of the beam splice joins on beam, inclination, and contact imprints

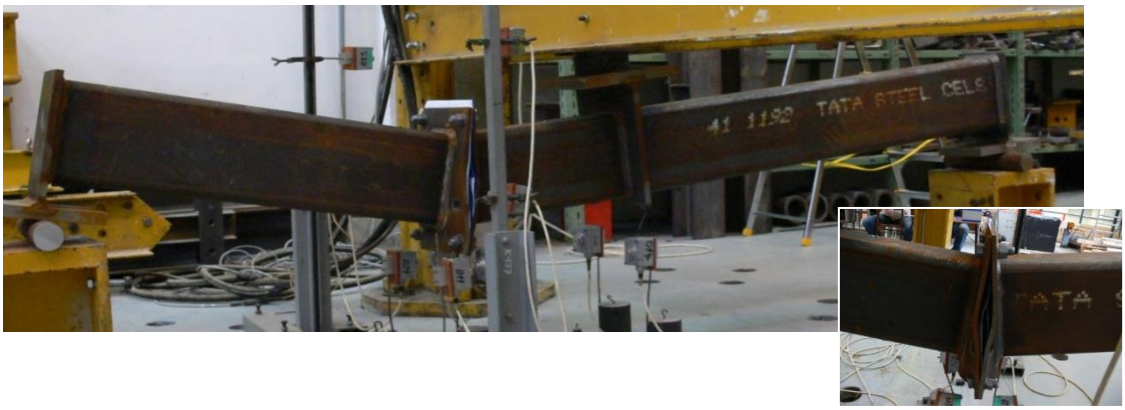

Fig. 5.4.2 The test sample with 0° inclination

5.4.3 Analytical model

The connections were designed according to EN 1993-1-8:2005. Four components are guiding the behavior: fillet welds, beam flange in compression and in tension, end plate in bending, and bolts in tension. Effective lengths for circular and noncircular failures are considered according to EN 1993-1-8:2005, Cl. 6.2.6. Three modes of collapse according to EN 1993-1-8:2005, Cl. 6.2.4.1 are considered. Bolts are designed according to Cl. 3.6.1 in EN 1993-1-8:2005. Design resistance considers punching shear resistance and rupture of the bolt. A linear interaction is recommended in EN 1993-1-8:2005 for component method. The quadratic interaction curve according to Neumann (2014) is included in the verification study.

5.4.4 Verification of resistance

Resistance calculated by CBFEM was compared with the results of CM and experimental results. The sensitivity study was focused on the ratio of bending moments in strong and week axis; see Fig. 5.4.4. CM with linear interaction gives conservative values of resistance. CM with quadratic interaction gives the highest resistances, which are still rather conservative to experimental results. CBFEM gives similar results as CM with quadratic interaction.

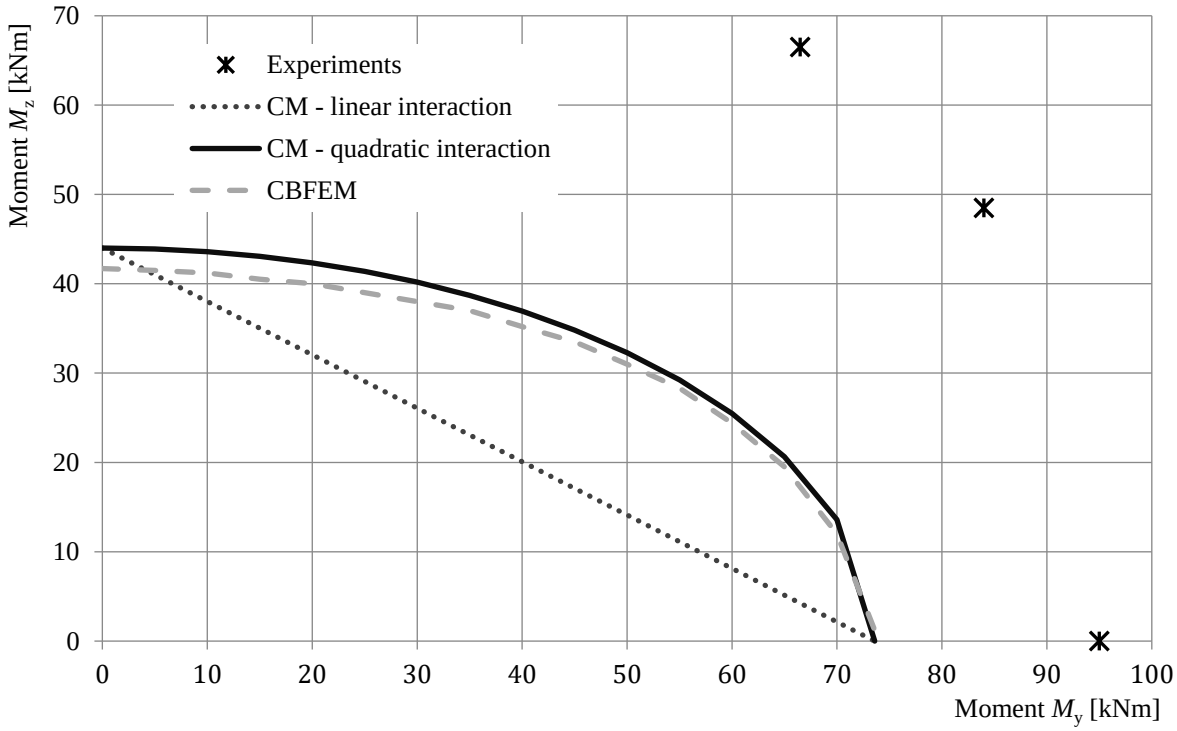

Fig. 5.4.4 Sensitivity study of the bending moment ratio

5.4.5 Global behavior

Comparison of the global behavior described by moment-rotation diagram was prepared. Attention was focused on initial stiffness, resistance, and deformation capacity. Sample 0° with strong axis bending moment was chosen as a reference; see Fig. 5.4.5 and Tab. 5.4.1. The comparison shows the overestimation of the initial stiffness by CM, which is often emphasized in the literature, e.g. in Dubina D., Iványi M (1999) and Bursi O.S., Jaspart J.P. (1997). In all cases resistances by CM and CBFEM are similar, and experimentally measured resistances are higher than both.

Tab. 5.4.1 Global behavior overview

		CM	CBFEM	Experiment	CM/CBFEM	Exp./CBFEM
Initial stiffness	[kNm/rad]	15675	2290	3350	6,84	1,46
Design resistance	[kNm]	69	65	95	1,06	1,46
Deformation capacity	[mrad]	31	50	116	0,62	2,32

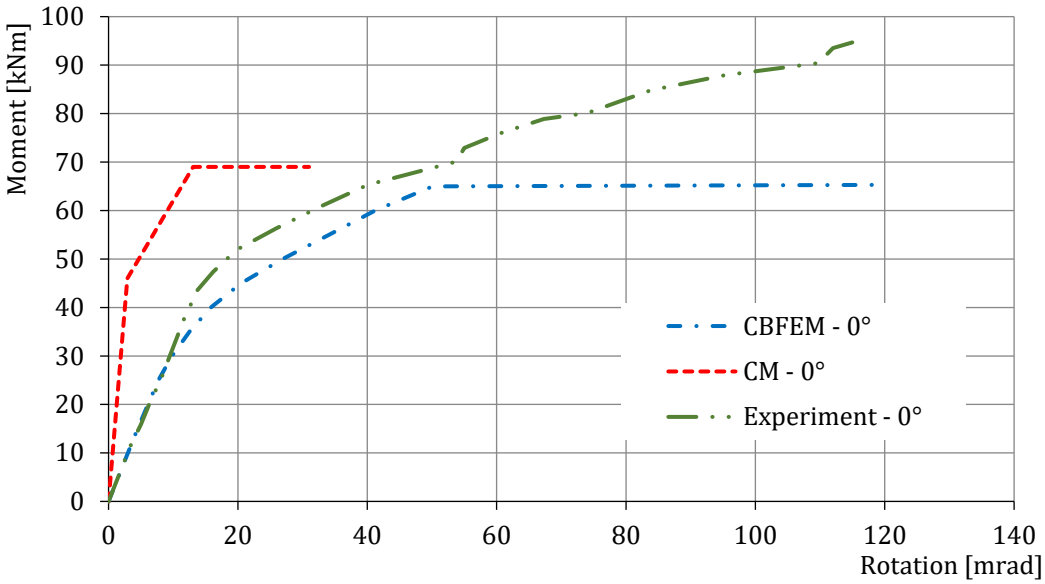

Fig. 5.4.5 Moment-rotational diagram in case of 0° rotation

5.4.6 Benchmark example

Inputs

Beam, see Fig. 5.4.6

- Steel S355
- Cross-section RHS 250×150×16

End plate

- Bolts 6 × M20 8.8
- Vertical distances of the bolts 35 – 230 – 100 – 35 mm
- Horizontal distances 30 – 240 – 30 mm
- End plate thickness 10 mm
- Fillet weld throat thickness 8 mm

Outputs

- Resistance in bending $M_{y,\mathrm{Rd}}$ = 65 kNm
- Vertical shear load V_{Ed} = 65 kN
- Critical component: bolts in tension in the second row

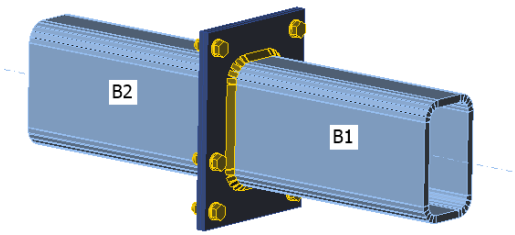

Fig. 5.4.6 Benchmark example for the generally loaded end plate joint in case of 0° rotation

5.5 Interaction of shear and tension

5.5.1. Description

The objective of this chapter is a verification of the component-based finite element method (CBFEM) for the interaction of shear and tension in a bolt to an analytical model (AM). A beam-to-beam joint with end plates and two rows of bolts was selected for verification; see Fig. 5.5.1. The bending stiffness of the joint is high enough to be classified as rigid.

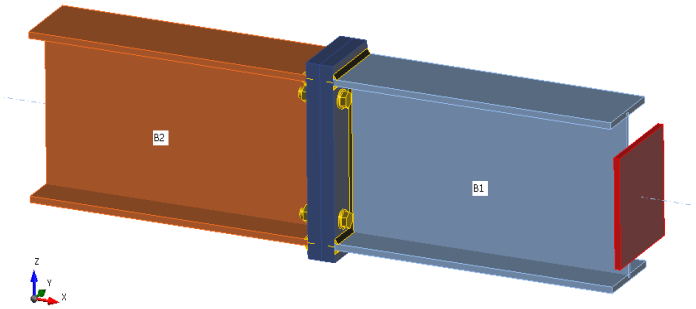

Fig. 5.5.1 Joint arrangement of bolted beam-to-beam joint

5.5.2. Analytical model

Bolt resistance in interaction of shear and tension is designed according to Tab. 3.4 in chapter 3.6.1 in EN 1993-1-8:2005. A bilinear relation is used. The geometry and the end plate dimensions of the joint are selected to limit the design resistance of the joint by bolt failure. The design resistance of equivalent T-stub in tension is modeled according to Tab. 6.2 in chapter 6.2.4 in EN 1993-1-8:2005.

5.5.3. Verification of resistance

Parameters of the model are a bolt diameter and a beam dimension; see Figs 5.5.2 to 5.5.5. Dimensions of the end plate and the bolt distances are modified to limit the joint resistance by the bolt failure. The shear and bending resistance of the joint is compared in loading at the bolt failure. The results are summarised in Tab. 5.5.1 and 5.5.2.

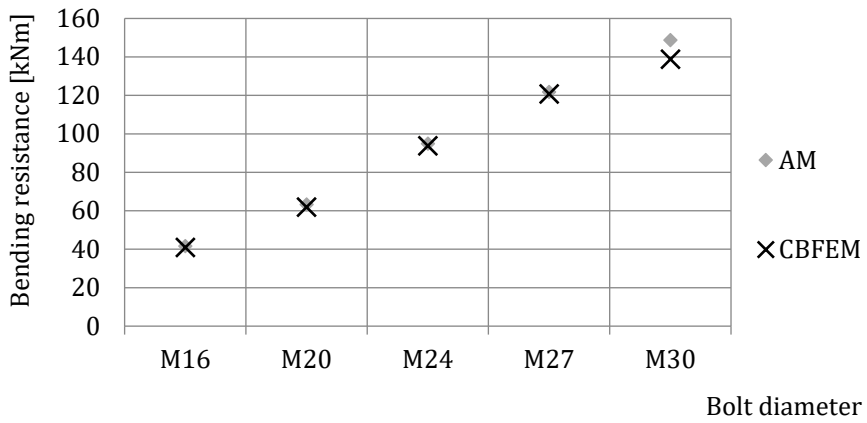

Fig. 5.5.2 Sensitivity study for resistance in bending with variation of bolt diameter

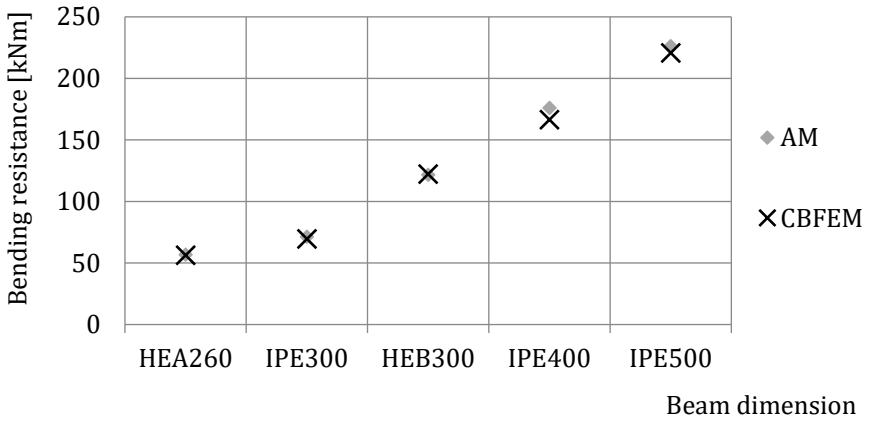

Fig. 5.5.3 Sensitivity study for resistance in bending with variation of beam dimension

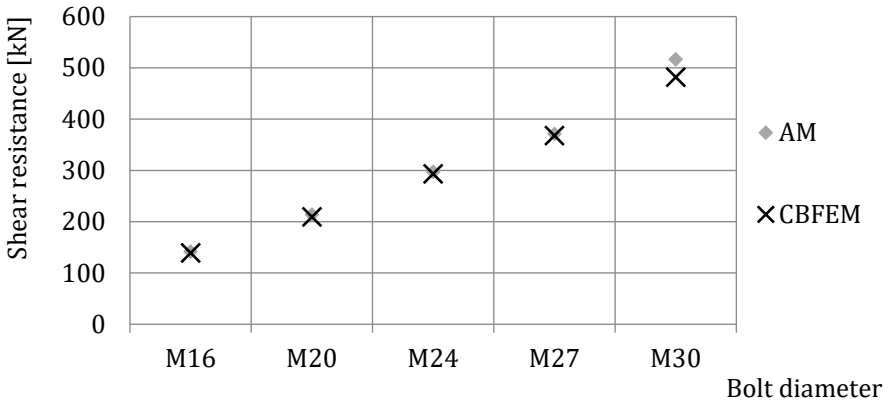

Fig. 5.5.4 Sensitivity study for resistance in shear with variation of bolt diameter

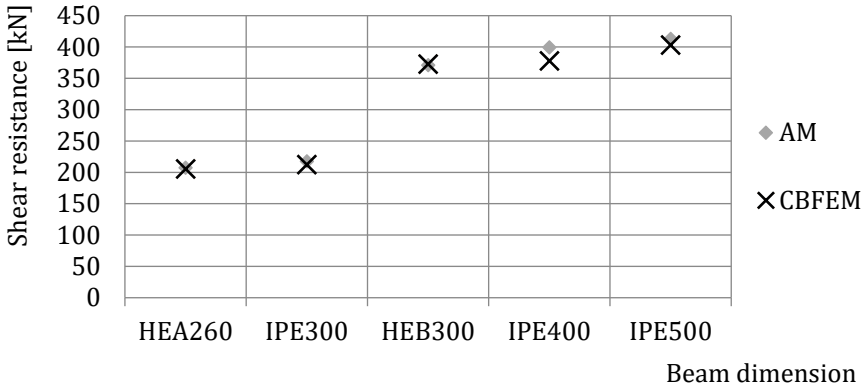

Fig. 5.5.5 Sensitivity study for resistance in shear with variation of beam dimension

Tab. 5.5.1 Sensitivity study for resistance with variation of bolt diameter

Parameter			AM		CBFEM		AM/CBFEM	
			Resistance		Resistance			
Beam; end plate	Diameter	Distances	M_{Rd} [kNm]	V_{Rd} [kN]	M_{Rd} [kNm]	V_{Rd} [kN]	M_{Rd}	V_{Rd}
IPE270; t_p = 30mm; 150×310mm	M16/8.8	e_1 = 60 mm; p_1 = 190 mm; w_1 = 30mm; w = 90 mm	42	142	41	140	1,02	1,02
	M20/8.8	e_1 = 70 mm; p_1 = 170 mm; w_1 = 50 mm; w = 90 mm	63	213	62	209	1,02	1,02
HEA300; t_p = 40mm; 300×330mm	M24/8.8	e_1 = 85 mm; p_1 = 160 mm; w_1 = 75 mm; w = 150 mm	95	297	94	294	1,01	1,01
	M27/8.8	e_1 = 95 mm; p_1 = 140 mm; w_1 = 75 mm; w = 150 mm	122	371	121	368	1,01	1,01
	M30/8.8	e_1 = 95 mm; p_1 = 140 mm; w_1 = 75 mm; w = 150 mm	145	516	139	482	1,07	1,07

Tab. 5.5.2 Sensitivity study for resistance with variation of the beam dimension

Parameter			AM Resistance		CBFEM Resistance		AM/CBFEM	
Beam; fin plate	Diameter	Distances	M_{Rd} [kNm]	V_{Rd} [kN]	M_{Rd} [kNm]	V_{Rd} [kN]	M_{Rd}	V_{Rd}
HEA260; t_p = 25mm; 260×290mm	M20/8.8	e_1 = 75 mm; p_1 = 140 mm; w_1 = 65 mm; w = 130 mm	57	207	56	205	1,01	1,01
IPE300; t_p = 30mm; 150×340mm	M20/8.8	e_1 = 70 mm; p_1 = 200 mm; w_1 = 35 mm; w = 90 mm	71	217	69	212	1,02	1,02
HEB300; t_p = 40mm; 300×340mm	M27/8.8	e_1 = 100 mm; p_1 = 140 mm; w_1 = 75 mm; w = 150 mm	122	371	122	373	1,00	1,00
IPE400; t_p = 45mm; 210×460mm	M27/8.8	e_1 = 105 mm; p_1 = 250 mm; w_1 = 40 mm; w = 130 mm	176	399	167	378	1,06	1,06
IPE500; t_p = 45mm; 220×560mm	M27/8.8	e_1 = 105 mm; p_1 = 350 mm; w_1 = 40 mm; w = 120 mm	226	413	221	403	1,02	1,02

The results of sensitivity studies are summarized in graphs in Fig. 5.5.6 and 5.5.7. The results show that the differences between the two calculation methods are below 10 %. The analytical model gives generally higher resistance.

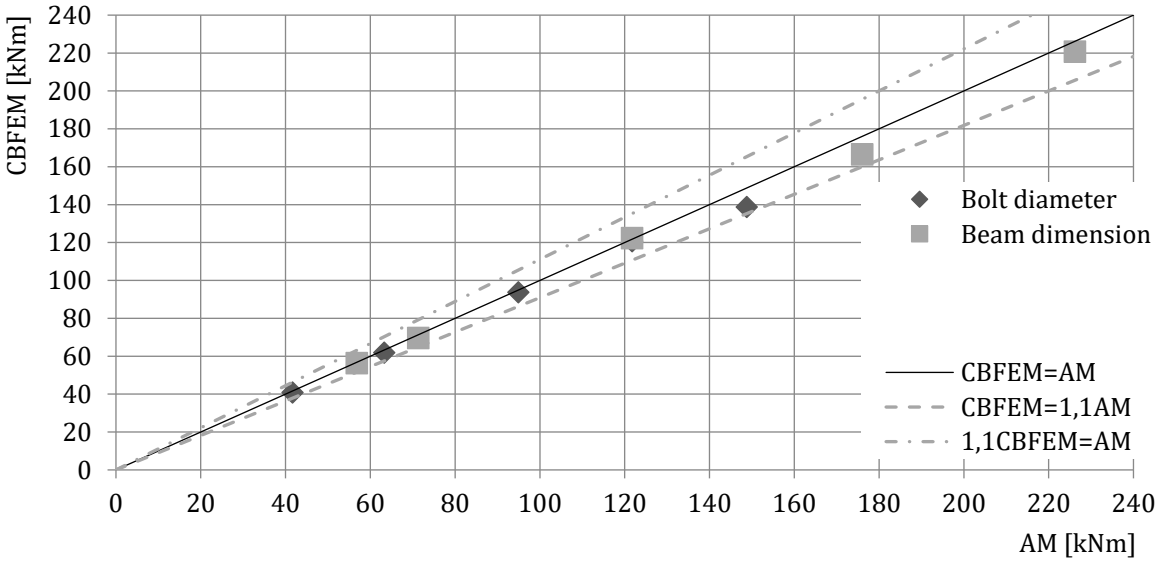

Fig. 5.5.6 Verification of CBFEM to AM for the interaction of shear and tension in bolt in case of loading to bending resistance of a joint

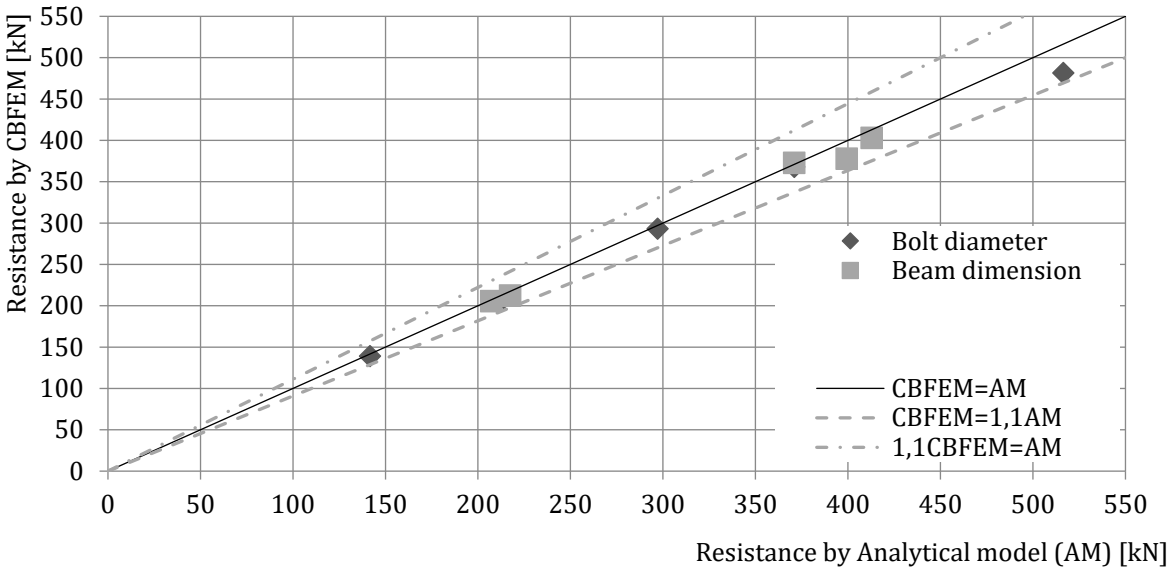

Fig. 5.5.7 Verification of CBFEM to AM for the interaction of shear and tension in bolt in case of loading to shear resistance of a joint

5.5.4. Benchmark example

Inputs

Connected members

- Steel S355
- Beams HEA300
- End plate thickness t_p = 40 mm
- End plate dimensions 300 × 330 mm

Bolts

- 4 × M24 8.8
- Distances e_1 = 85 mm; p_1 = 160 mm; w_1 = 75 mm; w = 150 mm

Outputs

- Design resistance in bending M_{Rd} = 94 kNm
- Design resistance in shear V_{Rd} = 294 kNm
- Collapse mode is bolt failure in interaction of shear and tension

5.6 Splices in shear in slip-resistant connection

5.6.1. Description

This study is focused on the verification of component-based finite element method (CBFEM) for the resistance of the symmetrical double splice slip-resistant connection to an analytical model (AM).

5.6.2. Analytical model

The slip resistance of a preloaded bolt is designed according to chapter 3.9.1 in EN 1993-1-8:2005. The preloading force is taken at 70 % of the ultimate strength of a bolt according to equation (3.7).

5.6.3. Verification of resistance

Design resistances calculated by CBFEM are compared with the results of analytical model (AM); see (Wald et al. 2018). The results are summarized in Tab. 5.6.1. The parameter is bolt diameter; see Fig. 5.6.1.

Tab. 5.6.1 Comparison of bolt resistance predicted by FE model to analytical one for bolt diameter

Parameter		Analytical Model (AM)		CBFEM		AM/ CBFEM
		Resist. [kN]	Critical component	Resist. [kN]	Critical component	
Diam.	Distances	Joint: splice 200/12 mm, bolts 2 × M× 8.8, plates 2 × 200/20 mm, steel S235				
M16	p = 55 e_1 = 40	211	Slip	205	Slip	1,03
M20	p = 70 e_1= 50	329	Slip	320	Slip	1,03
M24	p = 80 e_1 = 60	474	Slip	457	Slip	1,04
M27	p = 90 e_1 = 70	617	Slip	594	Slip	1,04
M30	p = 100 e_1 = 75	754	Slip	727	Slip	1,04

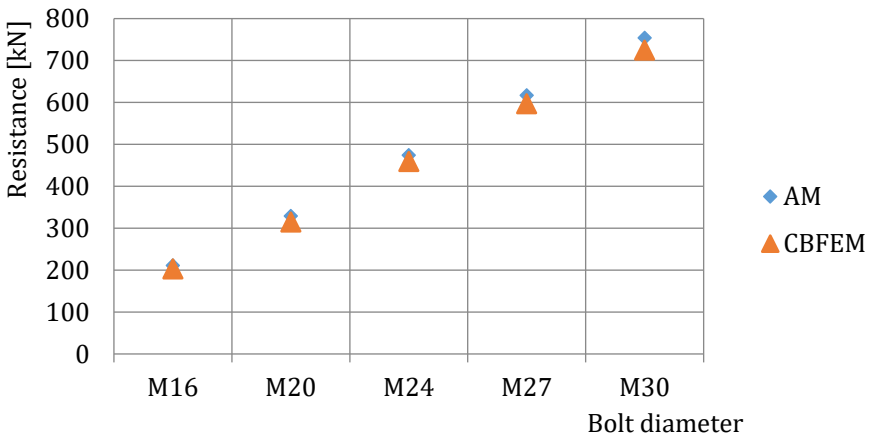

Fig. 5.6.1 Sensitivity study for the bolt diameter

The results of sensitivity studies are summarized in the graph in Fig. 5.6.2. The results show that the differences between the two calculation methods are below 5 %. Analytical model gives generally higher resistance.

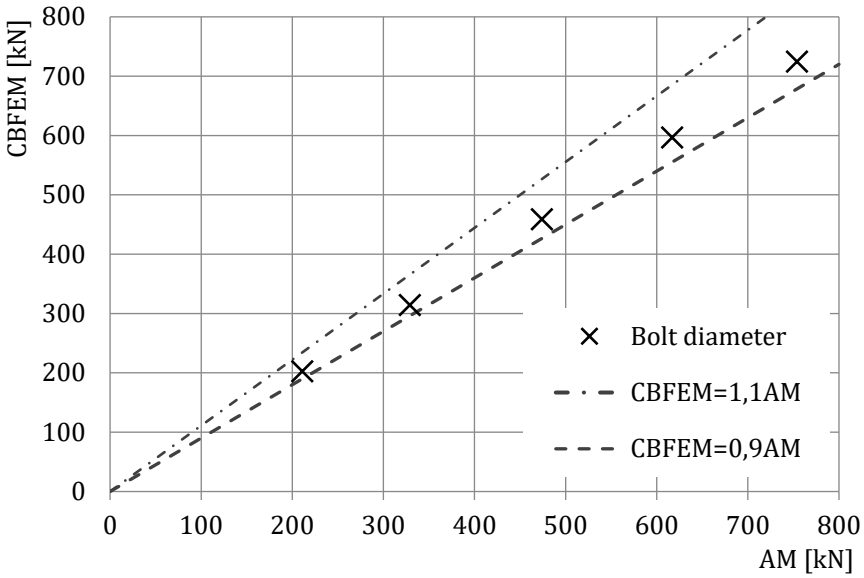

Fig. 5.6.2 Verification of CBFEM to AM for the slip-resistant double splice connection

5.6.4. Benchmark example

Inputs

Connected member

- Steel S235
- Splice 200×12 mm

Connectors

Bolts

- 3 × M20 8.8
- Distances e_1 = 50 mm, p = 70 mm

Two splices

- Steel S235
- Plate 240×200×20 mm

Outputs

- Design resistance F_{Rd} = 320 kN
- Design failure mode is slip of the bolts

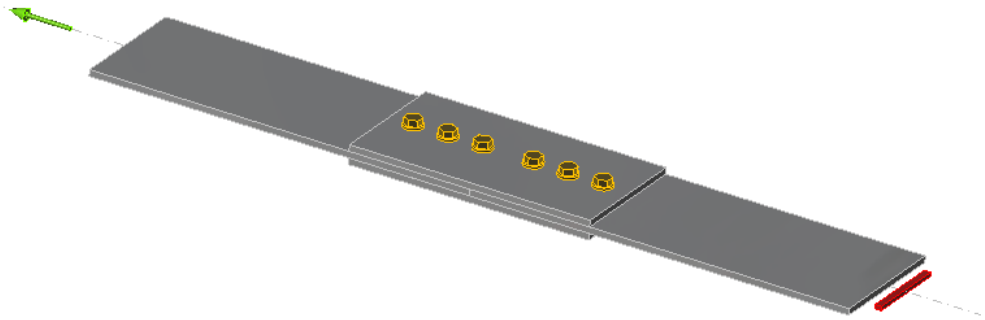

Fig. 5.6.3 Benchmark example of the bolted splices in shear

5.7 Block shear resistance

5.7.1 Description

This chapter is focused on the verification of component-based finite element method (CBFEM) for the resistance of block shear resistance of bolted connection loaded in shear to the validated research-oriented finite element model (ROFEM) and major analytical models (AM).

5.7.2 Analytical models

There are several analytical models for block shear resistance of bolted connection. The models from codes EN 1993-1-8:2005, EN 1993-1-8:2020, AISC 360-10, and CSA S16-9 are investigated. Furthermore, analytical models by Driver et al. (2005) and Topkaya et al. (2004) are used in comparison.

$$V_{\mathrm{eff,1,Rd}} = \frac{f_{\mathrm{u}} A_{\mathrm{nt}}}{\gamma_{\mathrm{M2}}} + \left(\frac{1}{\sqrt{3}}\right) f_{\mathrm{y}} A_{\mathrm{nv}} / \gamma_{\mathrm{M0}}$$ concentric loading (EN 1993-1-8:2005)

$$V_{\mathrm{eff,2,Rd}} = 0{,}5 \cdot \frac{f_{\mathrm{u}} A_{\mathrm{nt}}}{\gamma_{\mathrm{M2}}} + \left(\frac{1}{\sqrt{3}}\right) f_{\mathrm{y}} A_{\mathrm{nv}} / \gamma_{\mathrm{M0}}$$ eccentric loading (EN 1993-1-8:2005)

$$V_{\mathrm{eff,1,Rd}} = \left[A_{\mathrm{nt}} f_{\mathrm{u}} + \min\left(\frac{A_{\mathrm{gv}} \cdot f_{\mathrm{y}}}{\sqrt{3}}; \frac{A_{\mathrm{nv}} f_{\mathrm{u}}}{\sqrt{3}}\right)\right] / \gamma_{\mathrm{M2}}$$ concentric loading (prEN 1993-1-8:2020)

$$V_{\mathrm{eff,2,Rd}} = \left[0{,}5 A_{\mathrm{nt}} f_{\mathrm{u}} + \min\left(\frac{A_{\mathrm{gv}} \cdot f_{\mathrm{y}}}{\sqrt{3}}; \frac{A_{\mathrm{nv}} f_{\mathrm{u}}}{\sqrt{3}}\right)\right] / \gamma_{\mathrm{M2}}$$ eccentric loading (prEN 1993-1-8:2020)

$$\phi R_{\mathrm{n}} = \phi\big(0{,}6 f_{\mathrm{u}} A_{\mathrm{nv}} + U_{\mathrm{bs}} f_{\mathrm{u}} A_{\mathrm{nt}} \leq 0{,}6 f_{\mathrm{y}} A_{\mathrm{gv}} + U_{\mathrm{bs}} f_{\mathrm{u}} A_{\mathrm{nt}}\big)$$ U_{bs} = 1,0 for concentric and 0.5 for eccentric loading (AISC 360-16)

$$T_{\mathrm{r}} = \phi_{\mathrm{u}} \left[U_{\mathrm{t}} A_{\mathrm{nt}} f_{\mathrm{u}} + 0{,}6 A_{\mathrm{gv}} \frac{f_{\mathrm{y}} + f_{\mathrm{u}}}{2}\right]$$ U_{t} = 1.0 for concentric and 0.5 for eccentric loading (CSA S16-14)

where f_{y} is yield strength, f_{u} is ultimate strength, γ_{M2}, γ_{M2}, ϕ, ϕ_{u} are safety factors. For A_{nt}, A_{nv}, A_{gv} see Fig. 5.7.1.

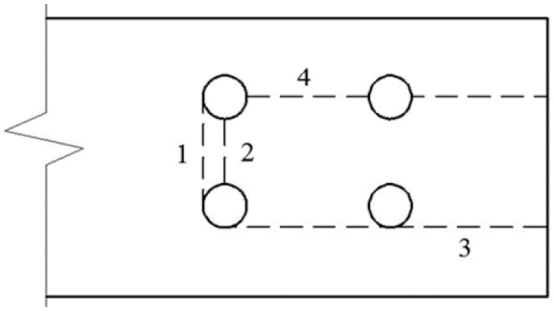

1. Gross tensile plane A_{gt}
2. Net tensile plane A_{nt}
3. Gross shear plane A_{gv}
4. Net shear plane A_{nv}

Fig. 5.7.1 Failure planes during the block shear failure

5.7.3 Validation and verification of resistance

The experiments by Huns et al. (2002) are used for validation of ROFEM created by Sekal (2019) in ANSYS software, see Fig. 5.7.2. True stress-strain material diagram is used. Only the thinnest plate meant to fail are modeled. Bolts are simplified as only bearing displacements on the half-circle of the bolt hole. The displacements in all holes are coupled. The ROFEM model shows very good agreement with the test results.

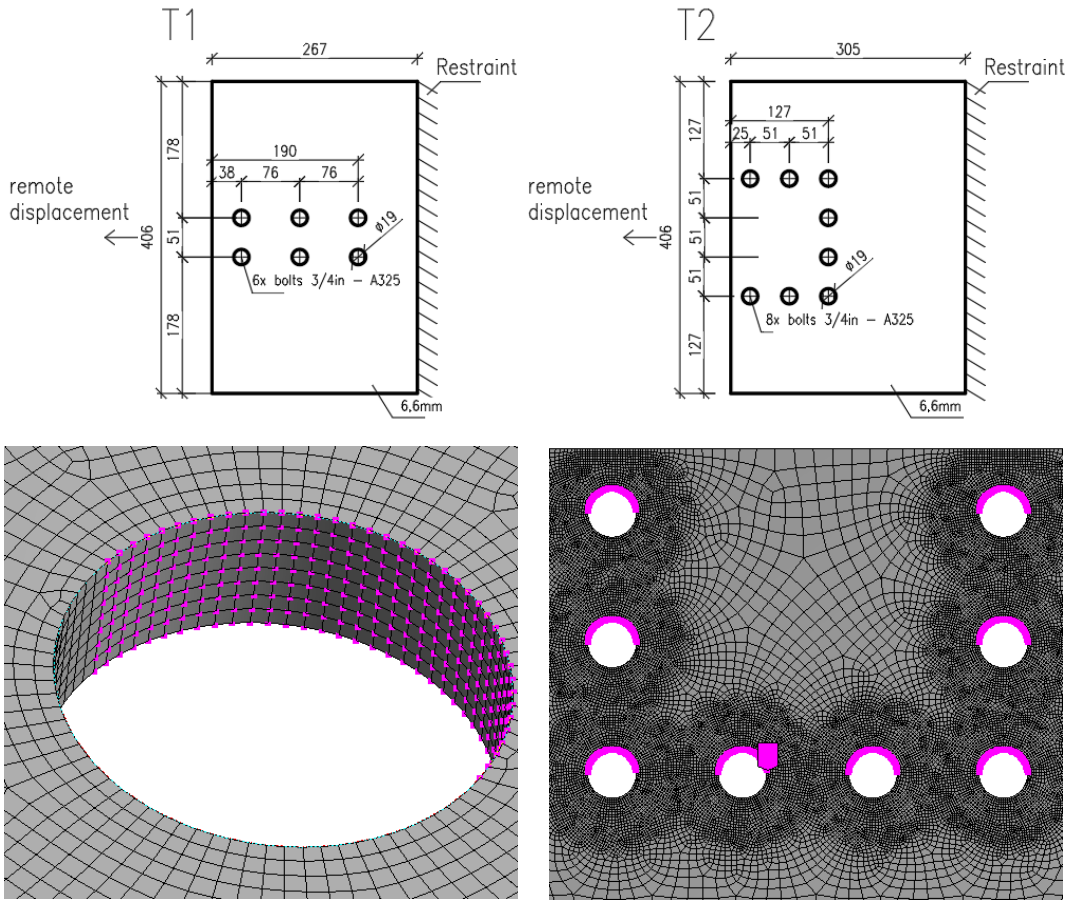

Fig. 5.7.2 ROFEM with fine mesh of the specimens tested by Huns et al. (Sekal, 2019)

Design-oriented CBFEM model uses shell elements with rather coarse mesh. The mesh is predefined near bolt holes. Bolts are modeled as nonlinear springs which are connected to the nodes at the edges of the bolts holes by links. The bilinear material diagram with negligible strain-hardening is used for plates. The limit resistance of a group of bolts in bearing is determined when the plastic strain at the plate reaches 5 % (EN 1993-1-5: 2005). The bearing and hole tear-out resistances of each individual bolt are checked by formulas in appropriate code.

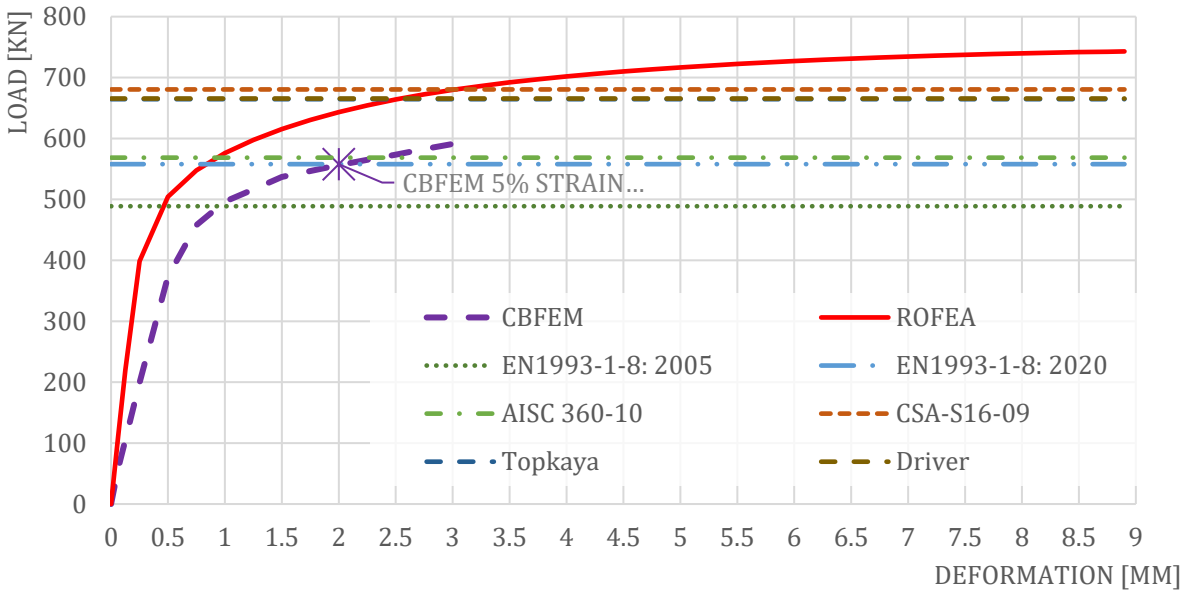

Fig. 5.7.3 Comparison of specimen T2 tested by Huns et al. (Sekal, 2019)

The comparison of ROFEM, CBFEM, and analytical models is shown in Fig. 5.7.3. The most conservative is the model in EN 1993-1-8: 2005 because, unlike other models, it uses the net shear plane in combination with yield strength. Yielding in the gross shear plane is observed in experiments and numerical models. In the next generation of Eurocodes (EN 1993-1-8: 2020), the formula for block shear resistance will be changed. The stiffness of CBFEM model is lower compared to ROFEM. In the experiments, the holes were drilled with the same diameter as bolts, so there was no initial slip. The ROFEM model also disregards any slip, but in CBFEM, the shear model of bolts is approximated with the assumption of the regular bolt holes.

5.7.4 Sensitivity study

Specimen T1 was used for the study how bolt pitch (Fig. 5.7.4) and plate thickness (Fig. 5.7.5) affects the block shear resistance. The models provide expected results. Again, the EN 1993-1-8: 2005 is the most conservative, followed by CBFEM, EN 1993-1-8:2020 and AISC 360-10.

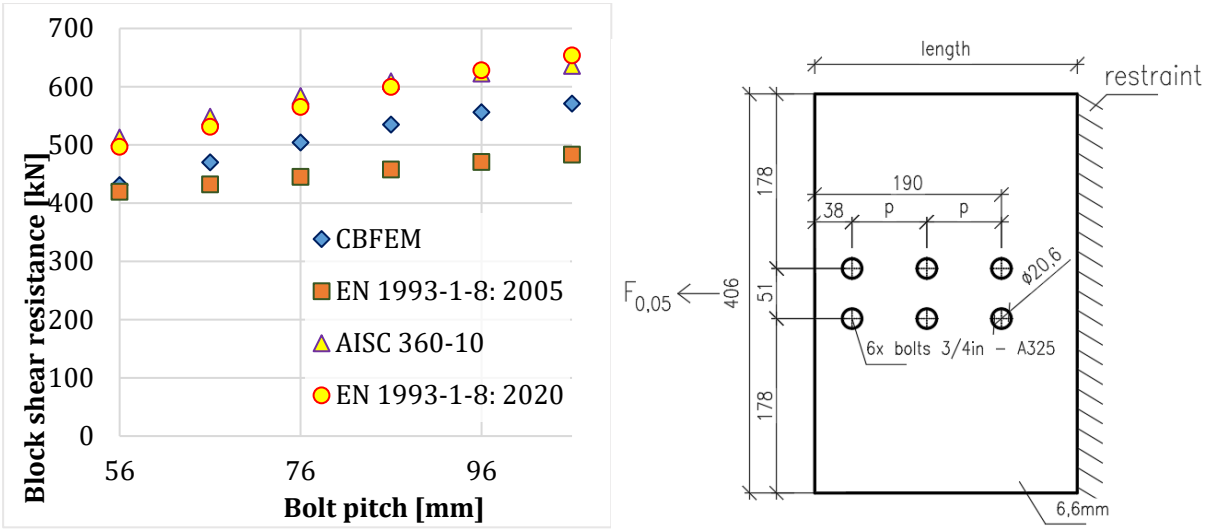

Fig. 5.7.4 Effect of bolt pitch (Sekal, 2019)

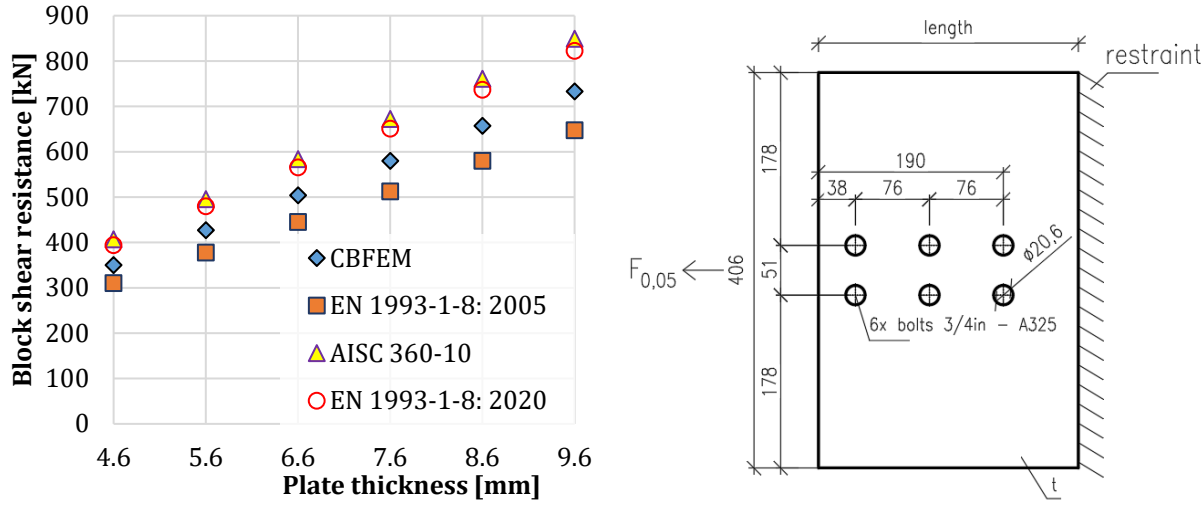

Fig. 5.7.5 Effect of plate thickness (Sekal, 2019)

In the study of eccentrically loaded bolted connection, the steel grade S235 and bolts M22 grade 10.9 are used. Material safety factors are set to 1. The comparison with analytical models is in Fig. 5.7.6. The analytical models used in codes use constant reduction factor regardless of the magnitude of the eccentricity. Topkaya (2004) and Driver (2005) claim that the effect of in plane eccentricity is not crucial for the total resistance (up to 10 % reduction). The results of CBFEM lie between their models and these used in codes.

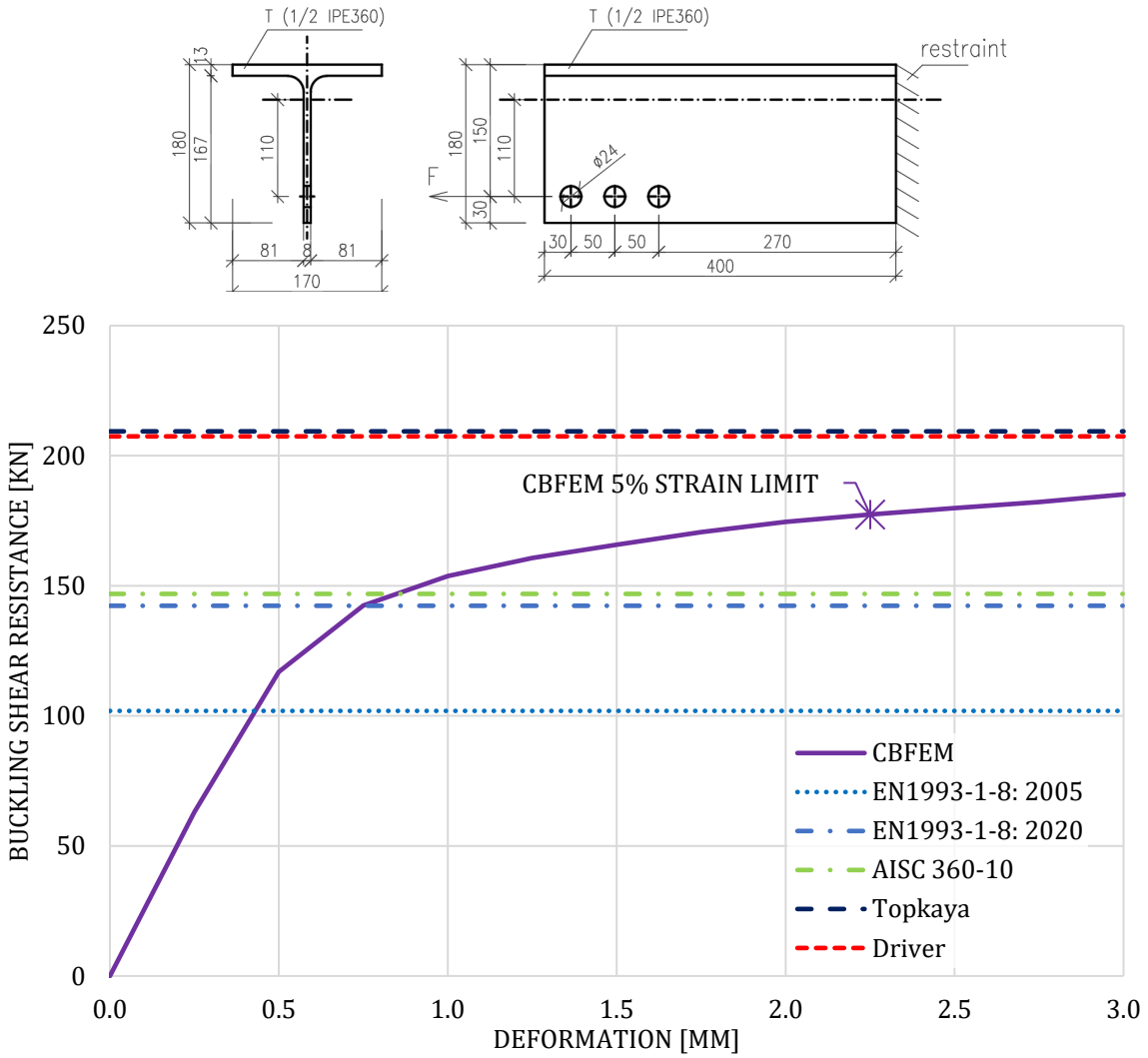

Fig. 5.7.6 Eccentric bolted connection (Sekal, 2019)

19 CBFEM models were created and compared to either two research-oriented finite element models or 6 different analytical models. The currently valid EN 1993-1-8: 2005 is excluded from the comparison. The CBFEM method is conservative for concentric connections but unsafe compared to analytical models for eccentric connections used in Codes; see Fig.5.7.7.

The CBFEM model uses bilinear material diagram with negligible strain-hardening. On the other hand, the analytical models use a combination of yield and ultimate strengths in their formulas. The CBFEM model provides lower block shear resistances compared to the analytical models if steel grade with a high ratio of ultimate to yield strength is used. Mesh refinement slightly decreases the block shear resistance; however, the mesh size near bolt holes is fixed.

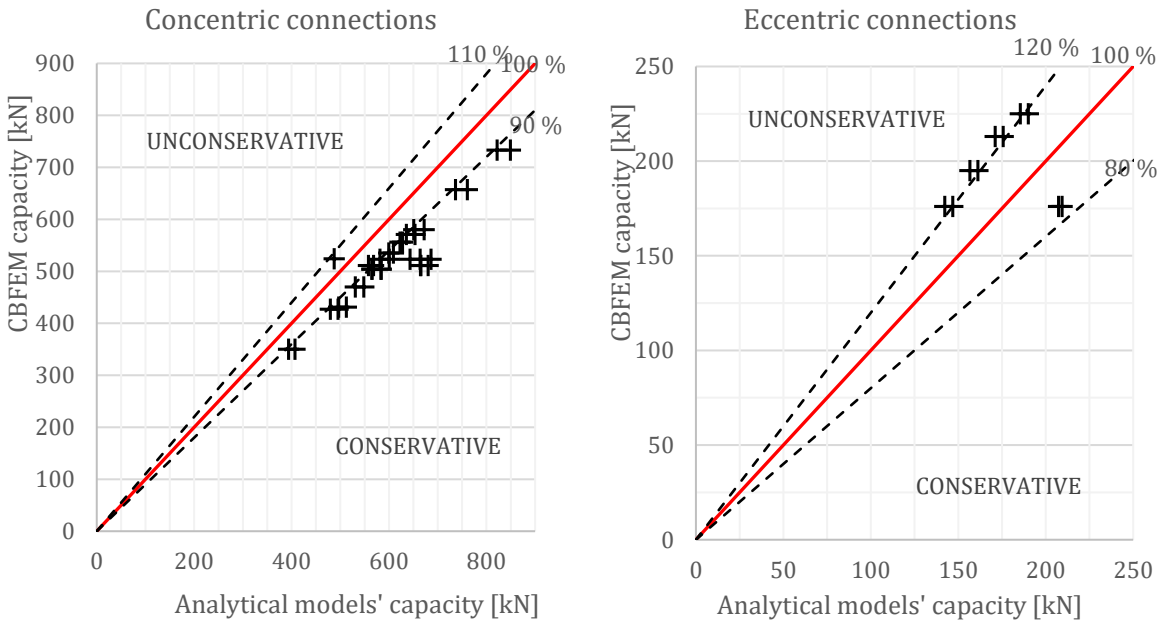

Fig. 5.7.7 Comparison between analytical models and CBFEM (Sekal, 2019)

5.7.5 Benchmark example

Inputs

Steel S235

Member – model type N-Vy-Vz

- 2× UPE 200

Plate – bearing member

- 450×410×8 mm
- Model type N-Vy-Vz

Connectors

Bolts

- 7 × M20 10.9
- Distances e_1 = 45 mm, p_1 = 70 mm, p_2 = 60 mm

Outputs

- Design resistance N_{Rd} = 541 kN
- Critical is plastic strain of gusset plate

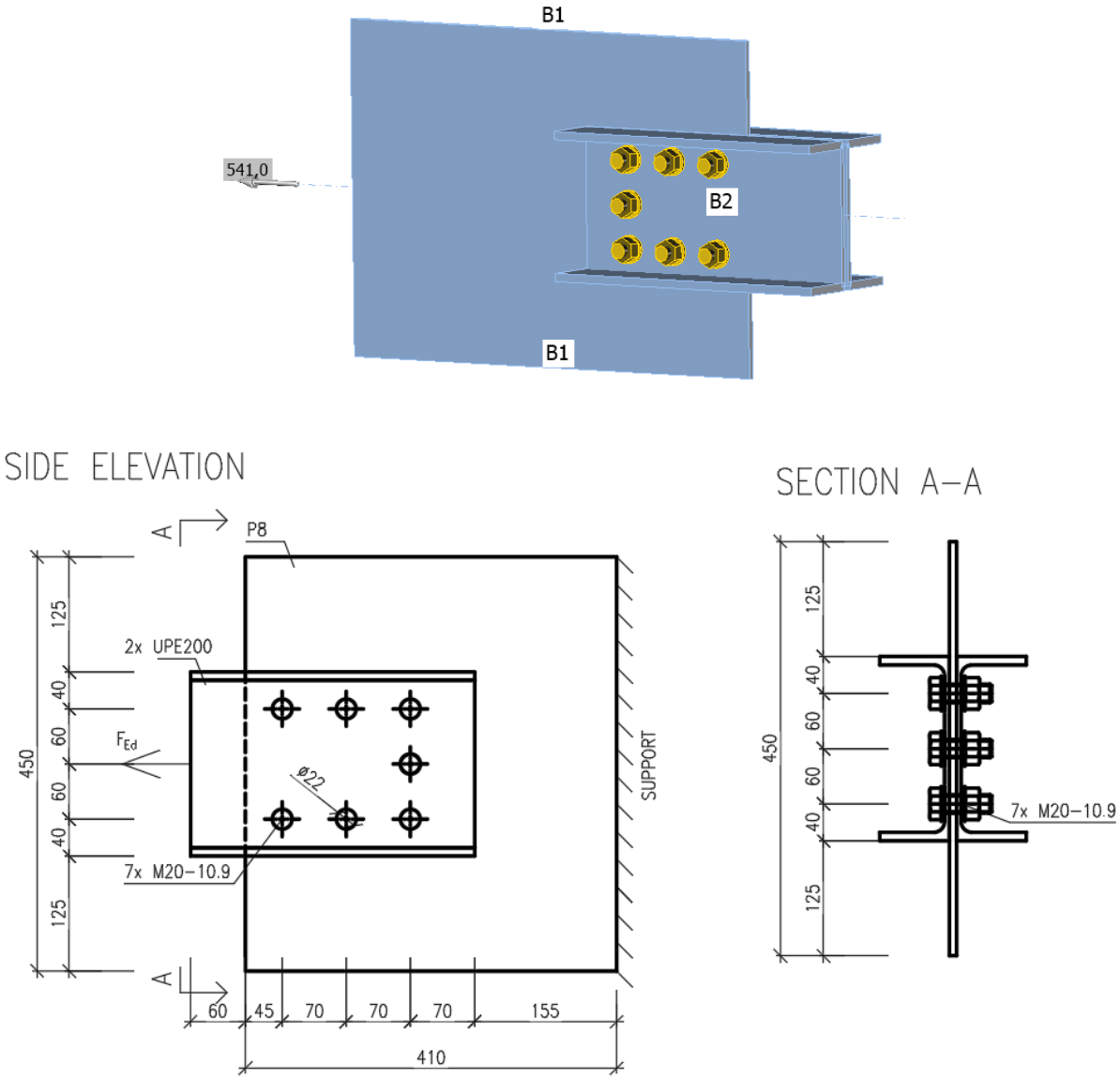

Fig. 5.7.8 geometry of the benchmark example

5.8 End plate connection with four bolts in row

5.8.1 Description

This study is focused on the verification of component-based finite element method (CBFEM) for the resistance of the end plate connection with four bolts in a row to an analytical model (AM), and a research-oriented finite element model (ROFEM) validated on experiments.

5.8.2 Analytical model

The bolt resistance in shear and tension and the plate resistance in bearing and punching shear are designed according to Tab. 3.4, Chapter 3.6.1 in EN 1993-1-8:2006. The equivalent T-stub in tension, according to Chapter 6.2.4, was modified by Jaspart et al. (2010).

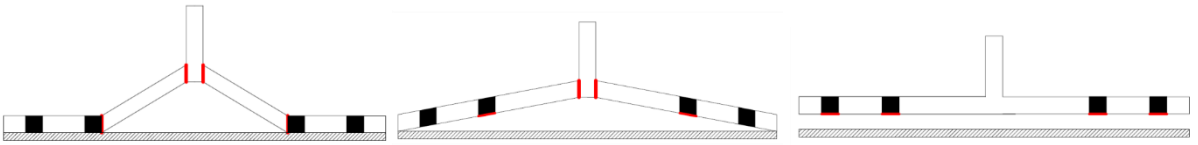

Fig. 5.8.1 Failure modes of T-stub with four bolts in a row: mode 1 (left), mode 2 (middle), mode 3 (right)

Tab. 5.8.1 Failure modes of T-stub with four bolts in a row (Jaspart et al. 2010)

Mode 1	$F_{\mathrm{T,Rd,1}} = \dfrac{(8n - 2e_{\mathrm{w}})M_{\mathrm{pl,1,Rd}}}{2mn - e_{\mathrm{w}}(m+n)}$
Mode 2	$F_{\mathrm{T,Rd,2}} = \min(F_{\mathrm{Rd,2,p}};\ F_{\mathrm{Rd,2,np}})$ $F_{\mathrm{Rd,2,p}} = \dfrac{2M_{\mathrm{pl,2,Rd}} + \frac{\sum F_{\mathrm{t,Rd}}}{2} \cdot \left(\frac{n_1^2 + 2n_2^2 + 2n_1 n_2}{n_1 + n_2}\right)}{(m + n_1 + n_2)}$ $F_{\mathrm{Rd,2,np}} = \dfrac{2M_{\mathrm{pl,1,Rd}} + \frac{\sum F_{\mathrm{t,Rd}}}{2} \cdot n_1}{(m + n_1)}$
Mode 3	$F_{\mathrm{T,Rd,3}} = \sum F_{\mathrm{t,Rd}}$

where $F_{\mathrm{t,Rd}}$ is bolt tensile resistance, $e_{\mathrm{w}} = d_{\mathrm{w}}/4$, d_{w} is the diameter of the washer, or the width across points of the bolt head or nut, as relevant, m, $n = e_1 + e_2$; $n \leq 1.25m$, $n_1 = e_1$, $n_2 = e_2$; $n_2 \leq 1{,}25m + n_1$ see Fig. 5.8.2, $M_{\mathrm{pl,1,Rd}} = 0.25 l_{\mathrm{eff,1}} t_{\mathrm{f}}^2 f_{\mathrm{y}}/\gamma_{\mathrm{M0}}$, $M_{\mathrm{pl,2,Rd}} = 0.25 l_{\mathrm{eff,2}} t_{\mathrm{f}}^2 f_{\mathrm{y}}/\gamma_{\mathrm{M0}}$, l_{eff} is effective length, t_{f} is the flange thickness, and f_{y} is the yield strength.

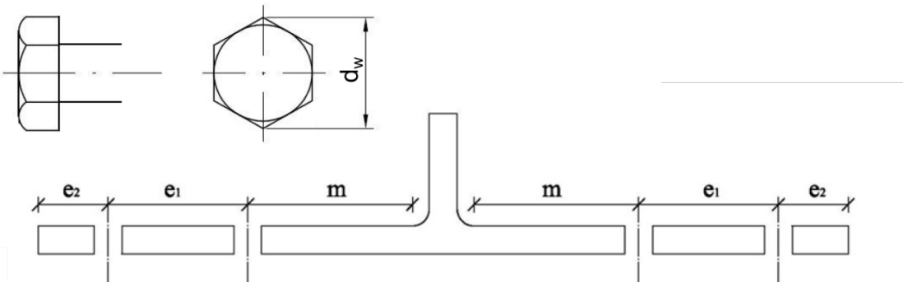

Fig. 5.8.2 T-stub geometry with four bolts in a row

5.8.3 Validation and verification of resistance

Design resistances calculated by CBFEM were compared with the results of the analytical model (Zakouřil, 2019) and experiments with research-oriented finite element model (Samaan et al. 2017); see Fig. 5.8.3. The results are summarised in Fig. 5.8.4. Bolt grade 8.8 and steel grade S450 were used. The yield and tensile strengths correspond closely to the experimental values, e.g. bolt yield strength is 684 MPa, bolt tensile strength is 864 MPa.

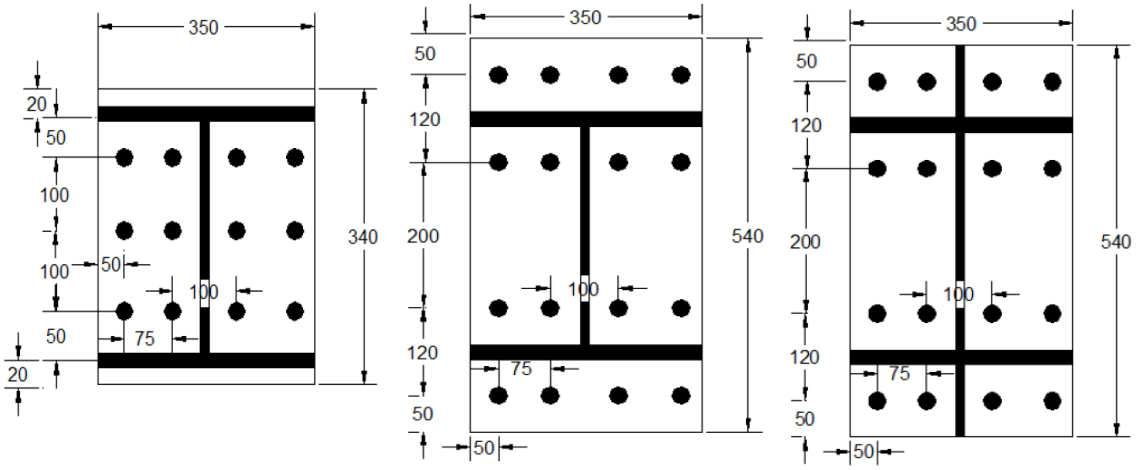

Fig. 5.8.3 Tested specimens – flushed end plate labeled F (left), extended unstiffened end plate labeled ENS (middle), extended stiffened labeled ES (right) – Samaan et al. (2017)

The bending moment resistance determined by CBFEM is usually between resistance determined by component method and experiment. Both component method and CBFEM underestimate the resistance of the specimen with flushed end plate (F20).

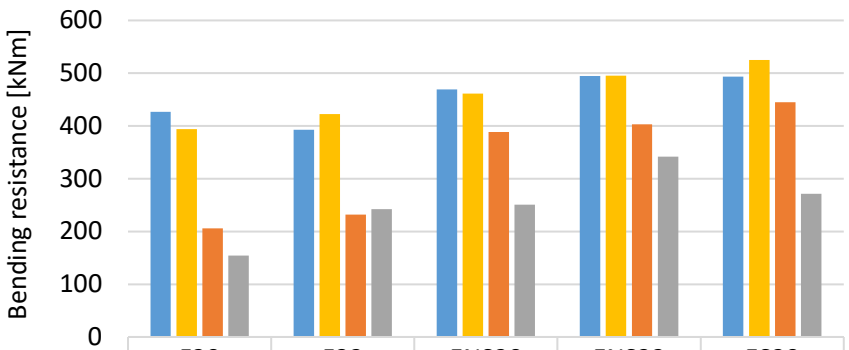

	F20	F32	ENS20	ENS32	ES20
Experiment	427	393	470	495	494
ROFEM	394	422	461	495	525
CBFEM	206	232	389	403	445
CM	154	242	251	342	272

Fig. 5.8.4 Comparisons of bending moment resistances – experimental, ROFEM, CBFEM, and modified component method

5.6.1. Benchmark example

Inputs

Column

- Steel S450
- h = 360 mm, b = 350 mm, t_f = 30 mm, t_w = 12 mm

Beam

- Steel S450
- h = 340 mm, b = 350 mm, t_f = 20 mm, t_w = 12 mm

End plate

- Steel S450
- Plate 540×350×20

Connectors

Bolts

- 16 × M20 8.8
- Distances e_1 = 50 mm, $p_{1,1}$ = 120 mm, $p_{1,2}$ = 200 mm, e_2 = 50 mm, $p_{2,1}$ = 100 mm, $p_{2,2}$ = 75 mm

Outputs

- Design resistance $M_{j,Rd}$ = 389 kNm, corresponding shear force 130 kN
- Critical components are bolts with forces increased by prying of end plate

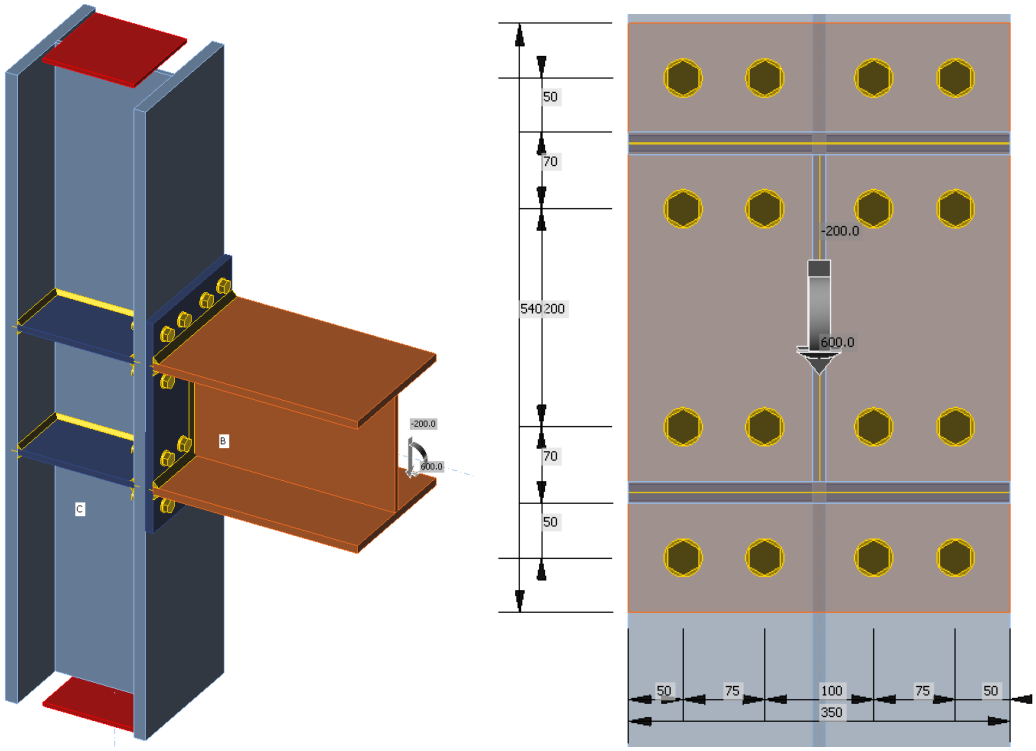

Fig. 5.8.5 Benchmark example of specimen ENS20

5.9 Single sided gusset plate connection

5.9.1 Description

This study is focused on the verification of component-based finite element method (CBFEM) for the resistance of the single-sided gusset plate connection to the research-oriented finite element model (ROFEM) validated on experiments and the analytical models (AM).

5.9.2 Analytical model

The analytical model was designed by Khoo et al. (2009). The collapse mechanism is by two plastic hinges at a gusset plate and a connecting plate.

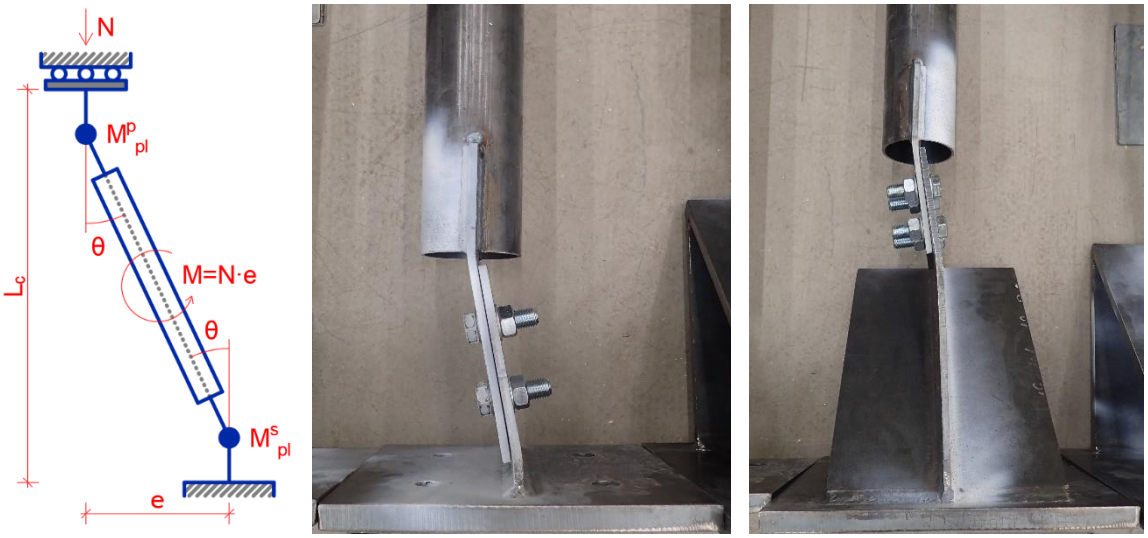

Fig. 5.9.1 Failure mode of single-sided gusset plate connection (Vesecký, 2019)

The resistance of such failure mode is linearly dependent on steel yield strength, length of the plastic hinge, free length of connecting and gusset plate, and quadratically on the thicknesses of gusset and connecting plate.

5.9.3 CBFEM model

The CBFEM model comprises only the joint with stubs of connected members. The member model type is set to N-Vy-Vz so that the bending moments are restrained. The applied forces are in the position of the center of the bolt group, see Fig. 5.9.2. The member is loaded by normal force N_{Ed} and, to simulate the bending of the gusset and connected plates, eccentricities and second order effects, shear force with the magnitude of

$$V_{Ed} = N_{Ed}/10 \qquad (5.9.1)$$

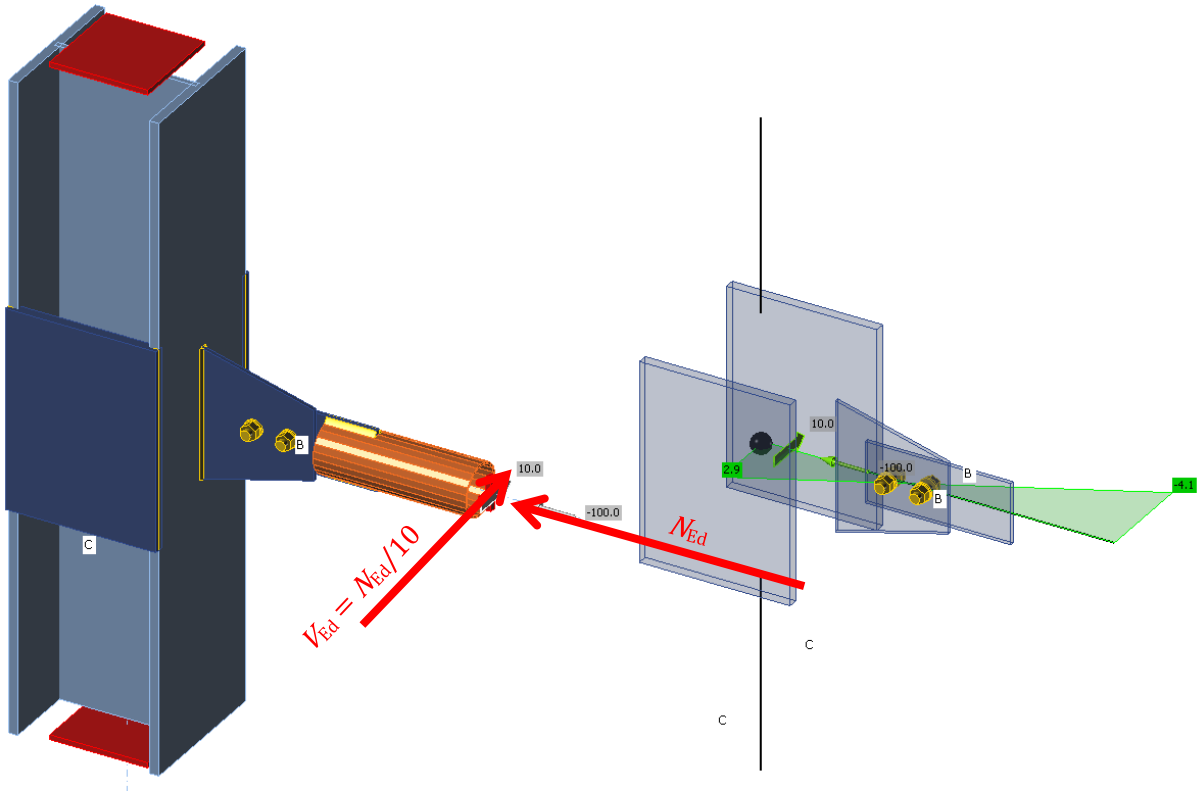

Fig. 5.9.2 CBFEM model with supports and bending moment diagram

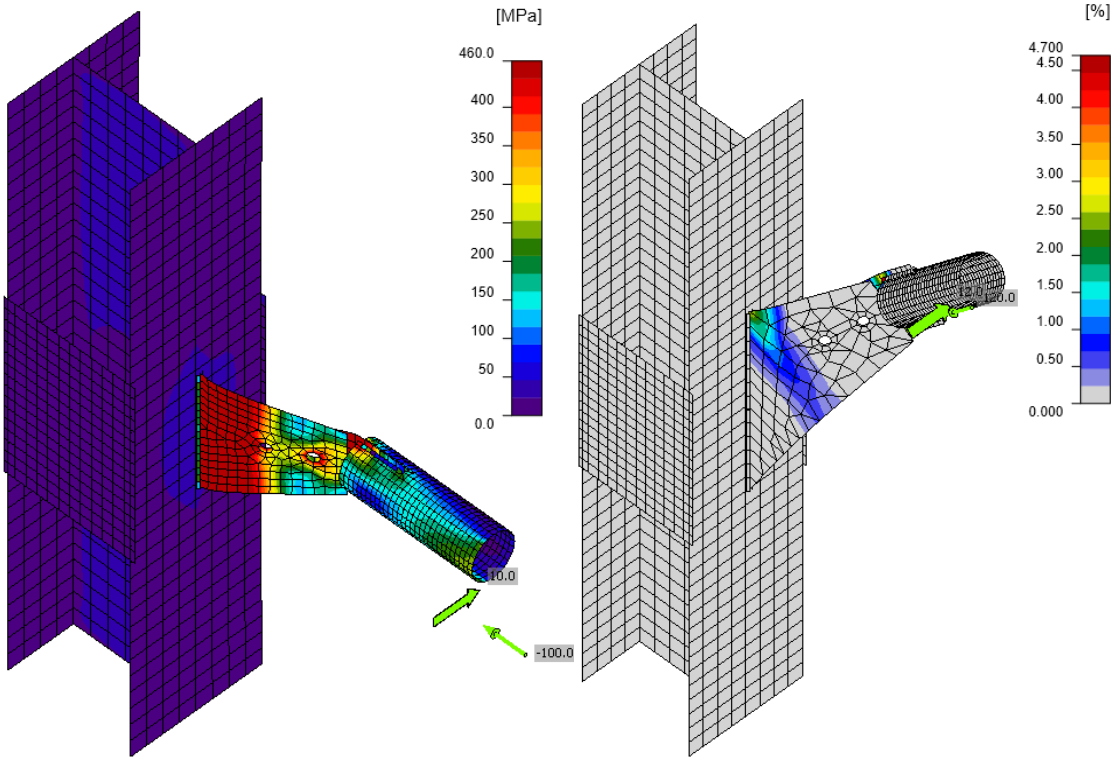

Fig. 5.9.3 Von Mises stress on specimen C2 and plastic strain on specimen D4, deformation scale 3

5.9.4 Verification and validation of resistance

Design resistances calculated by CBFEM were compared with the results of the analytical model, experiments, and research-oriented finite element model (Vesecký, 2019). The experiments were performed at ČVUT in 2018 and comprised six specimens. All members were tubes CHS 102×4 eccentrically connected via gusset plates and connecting plates with the thicknesses of 8 mm; see Fig. 5.9.4. The research-oriented finite element model was made in Abaqus software and validated on the experiments. ROFEM - DIC is using digital image correlation to apply the real imperfections; ROFEM - EN is using imperfections according to EN 1993-1-5 and EN 1090-2. The analytical models are labeled KPA1 and KPA2. Model KPA1 is Khoo-Perera-Albermani with minimal lengths of plastic hinges and minimal moments of inertias of gusset and connecting plates; model KPA2 is using average moments of inertia. The measured strengths of gusset plates and connecting plates were used in all models. The results are summarised in Fig. 5.9.5.

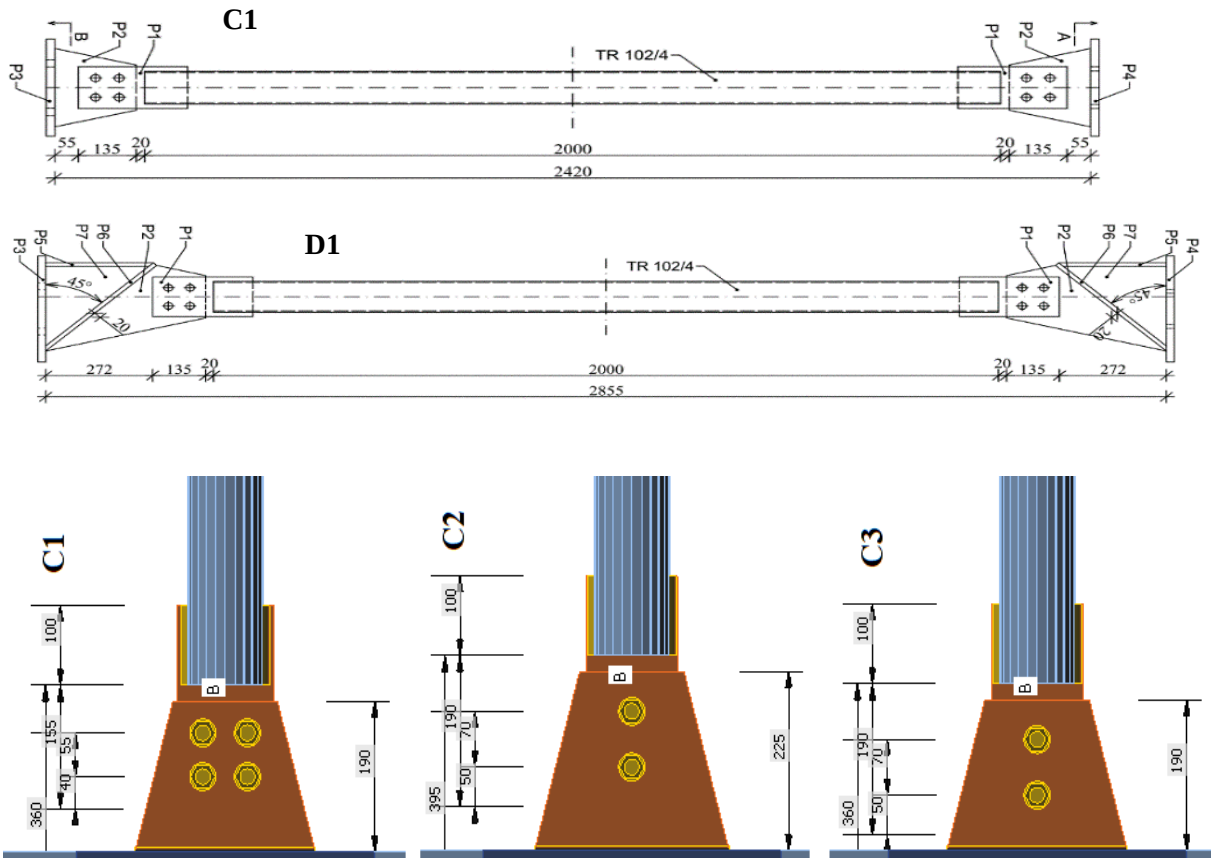

Fig. 5.9.4 Specimens of circular hollow sections connected by single-sided gusset plates (Vesecký et al. 2019)

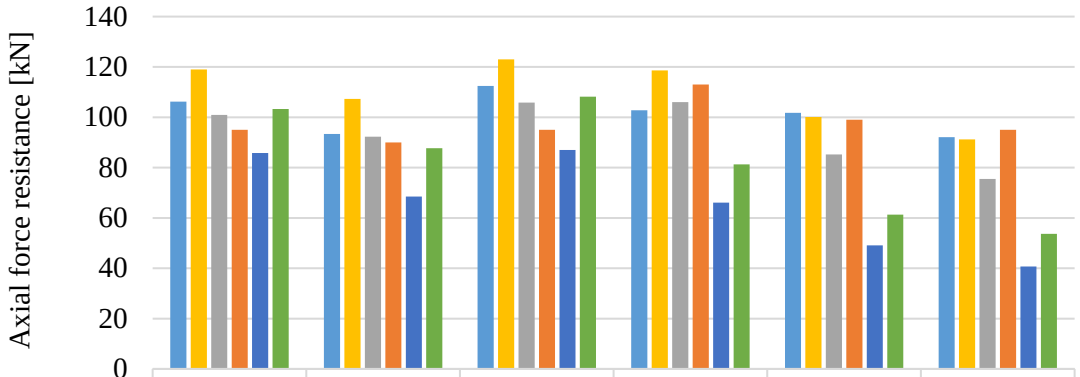

	C1	C2	C3	D1	D2	D4
Experiment	106	93	112	103	102	92
ROFEM - DIC	119	107	123	119	100	91
ROFEM - EN	101	92	106	106	85	76
CBFEM	95	90	95	113	99	95
KPA1	86	69	87	66	49	41
KPA2	103	88	108	81	61	54

Fig. 5.9.5 Comparison of experimental, FEM and analytical models of tested specimens

5.9.5 Sensitivity analysis

The ROFEM was further used for parametric study. The steel grade S355 and geometry parameters of specimen C2 were used unless stated otherwise. Always only one parameter was variable.

The resistance of the joint for varying free length is shown in Fig. 5.9.6. CBFEM follows the same slope as ROFEM. The resistance is linearly dependent on the free length.

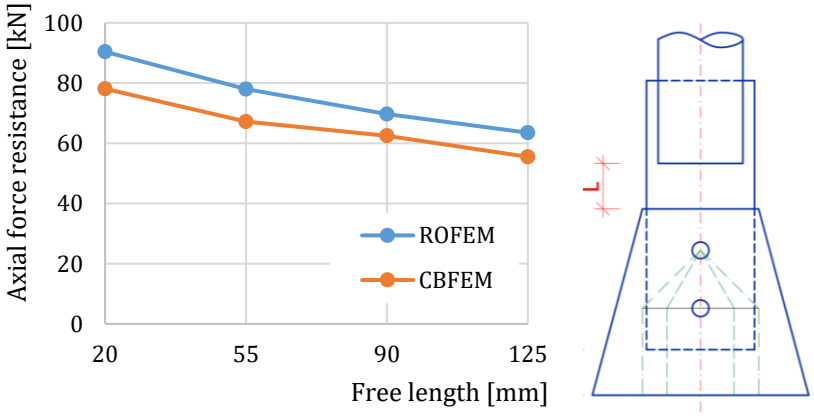

Fig. 5.9.6 Effect of free length of the connecting plate

The effect of varying thickness of gusset and connected plates is shown in Fig. 5.9.7. The CBFEM is slightly underestimating the resistance with higher thickness of the plates compared to the ROFEM.

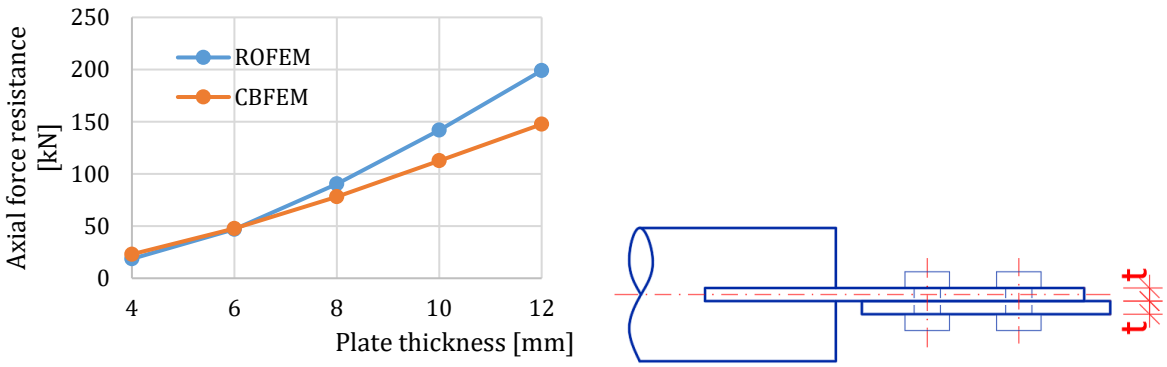

Fig. 5.9.7 Effect of thicknesses of gusset plate and connected plate

The number of bolts nearly does not affect the resistance of the connection, see Fig. 5.9.8. The effect was investigated on connection C2 and D4.

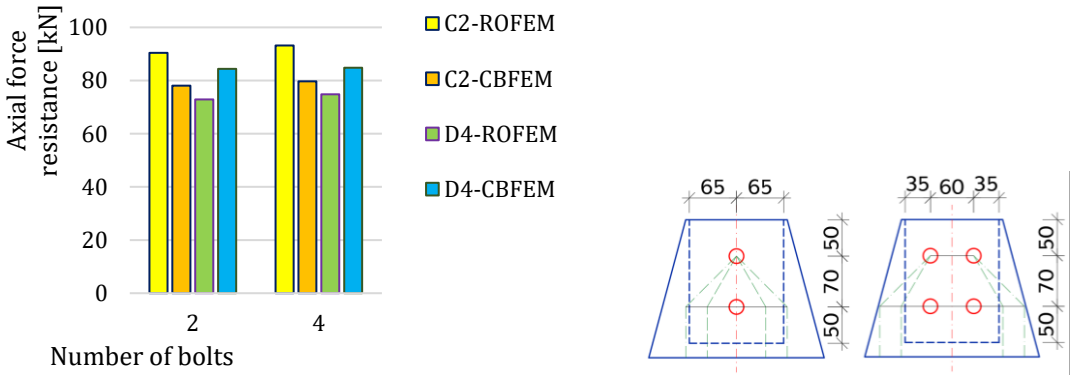

Fig. 5.9.8 Effect of number of bolts

The load resistance is linearly rising with increasing yield strength, see Fig. 7.5.9. The effect was investigated on connection C2 and D4.

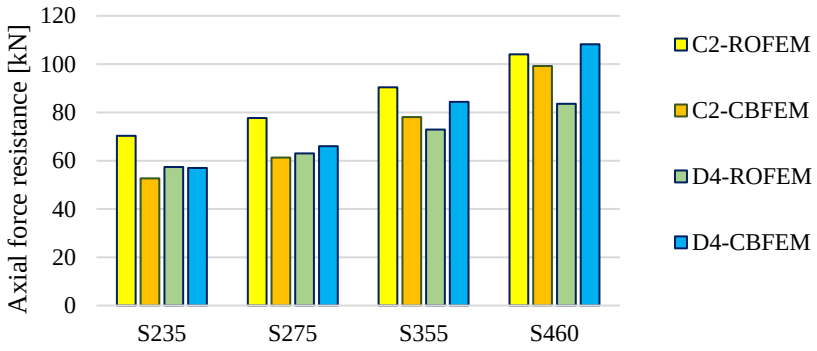

Fig. 5.9.9 Effect of steel grade

The comparison of load resistances using ROFEM and CBFEM is plotted in Fig. 5.9.10. The CBFEM is usually conservative except for specimens D2 and D4. However, for these specimens, the ROFEM is conservative compared to the experiments. The CBFEM model is much simpler and

uses geometrically linear analysis but the accuracy of its results is comparable to ROFEM and exceeds analytical models.

The resistance of the subsystem of the member including its joints will be natural future of design of gusset plate connection with single-sided splice member by CBFEM models.

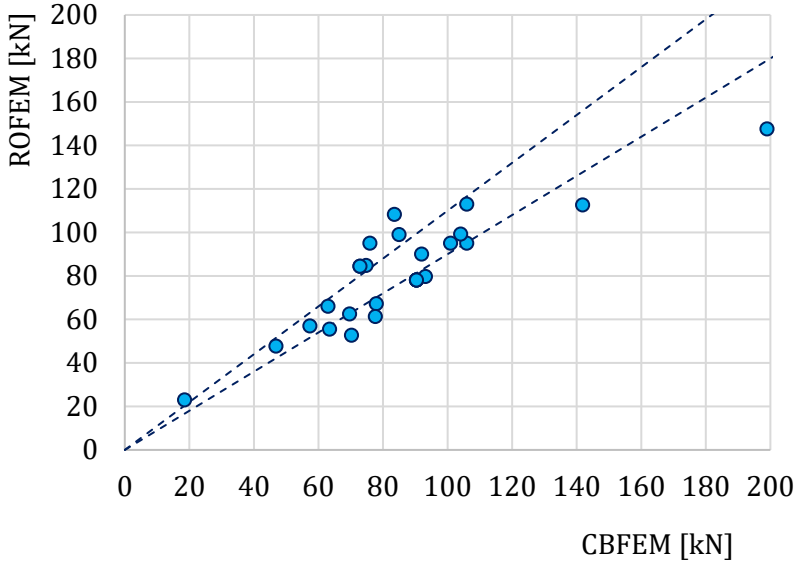

Fig. 5.9.10 Comparison between ROFEM and CBFEM

5.9.6 Benchmark example

Inputs

Steel S355

Column

- HEB 300

Beam

- CHS 102×4
- Model type N-Vy-Vz

Connecting plate

- Gusset plate 261×225×8
- Connecting plate 290×130×8

Connectors

Bolts

- 2 × M20 8.8
- Distances e_1 = 50 mm, $p_{1,1}$ = 70 mm

Outputs

- Design resistance N_{Rd} = 90 kN, equivalent shear force 9 kN
- Critical is plastic strain of gusset plate

6 SLENDER PLATE IN COMPRESSION

6.1 Triangular haunch

6.1.1 Description

The object of this study is verification of component-based finite element method (CBFEM) for a class 4 triangular haunch without a flange and a class 4 triangular haunch with a flange with reduced stiffness with research FEM model (RFEM) and design FEM model (DFEM).

6.1.2 Experimental investigation

Experimental results of six specimens of haunches with and without flanges are presented. Three specimens are without flanges and three specimens are supported by additional flanges. Unstiffened specimens differ in the web thickness t_w and the web width b_w. Reinforced specimens differ in the web thickness t_w, the flange thickness $t_{f,}$ and the flange width b_f. The dimensions of specimens are summarized in Tab. 6.1.1. The test set-up for the specimen without a flange is shown in Fig. 6.1.1 (top) and for the specimen with a flange in Fig. 6.1.1 (bottom). Material characteristics of the steel plates are summed up in Tab. 6.1.2.

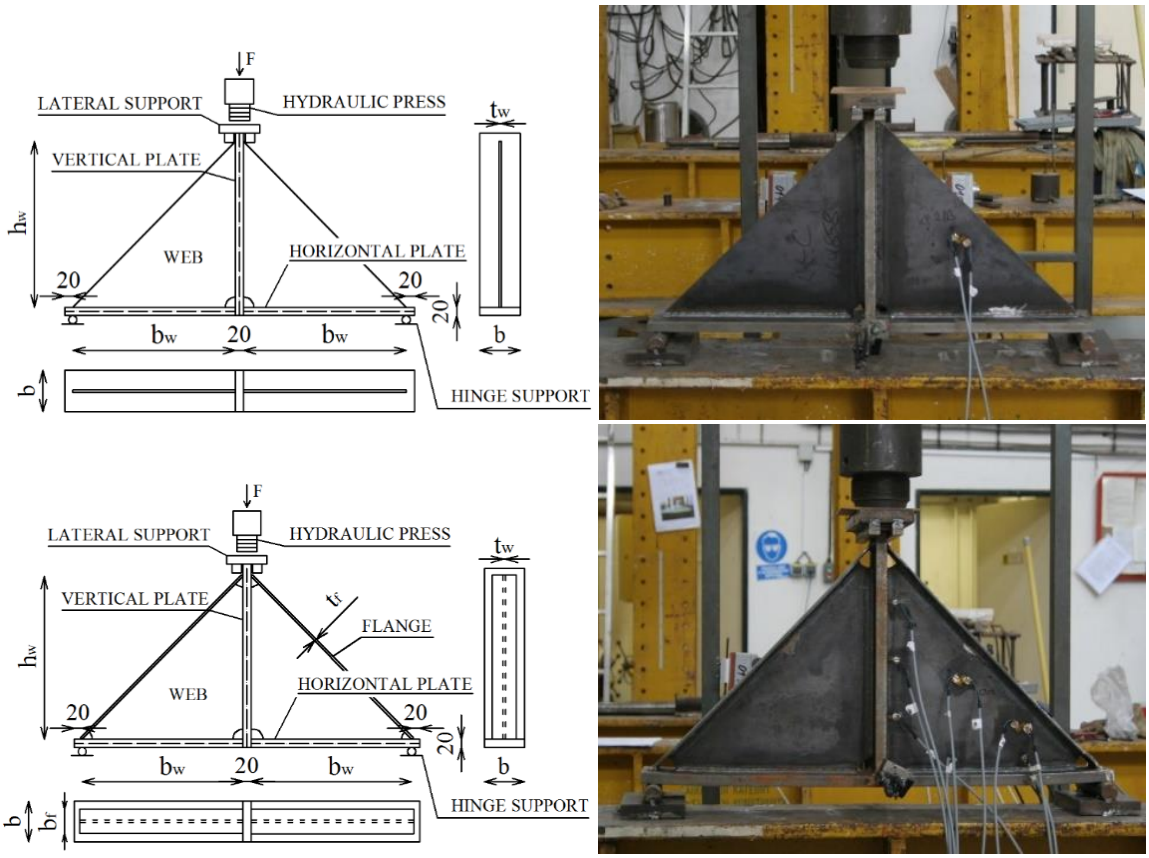

Fig. 6.1.1 Specimens geometry and test set-up

Tab. 6.1.1 Examples overview

Example	Triangular web			Flange	
	b_w	h_w	t_w	b_f	t_f
	[mm]	[mm]	[mm]	[mm]	[mm]
A	200	400	6	-	-
B	400	400	6	-	-
C	400	400	4	-	-
D	400	400	6	60	6
E	400	400	6	120	12
F	400	400	4	120	12

Tab. 6.1.2 Material characteristics used in numerical models

		Plate thickness [mm]			
Material characteristics		4	6	12	20
Young's Modulus	E [GPa]	163,0	158,7	159,8	160,0
Yield strength	f_y [MPa]	417,5	323,5	395,4	355,0
Ultimate tensile strength	f_u [MPa]	499,3	467,0	529,6	510,0

6.1.3 Research FEM model

Research FEM model (RFEM) is used to verify the DFEM model and is validated on the experiments. In the numerical model, 4-node quadrilateral shell elements with nodes at their corners are applied, with a maximum side length of 10 mm. Materially and geometrically nonlinear analysis with imperfections (GMNIA) is applied. Equivalent geometric imperfections are derived from the first buckling mode, and the amplitude is set according to Annex C of EN 1993-1-5:2006. Numerical models are shown in Fig. 6.1.2.

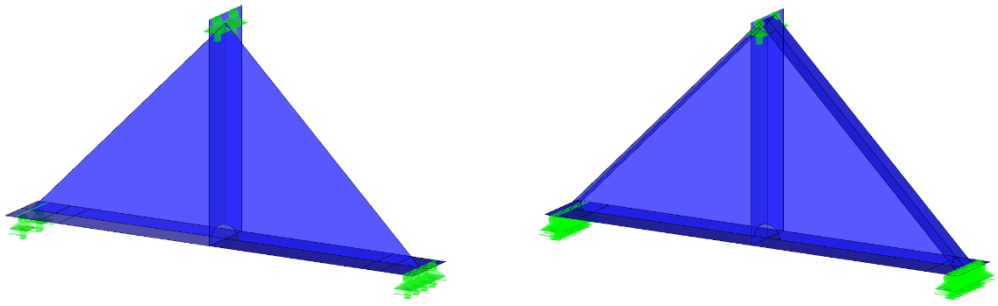

a) b)

Fig. 6.1.2 Research FEM model a) haunch without a flange b) haunch with a flange

An example of the comparison of RFEM and experimental test on the load-deflection behavior is shown in Fig. 6.1.3a. The comparison of resistances measured in the experiment and obtained from RFEM is shown in Fig. 6.1.3b. The resistance calculated in the numerical model is displayed

on the horizontal axis. The resistance measured in the experimental study is displayed on the vertical axis. It can be seen that a good agreement exists.

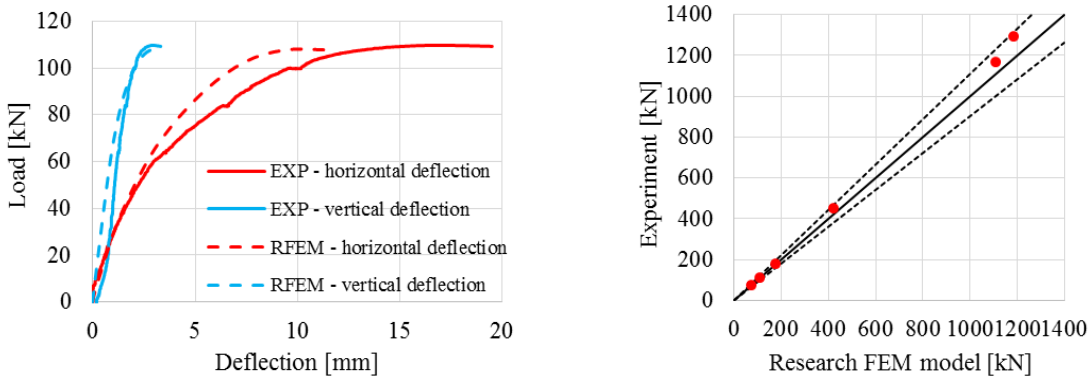

a) b)

Fig. 6.1.3 a) Load-deflection curve of a haunch without a flange
b) Experiments' resistances compared against RFEMs'

The comparisons of the final deformation states between numerical simulations and experimental results are performed at the end of the tests. Fig. 6.1.4 presents the comparison of the deformation of specimens A, B, and D after failure with RFEA. It can be found that good agreements between numerical models and experimental results of the haunches exist in the failure mode. For more details, see (Kurejková and Wald, 2017).

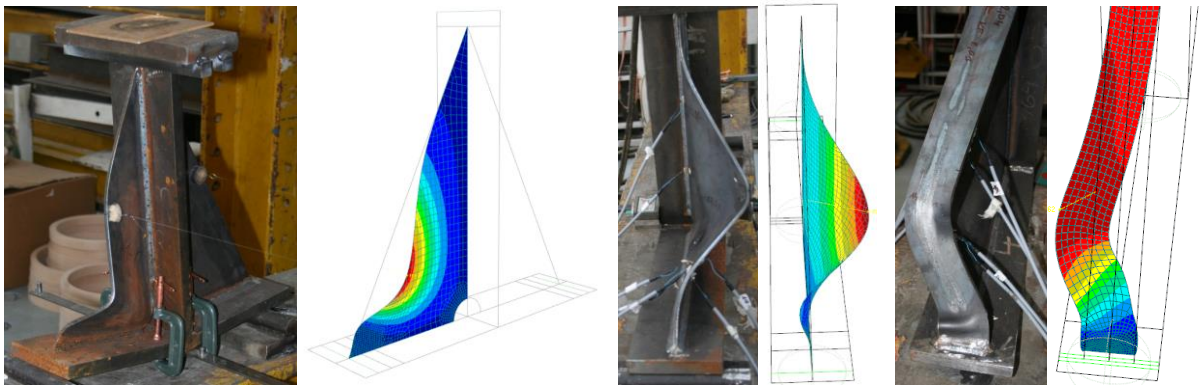

a) specimen A b) specimen B c) specimen D

Fig. 6.1.4 Experimental and numerical deflection of specimens A, B and D after failure

6.1.4 Design FEM model

Design procedure for class 4 cross-sections is described in section 3.10 Local buckling.

The design procedure is verified on the comparison of DFEM and RFEM models. Both models are created in Dlubal RFEM software. The procedure is applied in CBFEM models; see (Kurejková et al. 2015). The resistance governed by 5% plastic strain is obtained in the first step and followed by linear buckling analysis. The critical component in the buckling analysis is studied. The design resistance is interpolated until the condition $\rho \cdot \alpha_{ult,k} = 1$ is reached.

The first buckling mode of a haunch without a flange is shown in Fig. 6.1.4 a). The resistance is assessed according to formula (3.10.2) in section 3.10. The comparison of DFEM's and RFEM's resistances is shown in Fig. 6.1.4 b). The resistance calculated in the DFEM is displayed on the horizontal axis. The resistance calculated in RFEM is displayed on the vertical axis. It can be seen that a good agreement exists and the procedure is verified.

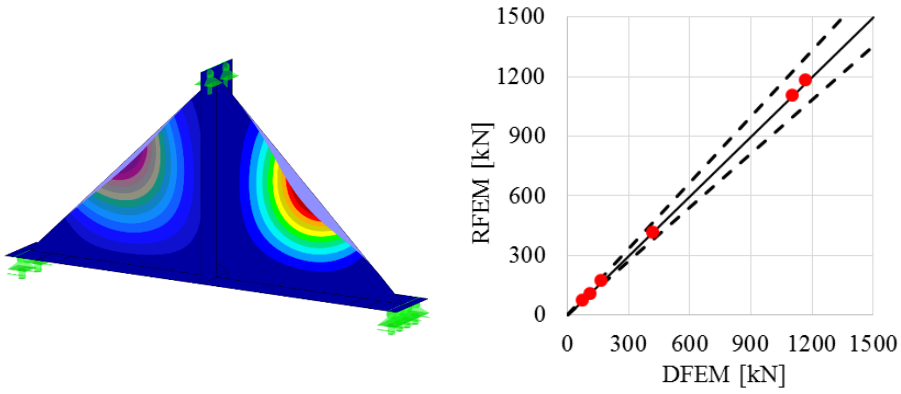

a) b)

Fig. 6.1.4 a) First buckling mode of DFEM model b) Comparison of DFEM and RFEM resistances

6.1.5 Global behavior and verification

Comparison of the global behavior of a haunch without flange described by load-deflection diagrams in DFEM model is prepared. The deflection is measured in the vertical direction in the middle of the specimen. Attention is focused on the main characteristics: design resistance and critical load. Two examples of a haunch without a flange are chosen to present as a reference; see Fig. 6.1.5. The design procedure in DFEM models covers the post-buckling reserve, which is observed in Fig. 6.1.5 a). The critical load F_{cr} is smaller than the design resistance F_{DFEM}. The post-buckling reserve is observed in cases with very slender plates. The typical diagram is shown in Fig. 6.1.5 b), where the design resistance F_{DFEM} does not reach the critical load F_{cr}. The load $F_{ult,k}$ refers to resistance by 5 % of plastic strain.

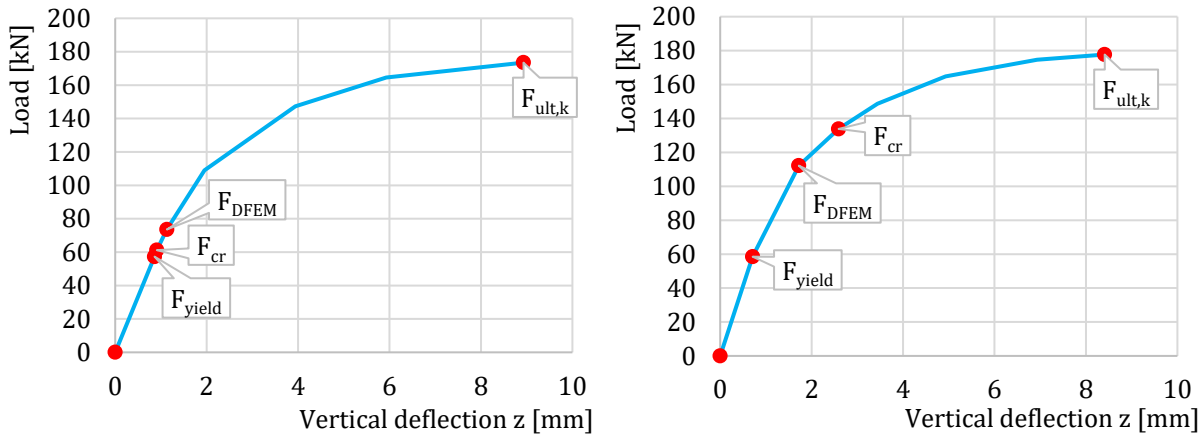

a) b)

Fig. 6.1.5 a) Load-deflection curve with post-buckling reserve
b) Load-deflection curve without post-buckling reserve (Kuříková et al. 2019)

The design procedure in CBFEM models is described in section 3.10 Local buckling. The buckling analysis is implemented in the software. The calculation of the design resistances is done manually according to the design procedure. F_{CBFEM} is interpolated by the user until the formula (2) is equal to 1. A beam-column joint with a haunch without a flange is studied. The thicknesses of beam and column webs are changing in the same way as the thickness of the triangular haunch. The same cross-section is used for beam and column. The geometry of the examples is described in Tab. 6.1.3. The joint is loaded by bending moment.

Tab. 6.1.3 Examples overview (Kuříková et al. 2019)

Example	Material	Triangular haunch			Beam/column flange		Beam/column web	
		b_w	h_w	t_w	b_f	t_f	h_w	t_w
		[mm]	[mm]	[mm]	[mm]	[mm]	[mm]	[mm]
tw3	S355	400	400	3	120	10	300	3
tw4	S355	400	400	4	120	10	300	4
tw5	S355	400	400	5	120	10	300	5
tw6	S355	400	400	6	120	10	300	6

6.1.6 Verification of resistance

The design resistance calculated by CBFEM is compared with the results obtained by RFEM. The comparison is focused on the design resistance and critical load. The results are ordered in Tab. 6.1.4. The diagram in Fig. 6.1.6 c) shows the influence of the haunch thickness on the resistances and critical loads in the examined examples.

The results show very good agreement in critical load and design resistance. The post-buckling reserve is observed for beam web and triangular haunch with thicknesses of 3 and 4 mm. The CBFEM model of the joint with a haunch with a thickness of 3 mm is shown in Fig. 6.1.6 a). The first buckling mode of the joint is shown in Fig. 6.1.6 b).

Tab. 6.1.4 Design resistance

Example	M_{cr}		α_{cr}	M		$\alpha_{ult,k}$	Difference
	RFEM	CBFEM	CBFEM	RFEM	CBFEM	CBFEM	M_{CBFEM}/M_{RFEM}
	[kNm]	[kNm]	[-]	[kNm]	[kNm]	[-]	[-]
tw3	22	20	0,63	41	31	3,00	0,76
tw4	50	42	0,8	60	52	2,33	0,87
tw5	89	74	0,96	85	77	1,94	0,91
tw6	142	144	1,14	120	102	1,66	0,85

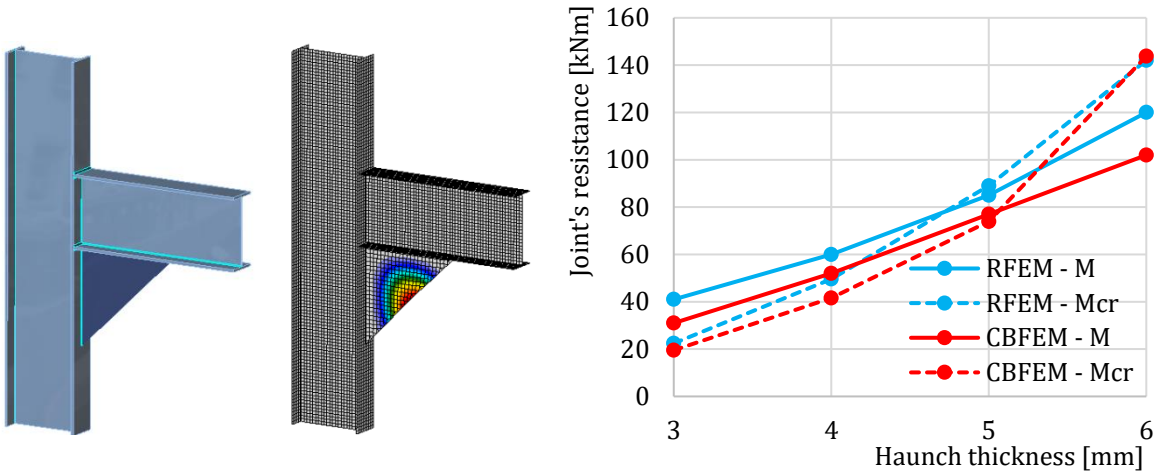

a) b) c)

Fig. 6.1.6 a) CBFEM model b) First buckling mode
c) Influence of haunch thickness on resistances and critical loads

Verification studies confirm the accuracy of the CBFEM model for the prediction of a triangular haunch behavior. The results of CBFEM are compared with the results of the RFEM. The design procedure is verified on the RFEM model, which is validated on experiments. All procedures predict similar global behavior of the joint.

6.1.7 Benchmark example

Inputs

Beam and column

- Steel S355
- Flange thickness t_f = 10 mm
- Flange width b_f = 120 mm
- Web thickness t_w = 3 mm
- Web height h_w = 300 mm

Triangular haunch

- Thickness t_w = 3 mm
- Width b_w = 400 mm
- Height h_w = 400 mm

Calculate

- Buckling analysis

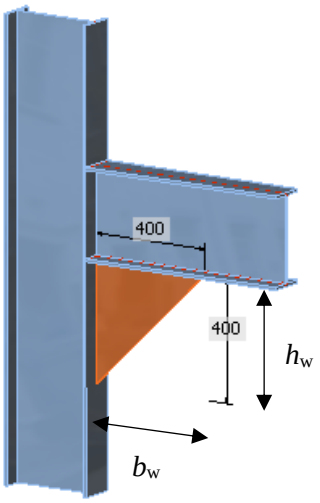

Fig. 6.1.7 Triangular haunch calculated in the benchmark example

Outputs

- Load by 5% plastic strain $M_{ult,k}$ = 93 kNm
- Design resistance M_{CBFEM} = 31 kNm
- Critical buckling factor (for M_{CBFEM} = 31 kNm) α_{cr} = 0,63
- Load factor by 5 % plastic strain $\alpha_{ult,k} = M_{ult,k} / M_{CBFEM}$ = 93 / 31 = 3,00

6.2 Column web panel in shear

6.2.1 Description

The objective of this study is verification of component-based finite element method (CBFEM) of a beam-column joint with a class 4 column web with a research FEM model (RFEM) and component method (CM).

6.2.2 Analytical model

The component column web panel in shear is described in cl. 6.2.6.1 in EN 1993-1-8:2005. The design method is limited to column web slenderness $d / t_w \leq 69\,\varepsilon$. Webs with higher slenderness are designed according to EN 1993-1-5:2006 cl. 5 and Annex A. The shear resistance is made of shear buckling resistance of the web panel and resistance of the frame made of the flanges and stiffeners surrounding the panel. The buckling resistance of the web panel is based on the shear critical stress

$$\tau_{cr} = k_\tau \sigma_E \tag{6.2.1}$$

where σ_E is the Euler critical stress of the plate

$$\sigma_E = \frac{\pi^2 E}{12(1-\nu^2)} \left(\frac{t_w}{h_w}\right)^2 \tag{6.2.2}$$

The buckling coefficient k_τ is obtained in EN 1993-1-5:2006, Annex A.3.

The slenderness of the web panel is

$$\bar{\lambda}_w = 0{,}76 \sqrt{\frac{f_{yw}}{\tau_{cr}}} \tag{6.2.3}$$

The reduction factor χ_w may be obtained in EN 1993-1-5:2006 cl. 5.3.

The shear buckling resistance of the web panel is

$$V_{bw,Rd} = \frac{\chi_w f_{yw} h_w t_w}{\sqrt{3}\gamma_{M1}} \tag{6.2.4}$$

The resistance of the frame may be designed according to cl. 6.2.6.1 in EN 1993-1-8:2005.

6.2.3 Research FEM model

Research FEM model (RFEM) is used to verify the CBFEM model. In the numerical model, 4-node quadrilateral shell elements with nodes at its corners are applied. Geometrically and materially nonlinear analysis with imperfections (GMNIA) is applied. Equivalent geometric imperfections are derived from the first buckling mode, and the imperfection amplitude is set according to EN 1993-1-5:2006, Annex C. A numerical model is shown in Fig. 6.2.1.

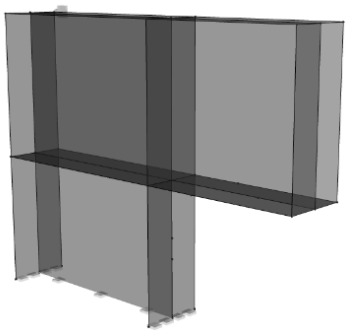

Fig. 6.2.1 Research FEM model of a beam-column joint with slender column panel

6.2.4 Design finite element model

The design procedure for slender plates is described in section 3.10. The linear buckling analysis is implemented in the software. The calculation of the design resistances is done according to the design procedure. F_{CBFEM} is interpolated by the user until $\rho \cdot \alpha_{ult,k}/\gamma_{M1}$ is equal to 1.

A beam-column joint with a slender column web is studied. The height of the beam web is changing; thus, the width of the column web panel is changing. The geometry of the examples is described in Tab. 6.2.1. The joint is loaded by bending moment.

Tab. 6.2.1 Examples overview

Example	Column flange		Column web		Beam	Material
	b_f	t_f	h_w	t_w	IPE	
	[mm]	[mm]	[mm]	[mm]		
IPE400	250	10	820	4	400	S235
IPE500	250	10	820	4	500	S235
IPE600	250	10	820	4	600	S235

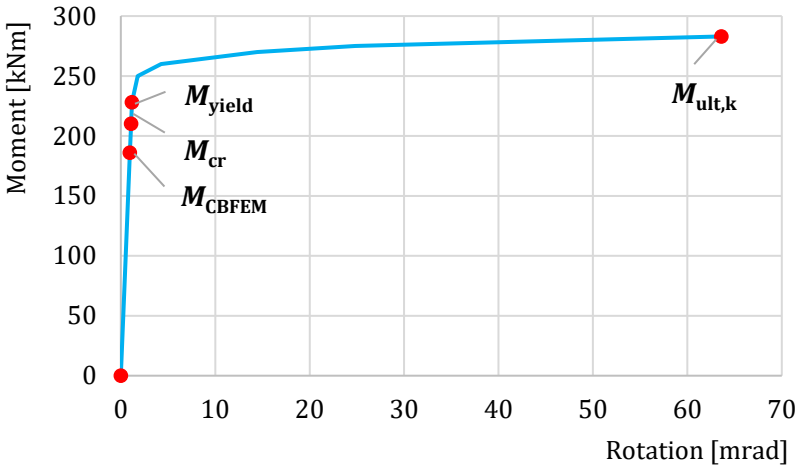

Fig. 6.2.2 Moment-rotation curve of example IPE600 (Kuříková et al. 2019)

6.2.5 Global behavior and verification

The global behavior of a beam-column joint with a slender column web described by moment-rotation diagram in CBFEM model is shown in Fig. 6.2.2. Attention is focused on the main characteristics: design resistance and critical load. The diagram is completed with a point where yielding starts and resistance by 5 % plastic strain.

6.2.6 Verification of resistance

The design resistance calculated by CBFEM is compared with RFEM and CM. The comparison is focused on the design resistance and critical load. The results are ordered in Tab. 6.2.2. The diagram in Fig. 6.2.3c shows the influence of the width of the column web on the resistances and critical loads in the examined examples.

Tab. 6.2.2 Design resistances and critical loads of RFEM, CBFEM, and CM

Example	M_{cr}			α_{cr}	M			$\alpha_{ult,k}$	Difference	
	RFEM	CM	CBFEM	CBFEM	RFEM	CM	CBFEM	CBFEM	M_{CBFEM} / M_{RFEM}	M_{CBFEM} / M_{CM}
	[kNm]	[kNm]	[kNm]	[-]	[kNm]	[kNm]	[kNm]	[-]	[%]	[%]
IPE400	256	275	301	1,59	170	177	189	1	1,11	1,07
IPE500	216	234	244	1,32	177	200	185	1,28	1,05	0,93
IPE600	195	210	215	1,14	200	220	189	1,51	0,95	0,86

The results show good agreement in critical load and design resistance. The CBFEM model of the joint with a beam IPE600 is shown in Fig. 6.2.3a. The first buckling mode of the joint is shown in Fig. 6.2.3b.

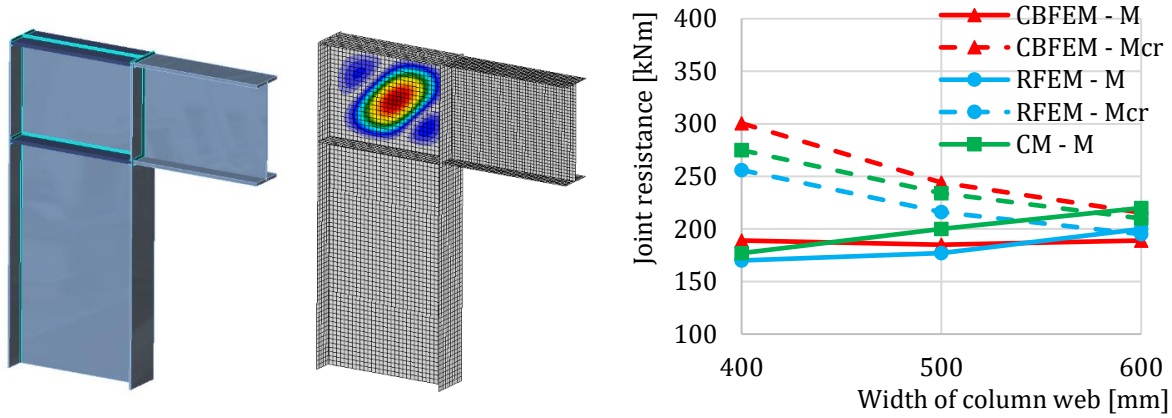

a) b) c)

Fig. 6.2.3 a) CBFEM model b) First buckling mode
c) Influence of width of column web on resistances and critical loads

Verification studies confirmed the accuracy of the CBFEM model for the prediction of a column web panel behavior. The results of CBFEM are compared with the results of the RFEM and CM.

The design procedure is verified on the RFEM model. Procedures predict similar global behavior of the joint.

6.2.7 Benchmark example

Inputs

Beam

- Steel S235
- IPE600

Column

- Steel S235
- Flange thickness t_f = 10 mm
- Flange width b_f = 250 mm
- Web thickness t_w = 4 mm
- Web height h_w = 800 mm
- Section height h = 820 mm

Web stiffener

- Steel S235
- Stiffener thickness t_w = 19 mm
- Stiffener width h_w = 250 mm
- Welds $a_{w,stiff}$ = 7 mm
- Stiffeners opposite to upper and lower flange

Outputs

- Load by 5 % plastic strain $M_{ult,k}$ = 285 kNm
- Design resistance M_{CBFEM} = 189 kNm
- Critical buckling factor (for M = 189 kNm) α_{cr} = 1,14
- Load factor by 5 % plastic strain $\alpha_{ult,k} = M_{ult,k} / M_{CBFEM}$ = 285/189 = 1,51

6.3 Column web stiffener

6.3.1 Description

The objective of this study is verification of component-based finite element method (CBFEM) of a class 4 column web stiffener in a beam-to-column joint with a research FEA model (RFEM) created in Dlubal RFEM software and component method (CM).

6.3.2 Research FEA model

Research FEA model (RFEM) is used to verify the CBFEM model. In the numerical model, 4-node quadrilateral shell elements with nodes at its corners are applied. Geometrically and materially nonlinear analysis with imperfections (GMNIA) is applied. Equivalent geometric imperfections are derived from the first buckling mode, and the amplitude is set according to Annex C in EN 1993-1-5:2006. The numerical model is shown in Fig. 6.3.1.

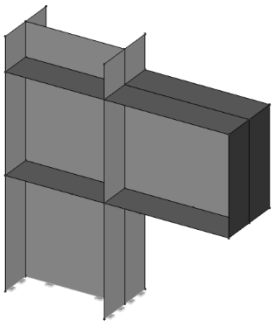

Fig. 6.3.1 Research FEA model of a beam-to-column joint with slender column web stiffener

6.3.3 CBFEM

The design procedure for slender plates is described in section 3.10. The linear buckling analysis is implemented in the software. The calculation of the design resistances is done according to the design procedure. F_{CBFEM} is interpolated by the user until $\rho \cdot \alpha_{ult,k}/\gamma_{M1}$ is equal to 1. A beam-to-column joint with a slender column web stiffener is studied. The same cross-section is used for the beam and the column. The thickness of the column web stiffener is changing. The geometry of the examples is described in Tab. 6.3.1. The joint is loaded by bending moment.

Tab. 6.3.1 Examples overview

Example	Column/beam flange		Column/beam web		Stiffener	Material
	b_f	t_f	h_w	t_w	t_s	
	[mm]	[mm]	[mm]	[mm]	[mm]	
t3	400	20	600	12	3	S235
t4	400	20	600	12	4	S235
t5	400	20	600	12	5	S235
t6	400	20	600	12	6	S235

6.3.4 Global behavior and verification

The global behavior of a beam-to-column joint with a slender column web stiffener of thickness 3 mm described by moment-rotation diagram in CBFEM model is shown in Fig. 6.3.2. Attention is focused on the main characteristics: design resistance and critical load. The diagram is completed with a point where yielding starts and resistance by 5 % plastic strain.

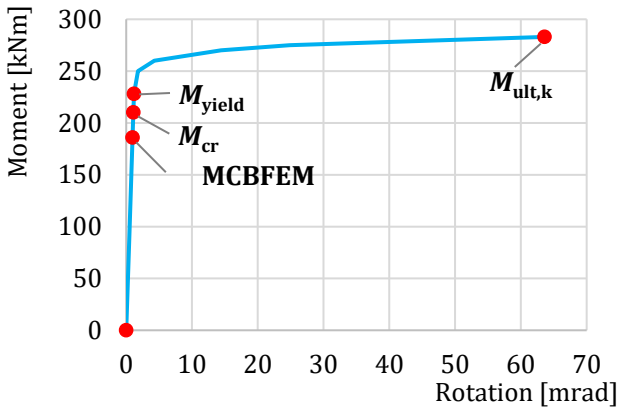

Fig. 6.3.2 Moment-rotation curve of example t3

6.3.5 Verification of resistance

The design resistance calculated by CBFEM Idea StatiCa software is compared with RFEM. The comparison is focused on the design resistance and critical load. The results are ordered in Tab. 6.3.2. The diagram in Fig. 6.3.3 c) shows the influence of the thickness of the column web stiffener on the resistances and critical loads in the examined examples.

Tab. 6.3.2 Design resistances and critical loads of RFEM and CBFEM

Example	M_{cr}		α_{cr}	M_{Rd}		$\alpha_{ult,k}$	Diff.
	RFEM	CBFEM	CBFEM	RFEM	CBFEM	CBFEM	M_{CBFEM} / M_{RFEM}
	[kNm]	[kNm]	[-]	[kNm]	[kNm]	[-]	[%]
t3	260	286	0,94	290	304	1,95	5
t4	511	565	1,33	419	425	1,43	2
t5	874	952	1,74	532	547	1,12	3
t6	1346	1467	2,37	580	619	1,00	6

The results show very good agreement in critical load and design resistance. The CBFEM model of the joint with web stiffener with the thickness of 3 mm is shown in Fig. 6.3.3a. The first buckling mode of the joint is shown in Fig. 6.3.3b.

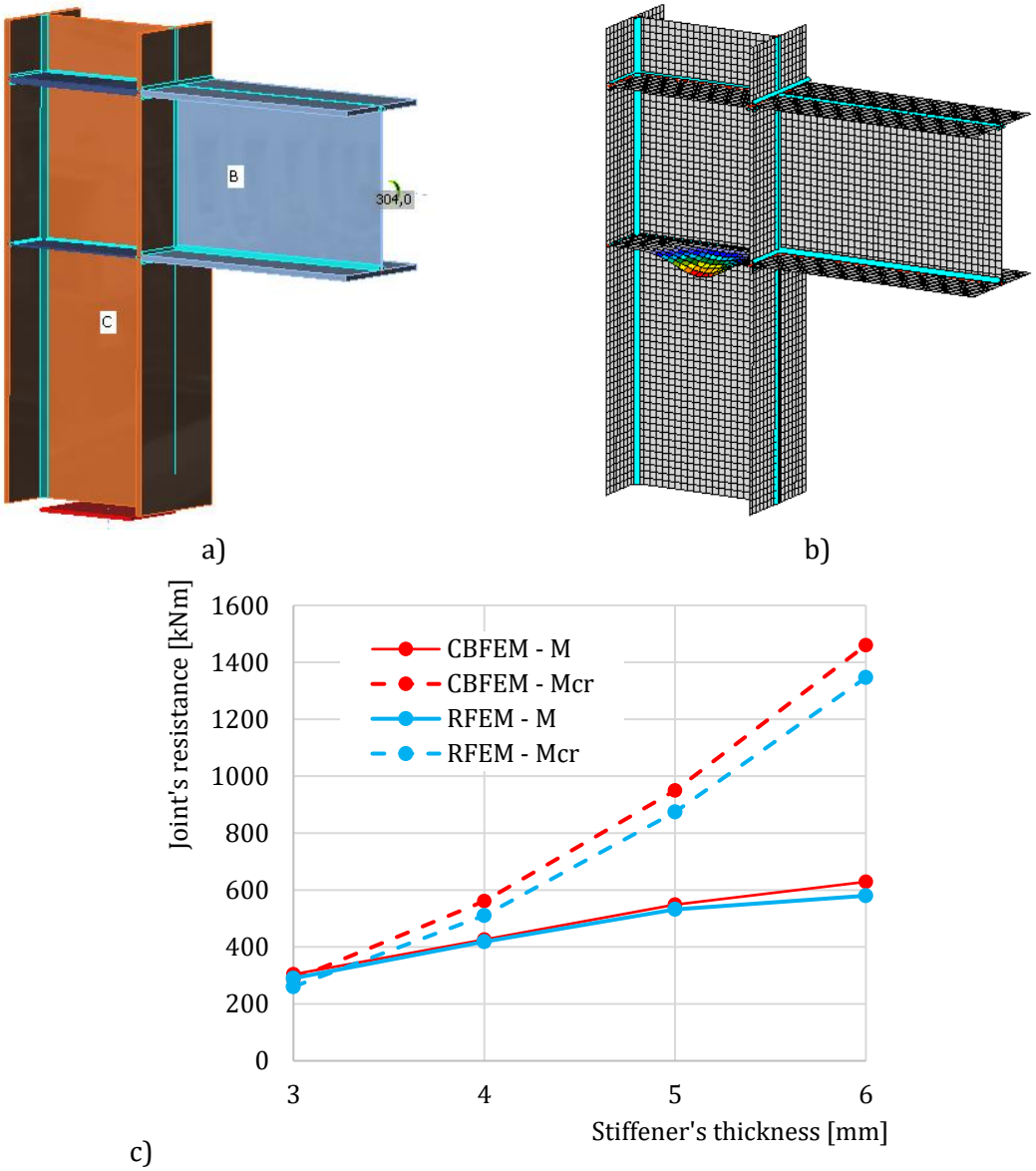

Fig. 6.3.3 a) Geometrical model b) First buckling mode
c) Influence of stiffener's thickness on resistances and critical loads

Verification studies confirmed the accuracy of the CBFEM model for the prediction of a column web stiffener behavior. The results of CBFEM are compared with the results of the RFEM. All procedures predict similar global behavior of the joint. The difference in design resistance is in all cases below 10%.

6.3.6 Benchmark example

Inputs

Beam

- Steel S235
- Flange thickness t_f = 20 mm
- Flange width b_f = 400 mm
- Web thickness t_w = 12 mm
- Web height h_w = 600 mm

Column

- Steel S235
- Flange thickness t_f = 20 mm
- Flange width b_f = 400 mm
- Web thickness t_w = 12 mm
- Web height h_w = 560 mm
- Section height h = 600 mm

Upper column web stiffener

- Steel S235
- Stiffener thickness t_w = 20 mm
- Stiffener width h_w = 400 mm

Lower column web stiffener

- Steel S235
- Stiffener thickness t_w = 3 mm
- Stiffener width h_w = 400 mm

Outputs

- Load by 5% plastic strain $M_{ult,k}$ = 594 kNm
- Design resistance M_{CBFEM} = 304 kNm
- Critical buckling factor (for M = 304 kNm) α_{cr} = 0,94
- Load factor by 5 % plastic strain $\alpha_{ult,k} = M_{ult,k} / M_{CBFEM}$ = 594/304 = 1,95

7 HOLLOW SECTION JOINTS

7.1 Circular hollow sections

7.1.1 Failure mode method

In this chapter, component-based finite element method (CBFEM) for design of uniplanar welded Circular Hollow Sections (CHS) is verified to Failure Mode Method (FMM): T, X, and K-joints. In CBFEM, the design resistance is limited by reaching 5 % of strain or a force corresponding to 3% d_0 joint deformation, where d_0 is chord diameter. The resistance in FMM is generally determined by peak load or 3% d_0 deformation limit, see (Lu et al. 1994). FMM is based on the principle of identifying modes that may cause joint failure. From the practical experience and experiments accomplished during the 70s and 80s, two modes of failure were identified for the CHS joints: chord plastification and chord punching shear. This calculation method is always limited to a probed geometry of joints. This means that different formulas always apply for each geometry. In the following studies, the welds are designed according to EN 1993-1-8:2006 not to be the weakest components in the joint.

Chord plastification

The design resistance of a CHS chord face can be determined using the method given by FMM model in Ch. 9 of prEN 1993-1-8:2020; see Fig. 7.1.1. The method is also given in ISO/FDIS 14346 and is described in more detail in (Wardenier et al. 2010). The design resistance of the axially loaded welded CHS joint is:

- for T and Y joint

$$N_{1,\mathrm{Rd}} = C_\mathrm{f} \cdot \frac{f_\mathrm{yo} \cdot t_0^2}{\sin\theta_1} \cdot (2{,}6 + 17{,}7 \cdot \beta^2) \cdot \gamma^{0,2} \cdot Q_\mathrm{f} / \gamma_{\mathrm{M5}} \tag{7.1.1}$$

- X joint

$$N_{1,Rd} = C_\mathrm{f} \cdot \frac{f_\mathrm{yo} \cdot t_0^2}{\sin\theta_1} \cdot \left(\frac{2{,}6 + 2{,}6 \cdot \beta}{1 - 0{,}7 \cdot \beta}\right) \cdot \gamma^{0,15} \cdot Q_\mathrm{f} / \gamma_{\mathrm{M5}} \tag{7.1.2}$$

- and for K gap joint

$$N_{1,Rd} = C_\mathrm{f} \cdot \frac{f_\mathrm{yo} \cdot t_0^2}{\sin\theta_1} \cdot (1{,}65 + 13{,}2 \cdot \beta^{1,6}) \cdot \gamma^{0,3} \cdot \left[1 + \frac{1}{1{,}2 + (g/t_0)^{0,8}}\right] \cdot Q_\mathrm{f} / \gamma_{\mathrm{M5}} \tag{7.1.3}$$

where:

d_i is an overall diameter of CHS member *i* (*i* = 0,1,2 or 3)
$f_\mathrm{y,i}$ is a yield strength of member *i* (*i* = 0,1,2 or 3)

g is a gap between braces of K joint
t_{i} is thickness of the wall of CHS member *i* (*i* = 0,1,2 or 3)
θ_{i} is an included angle between brace member *i* and the chord (*i* =1,2 or 3)
β is a ratio of the mean diameter or width of brace members, to that of the chord
γ is a ratio of a chord width or diameter to twice its wall thickness
Q_{f} is a chord stress factor
C_{f} is a material factor
γ_{M5} is partial safety factor for resistance of joints in hollow section lattice girders
$N_{\mathrm{i,Rd}}$ is a design resistance of a joint expressed in terms of the internal axial force in member *i* (*i* = 0, 1, 2 or 3)

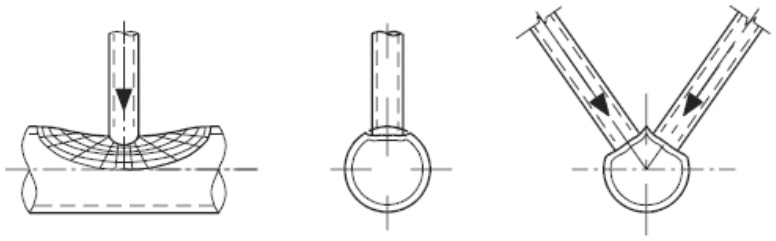

Fig. 7.1.1 Examined failure mode – chord plastification

Chord punching shear

(for $d_{\mathrm{i}} \leq d_0 - 2t_0$)

The design resistance of the axially loaded T, Y, X, and K joint of welded circular hollow sections for chord punching shear (Fig. 7.1.2) is:

$$N_{1,\mathrm{Rd}} = C_{\mathrm{f}} \cdot \frac{f_{\mathrm{yo}}}{\sqrt{3}} \cdot t_0 \cdot \pi \cdot d_i \cdot \frac{1 + \sin\theta_1}{2 \cdot \sin^2\theta_1} / \gamma_{\mathrm{M5}} \qquad (7.1.4)$$

where:

d_{i} is an overall diameter of CHS member *i* (*i* = 0,1,2 or 3)
t_{i} is thickness of the wall of CHS member *i* (*i* = 0,1,2 or 3)
$f_{\mathrm{y,i}}$ is yield strength of member *i* (*i* = 0,1,2 or 3)
θ_{i} is an included angle between brace member *i* and the chord (*i* = 1,2 or 3)
C_{f} is a material factor
$N_{\mathrm{i,Rd}}$ is a design resistance of a joint expressed in terms of the internal axial force in member *i* (*i* = 0, 1, 2 or 3)

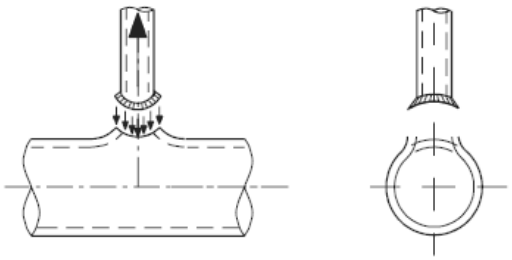

Fig. 7.1.2 Examined failure mode – chord punching shear

Chord shear

(for X joints, only if cos $\theta_1 > \beta$)

The design resistance of the axially loaded X joint of welded circular hollow sections for chord shear, see Fig. 7.1.3, is:

$$N_{1,\mathrm{Rd}} = \frac{f_{\mathrm{y0}}}{\sqrt{3}} \cdot \frac{(2/\pi) \cdot A_0}{\sin \theta_1} \Big/ \gamma_{\mathrm{M5}} \tag{7.1.5}$$

$$N_{\mathrm{gap,0,Rd}} = A_0 \cdot f_{\mathrm{y0}} \cdot \sqrt{1 - \left(\frac{N_{1,\mathrm{Ed}} \cdot \sin \theta_1}{(f_{\mathrm{y0}}/\sqrt{3})(2/\pi) \cdot A_0} \right)^2} \Big/ \gamma_{\mathrm{M5}} \tag{7.1.6}$$

where:

A_{i} is an area of cross-section *i* (*i* = 0,1,2 or 3)
$f_{\mathrm{y,i}}$ is yield strength of member *i* (*i* = 0,1,2 or 3)
θ_{i} is an included angle between brace member *i* and the chord (*i* = 1,2 or 3)
$N_{\mathrm{i,Rd}}$ is a design resistance of a joint expressed in terms of the internal axial force in member *i* (*i* = 0, 1, 2 or 3)

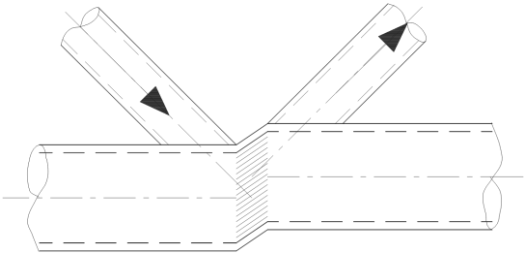

Fig. 7.1.3 Examined failure mode - Chord shear

Range of validity

CBFEM was verified for typical joints of the welded circular hollow sections. Range of validity for these joints is defined in Table 7.1.8 of prEN 1993-1-8:2020; see Tab 7.1.2. The same range of validity is applied to CBFEM model. Outside the range of validity of FMM, an experiment should be prepared for validation or verification performed for verification according to a validated research model.

Tab. 7.1.2 Range of validity for method of failure modes

General	$0{,}2 \le \frac{d_{\mathrm{i}}}{d_0} \le 1{,}0$	$\theta_{\mathrm{i}} \ge 30^{\mathrm{o}}$	$-0{,}55 \le \frac{e}{d_0} \le 0{,}25$
	$g \ge t_1 + t_2$	$f_{\mathrm{yi}} \le f_{\mathrm{y0}}$	$t_{\mathrm{i}} \le t_0$
Chord	Compression	Class 1 or 2 and $10 \le d_0/t_0 \le 50$ (but for X joints: $d_0/t_0 \le 40$)	
	Tension	$10 \le d_0/t_0 \le 50$ (but for X joints: $d_0/t_0 \le 40$)	
CHS braces	Compression	Class 1 or 2 and $d_{\mathrm{i}}/t_{\mathrm{i}} \le 50$	
	Tension	$d_{\mathrm{i}}/t_{\mathrm{i}} \le 50$	

7.1.2 Uniplanar T and Y-CHS joint

Overview of the considered examples in the study is given in Tab. 7.1.3. Selected cases cover a wide range of joint geometric ratios. Geometry of the joints with dimensions is shown in Fig. 7.1.2. In the selected cases, the joints failed according to the FMM by the chord plastification or punching shear.

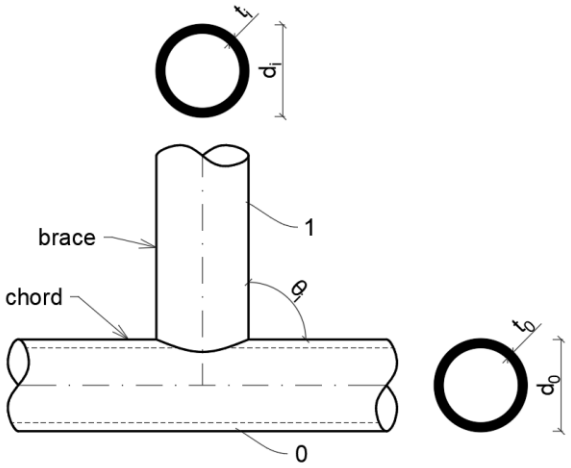

Fig. 7.1.4 Dimensions of T/Y joint

Tab. 7.1.3 Examples overview

Example	Chord	Brace	Angles	Material		
	Section	Section	θ	f_y	f_u	E
			[°]	[MPa]	[MPa]	[GPa]
1	CHS219.1/5.0	CHS48.3/5.0	90	355	490	210
2	CHS219.1/5.0	CHS114.3/6.3	90	355	490	210
3	CHS219.1/6.3	CHS114.3/6.3	90	355	490	210
4	CHS219.1/10.0	CHS60.3/5.0	90	355	490	210
5	CHS219.1/18,0	CHS159/14,0	90	355	490	210
6	CHS219.1/8.0	CHS48.3/5.0	90	355	490	210
7	CHS219.1/4.5	CHS168.3/8.0	60	355	490	210
8	CHS219.1/5.0	CHS60.3/5.0	60	355	490	210
9	CHS219.1/6.3	CHS219.1/8.0	60	355	490	210
10	CHS219.1/8.0	CHS88.9/5.0	60	355	490	210
11	CHS219.1/6.3	CHS60.3/5.0	60	355	490	210
12	CHS219.1/6.3	CHS76.1/5.0	60	355	490	210
13	CHS219.1/4.5	CHS48.3/5.0	30	355	490	210
14	CHS219.1/4.5	CHS193.7/10.0	30	355	490	210
15	CHS219.1/5,0	CHS139.7/10.0	30	355	490	210
16	CHS219.1/8,0	CHS114.3/6.3	30	355	490	210
17	CHS219.1/6.3	CHS139.7/10.0	30	355	490	210
18	CHS219.1/6.3	CHS88.9/5.0	30	355	490	210

Verification of resistance

The results of the method based on FMM are compared with the results of CBFEM. The comparison is focused on the resistance and design failure mode. The results are presented in Tab. 7.1.4.

The study shows a good agreement for the applied load cases. The results are summarized in a diagram comparing CBFEM's and FMM's design resistances; see Fig. 7.1.5. The results show that the difference between the two calculation methods is in all cases less than 11%.

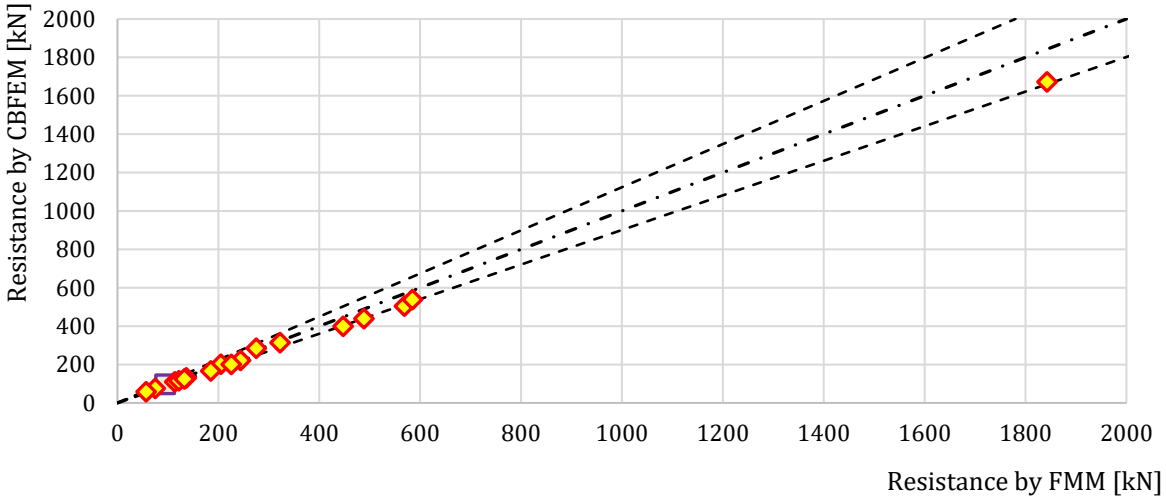

Fig. 7.1.5 Verification of CBFEM to FMM for the uniplanar CHS T and Y-joint

Tab. 7.1.4 Comparison of results of prediction by CBFEM and FMM

Example	Design resistance for loading in tension/compression				
	FMM [kN]	Mode of failure	CBFEM [kN]	Mode of failure	diff, [%]
1	56,9	Chord plastification	57,9	Chord plastification	2
2	122,0	Chord plastification	116,1	Chord plastification	5
3	185,0	Chord plastification	166,6	Chord plastification	10
4	225,8	Chord plastification	200,6	Chord plastification	11
5	1842,8	Chord punching shear	1672,0	Chord punching shear	9
6	132,7	Chord plastification	124,7	Chord plastification	6
7	205,0	Chord plastification	201,9	Chord plastification	2
8	74,9	Chord plastification	75,7	Chord plastification	1
9	584,7	Chord plastification	538,6	Chord plastification	8
10	244,1	Chord plastification	221,5	Chord plastification	9
11	113,5	Chord plastification	109,6	Chord plastification	3
12	136,4	Chord plastification	131,2	Chord plastification	4
13	94,2	Chord plastification	97,7	Chord plastification	4
14	447,4	Chord plastification	399,1	Chord plastification	11
15	322,4	Chord plastification	314,1	Chord plastification	3
16	568,8	Chord plastification	504,6	Chord plastification	11
17	488,7	Chord plastification	439,7	Chord plastification	10
18	275,1	Chord plastification	284,8	Chord plastification	4

Benchmark example

Inputs

Chord

- Steel S355
- Section CHS219.1/5.0

Brace

- Steel S355
- Sections CHS48.3/5.0
- Angle between the brace member and the chord 90°

Weld

- Butt weld around the brace

Loaded

- By force to brace in compression

Mesh size

- 64 elements along surface of the circular hollow member

Outputs

- The design resistance in compression is N_{Rd} = 57,9 kN
- The design failure mode is chord plastification

7.1.3 Uniplanar X-CHS joint

Overview of the considered examples in the study is given in the Tab. 7.1.5. Selected cases cover a wide range of joint geometric ratios. Geometry of the joints with dimensions is shown in Fig. 7.1.6. In the selected cases, the joints failed according to the FMM by the chord plastification or punching shear.

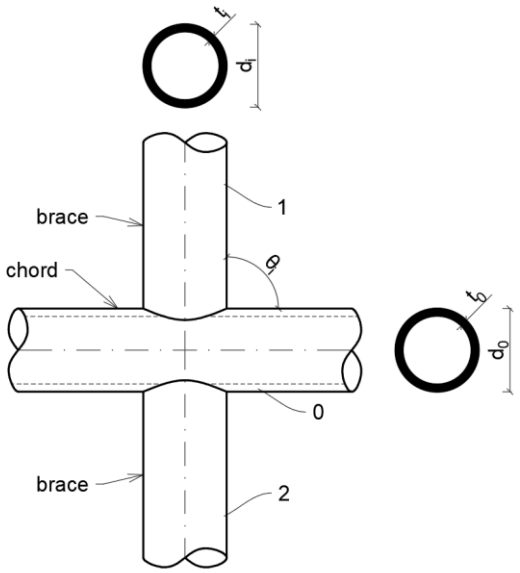

Fig. 7.1.6 Dimensions of X joint

Tab. 7.1.5 Examples overview

Example	Chord	Brace	Angles	Material		
	Section	Section	θ	f_y	f_u	E
			[°]	[MPa]	[MPa]	[GPa]
1	CHS219.1/6.3	CHS60.3/5.0	90	355	490	210
2	CHS219.1/8.0	CHS76.1/5.0	90	355	490	210
3	CHS219.1/10.0	CHS139.7/10.0	90	355	490	210
4	CHS219.1/12.5	CHS114.3/6.3	90	355	490	210
5	CHS219.1/10.0	CHS76.1/5.0	90	355	490	210
6	CHS219.1/8.0	CHS114.3/6.3	90	355	490	210
7	CHS219.1/6.3	CHS48.3/5.0	60	355	490	210
8	CHS219.1/6.3	CHS114.3/6.3	60	355	490	210
9	CHS219.1/8.0	CHS60.3/5.0	60	355	490	210
10	CHS219.1/10.0	CHS114.3/6.3	60	355	490	210
11	CHS219.1/12.5	CHS139.7/10.0	60	355	490	210
12	CHS219.1/8.0	CHS139.7/10.0	60	355	490	210
13	CHS219.1/6.3	CHS48.3/5.0	30	355	490	210
14	CHS219.1/6.3	CHS193.7/16.0	30	355	490	210
15	CHS219.1/6.3	CHS219.1/20.0	30	355	490	210
16	CHS219.1/8.0	CHS76.1/5.0	30	355	490	210
17	CHS219.1/8.0	CHS168.3/12.5	30	355	490	210
18	CHS219.1/12.5	CHS168.3/12.5	30	355	490	210

Verification of resistance

The results of CBFEM are compared with the results of FMM. The comparison is focused on the resistance and design failure mode. The results are presented in Tab. 7.1.6.

Tab. 7.1.6 Comparison of results of prediction by CBFEM and FMM

Example	Design resistance for loading in tension/compression				
	FMM [kN]	Mode of failure	CBFEM [kN]	Mode of failure	diff. [%]
1	88,8	Chord plastification	91,5	Chord plastification	3
2	155,7	Chord plastification	155,8	Chord plastification	0
3	390,9	Chord plastification	366,4	Chord plastification	6
4	478,7	Chord plastification	427,0	Chord plastification	11
5	235.3	Chord plastification	215.6	Chord plastification	8
6	209.7	Chord plastification	214.5	Chord plastification	2
7	93,7	Chord plastification	89,8	Chord plastification	4
8	155,6	Chord plastification	167,3	Chord plastification	8
9	159,5	Chord plastification	153,4	Chord plastification	4
10	365,8	Chord plastification	348,1	Chord plastification	5
11	682,1	Chord plastification	591,5	Chord plastification	13
12	298.7	Chord plastification	291.9	Chord plastification	2
13	162,3	Chord plastification	162,0	Chord plastification	0
14	555,8	Chord plastification	566,1	Chord plastification	2
15	749,7	Chord plastification	697,8	Chord plastification	7
16	311,4	Chord plastification	289,5	Chord plastification	7
17	669,1	Chord plastification	699,7	Chord plastification	5
18	1527.7	Chord plastification	1393.3	Chord plastification	9

The study shows a good agreement for most of the applied load cases. The results are summarized in a diagram comparing CBFEM's and FMM's design resistances; see Fig. 7.1.7. The results show that the difference between the two calculation methods is in most cases less than 11%. In one case, the CBFEM proves to be slightly conservative with the difference of 13%.

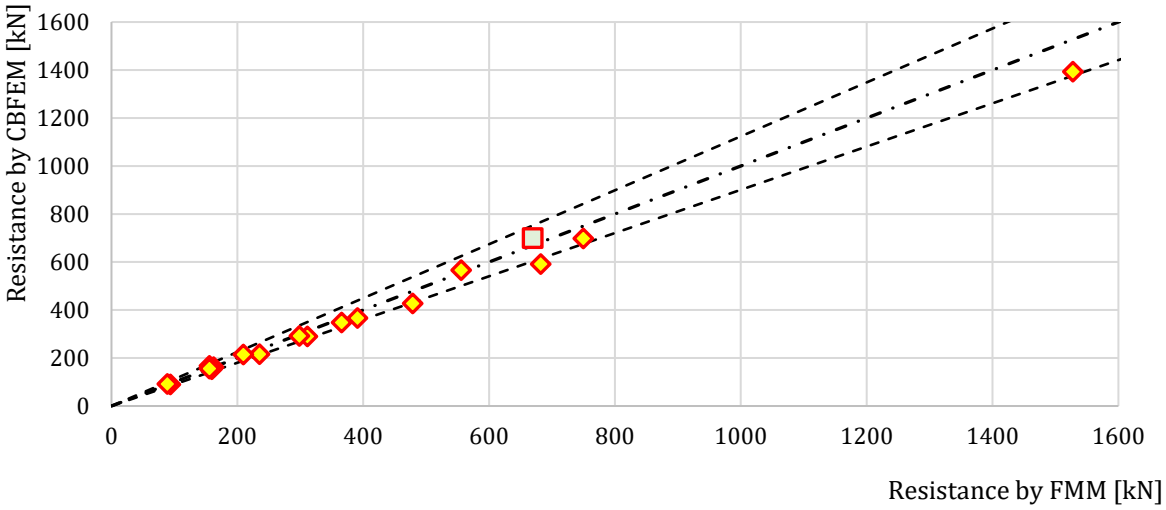

Fig. 7.1.7 Verification of CBFEM to FMM for the uniplanar CHS T and Y-joint

Benchmark example

Inputs

Chord

- Steel S355
- Section CHS219.1/6,3

Brace

- Steel S355
- Sections CHS60,3/5,0
- Angle between the brace member and the chord 90°

Weld

- Butt weld around the brace

Loaded

- By force to brace in compression

Mesh size

- 64 elements along surface of the circular hollow member

Outputs

- The design resistance in compression is NRd = 91,5 kN
- The design failure mode is chord plastification

7.1.4 Uniplanar K-CHS joint

Overview of the considered examples in the study is given in the Tab. 7.1.7. Selected cases cover a wide range of joint geometric ratios. Geometry of the joints with dimensions is shown in Fig. 7.1.8. In the selected cases, the joints failed according to the method based on the failure modes (FMM) by the chord plastification or punching shear.

Tab. 7.1.7 Examples overview

Example	Chord	Brace	Gap	Angles	Material		
	Section	Section	g	θ	f_y	f_u	E
			[mm]	[°]	[MPa]	[MPa]	[GPa]
1	CHS219.1/4,5	CHS139.7/10,0	20,1	60	355	490	210
2	CHS219.1/4,5	CHS219.1/20,0	39,9	60	355	490	210
3	CHS219.1/5,0	CHS88.9/5,0	9,9	60	355	490	210
4	CHS219.1/5,0	CHS219.1/20,0	39,9	60	355	490	210
5	CHS219.1/6,3	CHS48.3/5,0	9,9	60	355	490	210
6	CHS219.1/6,3	CHS60.3/5,0	9,9	60	355	490	210
7	CHS219.1/8,0	CHS114.3/6,3	12,5	60	355	490	210
8	CHS219.1/8,0	CHS139.7/10,0	20,1	60	355	490	210
9	CHS219.1/6.3	CHS114.3/6.3	12.5	60	355	490	210
10	CHS219.1/6.3	CHS139.7/10,0a	20.1	60	355	490	210

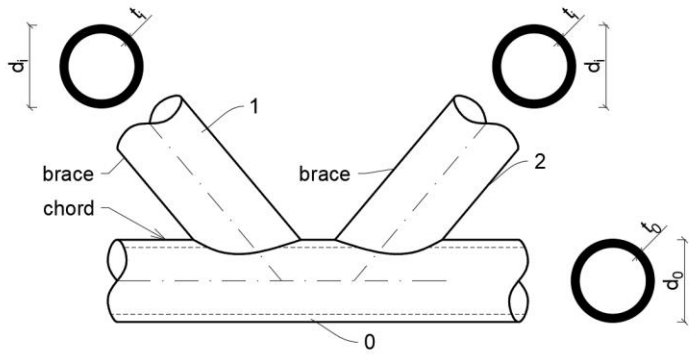

Fig. 7.1.8 Dimensions of K joint

Verification of resistance

The results of the method based on failure modes (FMM) are compared with the results of CBFEM. The comparison is focused on the resistance and design failure mode. The results are presented in Tab. 7.1.8 and in Fig. 7.1.9.

Tab. 7.1.8 Comparison of results of prediction by CBFEM and FMM

Example	Design resistance for loading in tension/compression				
	FMM	Mode of failure	CBFEM	Mode of failure	diff.
	[kN]		[kN]		[%]
1	213,3	Chord plastification	235,6	Chord plastification	10
2	367,5	Chord plastification	377,5	Chord plastification	3
3	165,4	Chord plastification	185,7	Chord plastification	12
4	443,6	Chord plastification	443,5	Chord plastification	0
5	149,2	Chord plastification	153,4	Chord plastification	3
6	175,7	Chord plastification	181,9	Chord plastification	4
7	501,1	Chord plastification	460,1	Chord plastification	8
8	605,6	Chord plastification	540,5	Chord plastification	11
9	324.4	Chord plastification	330.5	Chord plastification	2
10	392.4	Chord plastification	384.7	Chord plastification	2

The study shows a good agreement for the applied load cases. The results are summarized in a diagram comparing CBFEM's and FMM's design resistances; see Fig. 7.1.6. The results show that the difference between the two calculation methods is in all cases less than 12 %.

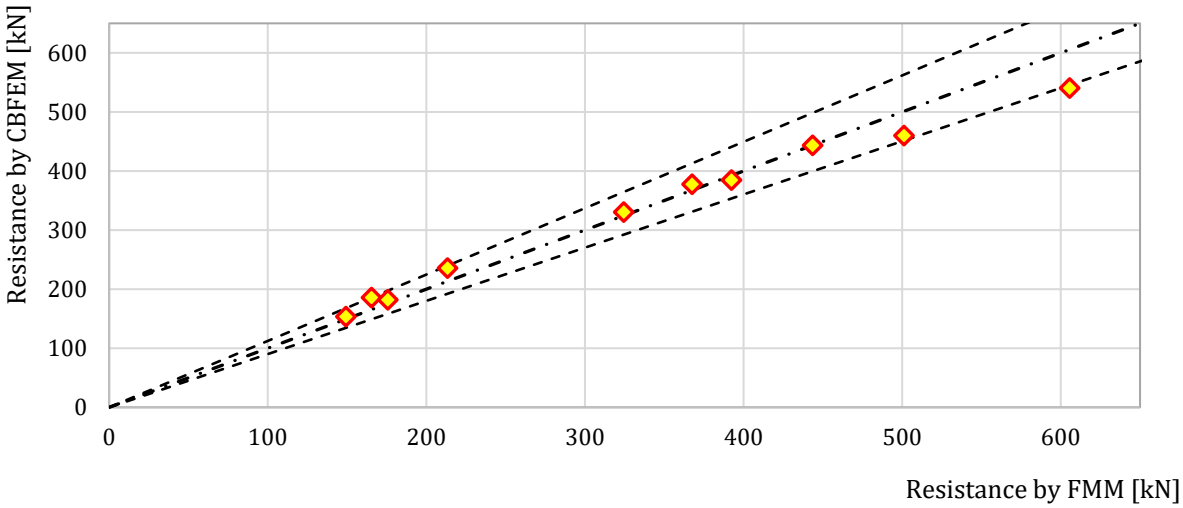

Fig. 7.1.9 Verification of CBFEM to FMM for the uniplanar CHS K-joint

Benchmark example

Inputs

Chord

- Steel S355
- Section CHS219.1/4,5

Brace

- Steel S355
- Sections CHS139,7/10
- Angle between the brace member and the chord 60°

Weld

- Butt weld around the brace

Loaded

- By force to brace in compression

Mesh size

- 64 elements along surface of the circular hollow member

Outputs

- The design resistance in compression is N_{Rd} = 235,6 kN
- The design failure mode is chord plastification

7.2 Rectangular hollow sections

7.2.1 Description

In this chapter, uniplanar welded rectangular, square, hollow sections T, X, and K-joints with gap predicted by CBFEM are verified. Square hollow sections (SHS) brace is welded directly onto an RHS chord without the use of reinforcing plates. The joints are loaded by an axial force. In CBFEM, the design resistance is limited by 5 % of strain or a force corresponding to $0{,}03b_0$ joint deformation and in FMM generally by plate out of plane deformation $0{,}03b_0$ where b_0 is the depth of the RHS chord; see Lu et al. (1994).

7.2.2 Failure mode method

In the case of the axially loaded T, Y, X or K-joint with gap of the welded rectangular hollow sections, five failure modes can occur. These are chord face failure, chord plastification, chord side wall failure, chord web failure, chord shear failure, punching shear failure, and brace failure. In this study, chord face failure, brace failure, and punching shear failure are examined for T, Y and X-joint and chord face failure, chord shear failure, brace failure, and punching shear failure are examined for K-joint with gap; see Fig. 7.2.1. The welds designed according to EN 1993-1-8:2005 are not the weakest components in the joint.

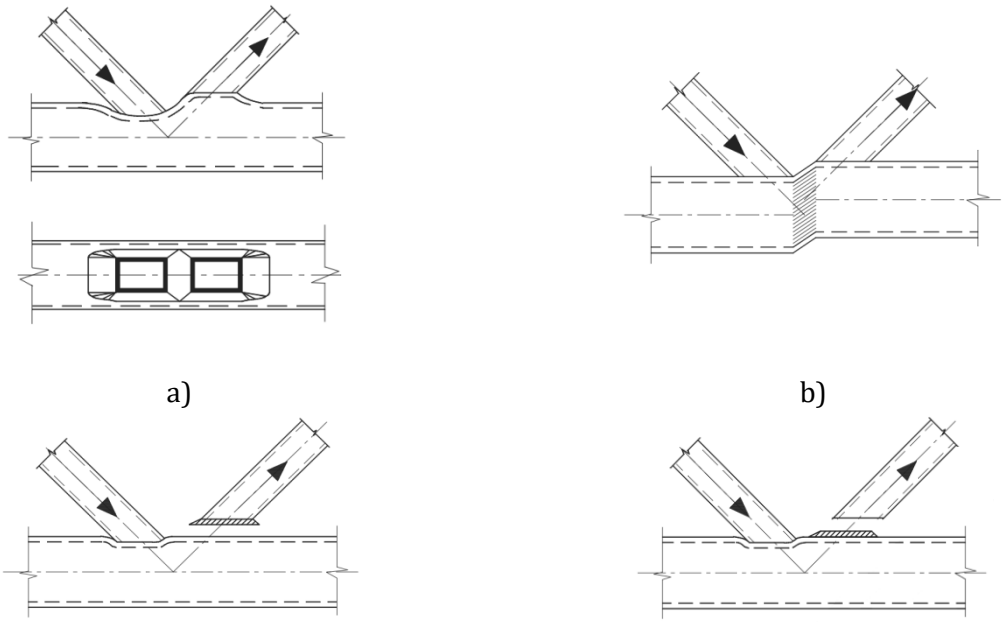

Fig. 7.2.1 Examined failure modes:
a) Chord face failure, b) Chord shear failure, c) Brace failure, and d) Punching shear failure

Chord face failure

The design resistance of an RHS chord face is determined by FMM model in section 9.5 of EN 1993-1-8:2020. The method is also given in the ISO/FDIS 14346 and is described in detail in Wardenier et al. (2010). The design resistance of the axially loaded T, Y or X-joint of welded rectangular hollow sections is

$$N_{\mathrm{i,Rd}} = C_f \frac{f_{\mathrm{y0}} t_0^2}{\sin\theta_{\mathrm{i}}} \left(\frac{2\eta}{(1-\beta)\sin\theta_{\mathrm{i}}} + \frac{4}{\sqrt{1-\beta}} \right) Q_{\mathrm{f}} / \gamma_{\mathrm{M5}} \qquad (7.2.1)$$

The design resistance of the axially loaded K-joint with gap of welded rectangular hollow sections is

$$N_{\mathrm{i,Rd}} = 8{,}9 C_{\mathrm{f}} \beta \gamma^{0{,}5} \frac{f_{\mathrm{y0}} t_0^2}{\sin\theta_1} Q_{\mathrm{f}} / \gamma_{\mathrm{M5}} \qquad (7.2.2)$$

where C_{f} is the material factor, f_{y0} is the yield stress of the chord, t_0 is the wall thickness of the chord, η is the brace height to the chord width ratio, β is the brace width to the chord width ratio, θ_i is the included angle between the brace member i and the chord (i = 1, 2), Q_{f} is the chord stress function, and γ is the chord slenderness ratio.

Brace failure

The design resistance of an RHS chord face can be determined using the method given by FMM model in section 9.5 of EN 1993-1-8:2020. The design resistance of the axially loaded T, Y or X-joint of welded rectangular hollow sections is

$$N_{\mathrm{i,Rd}} = C_{\mathrm{f}} f_{\mathrm{yi}} t_{\mathrm{i}} (2h_{\mathrm{i}} - 4t_{\mathrm{i}} + 2b_{\mathrm{eff}}) / \gamma_{\mathrm{M5}} \qquad (7.2.3)$$

The design resistance of the axially loaded K-joint with gap of welded rectangular hollow sections is

$$N_{\mathrm{i,Rd}} = C_{\mathrm{f}} f_{\mathrm{yi}} t_{\mathrm{i}} (2h_{\mathrm{i}} - 4t_{\mathrm{i}} + b_{\mathrm{i}} + b_{\mathrm{eff}}) / \gamma_{\mathrm{M5}} \qquad (7.2.4)$$

where C_{f} is the material factor, f_{yi} is the yield stress of the brace member i (i = 1, 2), t_{i} is the wall thickness of the brace member i, h_{i} is the height of the brace member i, b_{i} is the width of the brace member i, b_{eff} is the effective width of the brace member.

Punching shear

The design resistance of the axially loaded T, Y or X-joint of welded rectangular hollow sections is

$$N_{\mathrm{i,Rd}} = C_{\mathrm{f}} \frac{f_{\mathrm{y0}} t_0}{\sqrt{3}\sin\theta_{\mathrm{i}}} \left(\frac{2h_{\mathrm{i}}}{\sin\theta_{\mathrm{i}}} + 2b_{\mathrm{e,p}} \right) / \gamma_{\mathrm{M5}} \qquad (7.2.5)$$

The design resistance of the axially loaded K-joint with gap of welded rectangular hollow sections is

$$N_{\mathrm{i,Rd}} = C_{\mathrm{f}} \frac{f_{\mathrm{y0}} t_0}{\sqrt{3}\sin\theta_{\mathrm{i}}} \left(\frac{2h_{\mathrm{i}}}{\sin\theta_{\mathrm{i}}} + b_{\mathrm{i}} + b_{\mathrm{e,p}} \right) / \gamma_{\mathrm{M5}} \qquad (7.2.6)$$

Where C_f is the material factor, f_{y0} is the yield stress of the chord, t_0 is the wall thickness of the chord, θ_i is the included angle between the brace member i and the chord (i = 1, 2), h_i is the height of the brace member i, b_i is the width of the brace member i and $b_{e,p}$ is the effective width for punching shear.

Chord shear failure

The design resistance of the axially loaded K-joint with gap of welded rectangular hollow sections is

$$N_{i,Rd} = \frac{f_{y0} A_{v,0,gap}}{\sqrt{3}\sin\theta_i} / \gamma_{M5} \qquad (7.2.7)$$

where f_{y0} is the yield stress of the chord, $A_{v,0,gap}$ is the effective area for chord shear failure, and θ_i is the included angle between the brace member i and the chord (i = 1, 2).

Range of validity

CBFEM was verified for typical T, Y X, and K-joints with gap of the welded rectangular hollow sections. Range of validity for these joints is defined in Table 9.2 of prEN 1993-1-8:2020; see Tab. 7.2.1. The same range of validity is applied to CBFEM model. Outside the range of validity of FMM, an experiment should be prepared for validation or verification performed for verification according to a validated research model.

Tab. 7.2.1 Range of validity for method of failure modes, Table 9.2 of EN 1993-1-8:2020

General	$0{,}2 \le \frac{d_i}{d_0} \le 1{,}0$	$\theta_i \ge 30^o$	$\frac{e}{d_0} \le 0{,}25$
	$g \ge t_1 + t_2$	$f_{yi} \le f_{y0}$	$t_i \le t_0$
Chord	Compression	Class 1 or 2 and $d_0/t_0 \le 50$ (but for X joints: $d_0/t_0 \le 40$)	
	Tension	$d_0/t_0 \le 50$ (but for X joints: $d_0/t_0 \le 40$)	
RHS braces	Compression	Class 1 or 2; $b_i/t_i \le 35$ and $h_i/t_i \le 35$	
	Tension	$b_i/t_i \le 35$ and $h_i/t_i \le 35$	

7.2.2 Uniplanar T and Y-SHS joint

An overview of the considered examples is given in Tab. 7.2.2. Selected cases cover a wide range of joint geometric ratios. Geometry of joints with dimensions is shown in Fig. 7.2.2. Selected joints failed according to the method based on FMM by the chord face failure or brace failure.

Tab. 7.2.2 Examples overview

Example	Chord	Brace	Angles	Material		
	Section	Section	θ_1	f_y	f_u	E
			[°]	[MPa]	[MPa]	[MPa]
1	SHS200/6.3	SHS70/8.0	90	275	430	210
2	SHS200/8.0	SHS90/8.0	90	275	430	210
3	SHS200/10.0	SHS140/12.5	90	275	430	210
4	SHS200/12.5	SHS120/12.5	90	275	430	210
5	SHS200/16.0	SHS50/6.3	90	275	430	210
6	SHS200/6.3	SHS140/12.5	60	275	430	210
7	SHS200/8.0	SHS80/8.0	60	275	430	210
8	SHS200/10.0	SHS120/12.5	60	275	430	210
9	SHS200/12.5	SHS90/8.0	60	275	430	210
10	SHS200/16.0	SHS160/16.0	60	275	430	210
11	SHS200/6.3	SHS80/8.0	30	275	430	210
12	SHS200/8.0	SHS150/16.0	30	275	430	210
13	SHS200/10.0	SHS100/10.0	30	275	430	210
14	SHS200/12.5	SHS100/10.0	30	275	430	210
15	SHS200/16.0	SHS90/8.0	30	275	430	210

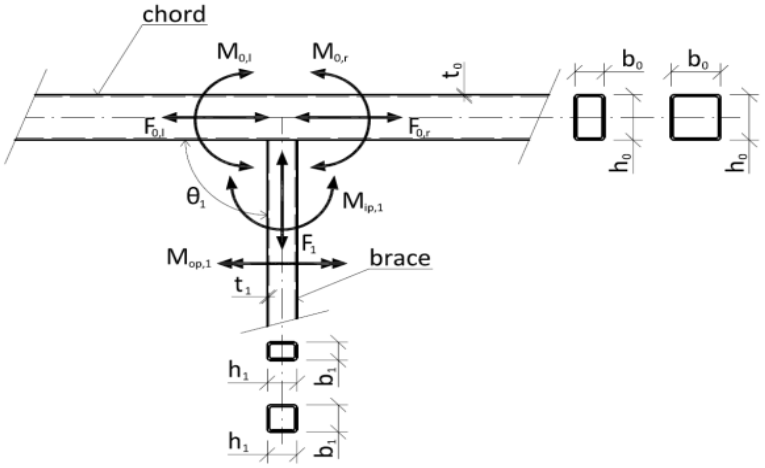

Fig. 7.2.2 Dimensions of T-joint

Verification of resistance

The results of FMM are compared with the results of CBFEM. The comparison is focused on the resistance and design failure mode. The results are presented in Tab. 7.2.3.

Tab. 7.2.3 Comparison of results predicted by CBFEM and FMM

Example	Design resistance loading in tension/compression				
	FMM [kN]	Mode of failure	CBFEM [kN]	Mode of failure	Diff. [%]
1	65,9	Chord face failure	63,0	Chord face failure	4
2	123,7	Chord face failure	113,7	Chord face failure	8
3	329,2	Chord face failure	354,0	Chord face failure	8
4	400,7	Chord face failure	419,5	Chord face failure	5
5	302,8	Brace failure	263,0	Brace failure	13
6	160,0	Chord face failure	160,5	Chord face failure	0
7	136,2	Chord face failure	125,3	Chord face failure	8
8	310,8	Chord face failure	306,5	Chord face failure	1
9	361,4	Chord face failure	327,0	Chord face failure	10
10	1478,0	Chord face failure	1373,7	Chord face failure	7
11	170,9	Chord face failure	160,9	Chord face failure	6
12	704,0	Chord face failure	638,5	Chord face failure	9
13	531,1	Chord face failure	468,6	Chord face failure	12
14	829,9	Chord face failure	731,9	Chord face failure	12
15	721,6	Brace failure	647,8	Brace failure	10

The study shows a good agreement for the applied load cases. The results are summarized in a diagram comparing design resistances of CBFEM and FMM; see Fig. 7.2.3. The results show that the difference between the two calculation methods is in all cases less than 13 %.

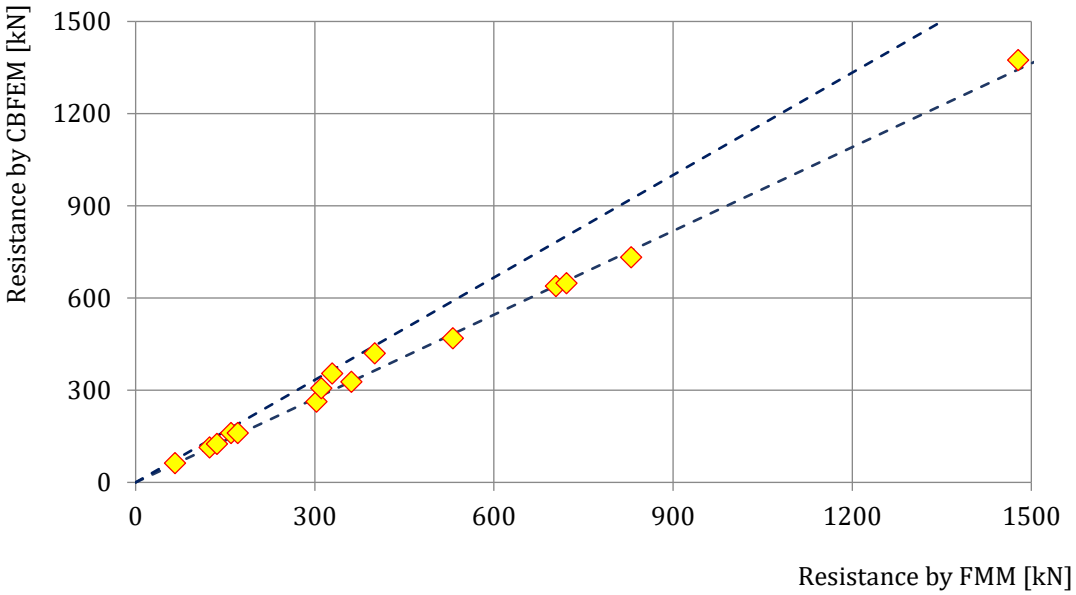

Fig. 7.2.3 Verification of resistance determined by CBFEM to FMM for the uniplanar SHS T and Y-joint

Benchmark example

Inputs

Chord

- Steel S275
- Section SHS 200×200×6,3

Brace

- Steel S275
- Section SHS 70×70×8,0
- Angle between the brace member and the chord 90°

Weld

- Butt weld

Mesh size

- 16 elements on the biggest web of rectangular hollow member

Loaded

- By force to brace in compression/tension

Outputs

- The design resistance in compression/tension is N_{Rd} = 63,0 kN
- The design failure mode is chord face failure

7.2.3 Uniplanar X-SHS joint

An overview of the considered examples is given in the Tab. 7.2.4. Selected cases cover a wide range of joint geometric ratios. The selected joints failed according to the method based on FMM by the chord face failure or brace failure.

Tab. 7.2.4 Examples overview

Example	Chord	Brace	Angles	Material		
	Section	Section	θ	f_y	f_u	E
			[°]	[MPa]	[MPa]	[MPa]
1	SHS200/6.3	SHS140/12.5	90	275	430	210
2	SHS200/8.0	SHS70/8.0	90	275	430	210
3	SHS200/10.0	SHS120/12.5	90	275	430	210
4	SHS200/12.5	SHS90/8.0	90	275	430	210
5	SHS200/16.0	SHS160/16.0	90	275	430	210
6	SHS200/6.3	SHS70/8.0	60	275	430	210
7	SHS200/8.0	SHS80/8.0	60	275	430	210
8	SHS200/10.0	SHS150/6.0	60	275	430	210
9	SHS200/12.5	SHS140/12.5	60	275	430	210
10	SHS200/16.0	SHS120/12.5	60	275	430	210
11	SHS200/6.3	SHS80/8.0	30	275	430	210
12	SHS200/8.0	SHS150/16.0	30	275	430	210
13	SHS200/10.0	SHS100/10.0	30	275	430	210
14	SHS200/12.5	SHS160/16.0	30	275	430	210
15	SHS200/16.0	SHS90/8.0	30	275	430	210

Verification of resistance

The results of the method based on failure modes (FMM) are compared with the results of CBFEM. The comparison is focused on the resistance and design failure mode; see Tab. 7.2.5.

Tab. 7.2.5 Comparison of results of prediction by CBFEM and FMM

Example	Design resistance loading in tension/compression				
	FM	Mode of failure	CBFEM	Mode of failure	Diff.
	[kN]		[kN]		[%]
1	130,6	Chord face failure	131,6	Chord face failure	1
2	106,3	Chord face failure	92,1	Chord face failure	13
3	256,4	Chord face failure	252,5	Chord face failure	2
4	302,1	Chord face failure	281,4	Chord face failure	7
5	1192,9	Chord face failure	1177,9	Chord face failure	1
6	78,2	Chord face failure	68,4	Chord face failure	12
7	136,2	Chord face failure	120,9	Chord face failure	11
8	474,0	Chord face failure	479,1	Chord face failure	1
9	629,7	Chord face failure	659,1	Chord face failure	5
10	795,7	Chord face failure	761,1	Chord face failure	4
11	170,9	Chord face failure	159,8	Chord face failure	7
12	704,0	Chord face failure	646,5	Chord face failure	8
13	531,1	Chord face failure	469,5	Chord face failure	12
14	1813,9	Brace failure	1670,8	Brace failure	8
15	721,6	Brace failure	650,3	Brace failure	10

The study shows a good agreement for the applied load cases. The results are summarized in a diagram comparing design resistances of CBFEM and FMM; see Fig. 7.2.4. The results show that the difference between the two calculation methods is in all cases less than 13 %.

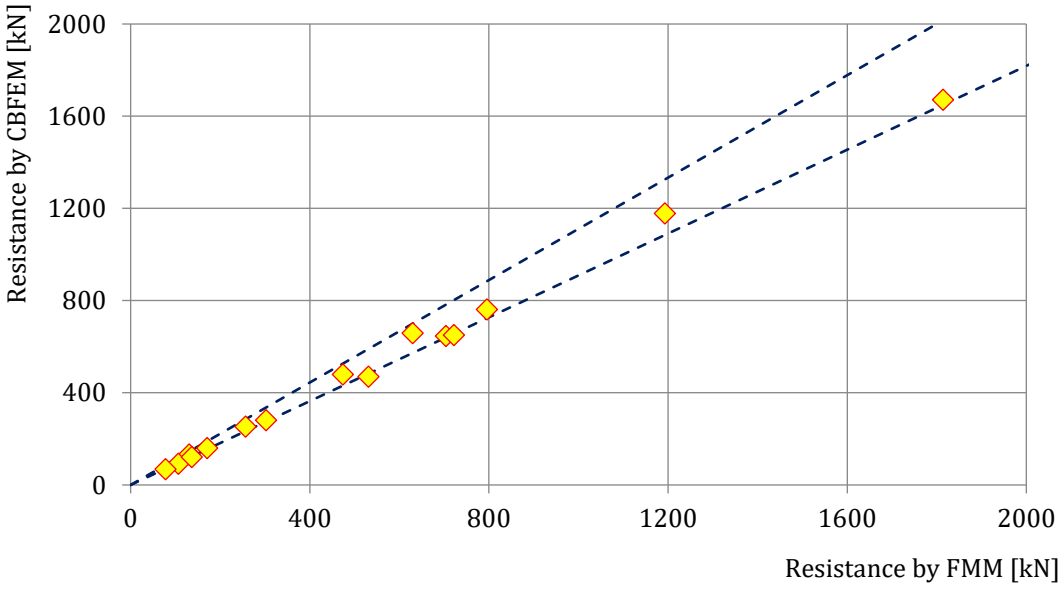

Fig. 7.2.4 Verification of resistance determined by CBFEM to FMM for the uniplanar SHS X-joint

Benchmark example

Inputs

Chord

- Steel S275
- Section SHS 200×200×6,3

Braces

- Steel S275
- Sections SHS 140×140×12,5
- Angle between the brace members and the chord 90°

Welds

- Butt welds

Mesh size

- 16 elements on the biggest web of rectangular hollow member

Loaded

- By force to brace in compression/tension

Outputs

- The design resistance in compression/tension is N_{Rd} = 131,6 kN
- The design failure mode is chord face failure

7.2.4 Uniplanar K-SHS joint

An overview of the considered examples is given in the Tab. 7.2.6. Selected cases cover a wide range of joint geometric ratios. The selected joints failed according to the method based on FMM by the chord face failure or brace failure.

Tab. 7.2.6 Examples overview

Example	Chord	Braces	Angles	Material		
	Section	Sections	θ	f_y	f_u	E
			[°]	[MPa]	[MPa]	[MPa]
1	SHS200/8.0	SHS160/16.0	45	275	430	210
2	SHS200/10.0	SHS150/16.0	45	275	430	210
3	SHS200/10.0	SHS160/16.0	45	275	430	210
4	SHS200/12.5	SHS140/12.5	45	275	430	210
5	SHS200/12.5	SHS150/16.0	45	275	430	210
6	SHS200/12.5	SHS160/16.0	45	275	430	210
7	SHS200/16.0	SHS50/6.3	45	275	430	210
8	SHS200/16.0	SHS70/8.0	45	275	430	210
10	SHS200/16.0	SHS80/8.0	45	275	430	210

Verification

The results of CBFEM are compared with the results of FMM. The comparison is focused on the resistance and design failure mode. The results are presented in Tab. 7.2.7.

Tab. 7.2.7 Comparison of results of prediction by CBFEM and FMM

Example	Design resistance loading in tension/compression				
	FM	Mode of failure	CBFEM	Mode of failure	diff
	[kN]		[kN]		[%]
1	626,6	Chord face failure	571,7	Chord face failure	9
2	800,1	Chord face failure	729,7	Chord face failure	9
3	875,6	Chord face failure	846,1	Chord face failure	3
4	1070,8	Chord face failure	968,5	Chord face failure	10
5	1147,3	Chord face failure	1097,9	Chord face failure	4
6	1223,8	Chord face failure	1236,8	Chord face failure	1
7	302,8	Brace failure	268,3	Brace failure	11
8	545,6	Brace failure	479,4	Brace failure	12
15	633,6	Brace failure	563,5	Brace failure	11

The study shows a good agreement for the applied load cases. The results are summarized in a diagram comparing design resistances of CBFEM and FMM; see Fig. 7.2.5. The results show that the difference between the two calculation methods is in all cases less than 12%.

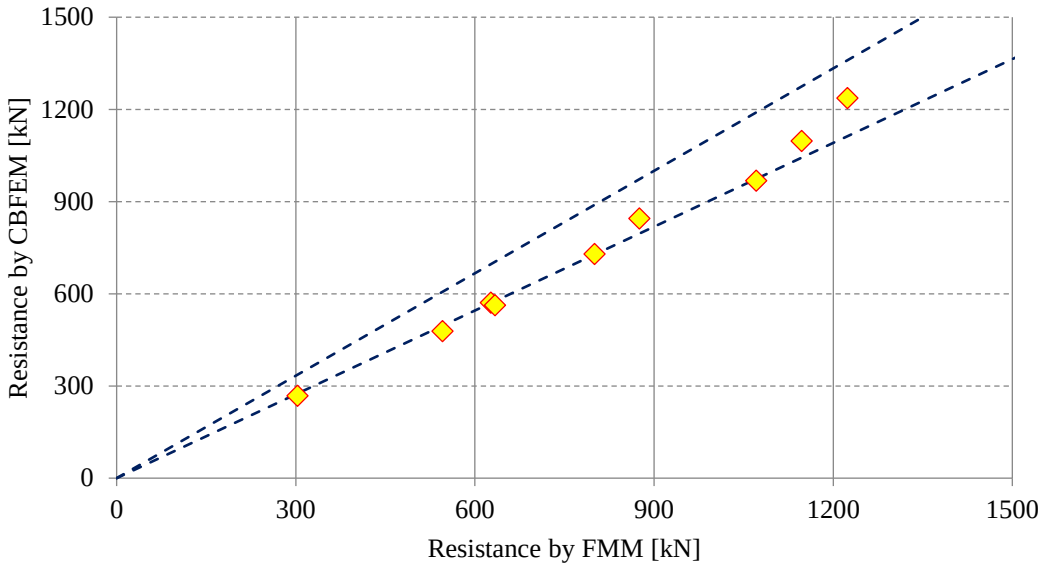

Fig. 7.2.5 Verification of resistance determined by CBFEM to FMM for the uniplanar SHS K-joint

Benchmark example

Inputs

Chord

- Steel S275
- Section SHS 200×200×8,0

Braces

- Steel S275
- Sections SHS 160×160×16,0
- Angle between the brace members and the chord 45°

Welds

- Butt welds

Mesh size

- 16 elements on the biggest web of rectangular hollow member

Loaded

- By force to brace in compression/tension

Outputs

- The design resistance in compression/tension is N_{Rd} = 571,7 kN
- The design failure mode is chord face failure

7.3 Plate to circular hollow section

7.3.1 Failure mode method

Uniplanar welded plate to circular hollow sections T-joints predicted by CBFEM are verified to FMM in this chapter. In CBFEM, the design resistance is limited by reaching 5 % of strain or a force corresponding to 3 % d_0 joint deformation, where d_0 is chord diameter. The FMM is based on the peak load limit or 3 % d_0 deformation limit; see Lu et al. (1994). The welds, designed according to EN 1993-1-8:2006, are not the weakest components in the joint.

Chord plastification

The design resistance of a CHS chord face is determined using the method given by FMM model in Ch. 9 of prEN 1993-1-8:2020 and in ISO/FDIS 14346; see Fig. 7.3.1. The design resistance of the axially loaded welded plate to CHS joint is:

T joint

Transverse

$$N_{1,\mathrm{Rd}} = 2{,}5 \cdot C_\mathrm{f} \cdot f_\mathrm{yo} \cdot t_0^2 \cdot (1 + 3 \cdot \beta^2) \cdot \gamma^{0{,}35} \cdot Q_\mathrm{f}/\gamma_\mathrm{M5} \qquad (7.3.1)$$

Longitudinal

$$N_{1,\mathrm{Rd}} = 7{,}4 \cdot C_\mathrm{f} \cdot f_\mathrm{yo} \cdot t_0^2 \cdot (1 + 0{,}4 \cdot \eta) \cdot Q_\mathrm{f}/\gamma_\mathrm{M5} \qquad (7.3.2)$$

X joint

Transverse

$$N_{1,\mathrm{Rd}} = 2{,}1 \cdot C_\mathrm{f} \cdot f_\mathrm{yo} \cdot t_0^2 \cdot (1 + 3 \cdot \beta^2) \cdot \gamma^{0{,}25} \cdot Q_\mathrm{f}/\gamma_\mathrm{M5} \qquad (7.3.3)$$

Longitudinal

$$N_{1,Rd} = 3{,}5 \cdot C_\mathrm{f} \cdot f_\mathrm{yo} \cdot t_0^2 \cdot (1 + 0{,}4 \cdot \eta) \cdot \gamma^{0{,}1} \cdot Q_\mathrm{f}/\gamma_\mathrm{M5} \qquad (7.3.4)$$

where:

$f_{\mathrm{y,i}}$ is a yield strength of member i (i = 0,1,2 or 3)
t_i is thickness of the wall of CHS member i (i = 0,1,2 or 3)
β is a ratio of the mean diameter or width of brace members, to that of the chord
η is the ratio of the brace member depth to the chord diameter or width
γ is a ratio of a chord width or diameter to twice its wall thickness
Q_f is a chord stress factor
C_f is a material factor
γ_M5 is partial factor for resistance of joints in hollow section lattice girders
$N_{\mathrm{i,Rd}}$ is a design resistance of a joint expressed in terms of the internal axial force in member i (i = 0,1,2 or 3)

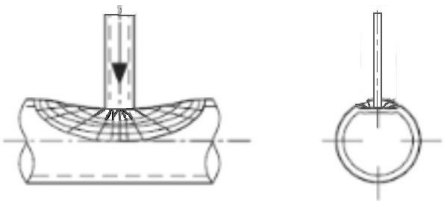

Fig. 7.3.1 Examined failure mode - chord plastification

Range of validity

CBFEM was verified for typical joints of the welded circular hollow sections. The range of validity for these joints is defined in Table 7.8 of prEN 1993-1-8:2020; see Tab 7.3.1. The same range of validity is applied to CBFEM model. Outside the range of validity of FMM, an experiment should be prepared for validation or verification performed for verification according to a validated research model.

Tab. 7.3.1 Range of validity for method of failure modes

General	$0{,}2 \leq \frac{d_\mathrm{i}}{d_0} \leq 1{,}0$	$\theta_\mathrm{i} \geq 30^\mathrm{o}$	$-0{,}55 \leq \frac{e}{d_0} \leq 0{,}25$
	$g \geq t_1 + t_2$	$f_\mathrm{yi} \leq f_\mathrm{y0}$	$t_\mathrm{i} \leq t_0$
Chord	Compression	Class 1 or 2 and $10 \leq d_0/t_0 \leq 50$ (but for X joints: $d_0/t_0 \leq 40$)	
	Tension	$10 \leq d_0/t_0 \leq 50$ (but for X joints: $d_0/t_0 \leq 40$)	
Transverse plate	-	$0{,}25 \leq \beta = b_1/d_0 \leq 1$	
Longitudinal plate	-	$0{,}6 \leq \eta = h_1/d_0 \leq 4$	

7.3.2 Validation

In this chapter, the CBFEM is validated to the FMM models of plate to CHS T-joints described in prEN 1993-1-8:2020. The models are compared against the data from mechanical tests in Tabs 7.3.2–7.3.3 with resistance based on deformation limit. Material and geometric properties of numerical tests are described in (Voth A.P. and Packer A.J., 2010). The experiments out of range of validity are marked in tables by star * and in graph indicated to show the quality of the boundary conditions.

Tab. 7.3.2 Geometric properties, material properties,
and resistances of connections from experiments and FMM models for transverse T-joint

ID	Reference	d_0 [mm]	t_0 [mm]	h_1 [mm]	h_1/d_0 [-]	d_0/t_0 [-]	f_{y0} [MPa]
TPT 1	Washio et al. (1970)	165,2	5,2	115,6	0,7	31,8	308,0
TPT 2	Washio et al. (1970)	165,2	5,2	148,7	0,9	31,8	308,0
TPT 3	Washio et al. (1970)	139,8	3,5	125,8	0,9	39,9	343,0
TPT 4	Voth et al. (2012)	219,2	4,5	100,3	0,5	48,8	388,8

ID	$N_{u,exp}$ [kN]	Branch type	$N_{u,exp}/(t_0^2 \cdot f_{y0})$	$N_{1,prEN}/(t_0^2 \cdot f_{y0})$	$N_{u,exp}/N_{1,prEN}$
TPT 1	169,4	Compression	20,34	16,25	1,25
TPT 2	250,5	Compression	30,08	22,58	1,33
TPT 3	184,8	Compression	43,98	24,45	1,80
TPT 4	282,5	Tension	36,04	12,45	2,89

Tab. 7.3.3 Geometric properties, material properties,
and resistances of connections from experiments and FMM models for longitudinal T-joint

ID	Reference	d_0 [mm]	t_0 [mm]	h_1 [mm]	h_1/d_0 [-]	d_0/t_0 [-]	f_{y0} [MPa]
TPL 1	Washio et al. (1970)	165,2	5,2	165,2	1,0	31,8	308,0
TPL 2	Washio et al. (1970)	165,2	5,2	330,4	2,0	31,8	308,0
*TPL 3	Voth et al. (2012)	219,2	4,5	99,9	0,5	48,8	388,8

ID	$N_{u,exp}$ [kN]	Branch type	$N_{u,exp}/(t_0^2 \cdot f_{y0})$	$N_{1,prEN}/(t_0^2 \cdot f_{y0})$	$N_{u,exp}/N_{1,prEN}$
TPL 1	107,6	Compression	12,92	10,36	1,25
TPL 2	127,4	Compression	15,30	13,32	1,15
*TPL 3	160,6	Tension	20,49	8,75	2,34

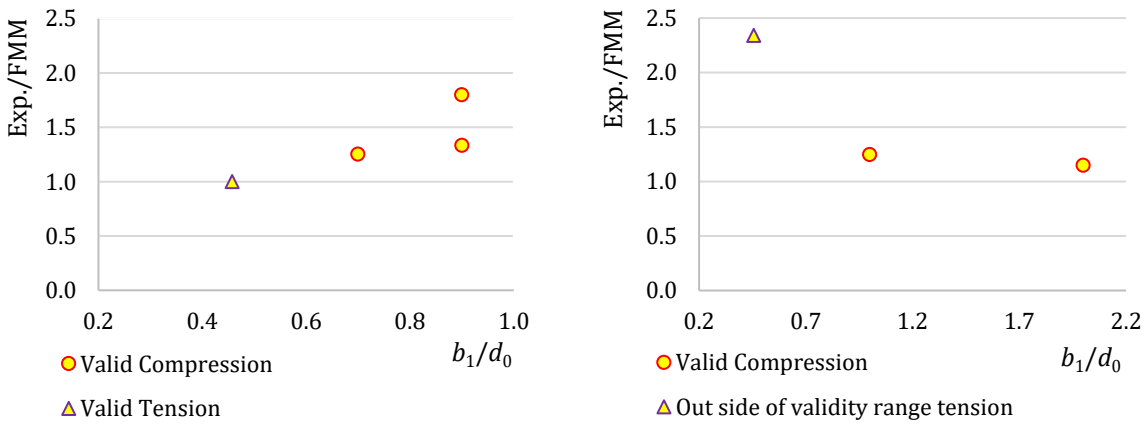

Fig. 7.3.2 Validation of FMM to mechanical experiments for transverse T-type plate-to-CHS connections (left) and to longitudinal T-type plate-to-CHS connections (right)

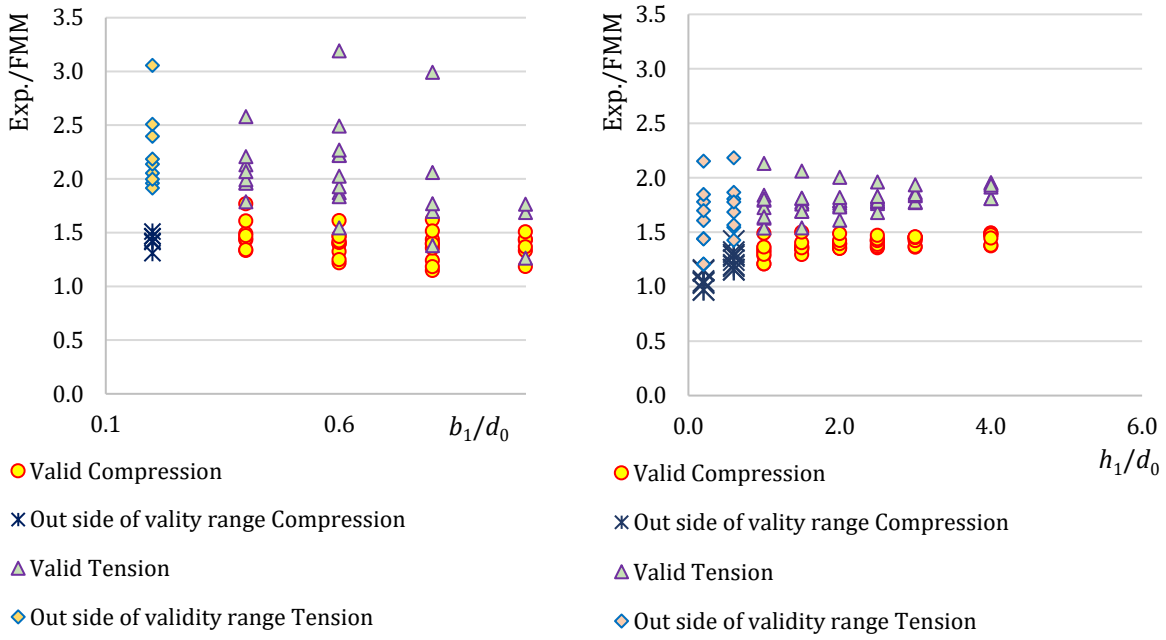

Fig. 7.3.3 Validation of FMM to mechanical experiments for transverse T-type plate-to-CHS connections (left) and longitudinal T-type plate-to-CHS connections (right)

The validation shown in Figs 7.3.2 and 7.3.3 demonstrates that differences to experiments are at least 15 % generally to the safe side. The experiments out of the range of validity are included and marked. The results indicate the good quality of the chosen boundary conditions.

7.3.3 Uniplanar plate T-joint

An overview of the considered examples in the study is given in the Tab. 7.3.4. Selected cases cover a wide range of joint geometric ratios. Geometry of the joints with dimensions is shown in Fig. 7.3.4. Plate thickness is 15 mm in all cases covered in this study.

Tab. 7.3.4 Examples overview

Example	Chord	Plate orientation	Plate width	Material		
	Section	-	b_1/h_1	f_y	f_u	E
			[mm]	[MPa]	[MPa]	[GPa]
1	CHS219.1/4,5	Transverse	80,0	355	490	210
2	CHS219.1/4,5	Transverse	140,0	355	490	210
3	CHS219.1/5,0	Transverse	80,0	355	490	210
4	CHS219.1/8,0	Transverse	115,0	355	490	210
5	CHS219.1/8,0	Transverse	170,0	355	490	210
6	CHS219.1/6,3	Transverse	90,0	355	490	210
7	CHS219.1/4,5	Longitudinal	180,0	355	490	210
8	CHS219.1/4,5	Longitudinal	250,0	355	490	210
9	CHS219.1/4,5	Longitudinal	380,0	355	490	210
10	CHS219.1/4,5	Longitudinal	500,0	355	490	210

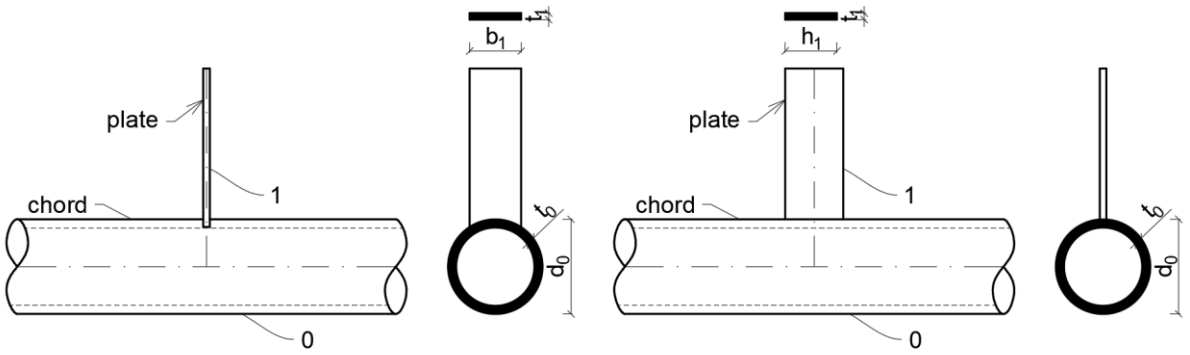

Fig. 7.3.4 Dimensions of plate to CHS T joint, transverse (left) and longitudinal (right)

Verification

The results of resistance and design failure mode of the FMM are compared with the results of CBFEM in Tab. 7.3.5 and in Fig. 7.3.5.

Tab. 7.3.5 Verification of prediction by CBFEM on FMM

Example	Design resistance for loading in tension/compression				
	FMM	Mode of failure	CBFEM	Mode of failure	diff.
	[kN]		[kN]		[%]
1	70,8	Chord plastification	72,5	Chord plastification	2
2	112,4	Chord plastification	117,0	Chord plastification	4
3	84,2	Chord plastification	80,0	Chord plastification	5
4	238,5	Chord plastification	230,5	Chord plastification	3
5	366,5	Chord plastification	390,5	Chord plastification	7
6	132,6	Chord plastification	129,0	Chord plastification	3
7	67,8	Chord plastification	64,5	Chord plastification	5
8	74,3	Chord plastification	76,0	Chord plastification	2
9	86,4	Chord plastification	92,0	Chord plastification	6
10	97,6	Chord plastification	97,5	Chord plastification	0

The study shows good agreement for the applied load cases. The results are summarized in a diagram comparing CBFEM's and FMM's design resistances; see Fig. 7.3.5. The results show that the difference between the two calculation methods is in all cases less than 7 %.

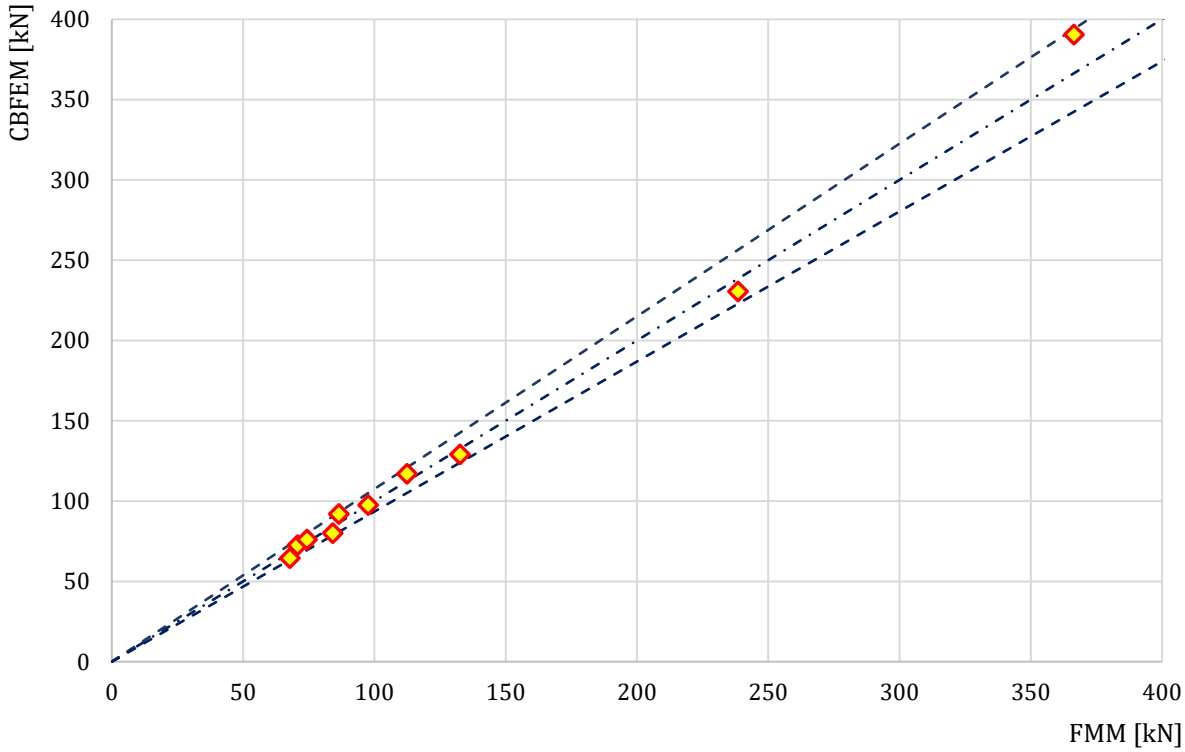

Fig. 7.3.5 Verification of CBFEM to FMM for the uniplanar Plate to CHS T-joint

Benchmark example

Inputs

Chord

- Steel S355
- Section CHS219.1/4,5

Brace

- Steel S355
- Plate 80/15 mm
- Angle between the brace member and the chord 90°

Weld

- Butt weld around the brace

Loaded

- By force to brace in compression

Mesh size

- 64 elements along surface of the circular hollow member

Outputs

- The design resistance in compression is N_{Rd} = 72,5 kN
- The design failure mode is chord plastification

7.4 Uniplanar T-joint between RHS brace and H/I chord

7.4.1 Description

A uniplanar T-joint of a rectangular hollow section brace to an open section chord, which is located in a lattice truss is studied. The RHS brace is welded directly onto the H or I chord (open sections) without use of reinforcing plates. The prediction by component-based finite element method (CBFEM) is verified with the failure modes method (FM) implemented in EN 1993-1-8:2005.

7.4.2 Analytical model

Three failure modes occur in the uniplanar T-joint of the welded rectangular hollow sections to the open sections: the local yielding of brace (brace failure), the chord web failure, and the chord shear. All these failure modes are examined in this study; see Fig. 7.4.1. Welds are designed not to be the weakest component in a joint according to EN 1993-1-8:2005. The elements of lattice trusses are loaded by normal forces and bending moments. A point of action of internal forces of T-joint is described as follows:

Axially loaded H/I chord

Normal forces in the chord right and left of a T-joint act in the direction of chord longitudinal axis.

Diffraction loaded H/I chord

Bending moments right and left of a T-joint in plane of the T-joint are considered in the chord, and these bending moments rotate around one of the axes in plane of the chord cross-section for rotation in plane of the T-joint.

Axially loaded RHS brace

The normal force in the brace of a T-joint acts in the direction of brace longitudinal axis.

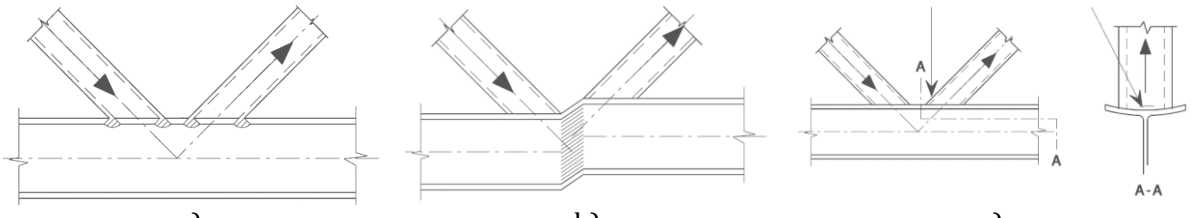

a) b) c)

Fig. 7.4.1 Major failure modes a) chord web failure, b) chord shear (in case of gap), c) brace failure

The resistance of the chord web is determined using the method given in section 7.6 of the EN 1993-1-8:2005, which is described in (Wardenier et al. 2010). The stresses from the brace are transferred through the flange of the chord to an effective area of the chord web. This area is located in the chord web at the point where the brace walls cross the chord web. The design axial resistance of the joint is the minimum of the design resistances:

Chord web failure

$$N_{\mathrm{i,Rd}} = \frac{f_{\mathrm{y0}}\, t_{\mathrm{w}}\ b_{\mathrm{w}}}{\sin\theta_{\mathrm{i}} \cdot \gamma_{\mathrm{M5}}} \tag{7.4.1}$$

Chord shear

$$N_{\mathrm{i,Rd}} = \frac{f_{\mathrm{y0}}\ A_{\mathrm{v}}}{\sqrt{3}\ \sin\theta_{\mathrm{i}} \cdot \gamma_{\mathrm{M5}}} \tag{7.4.2}$$

Brace failure:

$$N_{\mathrm{i,Rd}} = 2 f_{\mathrm{y1}} t_1 p_{\mathrm{eff}} / \gamma_{\mathrm{M5}} \tag{7.4.3}$$

where

$$p_{\mathrm{eff}} = t_{\mathrm{w}} + 2r + 7 t_{\mathrm{f}} f_{\mathrm{y0}} / f_{\mathrm{yi}} \tag{7.4.4}$$

and A_{v} is the effective shear area.

The design bending resistance of the joint is the minimum of the design resistances:

Chord web failure:

$$M_{\mathrm{ip,Rd}} = 0{,}5 f_{\mathrm{y0}} t_{\mathrm{w}} b_{\mathrm{w}} h_1 / \gamma_{\mathrm{M5}} \tag{7.4.5}$$

Brace failure:

$$M_{\mathrm{ip,Rd}} = f_{\mathrm{y1}} t_1 b_{\mathrm{eff}} (h_1 - t_1) / \gamma_{\mathrm{M5}} \tag{7.4.6}$$

where

$$b_{\mathrm{w}} = \frac{h_1}{\sin\theta_{\mathrm{i}}} + 5 \cdot \left(t_{\mathrm{f,0}} + r\right) \leq\ 2 \cdot t_{\mathrm{i}} + 10 \cdot \left(t_{\mathrm{f,0}} + r\right) \tag{7.4.7}$$

$$b_{\mathrm{eff}} = t_{\mathrm{w}} + 2r + 7 t_{\mathrm{f}} f_{\mathrm{y0}} / f_{\mathrm{y1}} \tag{7.4.8}$$

An overview of the considered examples loaded by axial force is described in Tab. 7.4.1. An overview of the considered examples loaded by bending moment is described in Tab. 7.4.2. A geometry of a joint with dimensions is shown in Fig. 7.4.2.

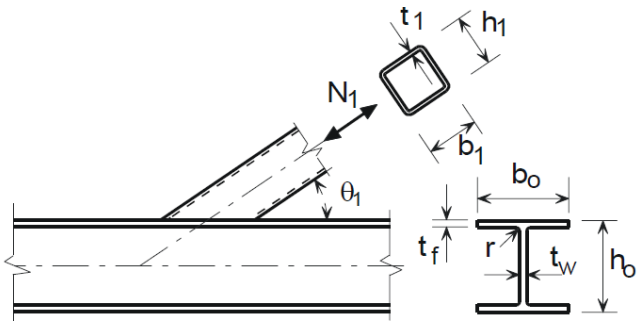

Fig. 7.4.2 Joint geometry with dimensions

Tab. 7.4.1 Examples overview

Example	Chord	Brace	Weld	Material		
	Section	Section	a	f_y	f_u	E
			[mm]	[MPa]	[MPa]	[GPa]
a1	IPN 220	RHS 140×70×10	11	235	360	210
a2	IPN 240	RHS 140×70×10	11	235	360	210
a3	IPN 260	RHS 140×70×10	10	235	360	210
a4	IPN 280	RHS 140×70×10	10	235	360	210
a5	IPE 200	RHS 140×70×10	10	235	360	210
a6	IPE 220	RHS 140×70×10	10	235	360	210
a7	IPE 270	RHS 140×70×10	10	235	360	210
a8	IPE 330	RHS 140×70×10	10	235	360	210
a9	IPE 360	RHS 140×70×10	10	235	360	210
a10	HEA 240	RHS 140×70×10	10	235	360	210
a11	HEA 280	RHS 140×70×10	10	235	360	210
a12	HEA 300	RHS 140×70×10	10	235	360	210
a13	HEA 320	RHS 140×70×10	10	235	360	210
a14	HEA 340	RHS 140×70×10	10	235	360	210
a15	HEA 360	RHS 140×70×10	10	235	360	210
b1	IPN 300	RHS 140×70×10	10	235	360	210
b2	IPN 320	RHS 140×70×10	10	235	360	210
b3	IPN 340	RHS 140×70×10	10	235	360	210
b4	IPN 360	RHS 140×70×10	10	235	360	210
b5	IPN 380	RHS 140×70×10	10	235	360	210
b6	IPN 400	RHS 140×70×10	10	235	360	210
b7	HEA 400	RHS 140×70×10	10	235	360	210
b8	HEB 300	RHS 140×70×10	10	235	360	210
b9	HEB 320	RHS 140×70×10	10	235	360	210
b10	HEB 340	RHS 140×70×10	10	235	360	210
c1	IPE 140	RHS 140×70×10	10	235	360	210
c2	IPE 160	RHS 140×70×10	10	235	360	210
c3	HEA 100	RHS 140×70×10	10	235	360	210
c4	HEA 120	RHS 140×70×10	10	235	360	210
c5	HEB 100	RHS 140×70×10	10	235	360	210
c6	HEB 120	RHS 140×70×10	10	235	360	210
c7	HEB 140	RHS 140×70×10	10	235	360	210
c8	HEB 160	RHS 140×70×10	10	235	360	210

Tab. 7.4.2 Examples of joints loaded by in-plane moment

Example	Chord	Brace	Weld	Material		
	Section	Section	a	f_y	f_u	E
			[mm]	[MPa]	[MPa]	[GPa]
a1	IPN 160	RHS 140×70×10	10	235	360	210
a2	IPN 180	RHS 140×70×10	10	235	360	210
a3	IPE 140	RHS 140×70×10	10	235	360	210
a4	IPE 160	RHS 140×70×10	10	235	360	210
a5	IPE 180	RHS 140×70×10	10	235	360	210
a6	IPE 200	RHS 140×70×10	10	235	360	210
a7	IPE 220	RHS 140×70×10	10	235	360	210
a8	HEA 120	RHS 140×70×10	10	235	360	210
a9	HEA 140	RHS 140×70×10	10	235	360	210
b1	IPE 240	RHS 140×70×10	11	235	360	210
b2	IPE 270	RHS 140×70×10	11	235	360	210
b3	IPE 300	RHS 140×70×10	11	235	360	210
b4	IPE 330	RHS 140×70×10	11	235	360	210
b5	HEA 200	RHS 140×70×10	11	235	360	210
b6	HEA 220	RHS 140×70×10	11	235	360	210

7.4.3 Verification of resistance

The study was focused on comparison of the failure models and the prediction of the design resistance. The results are presented in Tab. 7.4.3 and 7.4.4.

Tab. 7.4.3 Comparison of CBFEM and FM for axial force in brace

Example	Design resistance				
	FM [kN]	Mode of failure	CBFEM [kN]	Mode of failure	Difference [%]
a1	425	Chord web	449	Brace failure	5
a2	487	Chord web	501	Brace failure	3
a3	563	Chord web	571	Chord web	1
a4	631	Chord web	615	Chord web	-3
a5	296	Chord web	304	Chord web	3
a6	322	Chord web	349	Chord web	8
a7	413	Chord web	427	Chord web	3
a8	507	Chord web	511	Chord web	1
a9	552	Chord web	551	Chord web	0
a10	538	Chord web	492	Chord web	-9
a11	611	Chord web	558	Chord web	-9
a12	689	Chord web	613	Chord web	-12
a13	746	Chord web	661	Chord web	-13
a14	798	Chord web	700	Chord web	-14
a15	852	Chord web	738	Chord web	-15
b1	687	Brace failure	662	Brace failure	-4
b2	736	Brace failure	713	Brace failure	-3
b3	772	Brace failure	754	Brace failure	-2
b4	825	Brace failure	805	Brace failure	-2
b5	867	Brace failure	836	Brace failure	-4
b6	867	Brace failure	844	Brace failure	-3
b7	867	Brace failure	797	Brace failure	-9
b8	867	Brace failure	797	Brace failure	-9
b9	867	Brace failure	836	Brace failure	-4
b10	867	Brace failure	840	Brace failure	-3
c1	172	Chord shear	184	Chord shear	7
c2	213	Chord shear	223	Chord shear	4
c3	151	Chord shear	148	Chord shear	-2
c4	173	Chord shear	172	Chord shear	-1
c5	184	Chord shear	188	Chord shear	2
c6	229	Chord shear	242	Chord shear	5
c7	279	Chord shear	305	Chord shear	9
c8	368	Chord shear	387	Chord shear	5

Tab. 7.4.4 Comparison of CBFEM and FM for in-plane moment in brace

Example	Design resistance				
	FM [kNm]	Mode of failure	CBFEM [kNm]	Mode of failure	Difference [%]
a1	17,1	Chord web	18,8	Chord web	9
a2	20,3	Chord web	21,5	Chord web	6
a3	11,4	Chord web	12,9	Chord web	12
a4	14,1	Chord web	14,8	Chord web	5
a5	15,4	Chord web	17,2	Chord web	10
a6	19,2	Chord web	18,8	Chord web	-2
a7	20,9	Chord web	21,5	Chord web	3
a8	16,8	Chord web	15,6	Chord web	-8
a9	16,8	Chord web	18,4	Chord web	9
b1	23,2	Brace failure	22,7	Brace failure	-2
b2	23,6	Brace failure	25,0	Brace failure	6
b3	24,0	Brace failure	26,6	Brace failure	10
b4	25,2	Brace failure	29,7	Brace failure	15
b5	24,1	Brace failure	25,6	Brace failure	6
b6	24,8	Brace failure	27,7	Brace failure	10

The sensitivity study shows good agreement for all applied load cases. In the CBFEM method, the rounding of the wall of open cross-section is simplified, which brings a conservative estimate of the stress in the connected diagonal and the assumption of bearing capacity till 15 %. To illustrate the accuracy of the CBFEM model, the results of the parametric studies are summarized in a diagram comparing design resistances by CBFEM and FM; see Fig. 7.4.3.

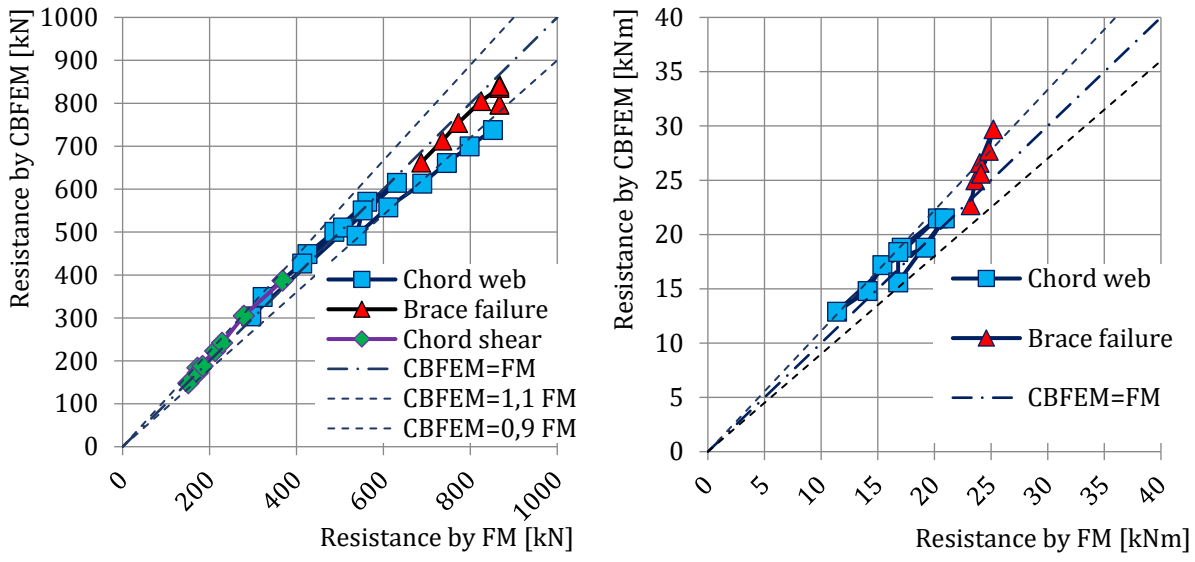

Fig. 7.4.3 Verification of CBFEM to FM for axial force and bending moment in the brace

7.4.4 Range of validity

Range of validity, on which is verified CBFEM for T-joints between rectangular hollow section and open section, is defined in Table 7.20 of EN 1993-1-8:2005, see Tab. 7.4.5. In case of application of the CBFEM model outside the range of validity of FM, the validation to experiments or verification to validated research model should be prepared to approve the quality of prediction.

Tab. 7.4.5 Range of validity of T-joints

Chord	Compression	Flange	class 1 or 2
		Web	class 1; $d_w \leq 400$ mm
	Tensile		-
RHS Brace	Compression		class 1; $b_i/t_i \leq 40$ and $h_i/t_i \leq 40$
	Tensile		$b_i/t_i \leq 40$ and $h_i/t_i \leq 40$
	Other		$0{,}5 \leq h_i/b_i \leq 2$
Angle between chord and brace			$\theta_i \geq 30$

7.4.5 Benchmark example

Inputs

Chord

- Steel S235
- IPE270

Brace

- Steel S235
- RHS 140×70×10

Weld

- Throat thickness a_w = 10 mm
- Fillet weld around the brace

Mesh size

- 16 elements on the biggest web of rectangular hollow member

Outputs

- Design resistance in compression/tension $F_{c,Rd}$ = 431 kN
- Collapse mode is full yielding of the chord web

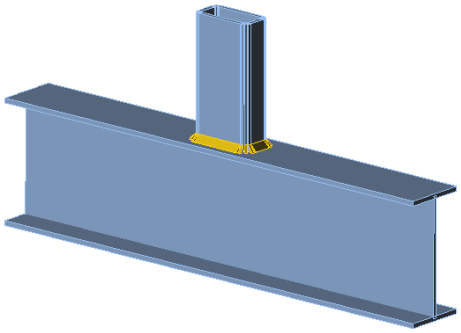

Fig. 7.4.4 Benchmark example for chord IPE270 and brace RHS 140×70×10

8 COLUMN BASE

8.1 Open section column in compression

8.1.1 Description

In this chapter, the Component-based Finite Element Method (CBFEM) of the column base under the steel open section column loaded in pure compression is verified on the component method (CM). The study is prepared for the column cross-section, dimension of base plate, grade of concrete, and dimensions of concrete block.

8.1.2 Component method

Three components are taken into account: column flange and web in compression, concrete in compression including grout, welds. Component column flange and web in compression is described in EN 1993-1-8:2005 Cl. 6.2.6.7. The concrete in compression including grout is modelled according to EN 1993-1-8:2005 Cl. 6.2.6.9 and EN1992-1-1:2005 Cl. 6.7. Two iterations of effective area are used to determine the resistance.

The weld is designed around the column cross-section; see EN 1993-1-8:2005 Cl. 4.5.3.2(6). The thickness of the weld on the flanges is selected the same as the thickness of the weld on the web. Shear force is transferred only by welds on the web, and plastic stress distribution is considered.

8.1.3 Base plate under HEB 240

This study is focused on the component concrete in compression including grout. An example of calculation is shown below for the concrete block with dimensions $a' = 1000$ mm, $b' = 1500$ mm, $h = 800$ mm from concrete grade C20/25 with base plate with dimensions $a = 330$ mm, b 440 mm, $t = 20$ mm from steel grade S235; see Fig. 8.1.2.

The joint stength of the concrete is calculated under the effective area in compression around the cross-section; see Fig. 8.1.1, iterating in two steps.

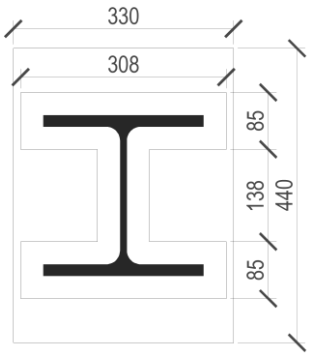

Fig. 8.1.1 Effective area under the base plate

For 1st step it is

$$f_{\mathrm{jd}} = \frac{\beta_{\mathrm{j}} \cdot k_{\mathrm{j}} \cdot f_{\mathrm{ck}}}{\gamma_{\mathrm{c}}} = \frac{0{,}67 \cdot 2{,}908 \cdot 20}{1{,}5} = 26 \text{ MPa}$$

$$c = t \cdot \sqrt{\frac{f_{\mathrm{y}}}{3 \cdot f_{\mathrm{jd}} \cdot \gamma_{\mathrm{M0}}}} = 20 \cdot \sqrt{\frac{235}{3 \cdot 26 \cdot 1{,}0}} = 35 \text{ mm}$$

$$l_{\mathrm{eff}} = b + 2 \cdot c = 240 + 2 \cdot 35 = 310 \text{ mm}$$

$$b_{\mathrm{eff}} = t_{\mathrm{f}} + 2 \cdot c = 17 + 2 \cdot 35 = 87 \text{ mm}$$

and for 2nd step it is

$$f_{jd} = \frac{\beta_j \cdot k_j \cdot f_{ck}}{\gamma_c} = \frac{0{,}67 \cdot 3 \cdot 20}{1.5} = 27 \text{ MPa}$$

$$c = t \cdot \sqrt{\frac{f_y}{3 \cdot f_{jd} \cdot \gamma_{M0}}} = 20 \cdot \sqrt{\frac{235}{3 \cdot 27 \cdot 1{,}0}} = 34 \text{ mm}$$

$$l_{eff} = b + 2 \cdot c = 240 + 2 \cdot 34 = 308 \text{ mm}$$

$$b_{eff} = t_f + 2 \cdot c = 17 + 2 \cdot 34 = 85 \text{ mm}$$

$$A_{eff} = 63\,463 \text{ mm}^2$$

The normal force resistance of the base plate by CM is

$$N_{Rd} = A_{eff} \cdot f_{jd} = 63\,436 \cdot 27 = 1701 \text{ kN}$$

The stresses calculated by CBFEM are presented in Fig. 8.1.2. The normal compressive force resistance of the base plate by CBFEM is 1683 kN.

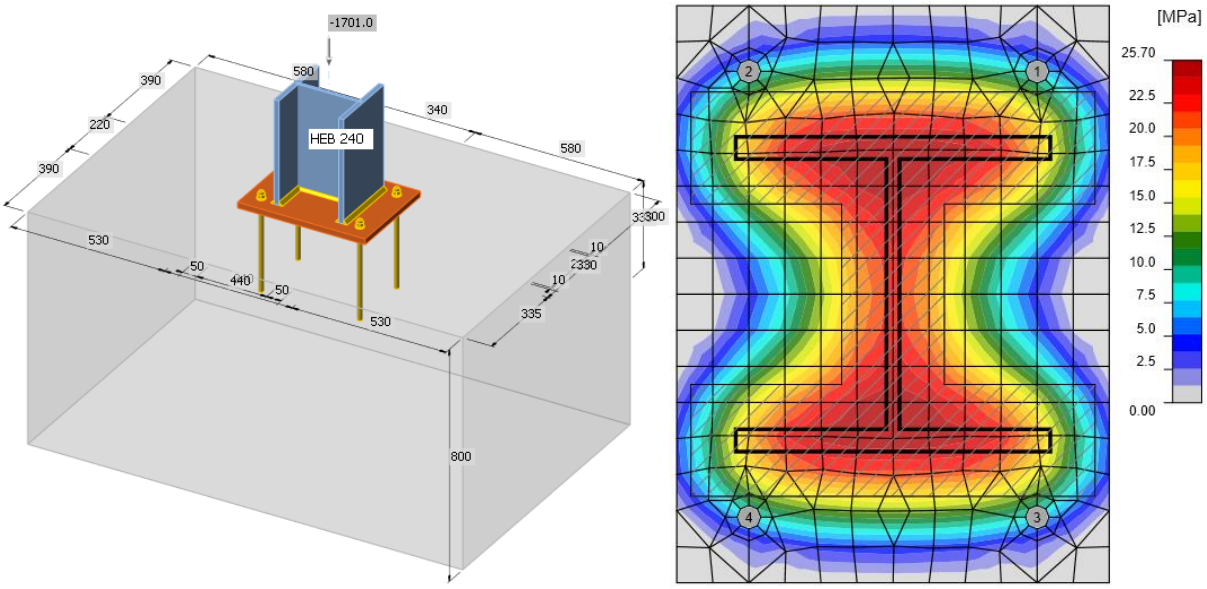

Fig. 8.1.2 Geometry of concrete block
and normal stresses under baseplate loaded by normal force only

8.1.4 Sensitivity study

The results of CBFEM software were compared with the results of the component method. The comparison was focused on the resistance and the critical component. Studied parameters are size of the column, dimensions of the base plate, concrete grade, and dimensions of the concrete pad. The column cross-sections are HEB 200, HEB 300, and HEB 400. The base plate width and length are chosen as 100 mm, 150 mm and 200 mm larger than the column section, the base plate thickness 15 mm, 20 mm, and 25 mm. The concrete block from grade C16/20, C25/30, and C35/45 of height 800 mm with width and length larger than the dimensions of the base plate by

200 mm, 300 mm, and 400 mm. The input parameters are summarized in Tab. 8.1.1. The fillet welds around the column cross-section have the throat thickness a = 8 mm.

Tab. 8.1.1 Selected parameters

Column section	HEB 200	HEB 300	HEB 400
Base plate offset	100 mm	150 mm	200 mm
Base plate thickness	15 mm	20 mm	25 mm
Concrete grade	C16/20	C25/30	C35/45
Concrete pad offset	200 mm	300 mm	400 mm

The resistances determined by CM are in Tab. 8.1.2. One parameter was changed, and the others were held constant at the middle value. N_{Rd} is the resistance of component concrete in compression including grout $F_{\mathrm{c,fc,Rd}}$ is the resistance of component column flange and web in compression and $F_{\mathrm{c,weld}}$ is the resistance of welds considering uniform distribution of stress. The joint coefficient β_{j} = 0,67 was used.

Table 8.1.2 Results of component method

Column	B.p. offset [mm]	B.p. thickness [mm]	Concrete	C.b. offset [mm]	N_{Rd} [kN]	2.$F_{c,fc,Rd}$ [kN]	$F_{c,weld}$ [kN]
HEB 200	150	20	C25/30	300	1753	1632	2454
HEB 300	150	20	C25/30	300	2352	3126	3466
HEB 400	150	20	C25/30	300	2579	4040	3822
HEB 300	**100**	20	C25/30	300	2296	3126	3466
HEB 300	**200**	20	C25/30	300	2408	3126	3466
HEB 300	150	**15**	C25/30	300	1909	3126	3466
HEB 300	150	**25**	C25/30	300	2795	3126	3466
HEB 300	150	20	**C16/20**	300	1789	3126	3466
HEB 300	150	20	**C35/45**	300	2908	3126	3466
HEB 300	150	20	C25/30	**200**	2064	3126	3466
HEB 300	150	20	C25/30	**400**	2517	3126	3466

The model in CBFEM was loaded by the compressive force until the concrete block was very close to 100 %. The same approach was used to get the resistance of welds $F_{c,weld}$.

Table 8.1.3 Results of CBFEM

Column	B.p. offset [mm]	B.p. thickness [mm]	Concrete grade	C.b. offset [mm]	Concrete block [kN]	$F_{c,weld}$ or $F_{c,Rd}$ [kN]
HEB 200	150	20	C25/30	300	1565	1835
HEB 300	150	20	C25/30	300	2380	3205
HEB 400	150	20	C25/30	300	2710	3650
HEB 300	**100**	20	C25/30	300	2385	3205
HEB 300	**200**	20	C25/30	300	2420	3205
HEB 300	150	**15**	C25/30	300	1870	3204
HEB 300	150	**25**	C25/30	300	2915	3204
HEB 300	150	20	**C16/20**	300	1850	3205
HEB 300	150	20	**C35/45**	300	2975	3205
HEB 300	150	20	C25/30	**200**	2380	3205
HEB 300	150	20	C25/30	**400**	2420	3205

Summary

Verification of CBFEM to CM for base plate loaded in compression is shown in Fig. 8.1.3. The dashed lines correspond to the 110 % and 90 % value of resistance. The difference is up to 14 % due to more accurate evaluation of the design bearing strength of the joint f_{jd} and effective area A_{eff} in CBFEM.

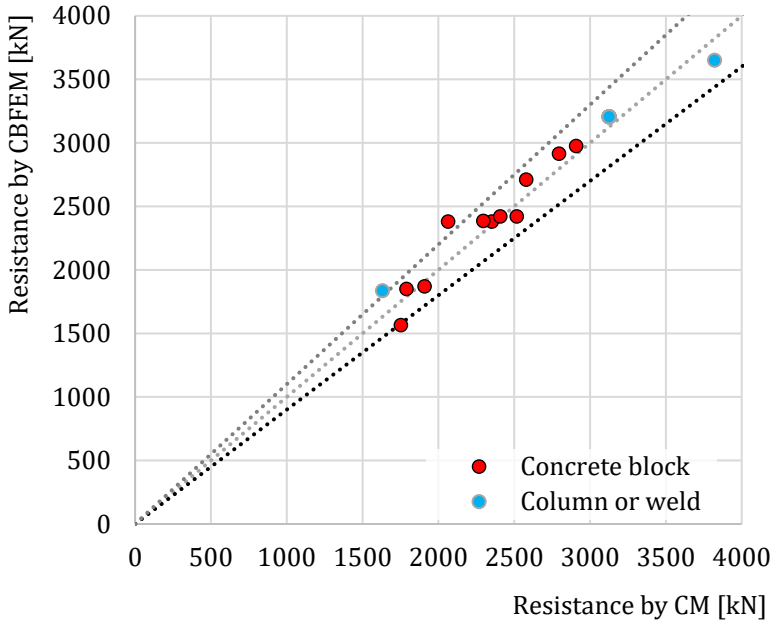

Fig. 8.1.3 Verification of CBFEM to CM for base plate loaded in compression

8.1.5 Benchmark case

Input

Column cross-section

- HEB 240
- Steel S235

Base plate

- Thickness 20 mm
- Offsets top 100 mm, left 45 mm
- Steel S235

Foundation concrete block

- Concrete C20/25
- Offset 335 mm, 530 mm
- Depth 800 mm
- Grout thickness 30 mm

Anchor bolt

- M20 8.8

Output

- Axial force resistance $N_{j.Rd}$ = −1683 kN

8.2 Open section column in bending to strong axis

8.2.1 Description

The object of this chapter is verification of component-based finite element method (CBFEM) of the column base of the steel open section column loaded in compression and bending around the stronger axis with the component method (CM). The study is prepared for size of the column, geometry, and thickness of base plate. In the study, five components are examined: column flange and web in compression, concrete in compression including grout, base plate in bending, anchors in tension, and welds. All components are designed according to EN 1993-1-8:2005, EN 1992-1-1:2005, and EN 1992-4.

8.2.2 Verification of resistance

An example of component method design is shown on the anchorage of column steel section HEB 240:

Concrete block has dimensions $a' = 1000$ mm , $b' = 1500$ mm , $h = 900$ mm and grade C20/25. Base plate dimensions are $a = 330$ mm; $b = 440$ mm; $t = 20$ mm, and steel grade is S235. Anchor bolts are 4 × M20, A_s = 245 mm², length 300 mm, with head diameter a = 60 mm and steel grade 8.8. Grout thickness is 30 mm.

The results of the analytical solution may be presented on an interaction diagram with distinctive significant points. Point −1 represents loading in pure tension, and point 4 represents the compression bearing resistance. Detailed description of points 0, 1, 2, and 3 is shown in Fig. 8.2.1; see (Wald, 1995) and (Wald et al. 2008).

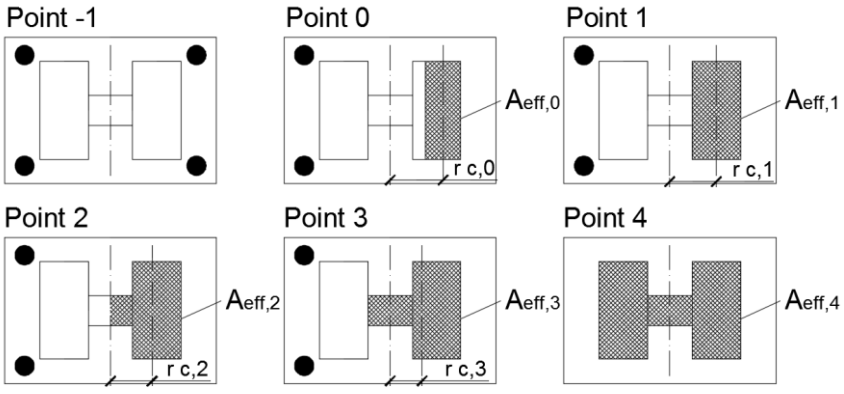

Fig. 8.2.1 Significant points on interaction diagram

The stress distribution for point 0 and 3 reached by CBFEM is displayed in Fig. 8.2.2 and 8.2.3.

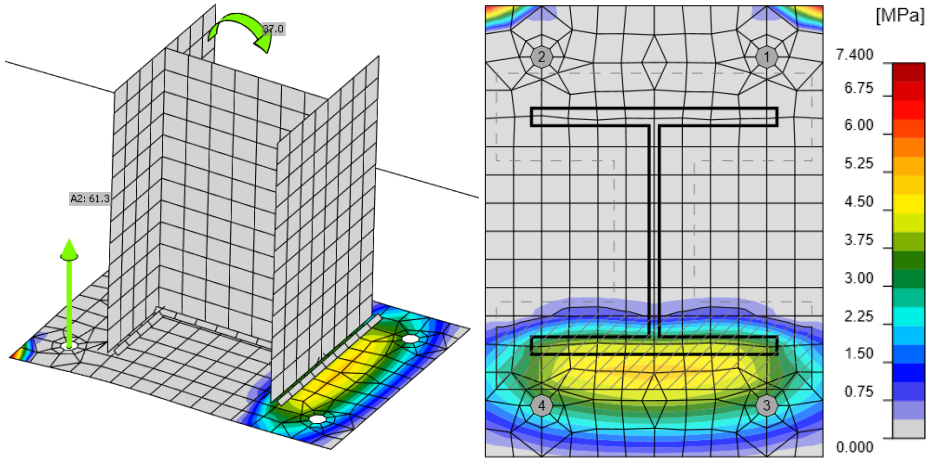

Fig. 8.2.2 Stress in concrete and forces in anchors for point 0 obtained by CBFEM (deform. scale 10)

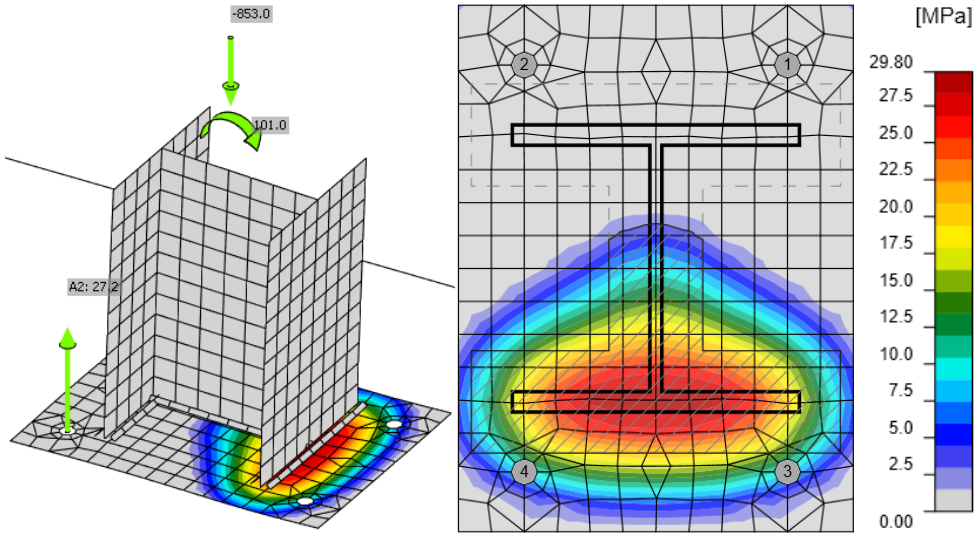

Fig. 8.2.3 Stress in concrete and forces in anchors for point 3 obtained by CBFEM (deform. scale 10)

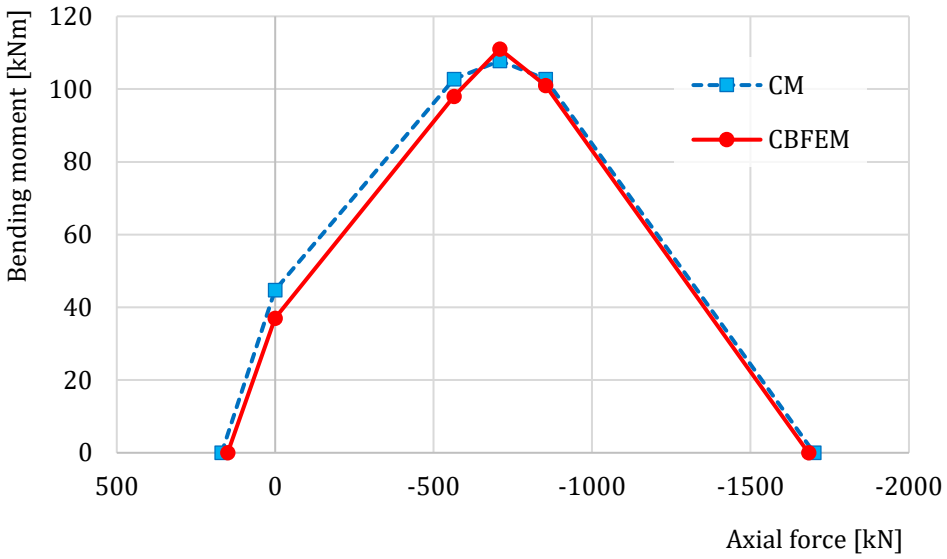

Fig. 8.2.4 Comparison of models on interaction diagram

The comparison of interaction diagram obtained by CBFEM to interaction diagram calculated according to CM is presented in Fig. 8.2.4 and Tab. 8.2.1.

Tab. 8.2.1 Comparison of results of interaction diagram for HEB 240 by analytic solution and by CBFEM

	Analytical solution		Results of CBFEM	
	Axial force [kN]	Bending resistance [kNm]	Axial force [kN]	Bending resistance [kNm]
Point -1	169	0	150	0
Point 0	0	45	0	37
Point 1	−564	103	−564	98
Point 2	−708	108	−708	111
Point 3	−853	103	−853	101
Point 4	−1700	0	−1683	0

8.2.3 Sensitivity study

The results of CBFEM were compared with the results of the component method. The comparison was made by bending moment resistance for the given level of normal force for each of the interaction diagram points.

In the sensitivity study, size of the column, dimensions of the base plate, and dimensions of concrete pad were changed. The selected column cross-sections were HEB 200, HEB 300, and HEB 400. The base plate width and length was chosen 100 mm, 150 mm, and 200 mm larger than the column section; the base plate thickness was 15 mm, 20 mm, and 25 mm. The concrete pad was from grade C25/30. The concrete pad height was for all cases 900 mm, and width and length were 200 mm larger than the dimensions of the base plate. Anchor bolts were M20 grade 8.8 with an

embedment depth of 300 mm. The parameters are summarized in Tab. 8.2.2. Welds were the same around the whole column section with sufficient throat thickness in order not to be the critical component. One parameter was changed while the others were held constant at the middle value.

Tab. 8.2.2 Selected parameters

Column section	HEB 200	HEB 300	HEB 400
Base plate offset	100 mm	150 mm	200 mm
Base plate thickness	15 mm	20 mm	25 mm

In Fig. 8.2.5, results for changes in the column cross-section are presented. In Fig. 8.2.6 and Fig. 8.2.7, the base plate offset and the base plate thickness are varied, respectively.

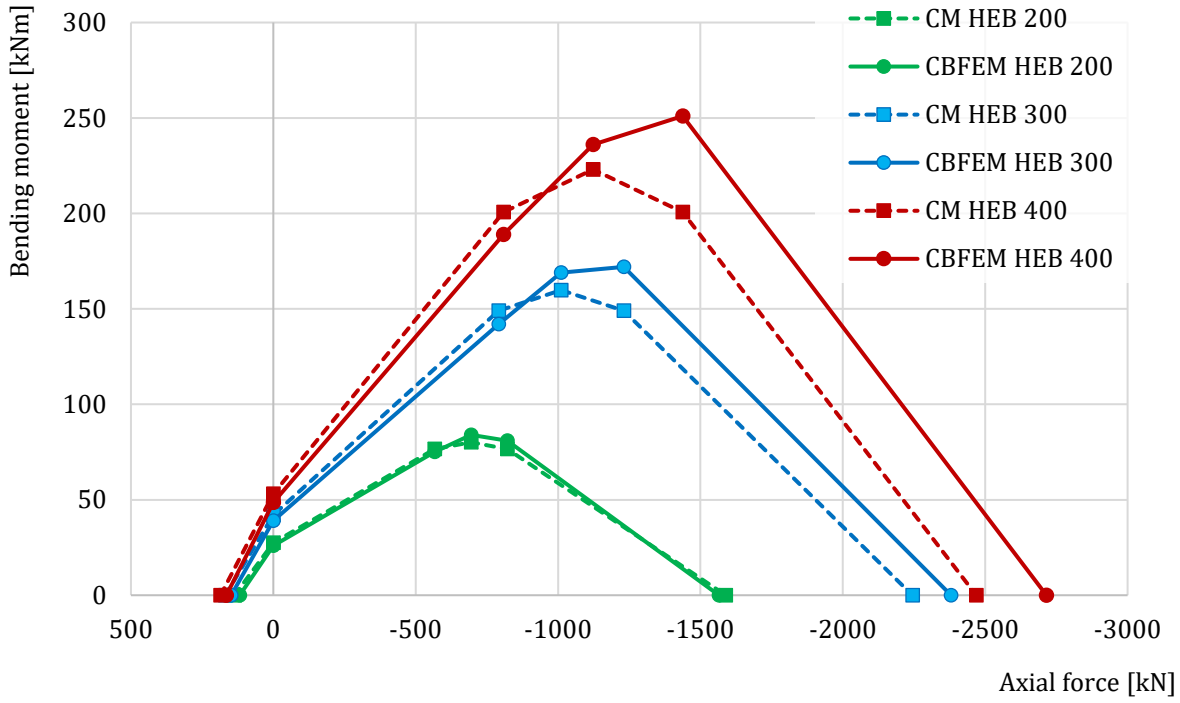

Fig. 8.2.5 Column section variation

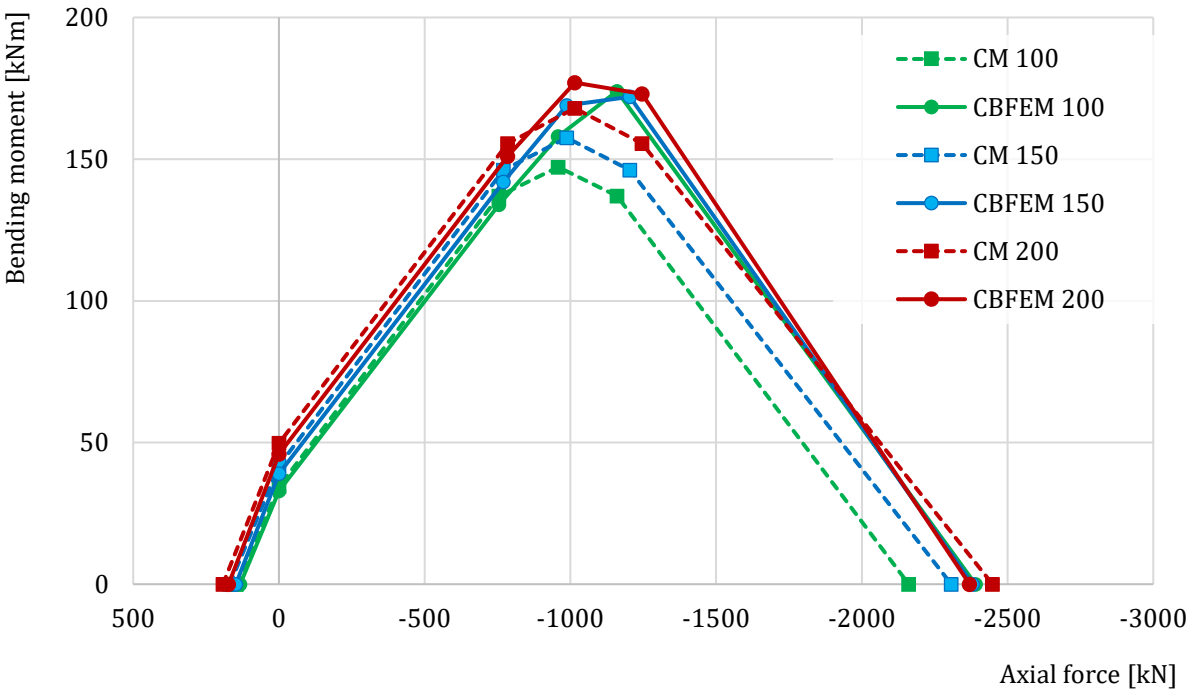

Fig. 8.2.6 Base plate offset variation – 100, 200, and 300 mm

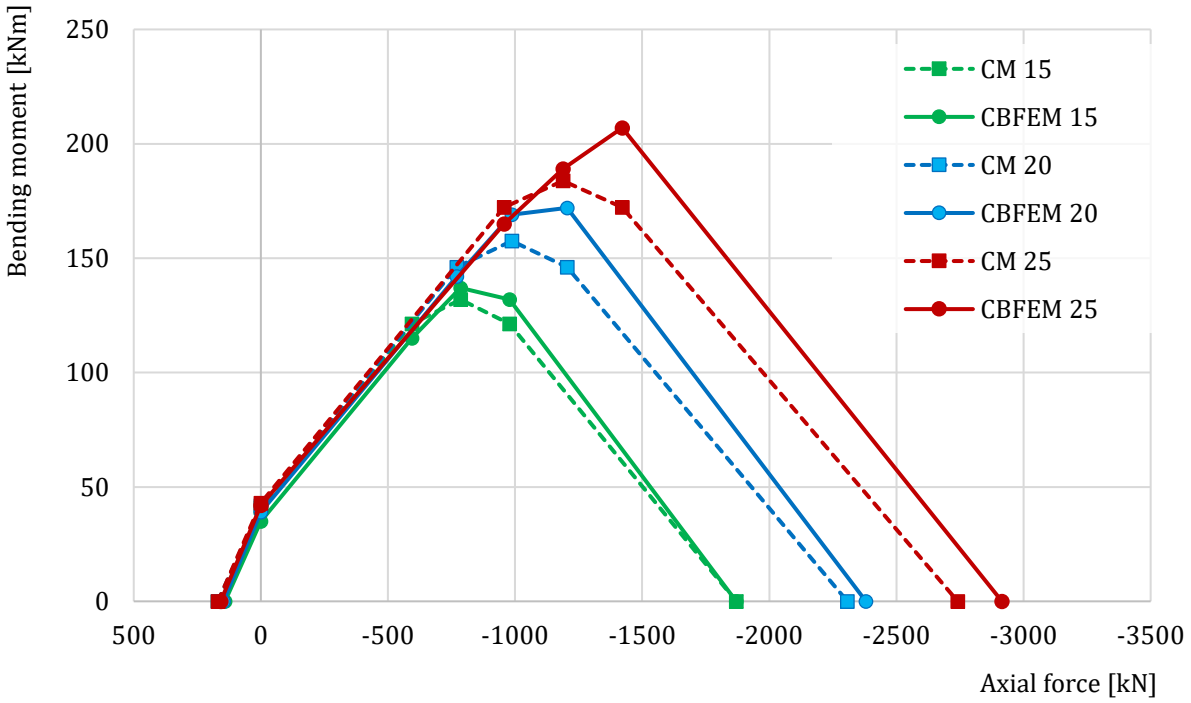

Fig. 8.2.7 Base plate thickness variation – 15, 20, and 25 mm

8.2.4 Benchmark case

Input

Column cross-section

- HEB 240
- Steel S235

Base plate

- Thickness 20 mm
- Offsets top 100 mm, left 45 mm
- Steel S235

Anchor bolt

- M20 8.8
- Anchoring length 300 mm
- Offsets top layers 50 mm, left layers -10 mm
- Shear plane in thread
- Welds both 8 mm

Foundation block

- Concrete C20/25
- Offset 335 mm and 530 mm
- Depth 900 mm
- Shear force transfer friction
- Grout thickness 30 mm

Loading

- Axial force N = −853 kN
- Bending moment M_y = 100 kNm

Output

- Anchor bolts 42,2 % ($N_{Ed,g}$ = 51,7 kN ≤ N_{Rdc} = 122,4 kN - concrete core breakout for anchors A1 and A2)
- Concrete block 99,5 % (σ = 26,7 MPa ≤ f_{jd} = 26,8 MPa)

8.3 Open section column in bending to weak axis

8.3.1 Description

Open section steel column is anchored with anchor bolts to concrete pad; the column is loaded by moment around the weaker axis and axial force. The compressed column is designed as a maximal 3rd class to avoid buckling. The study was performed for parameters: the size of the column, dimensions of the base plate, and thickness of the base plate. In the component method, components column flange in bending and web in compression, concrete including grout in compression, base plate in bending, anchor bolts in tension, and welds are activated. All components are designed according to EN 1993-1-8:2005, EN 1992-1-1:2005, and EN 1992-4.

8.3.2 Verification of resistance

An example of component method design is shown on the anchorage of the column steel cross-section HEB 240. Concrete block has dimensions $a' = 1000$ mm, $b' = 1500$ mm, $h = 900$ mm and grade C20/25. The base plate has dimensions $a = 330$ mm; $b = 440$ mm; $t = 20$ mm and is from steel S235. The anchor bolts are 4 × M20, A_s = 245 mm^2 with anchor head diameter a = 60 mm and steel grade 8.8. Grout has a thickness of 30 mm. Anchors are positioned with an offset from the column cross-section: top and bottom 50 mm, left and right −10 mm.

The results of the analytical solution are presented on an interaction diagram with distinctive points. Point 1 represents loading in pure tension, and point 4 represents the compression bearing resistance. A detailed description of points 0, 1, 2, and 3 is shown in Fig. 8.3.1; see (Wald, 1995) and (Wald et al. 2008).

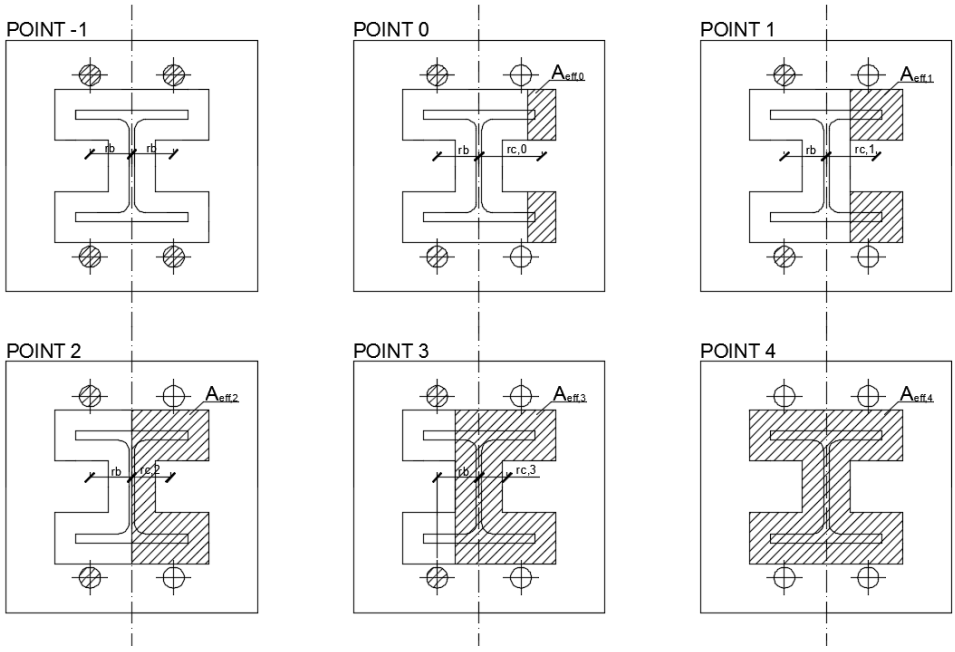

Fig. 8.3.1 Significant points on interaction diagram

Results by CBFEM are presented by the stress distribution for points 0 and 3, displayed in Fig. 8.3.2 and Fig. 8.3.3, and compared on the interaction diagram in Fig. 8.3.4.

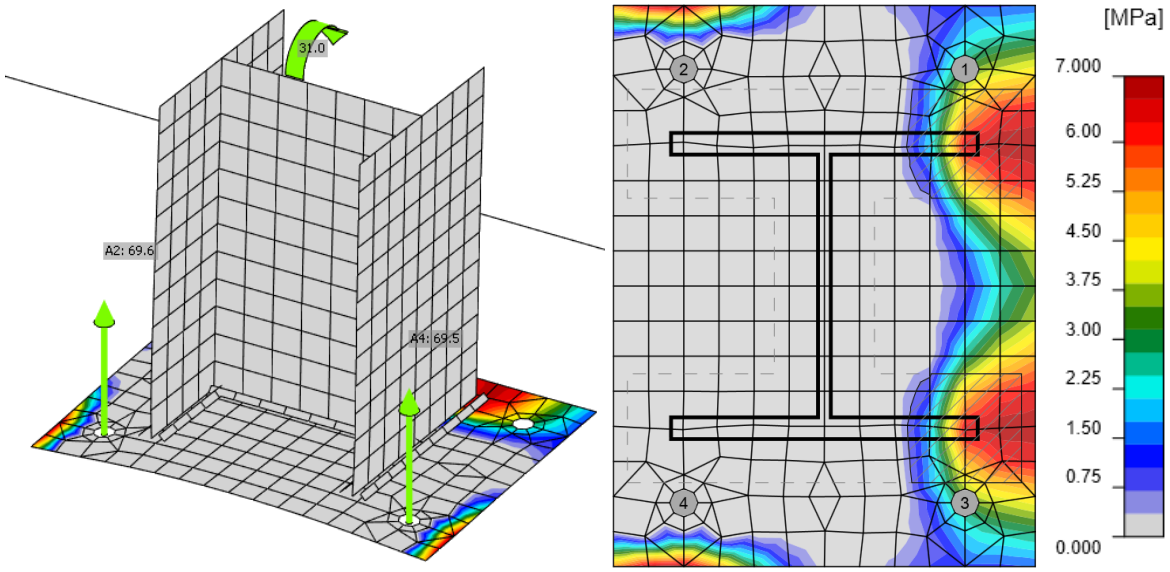

Fig 8.3.2 Stress distribution in concrete,
effective area (hatched) and forces in anchors for point 0

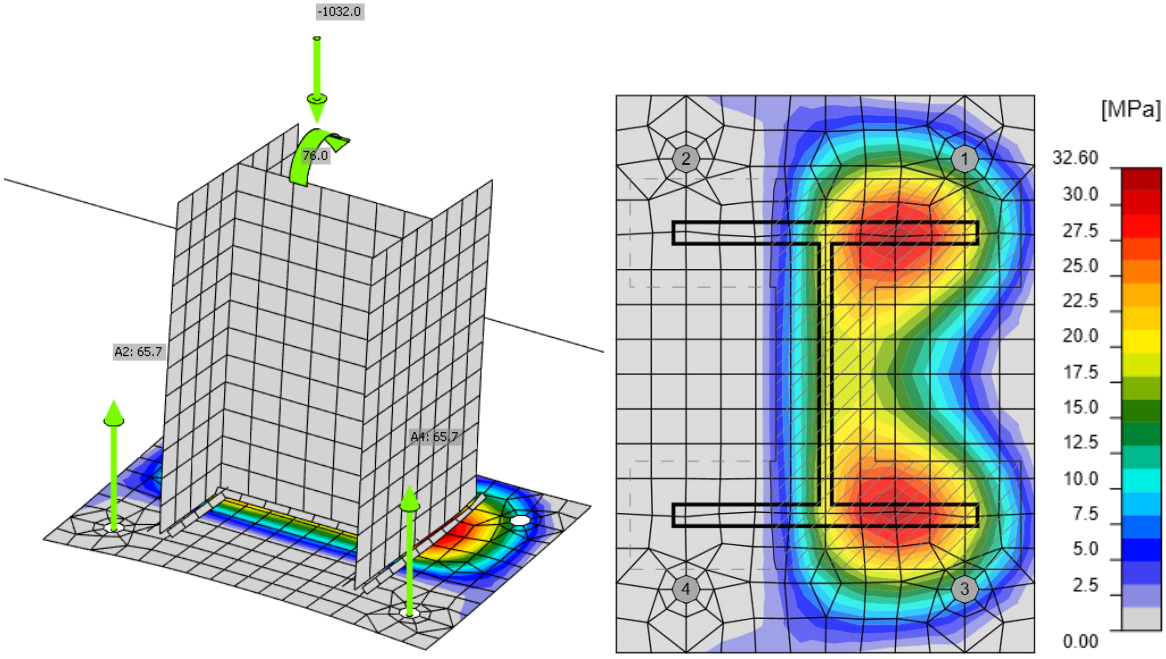

Fig. 8.3.3 Stress distribution in concrete,
effective area (hatched) and forces in anchors for point 3

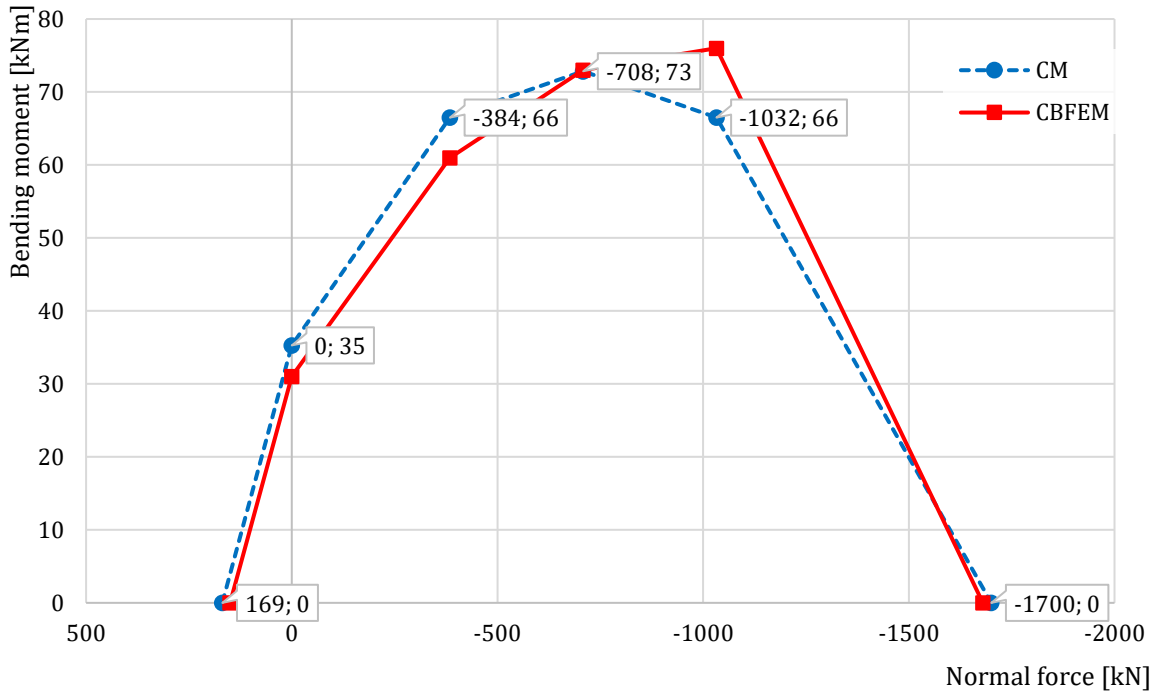

Fig. 8.3.4 Interaction diagram by CBFEM compared to CM

Tab. 8.3.1 Comparison of results of interaction diagram for HEB 240

	Analytic solution		Results of CBFEM	
	Axial force [kN]	Bending resistance [kNm]	Axial force [kN]	Bending resistance [kNm]
Point -1	169	0	150	0
Point 0	0	35	0	31
Point 1	−384	66	−384	61
Point 2	−708	73	−708	73
Point 3	−1032	66	−1032	76
Point 4	−1700	0	−1680	0

8.3.3 Sensitivity study

The results of CBFEM are compared with the results of the component method. The comparison is made for bending moment resistance for the given level of normal force for each of the interaction diagram points. The study is performed for the size of the column (Fig. 8.3.5), the thickness of the base plate (Fig. 8.3.6), and grade of concrete (Fig. 8.3.7). The selected columns were HEB 200, HEB 300, and HEB 400. The base plate thickness is chosen to be 15 mm, 20 mm, and 25 mm, and its offset from column cross-section is 100 mm. The concrete pad is from grade C16/20, C25/30, and C35/45. The concrete pad height is for all cases 900 mm, and width and length are 300 mm larger than the dimensions of the base plate. Steel grade is S355; anchors are M20, grade 8.8 with the same layout as in the previous example. The parameters are summarized in Tab. 8.3.2. Welds are the same around the whole column section with sufficient throat thickness

in order not to be the critical component. One parameter is changed while the others are held constant at the middle value.

Tab. 8.3.2 Selected parameters for sensitivity study

Column cross-section	HEB 200	HEB 300	HEB 400
Base plate thickness	15 mm	20 mm	25 mm
Concrete grade	C16/20	C25/30	C35/45

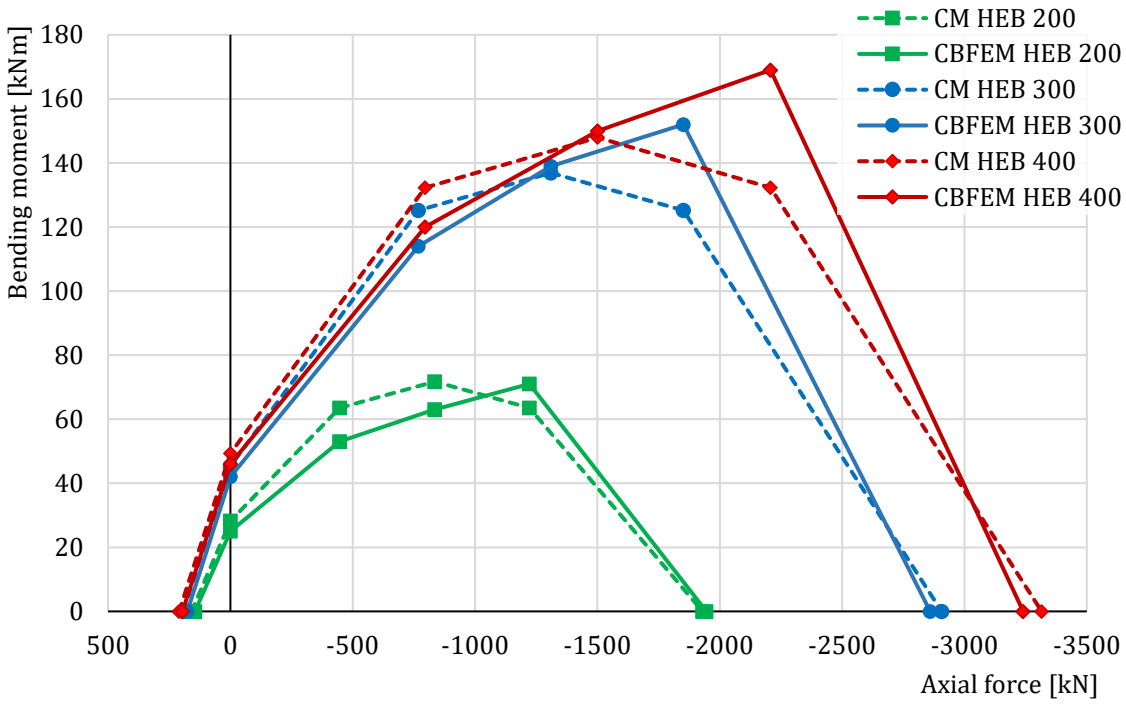

Fig. 8.3.5 Column section size variation

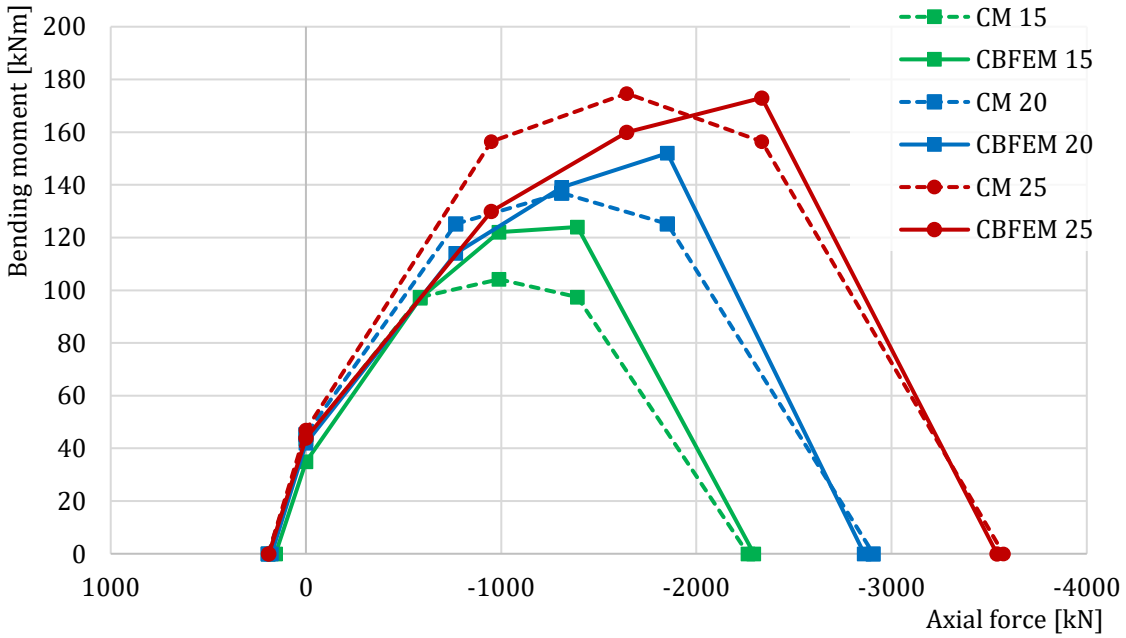

Fig. 8.3.6 Base plate thickness variation – 15, 20, and 25 mm

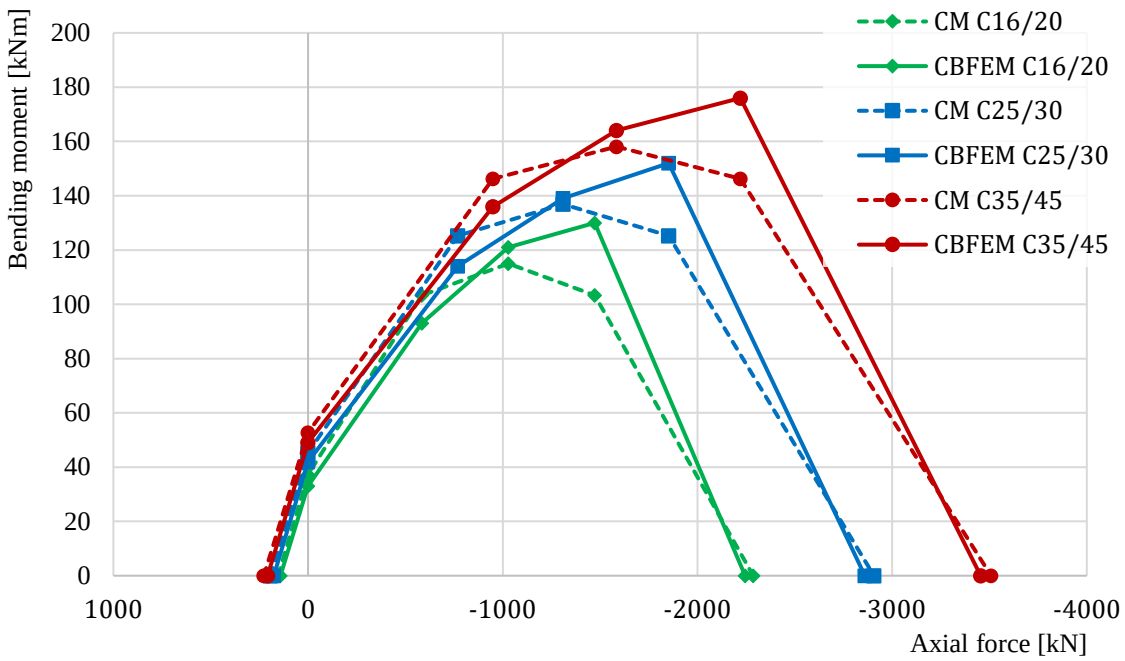

Fig. 8.3.7 Concrete grade variation

The resistances for point −1 (pure tension) are determined by the concrete cone breakout of a group of all four anchors. The resistances are the same for CM and CBFEM, but the forces in anchors slightly differ due to the occurrence of prying forces in CBFEM. Therefore, the load resistance of the column base is smaller for CBFEM. The same is happening for point 0 (pure bending), except the concrete cone breakout failure occurs only for a group of two tensioned anchors. For CBFEM, the resistances of points 1 and 2 are governed by the concrete cone breakout of anchors. The resistance of point 3 is governed either by concrete cone breakout of anchors or concrete in bearing. The differences in results by CBFEM and CM are the highest for point 3, which could be explained by a simplification in an assumption of the lever arm in CM. The resistances of CBFEM and CM for concrete in bearing for pure compression (point 4) are nearly identical.

8.3.4 Benchmark case

Input

Column cross-section

- HEB 240
- Steel S235

Base plate

- Thickness 20 mm
- Offsets top 100 mm, left 45 mm
- Fillet welds all around with the throat thickness 8 mm

- Steel S235

Anchors

- Type M20 8.8
- Anchoring length 300 mm
- Offsets top layers 50 mm, left layers −10 mm
- Shear plane in thread

Foundation block

- Concrete C20/25
- Offset 335, 530 mm
- Depth 900 mm
- Shear force transfer friction
- Grout thickness 30 mm

Loading

- Axial force N = −708 kN,
- Bending moment M_z = 73 kNm

Output

- Anchor bolts 97,5 % (N_{Ed} = 138,2 kN ≤ N_{Rdc} = 141,7 kN – concrete cone breakout for anchors A2 and A4)
- Concrete block 85,7 % (σ = 23,0 MPa ≤ f_{jd} = 26,8 MPa)
- Plates ε = 0,6 %
- Welds 99,2 % ($\sigma_{w,Ed}$ = 357,3 MPa ≤ $\sigma_{w,Rd}$ = 360 MPa)

8.4 Hollow section column

8.4.1 Description

The component-based finite element method (CBFEM) for the hollow section column base verified to the component method (CM) is described below. A compressed column is designed as at least class 3 cross-section. The sensitivity study is prepared for the size of the column, the dimension of the base plate, concrete grade, and the dimension of the concrete block. Four components are activated: the column flange and web in compression, the concrete in compression including grout, the anchor bolt in tension, and welds. This study is mainly focused on two components: concrete in compression including grout and anchor bolt in tension.

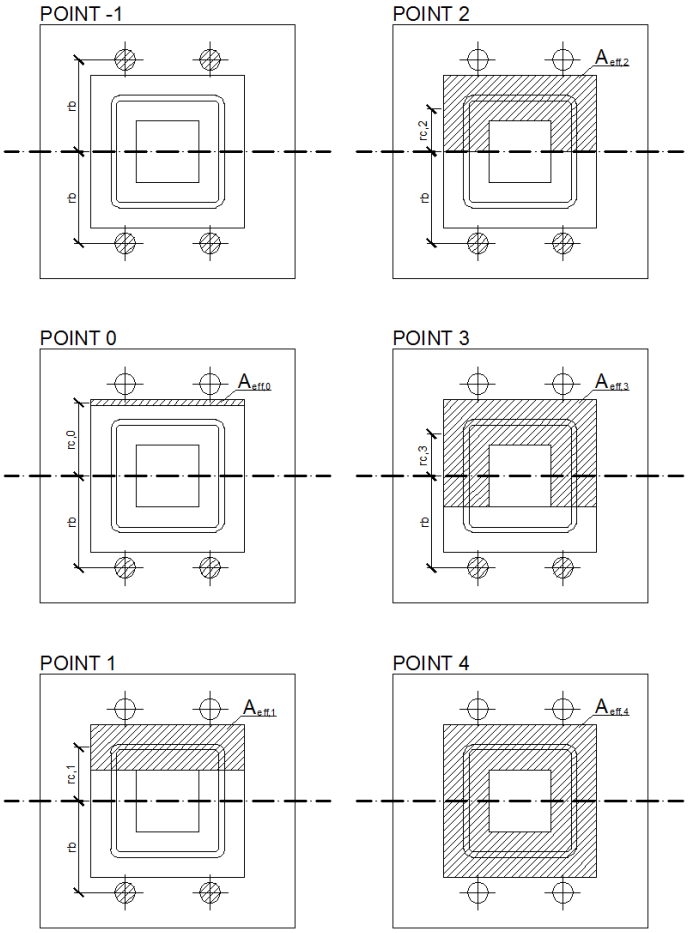

Fig. 8.4.1 Significant points of multilinear interaction diagram of square hollow section

8.4.2 Verification of resistance

In the following example, the column from square hollow section SHS 150×16 is connected to the concrete block with the area dimensions $a' = 750$ mm, $b' = 750$ mm and height $h = 800$ mm from concrete grade C20/25 by the base plate $a = 350$ mm; $b = 350$ mm; $t = 20$ mm from steel

grade S420. Anchor bolts are designed 4 × M20, A_s = 245 mm² with a head diameter a = 60 mm from steel grade 8.8 with the offsets at the top 50 mm and the left −20 mm and with an embedment depth 300 mm. Grout has a thickness of 30 mm.

The results of the analytical solution are presented as an interaction diagram with distinctive points. A detailed description of points −1, 0, 1, 2, and 3 is shown in Fig. 8.4.1; see (Wald, 1995) and (Wald et al. 2008), where point −1 represents pure tensile force, point 0 pure bending moment, points 1 to 3 combined compressive force and bending moment, and point 4 pure compressive force.

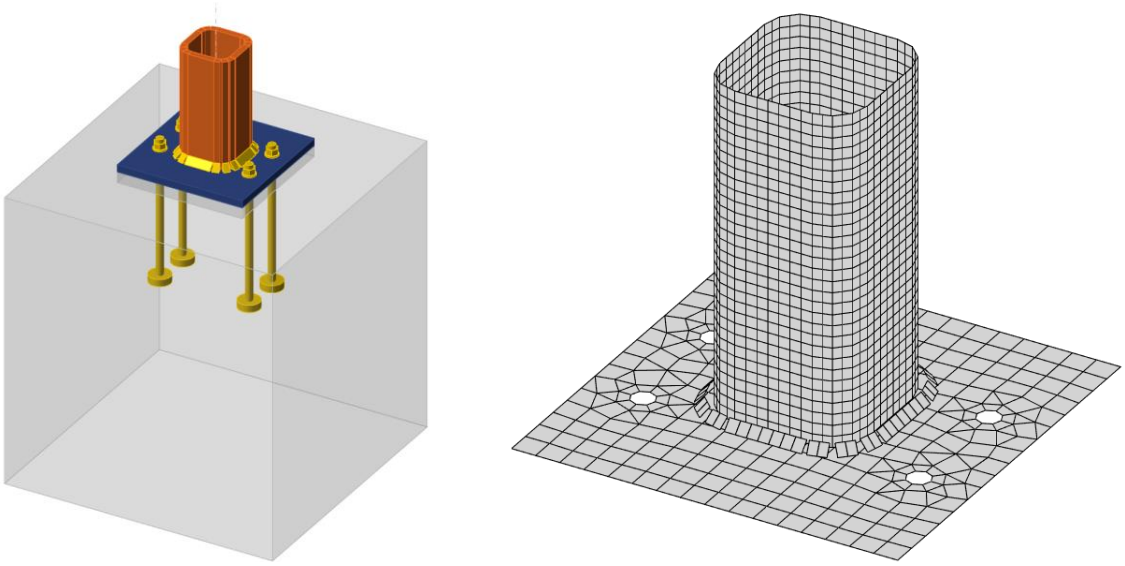

Fig.8.4.2 The column base for column SHS 150×16 and selected mesh of the base plate

In CBFEM, the prying forces occur in case of loading in pure tension loading; while in CM, no prying forces are developed by limiting the resistance to 1-2 failure mode only; see (Wald et al. 2008). Due to the prying forces, the difference in resistance is about 10 %. The numerical model of the column base is shown in Fig. 8.4.2. Results by CBFEM are presented by the bearing stress distribution on concrete for points 0 and 3, displayed in Fig. 8.4.3 and Fig. 8.4.4, and compared on the interaction diagram in Fig. 8.4.5.

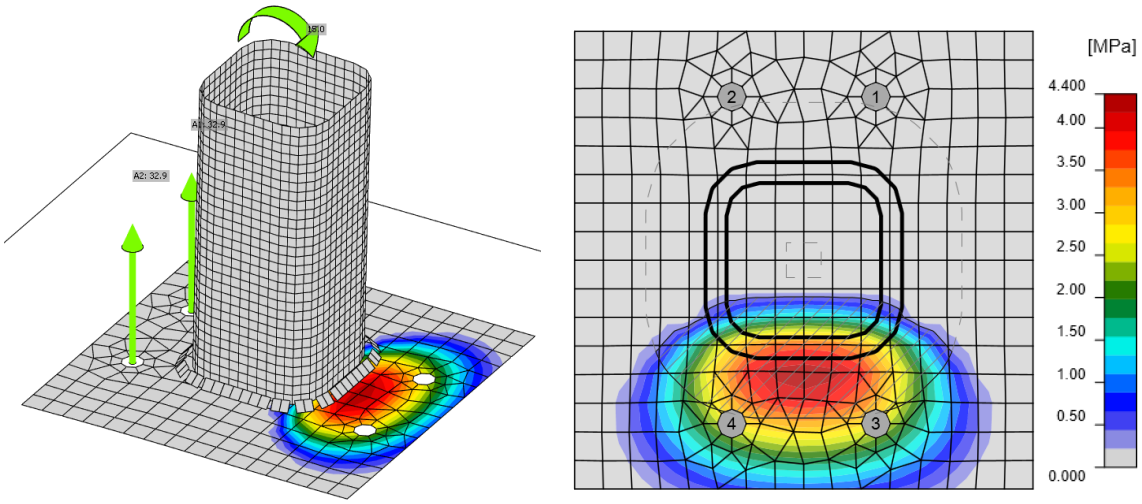

Fig. 8.4.3 CBFEM results for point 0, i.e. pure bending moment

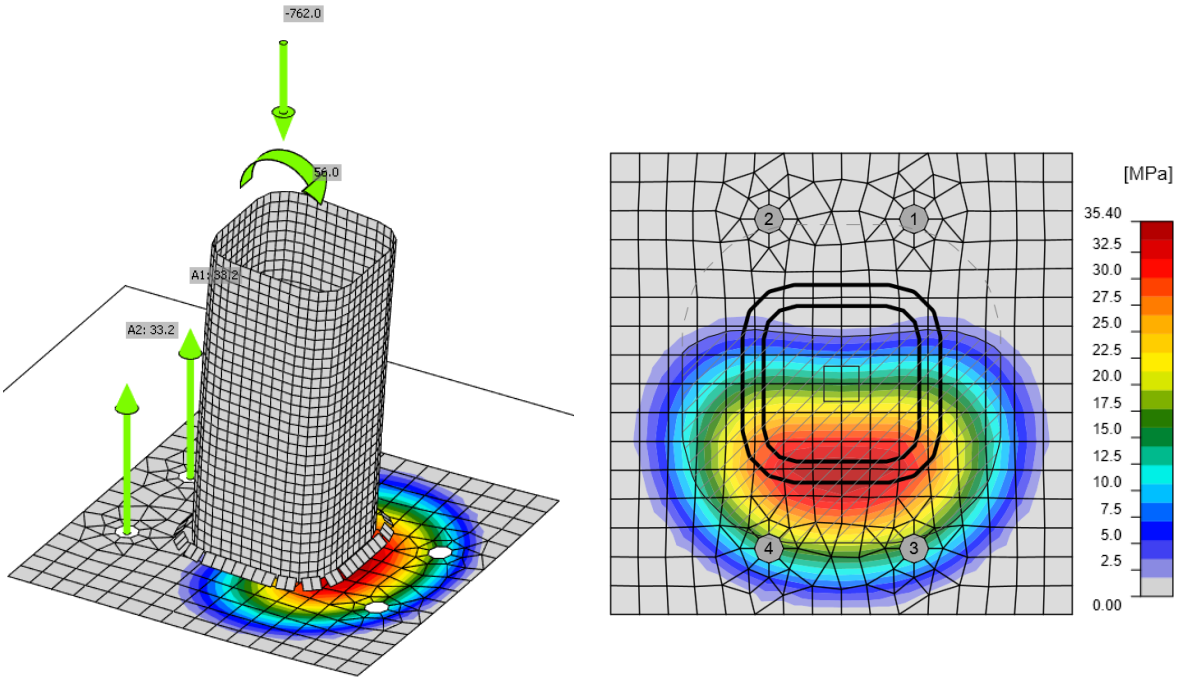

Fig. 8.4.4 CBFEM results for point 3, i.e. compressive force and bending moment

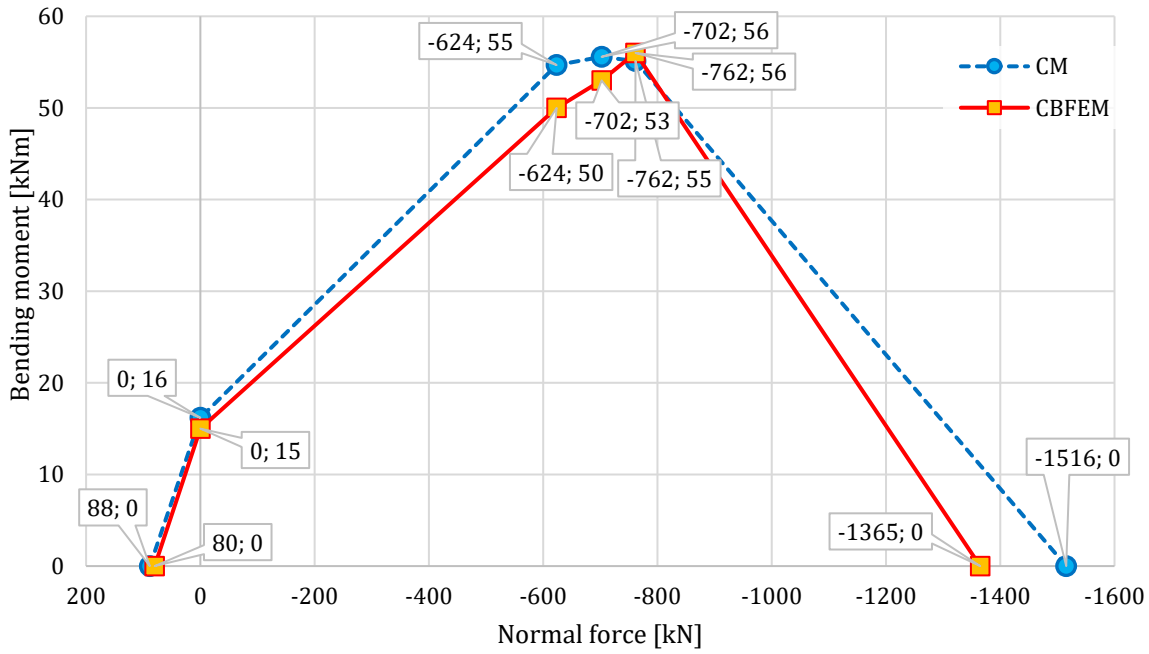

Fig. 8.4.5 Comparison of results of prediction of resistance by CBFEM and CM on interaction diagram for column base of column cross-section SHS 150×16

8.4.3 Sensitivity study

The sensitivity study is prepared for the column cross-section size, dimensions of the base plate, concrete grade, and dimensions of the concrete block. The columns are selected SHS 150×16, SHS 160×12.5, and SHS 200×16. The base plate is designed with area dimensions 100 mm, 150 mm and 200 mm larger than the column cross-section. The base plate thickness is 10 mm, 20 mm, and 30 mm. The foundation block is from concrete grade C20/25, C25/30, C30/37, and C35/45 with height for all cases 800 mm and with area dimensions 100 mm, 200 mm, 300 mm, and 500 mm larger than the dimensions of the base plate. One parameter was changed while the others were held constant. The parameters are summarized in Tab. 8.4.1. The fillet welds with thickness a = 12 mm were selected. The joint coefficient for grout with sufficient quality is taken as β_j = 0,67. Steel plates are from S420 with anchor bolts M20 grade 8.8 with embedment depth 300 mm in all cases.

Table 8.4.1 Selected parameters

Column cross section	SHS 150×16	SHS 16×12,5	SHS 200×16
Base plate offset, mm	100	150	200
Base plate thickness, mm	10	20	30
Concrete grade	C20/25	C30/37	C35/45
Concrete pad offset, mm	100	300	500

For the sensitivity study of column cross-section, the concrete grade C20/25, the base plate thickness 20 mm, the base plate offset 100 mm, and the concrete block offset 200 mm were used for varying parameters of the column section. The comparison of CBFEM to the analytical model by CM is shown in the interaction diagrams in Fig. 8.4.6.

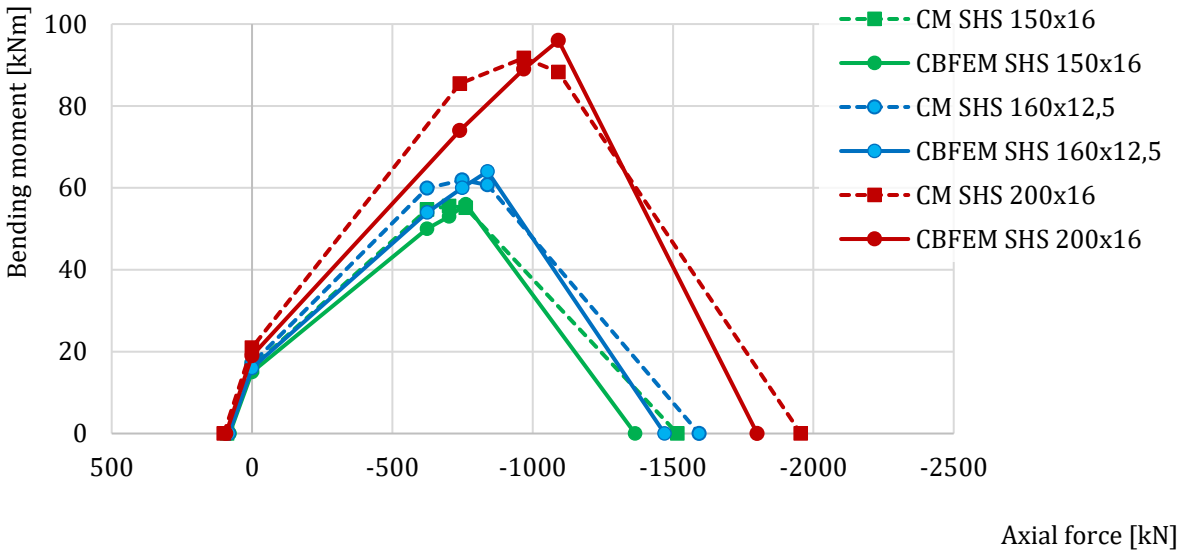

Fig. 8.4.6 Comparison of results of CBFEM to CM for the different column cross-sections

For the sensitivity study of base plate offset, the column cross-section SHS 200×16, concrete grade C25/30, base plate thickness 20 mm, and concrete block offset 200 mm were selected. The comparison of interaction diagrams is in Fig. 8.4.7. The most significant difference is in the resistance in pure tension of a large base plate where significant prying forces were present in CBFEM analyses, which are limited by analytical design.

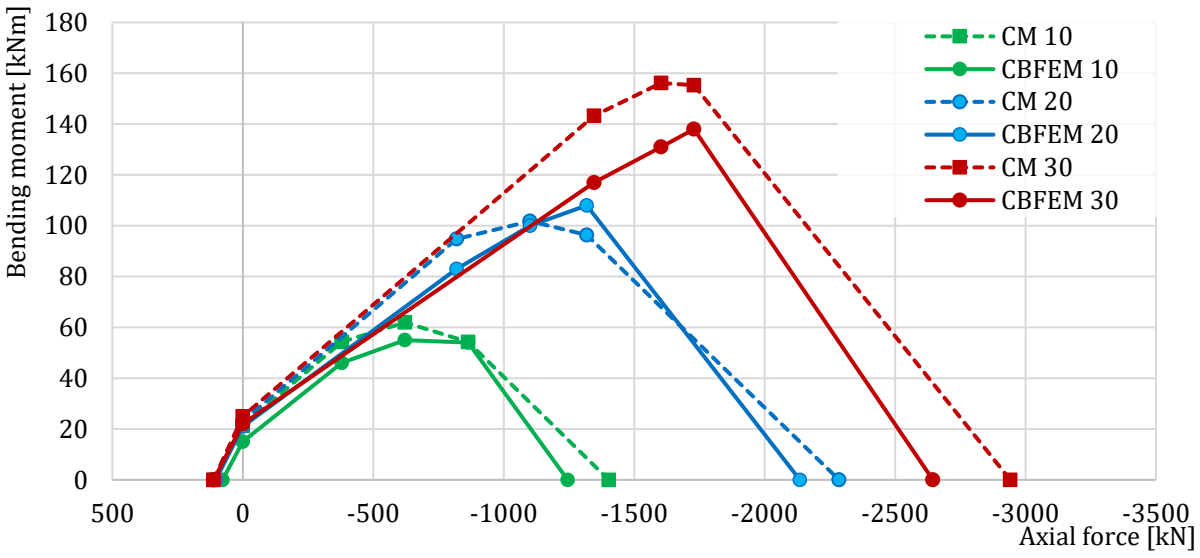

Fig. 8.4.7 Comparison of results of CBFEM to CM for the different base plate offsets

For sensitivity study of base plate thickness, the column cross-section SHS 200×16, concrete grade C25/30, base plate offset 100 mm, and concrete block offset 200 mm were selected. 10 mm, 20 mm, and 30 mm base plate thicknesses were used in this study. The comparison of interaction diagrams is in Fig. 8.4.8. The biggest difference is in the resistance in pure tension of a thin base plate where significant prying forces were present in CBFEM analyses, which are limited in analytical design by CM.

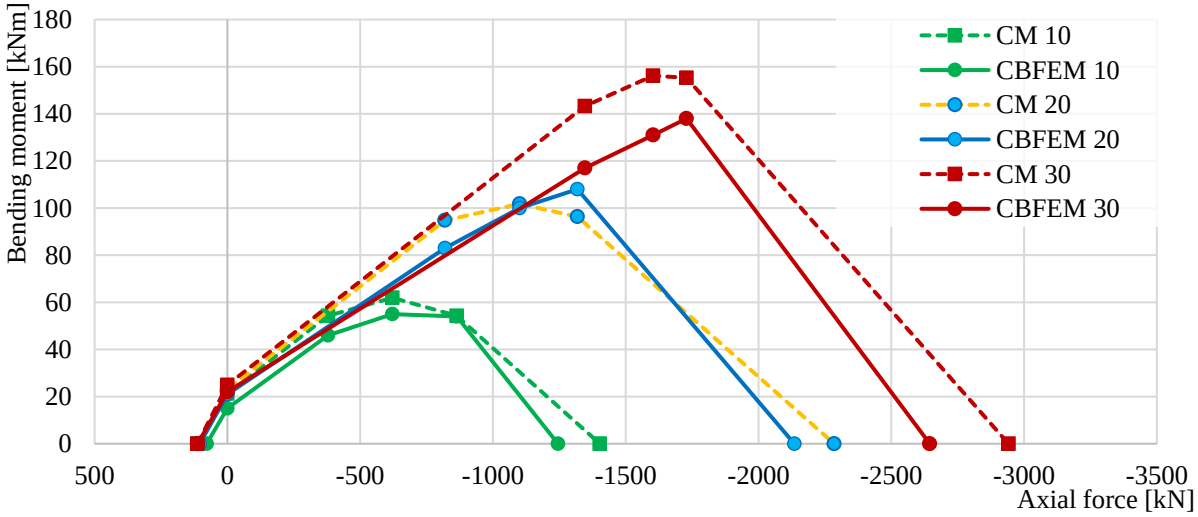

Fig. 8.4.8 Comparison of results of CBFEM to CM for the different base plate thickness

For the sensitivity study of concrete grade, the column cross-section SHS 150×16, base plate thickness 20 mm, base plate offset 100 mm, and concrete block offset 200 mm were selected. Concrete grades C20/25, C30/37, and C35/45 were used in this study. The comparison of interaction diagrams is in Fig. 8.4.9.

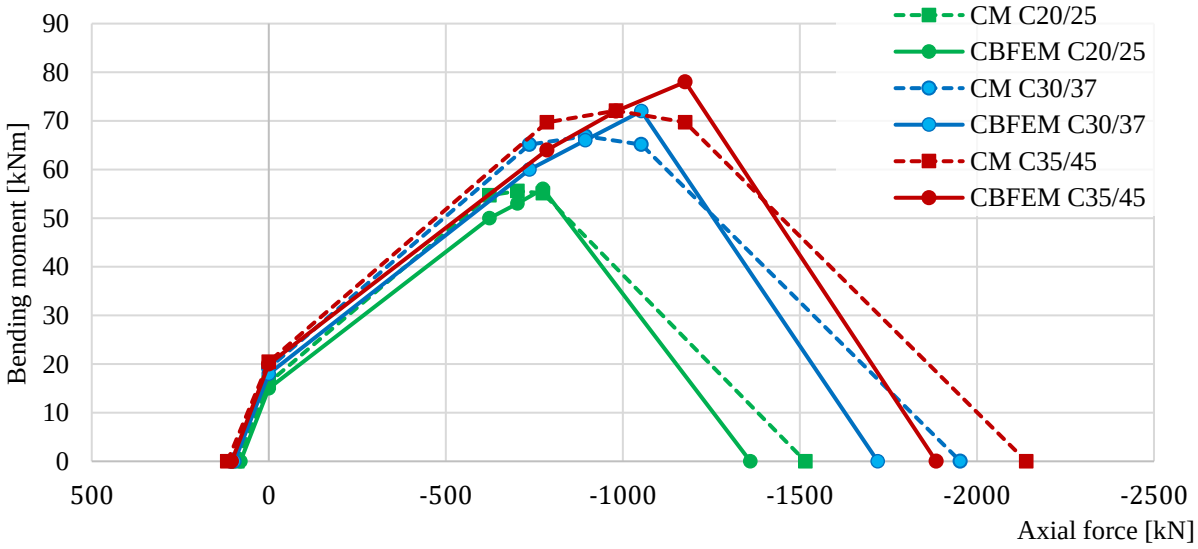

Fig. 8.4.9 Comparison of results of CBFEM to CM for the different concrete grades

For the sensitivity study of concrete block offset, the column cross-section SHS 160×12.5, base plate thickness 20 mm, base plate offset 100 mm, and concrete grade C25/30 were selected. 100 mm, 300 mm, and 500 mm concrete block offsets were used in this study. The comparison of interaction diagrams is in Fig. 8.4.10.

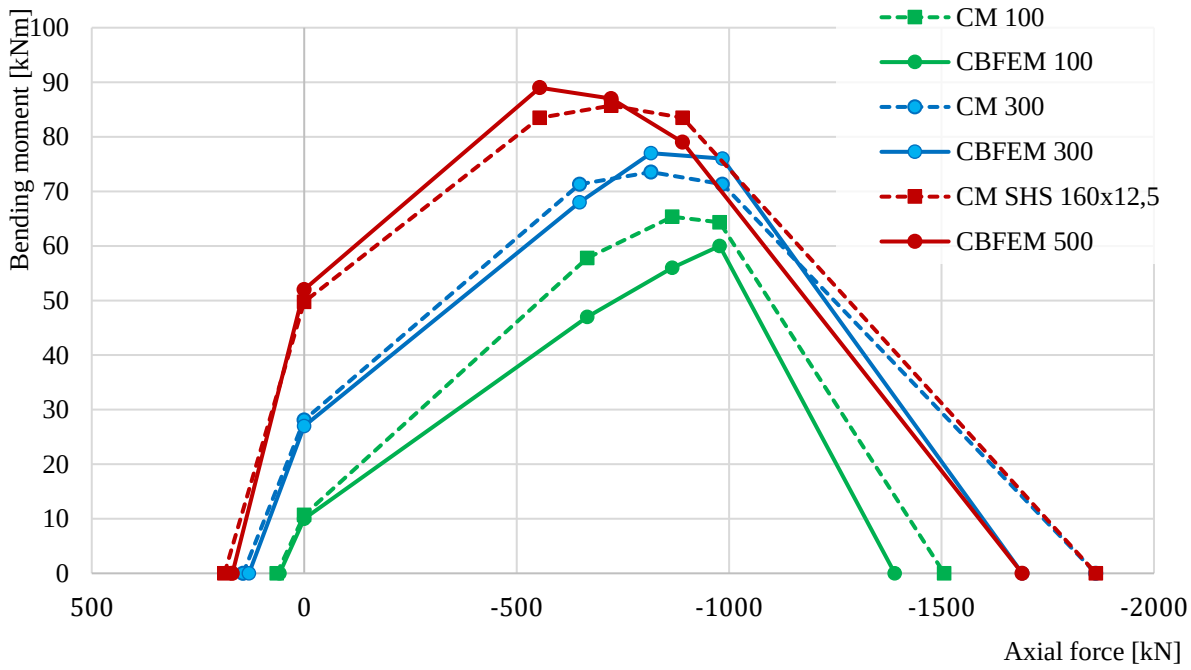

Fig. 8.4.10 Comparison of results of CBFEM to CM for the different concrete block offsets

The differences in the prediction of resistance of column base by CBFEM and CM are mainly in accepting the prying forces in CBFEM and avoiding it by CM according to EN 1993-1-8:2005.

Tab. 8.4.2 Interaction diagram comparison of CBFEM and CM

Difference CBFEM/CM	Point -1	Point 0	Point 1	Point 2	Point 3	Point 4
Maximum %	100%	105%	107%	105%	112%	93%
Minimum %	69%	71%	81%	84%	89%	88%

8.4.4 Benchmark case

Input

Column cross-section

- SHS 150×16
- Steel S420

Base plate

- Thickness 20 mm
- Offsets at top 100 mm, left 100 mm
- Welds – butt welds
- Steel S420

Anchors

- M20 8.8.
- Anchoring length 300 mm
- Offsets top layers 50 mm, left layers −20 mm
- Shear plane in thread

Foundation block

- Concrete C20/25
- Offset 200 mm
- Depth 800 mm
- Shear force transfer friction
- Grout thickness 30 mm

Loading

- Axial force N = −762 kN
- Bending moment M_y = 56 kNm

Output

- Plates $\varepsilon = 0{,}6$ %
- Anchor bolts 97,8 % ($N_{\mathrm{Ed,g}} = 65{,}7$ kN $\leq N_{\mathrm{Rd,c}} = 67{,}2$ kN
  (critical component concrete cone breakout for group of anchors A1 and A2)
- Concrete block 91,5 % ($\sigma = 24{,}5$ MPa $\leq f_{\mathrm{jd}} = 26{,}8$ MPa)
- Secant rotational stiffness $S_{\mathrm{js}} = 6{,}3 \frac{\mathrm{MNm}}{\mathrm{rad}}$

9 COLUMN WEB PANEL IN SHEAR

9.1 Welded portal frame eaves moment connection

9.1.1 Description

In this chapter, the component-based finite element method (CBFEM) for a welded portal frame eaves moment connection is verified on the component method (CM). An open section beam is welded to an open section column. The column is stiffened with two horizontal stiffeners opposite to beam flanges. Compressed plates, e.g. horizontal stiffeners of a column, column web panel in shear, compressed beam flange, are limited to 3rd class to avoid buckling. The rafter is loaded by shear force and bending moment.

9.1.2 Analytical model

Five components are examined in the study, namely the web panel in shear, the column web in transverse compression, the column web in transverse tension, the column flange in bending, and the beam flange in compression. All components are designed according to EN 1993-1-8:2005. Fillet welds are designed not to be the weakest component in the joint. The verification study of a fillet weld in a stiffened beam-to-column joint is in chapter 4.4.

Web panel in shear

The thickness of the column web is limited by slenderness to avoid stability problem; see EN 1993-1-8:2005, Cl 6.2.6.1(1). A class 4 column web panel in shear is studied in chapter 6.2. Two contributions to the load capacity are considered: resistance of the column panel in shear and the contribution from the frame mechanism of the column flanges and horizontal stiffeners; see EN 1993-1-8:2005, Cl. 6.2.6.1 (6.7 and 6.8).

Column web in transverse compression

Effect of the interaction of the shear load is considered; see EN 1993-1-8:2005, Cl. 6.2.6.2, Tab. 6.3. Influence of longitudinal stress in the column panel is considered; see EN 1993-1-8:2005, Cl. 6.2.6.2(2). The horizontal stiffeners are included in the load capacity of this component.

Column web in transverse tension

Effect of the interaction of the shear load is considered; see EN 1993-1-8:2005, Cl. 6.2.6.2, Tab. 6.3. The horizontal stiffeners are included in the load capacity of this component.

Column flange in bending

Horizontal stiffeners brace column flange; this component is not considered.

Beam flange in compression

The horizontal beam is designed to be class 3 cross-section or better to avoid buckling.

Overview of the considered examples and the material are given in the Tab. 9.1.1. Geometry of the joint with dimensions is shown in Fig. 9.1.1. The considered parameters in the study are beam cross-section, column cross-section, and thickness of the column web panel.

Tab. 9.1.1 Examples overview

Example	Material					Beam	Column	Column stiffener	
	f_y	f_u	E	γ_{M0}	γ_{M2}	Section	Section	b_s	t_s
	[MPa]	[MPa]	[GPa]	[-]	[-]			[mm]	[mm]
IPE140	235	360	210	1	1,25	IPE140	HEB260	73	10
IPE160	235	360	210	1	1,25	IPE160	HEB260	82	10
IPE180	235	360	210	1	1,25	IPE180	HEB260	91	10
IPE200	235	360	210	1	1,25	IPE200	HEB260	100	10
IPE220	235	360	210	1	1,25	IPE220	HEB260	110	10
IPE240	235	360	210	1	1,25	IPE240	HEB260	120	10
IPE270	235	360	210	1	1,25	IPE270	HEB260	135	10
IPE300	235	360	210	1	1,25	IPE300	HEB260	150	10
IPE330	235	360	210	1	1,25	IPE330	HEB260	160	10
IPE360	235	360	210	1	1,25	IPE360	HEB260	170	10
IPE400	235	360	210	1	1,25	IPE400	HEB260	180	10
IPE450	235	360	210	1	1,25	IPE450	HEB260	190	10
IPE500	235	360	210	1	1,25	IPE500	HEB260	200	10

Example	Material					Beam	Column	Column stiffener	
	f_y	f_u	E	γ_{M0}	γ_{M2}	Section	Section	b_s	t_s
	[MPa]	[MPa]	[GPa]	[-]	[-]			[mm]	[mm]
HEB160	235	360	210	1	1,25	IPE330	HEB160	160	10
HEB180	235	360	210	1	1,25	IPE330	HEB180	160	10
HEB200	235	360	210	1	1,25	IPE330	HEB200	160	10
HEB220	235	360	210	1	1,25	IPE330	HEB220	160	10
HEB240	235	360	210	1	1,25	IPE330	HEB240	160	10
HEB260	235	360	210	1	1,25	IPE330	HEB260	160	10
HEB280	235	360	210	1	1,25	IPE330	HEB280	160	10
HEB300	235	360	210	1	1,25	IPE330	HEB300	160	10
HEB320	235	360	210	1	1,25	IPE330	HEB320	160	10
HEB340	235	360	210	1	1,25	IPE330	HEB340	160	10
HEB360	235	360	210	1	1,25	IPE330	HEB360	160	10
HEB400	235	360	210	1	1,25	IPE330	HEB400	160	10
HEB450	235	360	210	1	1,25	IPE330	HEB450	160	10
HEB500	235	360	210	1	1,25	IPE330	HEB500	160	10

Example	Material					Beam	Column		Column stiffener	
	f_y	f_u	E	γ_{M0}	γ_{M2}	Section	Section	t_w	b_s	t_s
	[MPa]	[MPa]	[GPa]	[-]	[-]			[mm]	[mm]	[mm]
tw4	235	360	210	1	1,25	IPE330	HEA320	4	160	10
tw5	235	360	210	1	1,25	IPE330	HEA320	5	160	10
tw6	235	360	210	1	1,25	IPE330	HEA320	6	160	10
tw7	235	360	210	1	1,25	IPE330	HEA320	7	160	10
tw8	235	360	210	1	1,25	IPE330	HEA320	8	160	10
tw9	235	360	210	1	1,25	IPE330	HEA320	9	160	10
tw10	235	360	210	1	1,25	IPE330	HEA320	10	160	10
tw11	235	360	210	1	1,25	IPE330	HEA320	11	160	10
tw12	235	360	210	1	1,25	IPE330	HEA320	12	160	10
tw13	235	360	210	1	1,25	IPE330	HEA320	13	160	10
tw14	235	360	210	1	1,25	IPE330	HEA320	14	160	10
tw15	235	360	210	1	1,25	IPE330	HEA320	15	160	10
tw16	235	360	210	1	1,25	IPE330	HEA320	16	160	10

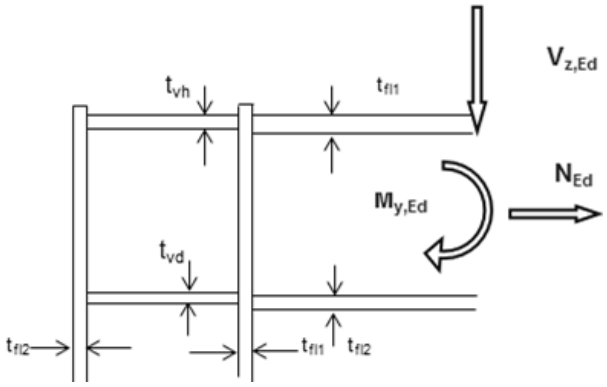

Fig. 9.1.1 Joint geometry and dimensions

9.1.3 Numerical model

Nonlinear elastic-plastic material status is investigated in each layer of an integration point. Assessment is based on the maximum strain given according to EN 1993-1-5:2006 by the value of 5%.

9.1.4 Global behavior

Comparison of the global behavior of a portal frame moment connection, described by moment-rotation diagram, is presented. Main characteristics of the moment-rotation diagram are initial stiffness, elastic resistance, and design resistance. An open section beam IPE 330 is welded to a column HEB 260 in the example. A portal frame moment connection with horizontal stiffeners in the column is considered according to component method as a rigid joint with $S_{j,ini} = \infty$. Therefore a joint without horizontal stiffeners in the column is analyzed. The moment-rotation

diagram is shown in Fig. 9.1.2, and the results are summarised in Tab. 9.1.2. The results show very good agreement in initial stiffness and joint global behavior.

Tab. 9.1.2 Rotational stiffness of a portal frame moment connection in CBFEM and CM

		CM	CBFEM	CM/CBFEM
Initial stiffness $S_{j,ini}$	[kNm/rad]	48423,7	58400,0	0,83
Elastic resistance *2/3* $M_{j,Rd}$	[kNm]	93,3	93,0	1,00
Design resistance $M_{j,Rd}$	[kNm]	140,0	139,0	0,99

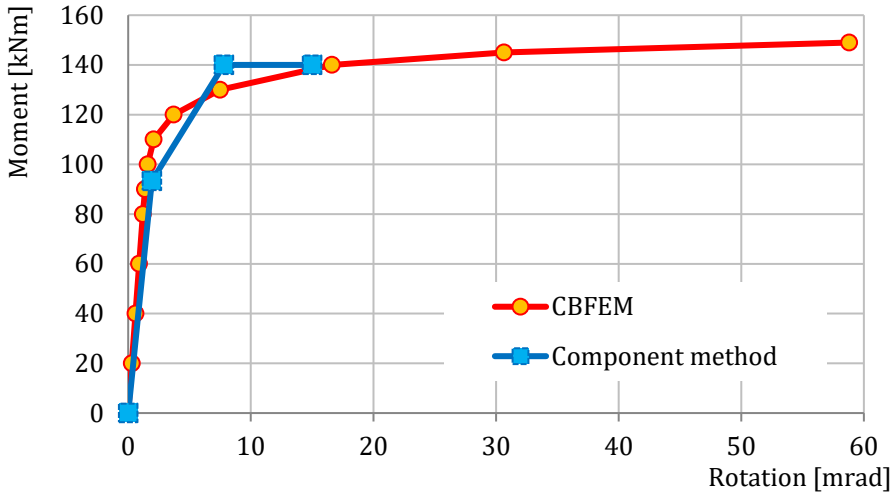

Fig. 9.1.2 Moment-rotation diagram for a joint without column stiffeners

9.1.5 Verification of resistance

The results calculated by CBFEM are compared with CM. The comparison is focused on the design resistance and the critical component. The study is performed for three different parameters: beam cross-section, column cross-section, and thickness of the column web panel.

An open section column HEB 260 is used in an example where the parameter is beam cross-section. The column is stiffened with two horizontal column stiffeners of thickness 10 mm opposite to the beam flanges. The width of stiffeners is corresponding to the width of beam flange. The beam IPE sections are selected from IPE 140 to IPE 500. The results are shown in Tab. 9.1.3. The influence of beam cross-section on the design resistance of a welded portal frame moment connection is shown in Fig. 9.1.3.

Tab. 9.1.3 Design resistances and critical components in CBFEM and CM

Parameter	Component method		CBFEM	
	Resistance [kN/kNm]	Critical component	Resistance [kN/kNm]	Critical component
IPE140	24	Beam flange in compression	27	Beam flange in compression
IPE160	33	Beam flange in compression	34	Beam flange in compression
IPE180	44	Beam flange in compression	48	Beam flange in compression
IPE200	59	Beam flange in compression	67	Beam flange in compression
IPE220	77	Beam flange in compression	80	Beam flange in compression
IPE240	98	Beam flange in compression	103	Beam flange in compression
IPE270	113	Beam flange in compression	125	Beam flange in compression
IPE300	142	Web panel in shear	142	Beam flange in compression
IPE330	155	Web panel in shear	154	Beam flange in compression
IPE360	168	Web panel in shear	167	Web panel in shear
IPE400	186	Web panel in shear	183	Web panel in shear
IPE450	209	Web panel in shear	202	Web panel in shear
IPE500	231	Web panel in shear	223	Web panel in shear

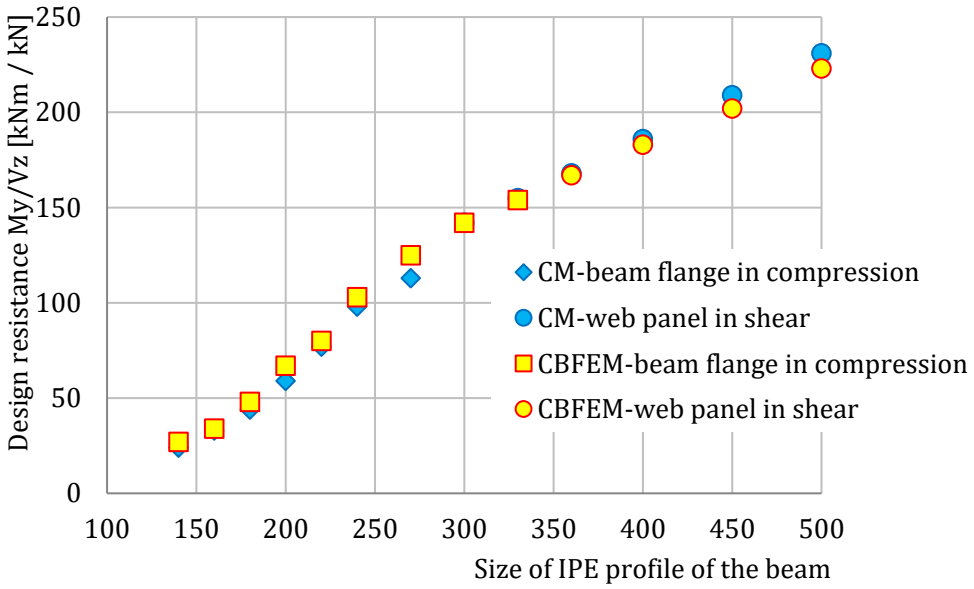

Fig. 9.1.3 Sensitivity study of beam size in a portal frame moment connection

An open section beam IPE330 is used in an example where the parameter is column cross-section. The column is stiffened with two horizontal column stiffeners with a thickness of 10 mm opposite to the beam flanges. The width of stiffeners is 160 mm. The column sections are selected from HEB 160 to HEB 500. The results are shown in Tab. 9.1.4. The influence of column cross-section on the design resistance of a welded portal frame moment connection is shown in Fig. 9.1.4.

Tab. 9.1.4 Design resistances and critical components of a moment connection in CBFEM and CM

Parameter	Component method		CBFEM	
	Resistance [kN/kNm]	Critical component	Resistance [kN/kNm]	Critical component
HEB160	73	Web panel in shear	70	Web panel in shear
HEB180	84	Web panel in shear	88	Web panel in shear
HEB200	103	Web panel in shear	101	Web panel in shear
HEB220	116	Web panel in shear	124	Web panel in shear
HEB240	139	Web panel in shear	139	Web panel in shear
HEB260	155	Web panel in shear	154	Web panel in shear
HEB280	170	Web panel in shear	179	Beam flange in compression
HEB300	198	Web panel in shear	196	Beam flange in compression
HEB320	216	Web panel in shear	226	Beam flange in compression
HEB340	226	Beam flange in compression	240	Beam flange in compression
HEB360	228	Beam flange in compression	245	Beam flange in compression
HEB400	234	Beam flange in compression	251	Beam flange in compression
HEB450	241	Beam flange in compression	258	Beam flange in compression
HEB500	248	Beam flange in compression	266	Beam flange in compression

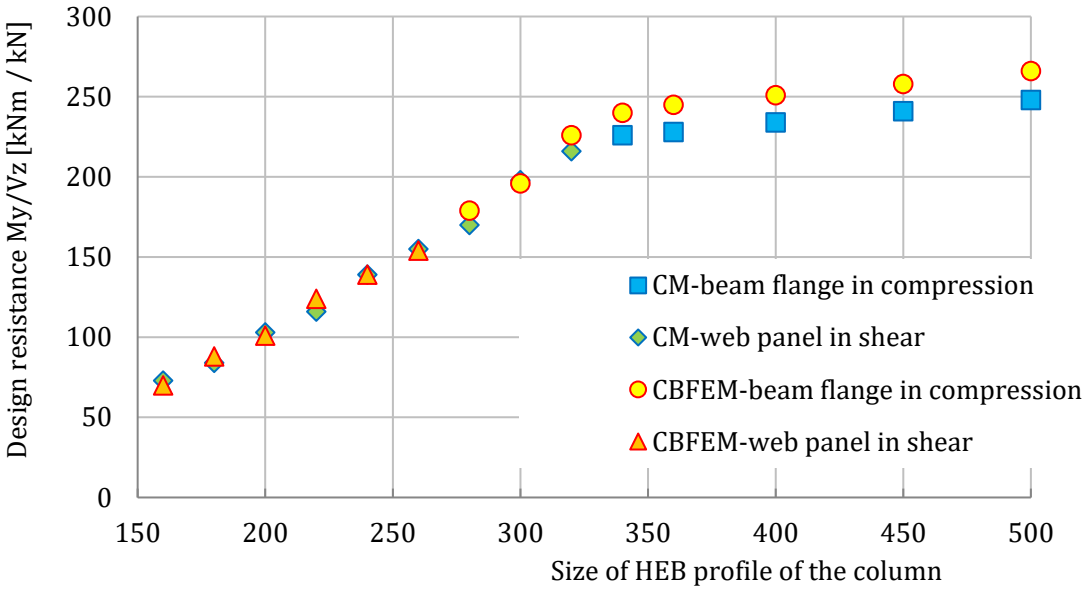

Fig. 9.1.4 Sensitivity study of column size in a portal frame moment connection

Third example presents a portal frame moment connection made out of an open section beam IPE 330 and column HEA 320. The parameter is the thickness of the column web. The column is stiffened with two horizontal column stiffeners with a thickness of 10 mm and width 160 mm. The column web thickness is chosen from 4 to 16 mm. The results are summarised in Tab. 9.1.5. The influence of column web thickness on the design resistance of a welded portal frame moment connection is shown in Fig. 9.1.5.

Tab. 9.1.5 Design resistances and critical components of a moment connection in CBFEM and CM

Parameter	Component method		CBFEM	
	Resistance [kN/kNm]	Critical component	Resistance [kN/kNm]	Resistance [kN/kNm]
tw4	82	Web panel in shear	99	Web panel in shear
tw5	94	Web panel in shear	115	Web panel in shear
tw6	106	Web panel in shear	131	Web panel in shear
tw7	118	Web panel in shear	147	Web panel in shear
tw8	130	Web panel in shear	162	Web panel in shear
tw9	142	Web panel in shear	177	Web panel in shear
tw10	155	Web panel in shear	190	Beam flange in compression
tw11	167	Web panel in shear	203	Beam flange in compression
tw12	179	Web panel in shear	216	Beam flange in compression
tw13	191	Web panel in shear	227	Beam flange in compression
tw14	203	Web panel in shear	236	Beam flange in compression
tw15	215	Beam flange in compression	240	Beam flange in compression
tw16	222	Beam flange in compression	241	Beam flange in compression

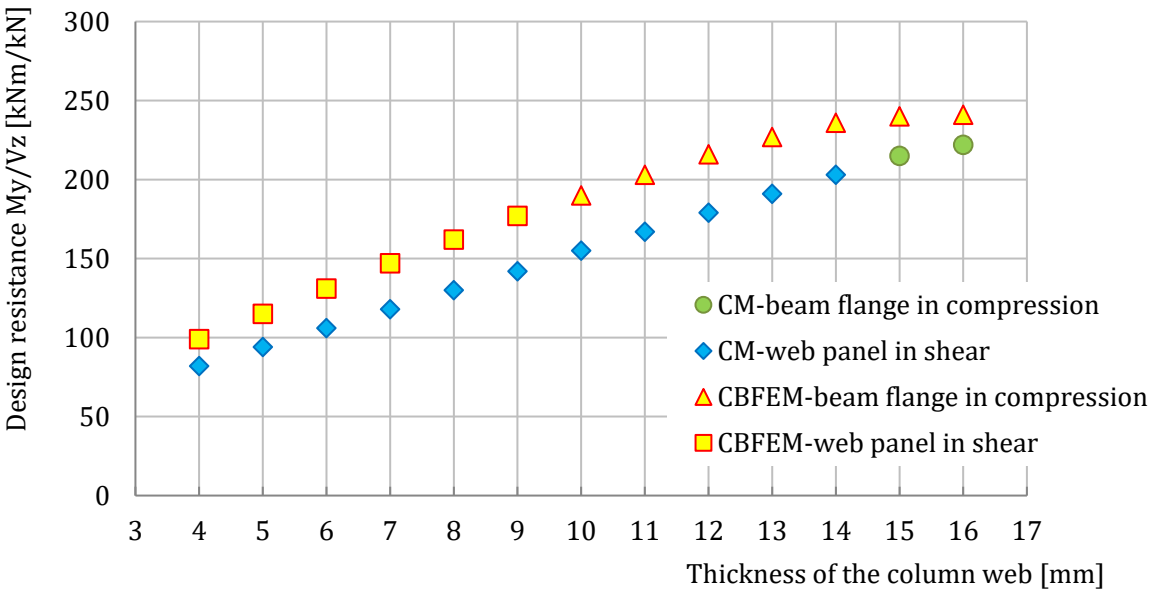

Fig. 9.1.5 A sensitivity study of column web thickness

To illustrate the accuracy of the CBFEM model, the results of the parametric studies are summarized in a diagram comparing the resistances of CBFEM and component method; see Fig. 9.1.6. The results show that the difference between the two calculation methods is less than 5%, which is a generally acceptable value. The study with parameter column web thickness gives higher resistance for CBFEM model compared to component method. This difference is caused by considering welded cross-sections. The transfer of shear load is in component method considered only in web and contribution of the flanges is neglected.

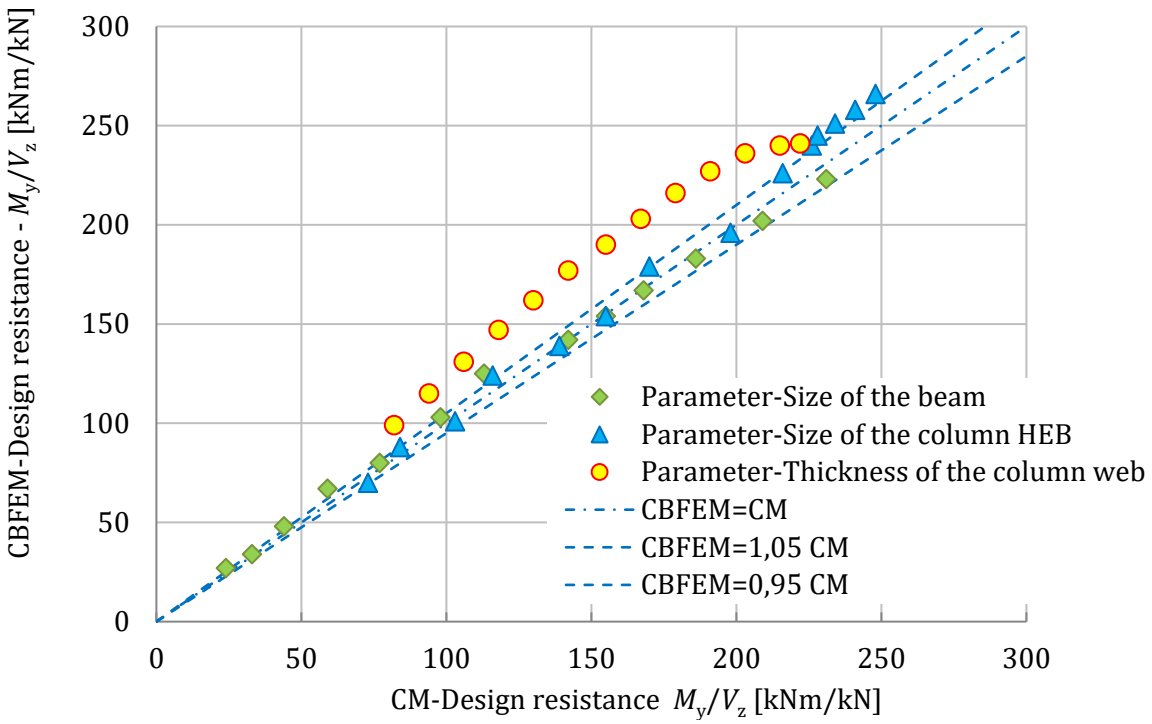

Fig. 9.1.6 Verification of CBFEM to CM

9.1.6 Benchmark example

Inputs

Column

- Steel S235
- HEB260

Beam

- Steel S235
- IPE330

Column stiffeners

- Thickness t_s = 10 mm
- Width b_s = 160 mm
- Opposite to beam flanges

Weld

- Flange weld throat thickness a_f = 9 mm
- Web weld throat thickness a_w = 5 mm
- Fillet weld

Outputs

- Design resistance in shear V_{Rd} = 154 kN
- Design resistance in bending M_{Rd} = 154 kNm

9.2 Bolted portal frame eaves moment connection

9.2.1. Description

The objective of this study is verification of bolted portal frame eaves connection, as shown in Fig. 9.2.1. Rafter is bolted using end plate on the column flange. The column is stiffened with two horizontal stiffeners in levels of the beam flanges. Compressed plates, e.g. horizontal stiffeners of column, web panel in shear or compression, and compressed beam flange, are designed as cross-section class 3. Horizontal beam is 6 m long loaded by continuous load over the entire length.

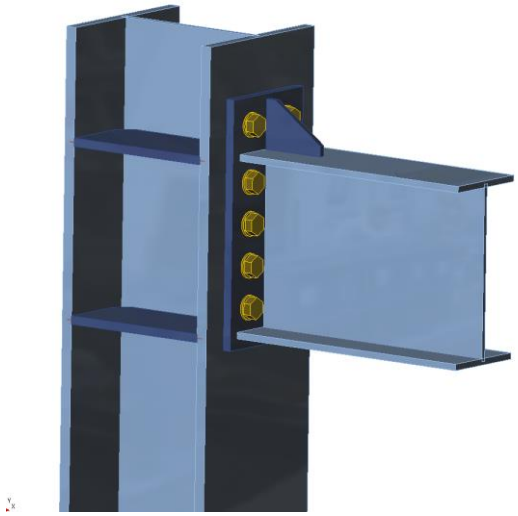

Fig. 9.2.1 Bolted portal frame eaves connection

9.2.2. Analytical model

Eight components are examined: fillet weld, web panel in shear, column web in transverse compression, column web in transverse tension, beam flange in compression and tension, column flange in bending, end plate in bending, and bolts. All components are designed according to EN 1993-1-8:2005. Design loads of components depend on the position. The web panel in shear is loaded by design loads on the vertical axis of the column. Other components are loaded by reduced design loads in column flange to which horizontal beam is connected.

Fillet weld

The weld is closed around the whole cross-section of the beam. The thickness of the weld on the flanges can differ from the thickness of the weld on the web. Vertical shear force is transferred only by welds on the web and plastic stress distribution is considered. Bending moment is transferred by whole weld shape, and elastic stress distribution is considered. Effective weld width depending on the horizontal stiffness of the column is considered (because of bending of the unstiffened column flange). Design of the weld is done according to EN 1993-1-8:2005,

Cl. 4.5.3.2(6). The assessment is carried out in two major points: on the upper or lower edge of the flange (maximum bending stress) and in the crossing of the flange and the web (combination of shear force and bending moment stresses).

Web panel in shear

The thickness of the column web is designed to be third class at most; see EN 1993-1-8:2005, Cl. 6.2.6.1(1). Two contributions to the load capacity are considered: resistance of the column wall in shear and the contribution from the frame behavior of the column flanges and horizontal stiffeners; see EN 1993-1-8:2005, Cl. 6.2.6.1 (6.7 and 6.8).

Column web in transverse compression or tension

Effect of the interaction of the shear load is considered; see EN 1993-1-8:2005, Cl. 6.2.6.2 and Tab. 6.3. Influence of longitudinal stress in the wall of the column is considered; see EN 1993-1-8:2005, Cl. 6.2.6.2(2). Horizontal stiffeners prevent buckling and are included in the load capacity of this component with the effective area.

Beam flange in compression

The horizontal beam is designed to be maximally third class.

Column flange or end plate in bending

Effective lengths for circular and noncircular failures are considered according to EN 1993-1-8:2005, Cl. 6.2.6. Three modes of collapse according to EN 1993-1-8:2005, Cl. 6.2.4.1 are considered.

Bolts

Bolts are designed according to EN 1993-1-8:2005, Cl. 3.6.1. Design resistance considers punching shear resistance and rupture of the bolt.

9.2.3. Numerical design model

T-stub is modeled by 4-node shell elements as described in Chapter 3 and summarized further. Every node has 6 degrees of freedom. Deformations of the element consist of membrane and flexural contributions. Nonlinear elastic-plastic material status is investigated in each layer of integration point. Assessment is based on the maximum strain given according to EN 1993-1-5:2006 by value of 5 %. Bolts are divided into three sub-components. The first is the bolt shank, which is modeled as a nonlinear spring and caries tension only. The second sub-component transmits tensile force into the flanges. The third sub-component solves shear transmission.

9.2.4. Global behavior

Comparison of the global behavior of the joint, described by moment-rotation diagrams for both design procedures mentioned above, was done. Attention was focused on the main characteristics of the moment-rotation diagram: initial stiffness, design resistance, and deformation capacity.

Beam IPE 330 is connected to column HEB 300 using extended end plate with 5 rows of the bolts M24 8.8. The results of both design procedures are shown in the graph in Fig. 9.2.2 and in Tab. 9.2.1. CM generally gives higher initial stiffness compared to CBFEM. CBFEM gives slightly higher design resistance compared to CM in all cases, as shown in Chapter 9.2.5. The difference is up to 10%. Deformation capacity is also compared. Deformation capacity was calculated according to (Beg et al. 2004) because EC3 provides limited background for deformation capacity of endplate joints.

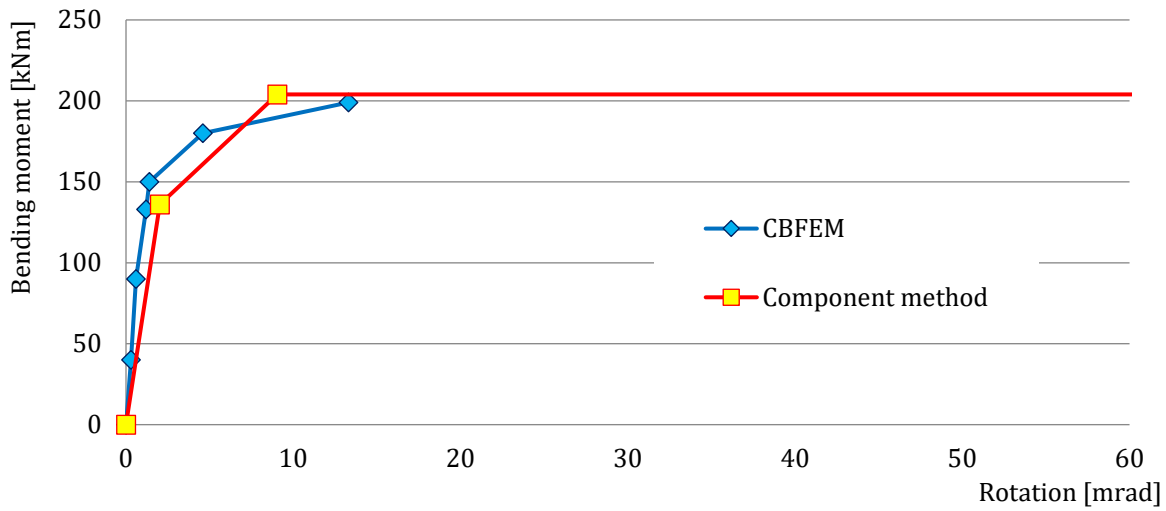

Fig. 9.2.2 Moment-rotation diagram

Tab. 9.2.1 Global behavior overview

		CM	CBFEM	CM/CBFEM
Initial stiffness	[kNm/rad]	67400	112000	0,60
Design resistance	[kNm]	204	199	0,98
Deformation capacity	[mrad]	242	47	5,14

9.2.5. Verification of resistance

Design resistance calculated by CBFEM was compared with the results of the component method in the next step. The comparison was focused on the resistance and also the critical component. The study was performed for the column cross-section parameter. Beam IPE 330 is connected to the column by extended endplate with 5 bolt rows. Bolts M24 8.8 are used. The dimensions of the end plate P15 with bolt end distances and spacing in millimeters are the height 450 (50-103-75-75-75-73) and the width 200 (50-100-50). The outer edge of the upper flange is 91 mm from the edge of the end plate. Beam flanges are connected to the end plate with welds with the throat thickness of 8 mm. The beam web is connected with the weld throat thickness of 5 mm. The column is stiffened with horizontal stiffeners opposite to beam flanges. The Stiffeners are 15 mm

thick, and their width corresponds to the column width. The thickness of the end plate stiffener is 10 mm, and its width is 90 mm. The results are shown in Tab. 9.2.2 and Fig. 9.2.3.

Tab. 9.2.2 Design resistance for parameter – column profile

Column cross section	CM		CBFEM		CM/ CBFEM
	Resistance kNm	Component	Resistance kNm	Component	
HEB 200	107	Column web in shear	106	Column web in shear	1,01
HEB 220	121	Column web in shear	136	Column web in shear	0,89
HEB 240	143	Column web in shear	155	Column web in shear	0,92
HEB 260	160	Column web in shear	169	Column web in shear	0,95
HEB 280	176	Column web in shear	187	Column web in shear	0,94
HEB 300	204	Column web in shear	199	Beam flange in tension/compression	0,98
HEB 320	222	Column web in shear	225	Beam flange in tension/compression	0,99
HEB 340	226	Beam flange in tension/compression	242	Beam flange in tension/compression	0,93
HEB 360	229	Beam flange in tension/compression	239	Beam flange in tension/compression	0,96
HEB 400	234	Beam flange in tension/compression	253	Beam flange in tension/compression	0,92
HEB 450	241	Beam flange in tension/compression	260	Beam flange in tension/compression	0,93
HEB 500	248	Beam flange in tension/compression	268	Beam flange in tension/compression	0,93

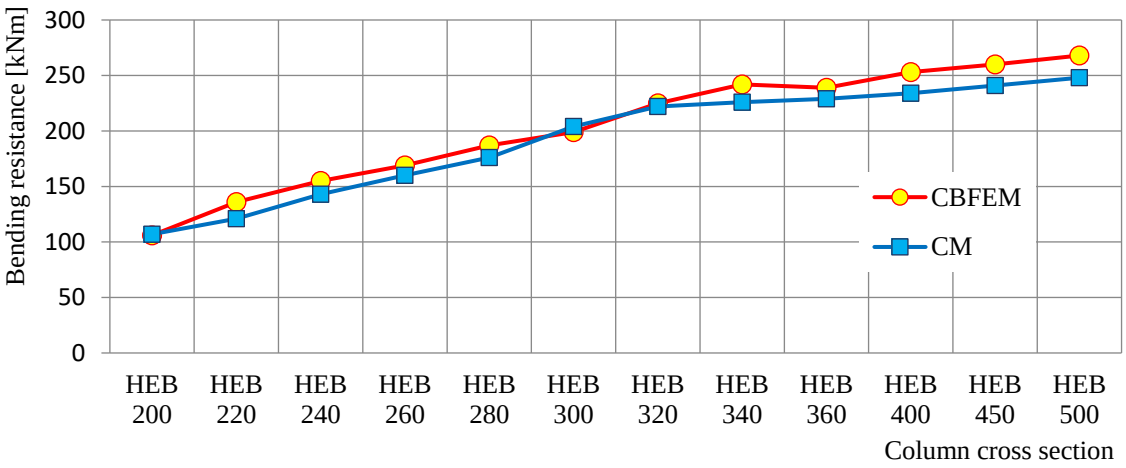

Fig. 9.2.3 Design resistance depending on column cross-section

To illustrate the accuracy of the CBFEM model, the results of the parametric studies are summarized in the graph comparing resistances predicted by CBFEM and by CM; see Fig. 9.2.4. The results show that CBFEM provides slightly higher design resistance compared to CM in nearly all cases. The difference between both methods is up to 10%.

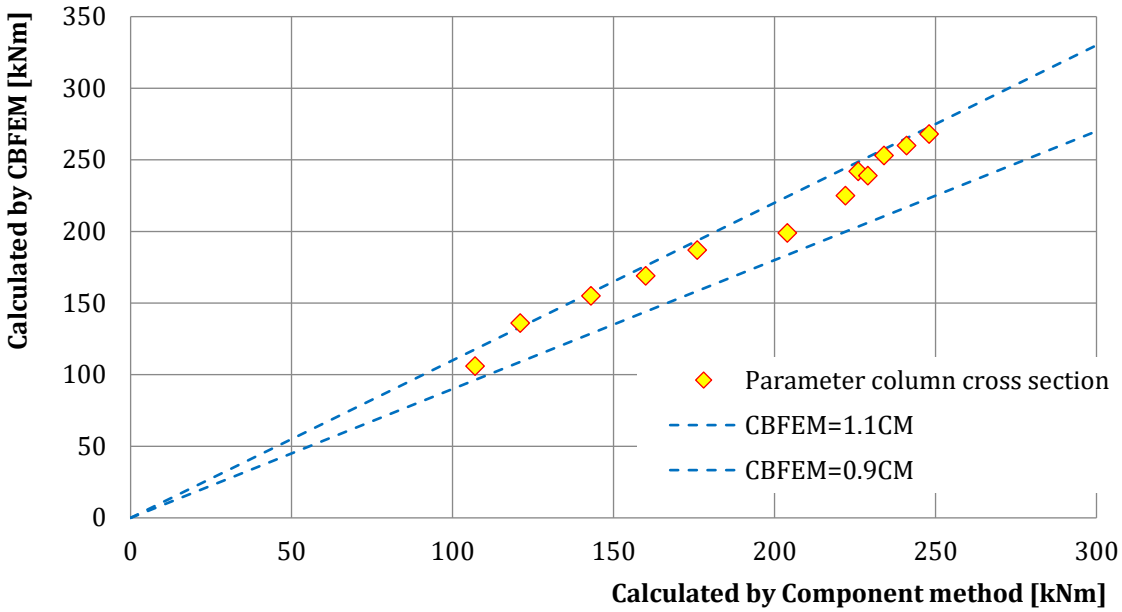

Fig. 9.2.4 Verification of CBFEM to CM

9.2.6. Benchmark example

Inputs

- Steel S235
- Beam IPE 330
- Column HEB 300
- End plate height h_p = 450 (50-103-75-75-75-73) mm
- End plate width b_p = 200 (50-100-50) mm
- End plate P15
- Column stiffeners 15 mm thick and 300 mm wide
- End plate stiffener 10 mm thick and 90 mm wide
- Flange weld throat thickness a_f = 8 mm
- Web weld throat thickness a_w = 5 mm
- Bolts M24 8.8

Outputs

- Design resistance in bending M_{Rd} = 199 kNm
- Corresponding vertical shear force V_{Ed}= 199 kN
- Collapse mode - yielding of the beam stiffener on upper flange
- Utilization of the bolts 88,9 %
- Utilization of the welds 87,5 %

10 PREDICTION OF STIFFNESS

10.1 Bending stiffness of welded joint of open sections

10.1.1 Description

The prediction of rotational stiffness is described on a welded eaves moment joint. A welded joint of open section column HEB and beam IPE is studied, and the joint behavior is described on a moment-rotation diagram. The results of the analytical model by component method (CM) are compared with the numerical results obtained by component-based finite element method (CBFEM). A benchmark case is available.

10.1.2 Analytical model

The rotational stiffness of a joint should be determined from a deformation of its basic components, which are represented by the stiffness coefficient k_i. The rotational stiffness of the joint S_j is obtained from:

$$S_j = \frac{Ez^2}{\mu \sum_i \frac{1}{k_i}} \qquad (10.1.1)$$

where k_i is the stiffness coefficient for the joint component i;

z is the lever arm; see 6.2.7;

μ is the stiffness ratio; see 6.3.1.

The joint components that are taken into account in this example are column web panel in shear k_1, column web in compression k_2, and column web in tension k_3. The stiffness coefficients are defined in Table 6.11 in EN 1993-1-8:2005. The initial stiffness $S_{j,ini}$ is obtained for a moment $M_{j,Ed} \leq 2/3\ M_{j,Rd}$.

An open section beam IPE 400 is welded to a column HEB 300 in the example. Beam flanges are connected to the column flange with welds with the throat thickness of 9 mm. The beam web is connected with welds with the throat thickness of 5 mm. Plastic stress distribution is considered in welds. The material of the beam and column is S235. The design resistance is limited by the components column web in compression and column web in tension. The calculated stiffness coefficients of the basic components, initial stiffness, stiffness by design resistance, and rotation of the beam are summarised in Tab. 10.1.1.

Tab. 10.1.1 Results of the analytical model

	k_1	k_2	k_3	$2/3\ M_{j,Rd}$	$S_{j,ini}$	φ_{ini}	$M_{j,Rd}$	S_j	φ
CM	[-]	[-]	[-]	[kNm]	[MNm/rad]	[mrad]	[kNm]	[MNm/rad]	[mrad]
	4,7	9,6	9,6	123	74,3	1,7	185	26,0	7,1

10.1.3 Numerical model

Detailed information about the prediction of stiffness in CBFEM may be found in chapter 3.9. The same eaves moment joint is modeled, and the results are in Tab. 10.1.2. The design resistance is reached by 5% plastic strain in the component column web in tension. The CBFEM analyses allow calculating rotational stiffness at any stage of loading.

Tab. 10.1.2 Results of CBFEM

Bending moment $M_{j,Ed}$	Secant stiffness S_j	Rotation φ
[kNm]	[MNm/rad]	[mrad]
0	0,0	0,0
60	85,9	0,7
132	82,2	1,6
150	63,2	2,4
170	28,6	6,0
180	17,1	10,5
198	4,7	42,3

10.1.4 Global behavior and verification

A comparison of the global behavior of a welded eaves moment joint described by a moment-rotation diagram is prepared. The joint is analyzed, and the stiffness of the connected beam is calculated. The main characteristic is the initial stiffness calculated at $2/3M_{j,Rd}$, where $M_{j,Rd}$ is the design moment resistance of the joint. $M_{c,Rd}$ stands for design moment resistance of the analyzed beam. The moment-rotation diagram is shown in Fig. 10.1.1.

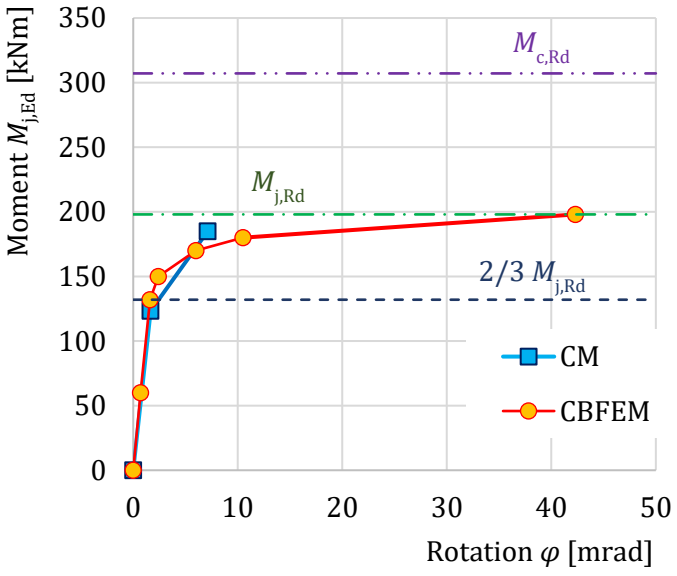

Fig. 10.1.1 Moment-rotation diagram for a welded eaves moment joint

10.1.5 Verification of stiffness

The rotational stiffness calculated by CBFEM is compared with CM. The comparison shows good agreement in initial stiffness and correspondence of joint behavior. The calculated stiffness from CBFEM and CM are summarised in Tab. 10.1.3.

Tab. 10.1.3 Rotational stiffness of a eaves moment joint in CBFEM and CM

CM				CBFEM			
$M_{j,Ed}$		$S_{j,ini}$	S_j	$M_{j,Ed}$		$S_{j,ini}$	S_j
[kNm]		[MNm/rad]	[MNm/rad]	[kNm]		[MNm/rad]	[MNm/rad]
2/3 $M_{j,Rd}$	123	74,3	-	2/3 $M_{j,Rd}$	132	82,1	-
$M_{j,Rd}$	185	-	26,0	$M_{j,Rd}$	198	-	4,7

10.1.6 Benchmark case

Inputs

Beam and column

- Steel S235
- Column HEB 300
- Beam IPE 400
- Flange weld throat thickness a_f = 9 mm
- Web weld throat thickness a_w = 5 mm
- Column offset s = 150 mm
- Double fillet weld

Outputs

- Design resistance $M_{j,Rd}$= 198 kNm
- Load $M_{j,Ed}$ = 2/3 $M_{j,Rd}$ = 132 kNm
- Rotational deformation ϕ = 1,6 mrad
- Secant rotational stiffness S_{js} = 82,2 MNm/rad

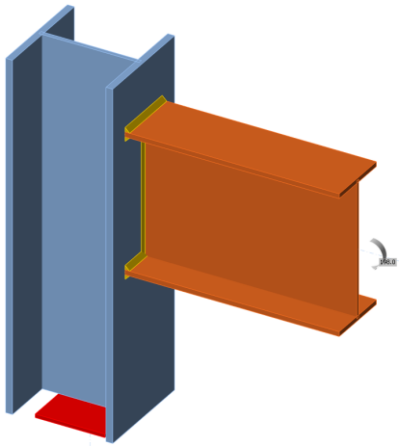

Fig. 10.1.2 Benchmark case for welded eaves moment joint (IPE 400 to HEB 300)

10.2 Bending stiffness of bolted joint of open sections

10.2.1 Description

The prediction of rotational stiffness is verified on a bolted eaves moment joint. A bolted joint of open section column HEB and beam IPE is studied, and the joint behavior is described on a moment-rotation diagram. The results of analytical model by the component-based finite element method (CBFEM) are compared with the component method (CM). The numerical results in the form of a benchmark case are available.

10.2.2 Analytical model

The rotational stiffness of a joint should be determined from deformation of its basic components, which represented by the stiffness coefficient k_i. The rotational stiffness of the joint S_j is obtained from:

$$S_j = \frac{Ez^2}{\mu \sum_i \frac{1}{k_i}} \qquad (10.2.1)$$

where k_i is the stiffness coefficient for the joint component i;

z is the lever arm, see 6.2.7;

μ is the stiffness ratio, see 6.3.1.

The joint components that are taken into account in this example are column web panel in shear k_1 and a single equivalent stiffness coefficient k_{eq} for end plate joint with two or more bolt-rows in tension. The stiffness coefficients are defined in Table 6.11 in EN 1993-1-8:2005. The equivalent stiffness coefficient may be obtained in chapter 6.3.3 in EN 1993-1-8:2005. The initial stiffness $S_{j,ini}$ is obtained for a moment $M_{j,Ed} \leq 2/3\ M_{j,Rd}$.

An open section beam IPE 330 is connected with bolted end plate to a column HEB 200 in the example. The end plate thickness is 15 mm, the bolt type is M24 8.8, and the assembly is shown in Fig. 10.2.1. The stiffeners are inside the column opposite to beam flanges with a thickness of 15 mm. Beam flanges are connected to the end plate with welds throat thickness of 8 mm. The beam web is connected with a weld with a throat thickness of 5 mm. Plasticity is applied in welds. The material of the beam, column, and end plate is S235. The joint is loaded in bending. The design resistance is limited by the component column web panel in shear. The calculated stiffness coefficients of the basic components, initial stiffness, secant stiffness at design resistance, and rotation of the beam are summarised in Tab. 10.2.1.

Tab. 10.2.1 Results of the analytical model

	k_1	k_{eq}	$2/3\ M_{j,Rd}$	$S_{j,ini}$	φ_{ini}	$M_{j,Rd}$	S_j	φ
CM	[-]	[-]	[kNm]	[MNm/rad]	[mrad]	[kNm]	[MNm/rad]	[mrad]
	3,0	10,8	71	40,2	1,8	107	13,4	8,0

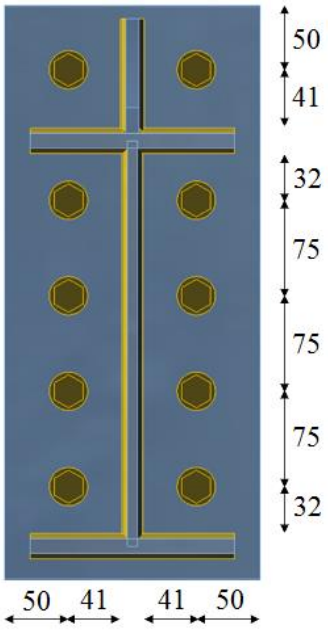

Fig. 10.2.1 Benchmark case for bolted eaves moment joint (IPE 330 to HEB 200)

10.2.3 Numerical model

Detailed information about the prediction of stiffness in CBFEM may be found in chapter 3.9. For this end plate joint, the results are summarised in Tab. 10.2.2. The CBFEM analysis allows calculating secant rotational stiffness in any stage of loading. The design resistance is reached by 5% plastic strain in a component column web panel in shear.

Tab. 10.2.2 Results of CBFEM

	$M_{j,Ed}$	S_j	φ
	[kNm]	[MNm/rad]	[mrad]
CBFEM	0	0	0,0
	40	41,0	1,0
	70	$S_{j,ini}$ = 39,7	1,8
	80	23,4	3,4
	90	11,6	7,8
	100	4,8	20,7
	105	2,5	42,2

10.2.4 Global behavior and verification

A comparison of the global behavior of a bolted eaves moment joint described by the moment-rotation diagram is prepared. The joint is analyzed, and the stiffness of the connected beam is calculated. The main characteristic is the initial stiffness calculated by $2/3M_{j,Rd}$, where $M_{j,Rd}$ is the design moment resistance of the joint. $M_{c,Rd}$ stands for a design moment resistance of the analyzed beam. The moment-rotation diagram is shown in Fig. 10.2.2.

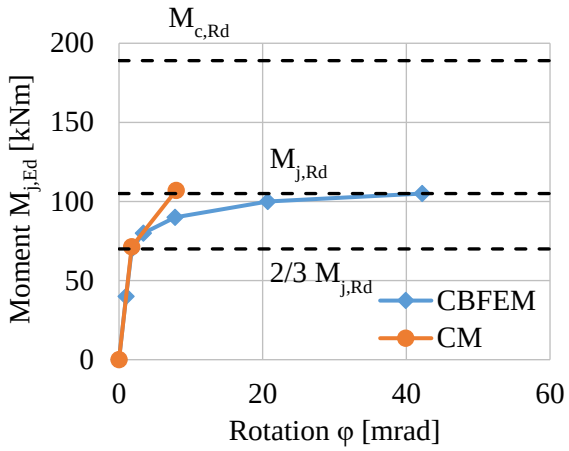

Fig. 10.2.2 Moment-rotation diagram for a bolted eaves moment joint

10.2.5 Verification of stiffness

The rotational stiffness calculated by CBFEM is compared with CM. The comparison shows good agreement in initial stiffness and correspondence of joint behavior. The calculated stiffness from CBFEM and CM are summarised in Tab. 10.2.3.

Tab. 10.2.3 Rotational stiffness of an eaves moment joint in CBFEM and CM

CM				CBFEM			
$M_{j,Ed}$		$S_{j,ini}$	S_j	$M_{j,Ed}$		$S_{j,ini}$	S_j
[kNm]		[MNm/rad]	[MNm/rad]	[kNm]		[MNm/rad]	[MNm/rad]
2/3 $M_{j,Rd}$	71	40,2	-	2/3 $M_{j,Rd}$	70	39,7	-
$M_{j,Rd}$	107	-	13,4	$M_{j,Rd}$	105	-	2,5

10.2.6 Benchmark case

Inputs

Beam and column

- Steel S235
- Column HEB 200
- Beam IPE 330
- Column offset s = 200 mm

Weld

- Flange weld throat thickness a_f = 8 mm
- Web weld throat thickness a_w = 5 mm

End-plate

- Thickness t_p = 15 mm
- Height h_p = 450 mm
- Width b_p = 200 mm

- Bolts M24 8.8
- Bolts assembly in Fig. 10.2.3

Column stiffeners

- Thickness t_s = 15 mm
- Width b_s = 95 mm
- Related to beam flange, position upper and lower
- Weld throat thickness a_s = 6 mm

End-plate stiffener

- Thickness t_{st} = 10 mm
- Height h_{st} = 90 mm
- Weld throat thickness a_{st} = 5 mm

Outputs

- Design resistance $M_{j,Rd}$= 105 kNm
- Load $M_{j,Ed}$ = 2/3 $M_{j,Rd}$ = 70 kNm
- Rotational deformation ϕ = 1,8 mrad
- Initial rotational stiffness $S_{j,ini}$ = 39,7 MNm/rad

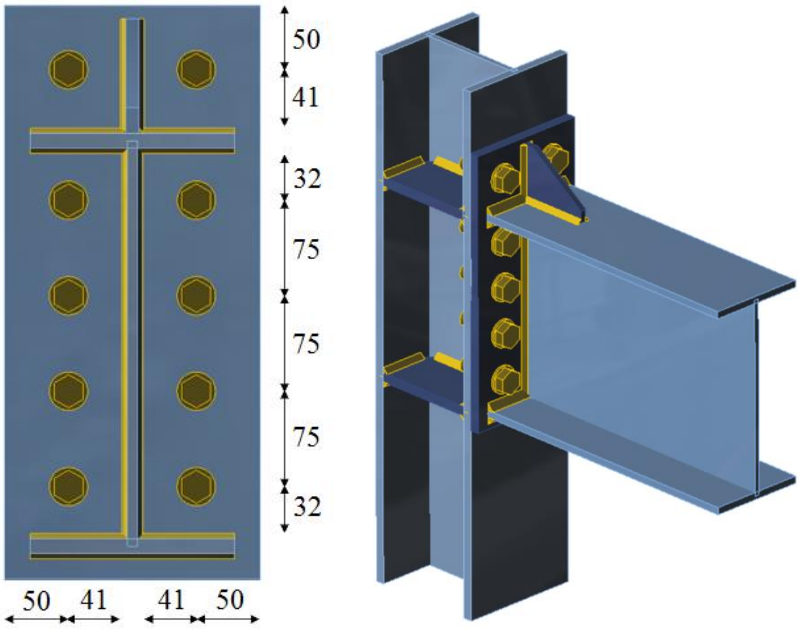

Fig. 10.2.3 Benchmark case for bolted eaves moment joint (IPE 330 to HEB 200)

10.3 Bending stiffness of column base

10.3.1 Description

The bending stiffness of the open and hollow section column base loaded by a combination of axial force and bending moment is studied. The design numerical model is validated to experiments presented at a paper by Bajer et al. (2014) and verified to the research numerical model in ATENA code and results of the component method.

10.3.2 Validation

Under project MERLION the column base of column HEB 240 was tested, with a concrete block of sizes $a' = 1000$ mm, $b' = 1500$ mm, $h = 400$ mm and concrete grade C20/25 with base plate $a = 330$ mm; $b = 440$ mm; $t = 20$ mm of steel grade S235, with cast-in anchor bolts 4 × M20, A_s = 245 mm² from grade 8.8, head diameter a = 60 mm, offset at top 50 mm and left −20 mm and grout thickness approximately 30 mm.

Fig. 10.3.1 Test set-up and deformed base plate and anchor bolts

Two specimens of this column base were tested at the laboratory in Brno University of Technology; see (Bajer et al. 2014). The experimental initial stiffness was 10 MNm/rad. The specimens did not exhibit any significant damage until load combination with axial force −400 kN and bending moment 180 kNm, which created rotation 0,04 rad. Then, concrete cracked with steel yielding of anchor bolts, base plate, and column. At the end of loading, the joint was still able to transfer bending moment 190 kNm up to rotation 0,15 rad.

ATENA software (Červenka et al. 2014) was used for a research model of the column base. The software includes a fracture-plastic material model for concrete, a material model with von Mises failure criterion for steel, and a Mohr-Coulomb criterion for the interfaces. The base plate is modeled by shell elements, and anchors are presented as reinforcement elements without a longitudinal bond. The anchors are fixed to the concrete at the location of the anchor heads. Supports by the concrete block are realized by springs. The model was validated using data from the experiment. It represents well the progress of cracking in the concrete block and deformation of steel parts. However, the idealization of the model brings a higher initial stiffness compared to the measured one.

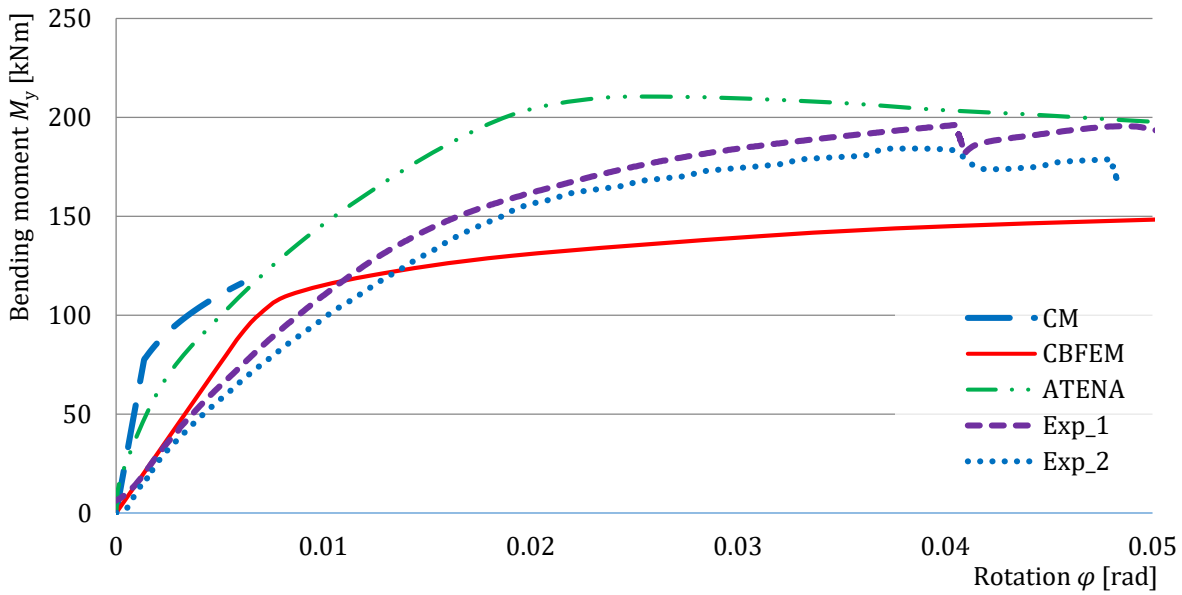

Fig. 10.3.2 Stiffness comparison of HEB 240 column base

The same column base was examined by the design-oriented model using CBFEM. For this comparison, all safety factors were set to 1 and anchor length for stiffness calculation to 12. The initial stiffness is also lower than 29 MNm/rad determined by CM. The concrete cone breakout failure according to EN 1992-4 should occur at load combination of axial force −400 kN and bending moment 100 kNm. Steel plates yield by more than 5 %, which is a recommended value by EN 1993-1-5:2006, at −400 kN and 153 kNm.

The comparison of moment-rotational diagrams predicted by design-oriented models, CM and CBFEM, and research-oriented model by ATENA code to the experimental results is in Fig. 10.3.2.

10.3.3 Verification

The verification is prepared for a base plate with geometry $a = 350$ mm; $b = 350$ mm; $t = 20$ mm from steel S420 under column SHS 150×16 with anchor bolts 4 × M20, steel grade 8.8, A_s = 245 mm², anchor head diameter a = 60 mm, grout thickness 30 mm, concrete block dimensions of $a' = 750$ mm, $b' = 750$ mm, $h = 800$ mm from concrete grade C20/25. The guiding component is mostly the concrete in compression including grout. An example of the calculation of this component resistance is shown below. The interaction diagram of this column base example is shown in Chapter 8.4.3. For stiffness calculation, an example of a load combination of compressive axial force −762 kN and bending moment 56 kNm is selected.

In CM, the weakest component is concrete cone breakout for two anchor bolts in tension, whose resistance is 67,2 kN. The stiffness coefficients of components are summarized in Tab. 10.3.1. The initial stiffness is 29 MNm/rad.

Tab. 10.3.1 Stiffness coefficients of components

Component	Stiffness coefficient
Concrete in compression (including grout)	k_{13} = 15 mm
Base plate in bending under tension	k_{15} = 11 mm
Anchor bolts in tension	k_{16} = 2 mm

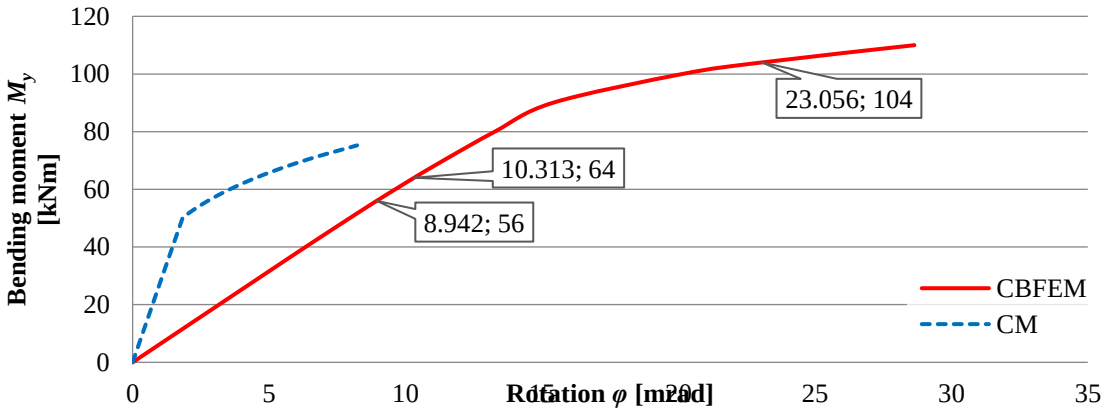

Fig. 10.3.3 Stiffness comparison of SHS 150×16 column base

In CBFEM, the weakest component is also a brittle component, the concrete cone breakout, which gives the bending moment resistance 56 kNm. The program informs the user also about virtual next failure modes, which are concrete bearing failure at 64 kNm, then anchor bolts rupture at 104 kNm and, at the same load, 5% limit plastic strain is reached. The initial stiffness is 6,3 MNm/rad. The results of the prediction by CM and CBFEM are compared in Fig. 10.3.3.

10.3.4 Benchmark case

Input

Cross-section

- SHS 150×16
- Steel S420

Base plate:

- Thickness 20 mm
- Offsets top 100 mm, left 100 mm
- Full penetration butt welds
- Steel S420

Anchors

- Type M20 8.8
- Anchoring length 300 mm
- Offsets top layers 50 mm, left layers −20 mm
- Shear plane in thread

Foundation block

- Concrete C20/25
- Offset 200 mm
- Depth 800 mm
- Shear force transfer friction
- Mortar joint thickness 30 mm

Loading

- Axial force N = −756 kN
- Bending moment M_y = 56 kNm

Output

Utilization

- Plates $\varepsilon = 0{,}2$ %
- Anchors 97,8 % ($N_{\mathrm{Ed}} = 65{,}7$ kN $\leq N_{\mathrm{Rd,c}} = 67{,}2$ kN – Concrete cone breakout for A1 and A2)
- Concrete block 91,5 % ($\sigma = 24{,}5$ MPa $\leq f_{\mathrm{jd}} = 26{,}8$ MPa)

Stiffness

- Rotational deformation 8,942 mrad
- Secant rotational stiffness 6,262 MNm/rad

11 PREDICTION OF DEFORMATION CAPACITY

11.1 Deformation capacity of welded joint of open sections

11.1.1 Description

The prediction of deformation capacity is described on a welded eaves moment joint, see Fig. 11.1.1. An unstiffened welded joint of open section column HEB 300 and beam HEB 260 is studied, and the joint behavior is described by a moment-rotation diagram. The results of component method (CM) are compared with component-based finite element method (CBFEM), and a benchmark case is prepared.

11.1.2 Analytical model

According to EN 1993-1-8:2005, Cl. 6.4.3, an unstiffened welded eaves moment joint may be assumed to have a rotation capacity at least 0,015 radians.

An example of an eaves moment joint is studied. An open section beam HEB 260 is welded to a column HEB 300. Welds with a throat thickness of 11 mm are used to connect beam flanges to column flange and of 6 mm to connect the beam web. The material of the beam and column is S235. The design resistance is limited by the component column web in compression and column web in tension.

11.1.3 Numerical model

Detailed information about the prediction of deformation capacity in CBFEM may be found in chapter 3.13. The eaves moment joint is modeled, and the limit plastic strain is set to 15 % to obtain the deformation capacity of the joint at an accidental location. The calculated rotations and stiffness are summarised in Tab. 11.1.1.

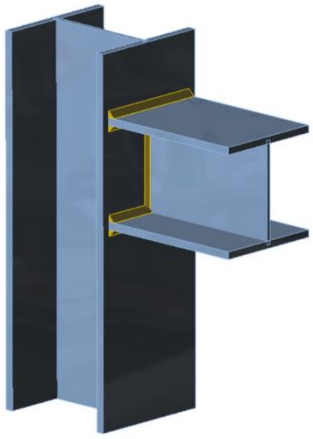

Fig. 11.1.1 Benchmark case for welded eaves moment joint (HEB 260 to HEB 300)

Tab. 11.1.1 Results of CBFEM

	Bending moment $M_{j,Ed}$	Secant stiffness S_j	Rotation φ
CBFEM	[kNm]	[MNm/rad]	[mrad]
	0	0	0,0
	84	32,5	2,6
	100	24,1	4,1
ε = 5%	126	5,0	25,1
ε = 15%	135	2,0	68,6

11.1.4 Verification

A comparison of the global behavior of a welded eaves moment joint described by a moment-rotation diagram is prepared. The joint is analyzed, and the rotation of the connected beam is calculated. The main characteristic is the rotation capacity calculated by limit plastic strain ε = 15 %. The joint design resistance by ε = 5 % is marked as $M_{j,Rd}$, while $M_{c,Rd}$ stands for a design moment resistance of the analyzed beam. The moment-rotation diagram is shown in Fig. 11.1.2.

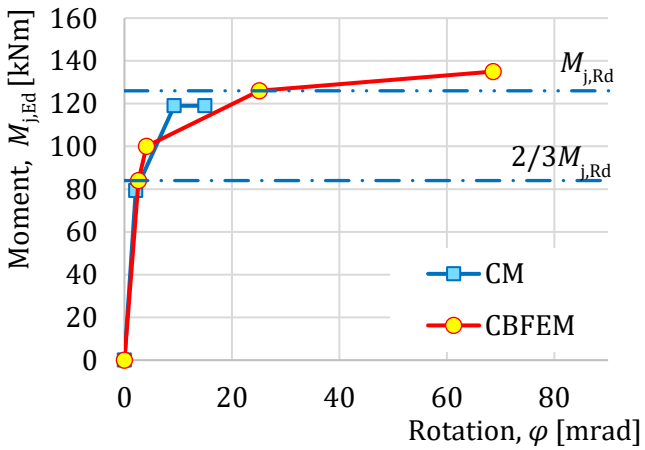

Fig. 11.1.2 Moment-rotation diagram for a welded eaves moment joint

The resistance of welds connecting the analyzed beam to the column is verified to avoid brittle fracture. The plastic strain in welds is limited to 5 %, while the plastic strain of 15 % in plates is allowed. The limit plastic strain 15 % is reached in the component column web in compression, as is shown in Fig. 11.1.3. The weld design resistance is not reached. The equivalent design stress in the design throat verification plane $f_{w.Ed}$ = 355,5 MPa ≤ f_u / β_w γ_{M2} = 360,0 MPa.

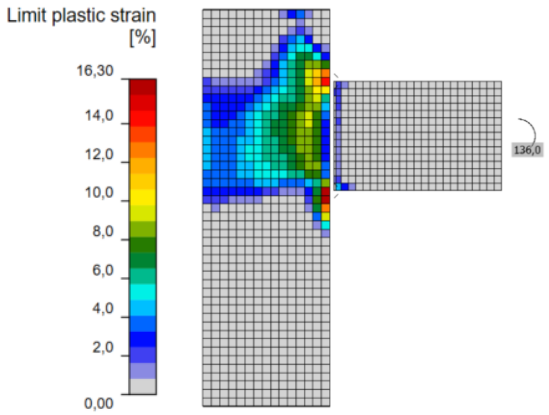

Fig. 11.1.3 Strains in eaves moment joint with yield strength f_y = 235 MPa

11.1.5 Capacity design check

In capacity design checks, the possibility that the actual yield strength of steel is higher than the nominal yield strength is taken into account by material overstrength factor γ_{ov} = 1,25. The influence of not guaranteed values of yield strength on the ductility of connections is shown in Fig. 11.1.4. The rotation capacity is calculated for the enlarged yield stress $f_{y,max} = \gamma_{ov} f_y$, and the weld design resistance is checked. The equivalent design stress in the design throat verification plane $f_{w.Ed}$ = 357,0 MPa ≤ f_u / β_w γ_{M2} = 360,0 MPa confirms the adequate weld resistance.

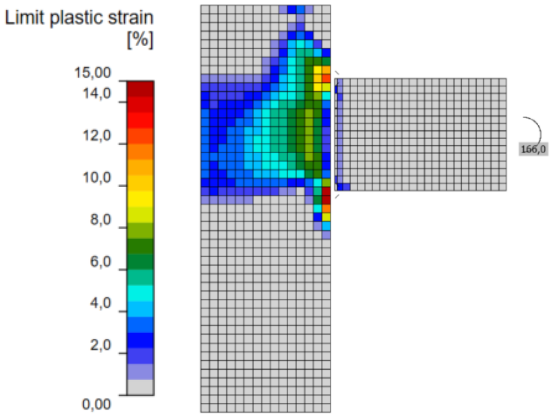

Fig. 11.1.4 Strains in the eaves moment joint with yield strength f_y = 1,25 · 235 = 293 MPa

If the connection is located in a dissipative zone, its design should conform to the upper value of the yield strength of steel $f_{y,max}$ = 1,1 γ_{ov} f_y; see EN 1998-1:2004. The rotation capacity is calculated, and the weld resistance is assessed, as is shown in Fig. 11.1.5. The equivalent design stress in the design throat verification plane $f_{w.Ed}$ = 359,8 MPa ≤ f_u / β_w γ_{M2} = 360,0 MPa confirms in this case the adequate weld resistance. The influence of the increased yield strength of steel on the rotation capacity is shown in Fig. 11.1.6.

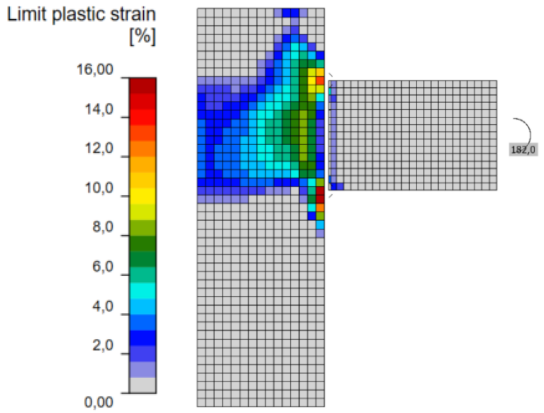

Fig. 11.1.5 Strains in the eaves moment joint with yield strength f_y = 1,25 · 1,1 · 235 = 323 MPa

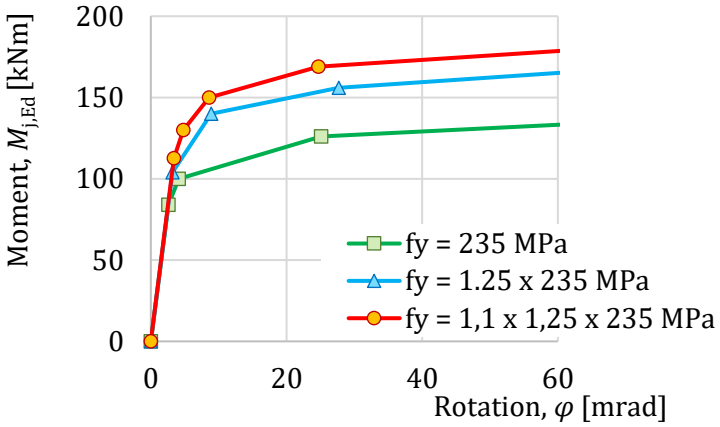

Fig. 11.1.6 Moment-rotational diagram for eaves moment joint
for changed yield strengths of steel

11.1.6 Verification of deformation capacity

The rotational capacity φ_{Cd} = 139,1 mrad calculated by CBFEM is larger than the minimal guaranteed value φ_{Cd} = 15 mrad in EN 1993-1-8:2005. The conservative prediction in standard is confirmed. It is expected that the deformation capacity in unstiffened eaves moment joint is larger than the prediction assumed in the standard.

11.1.7 Benchmark example

Inputs

Beam and column, see Fig. 11.1.1,

- Steel S235
- Column HEB 300
- Beam HEB 260
- Double fillet welds
- Flange weld throat thickness a_f = 11 mm
- Web weld throat thickness a_w = 6 mm

Outputs

- Design resistance by limit plastic strain ε = 15% is $M_{j,Rd}$ = 136 kNm
- Rotational capacity φ_{Cd} = 139,1 mrad

11.2 Deformation capacity of bolted joint of open sections

11.2.1 Description

The prediction of deformation capacity is verified on a bolted eaves moment joint. An unstiffened bolted joint of open section column HEB 300 and beam HEB 260 is studied, and the joint behavior is presented on a moment-rotation diagram. The results of the component-based finite element method (CBFEM) are compared with component method (CM). A benchmark case is prepared.

11.2.2 Analytical model

According to EN 1993-1-8:2005, Cl. 6.4.2, the bolted eaves moment joint may be assumed to have adequate rotation capacity if the design moment resistance of the joint is governed by the column web panel in shear with $d/t_w \leq 69\varepsilon$.

An open section beam IPE 330 is connected with bolted end-plate to a column HEB 200 in the example. The end plate thickness is 15 mm, the bolt type is M27 10.9, and the assembly is shown in Fig. 11.2.1. The stiffeners are inside the column opposite to beam flanges with a thickness of 15 mm. Beam flanges are connected to the end plate with a weld throat thickness of 12 mm. The beam web is connected with a weld throat thickness of 6 mm. Plastic stress distribution is assumed in welds. The material of the beam, column, and end plate is S235. The design resistance is limited by the component column web panel in shear.

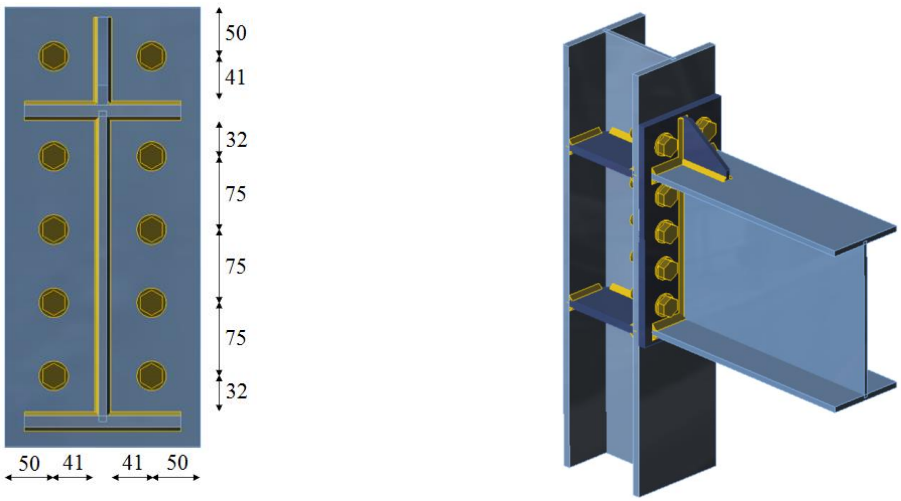

Fig. 11.2.1 Benchmark case for bolted eaves moment joint (IPE 330 to HEB 200)

11.2.3 Numerical model

Detailed information about the prediction of deformation capacity in CBFEM may be found in chapter 3.10. The eaves moment joint is modeled, and the limit plastic strain is set to 15 %

to obtain the deformation capacity of the joint. The results of the calculated rotations and stiffness are summarised in Tab. 11.2.1.

Tab. 11.2.1 Results of CBFEM

	Bending moment $M_{j,Ed}$	Secant stiffness S_j	Rotation φ
CBFEM	[kNm]	[MNm/rad]	[mrad]
	0	0	0,0
	73	39,7	1,8
	90	13,6	6,6
ε = 5%	110	2,0	53,9
ε = 15%	120	0,6	205,3

11.2.4 Verification

A comparison of the global behavior of a bolted eaves moment joint described by a moment-rotation diagram is prepared. The joint is analyzed, and the rotation of the connected beam is calculated. The main characteristic is the rotation capacity calculated by limit plastic strain ε = 15 %. The joint design resistance by ε = 5 % is marked as $M_{j,Rd}$, while $M_{c,Rd}$ stands for a design moment resistance of the analyzed beam. The moment-rotation diagram is shown in Fig. 11.2.2.

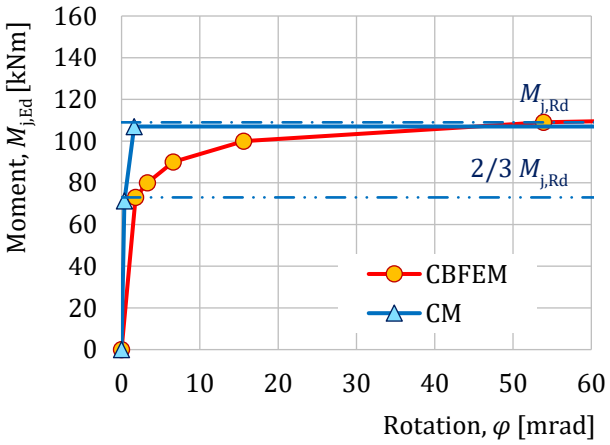

Fig. 11.2.2 Moment-rotation diagram for a bolted eaves moment joint

The resistances of bolts connecting the analyzed beam to the column are verified to avoid brittle fracture. The plastic strain in bolts is limited to ¼ of their guaranteed elongation, while the plastic strain of 15 % in plates is allowed. The limit plastic strain 15 % is reached in the component column web panel in shear, as is shown in Fig. 11.2.3. The tension resistance of bolts is not reached. The tension force in first bolt row $F_{t,1}$ = 316,0 kN ≤ $F_{t,Rd}$ = 330,5 kN.

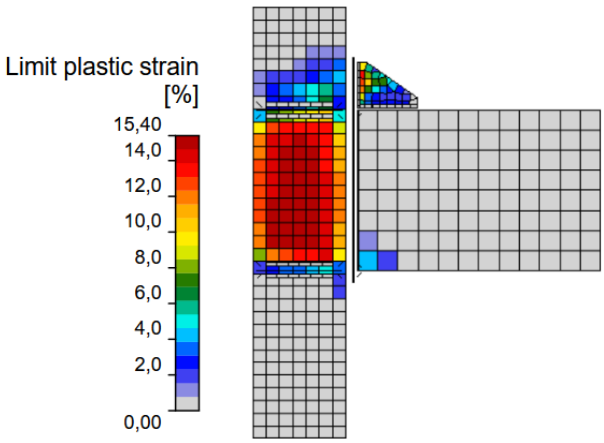

Fig. 11.2.3 Strains in eaves moment joint with yield strength f_y = 235 MPa

11.2.5 Capacity design check

In capacity design checks, the possibility that the actual yield strength of steel is higher than the nominal yield strength is taken into account by material overstrength factor γ_{ov} = 1,25. The influence of not guaranteed values of yield strength on the ductility of connections is shown in Fig. 11.2.4. The rotation capacity is calculated for enlarged yield stress $f_{y,max} = \gamma_{ov} f_{y,}$ and the bolt tension resistance is checked. The tension force in first bolt row $F_{t,1}$ = 322,7 kN ≤ $F_{t,Rd}$ = 330,5 kN confirms the adequate bolt resistance.

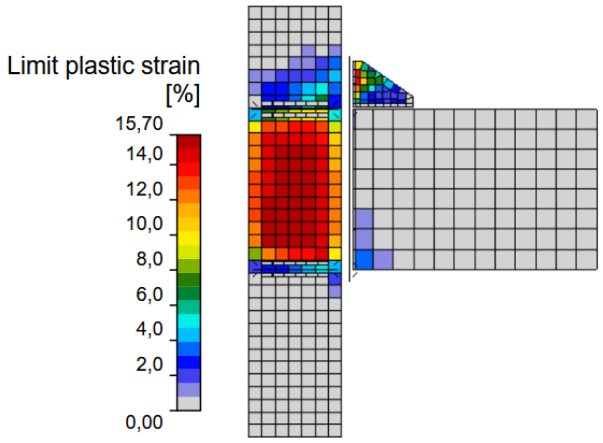

Fig. 11.2.4 Strains in the eaves moment joint with yield strength f_y = 1,25 · 235 = 293 MPa

If the connection is located in a dissipative zone, its design should conform to the upper value of the yield strength of steel $f_{y,max}$ = 1,1 γ_{ov} f_y; see EN 1998-1:2004. The rotation capacity is calculated, and the bolt resistances are assessed. The limit plastic strain 15 % is reached in the component column web panel in shear, as is shown in Fig. 11.2.5. The tension force in the first bolt row $F_{t,1}$ = 325,5 kN ≤ $F_{t,Rd}$ = 330,5 kN confirms the adequate tension bolt resistance in this case.

The influence of the increased yield strength of steel on the rotation capacity is shown in Fig. 11.2.6.

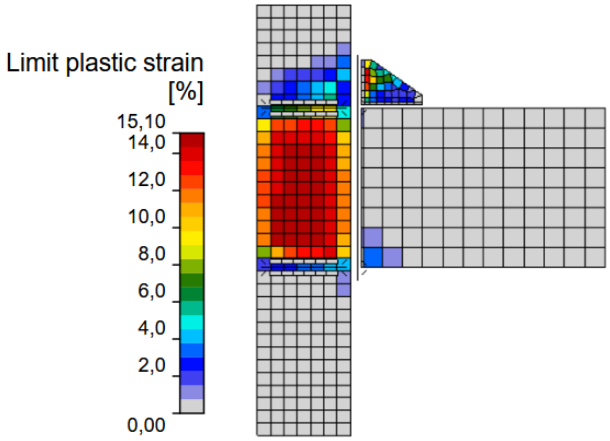

Fig. 11.2.5 Strains in the eaves moment joint with yield strength f_y = 1,25 · 1,1 · 235 = 323 MPa

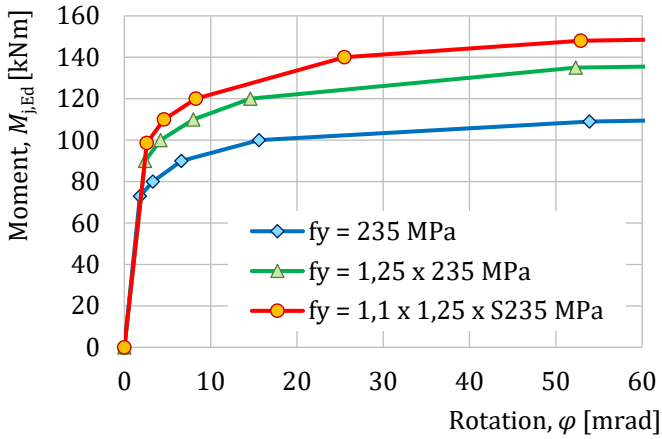

Fig. 11.2.6 Moment-rotation diagram for eaves moment joint for changed yield strengths of steel

11.2.6 Verification of deformation capacity

The rotational capacity φ_{Cd} = 233,4 mrad is calculated by CBFEM. The prediction in the standard is confirmed, and the joint has adequate rotational capacity. The design resistance is limited by column web panel in shear, while the tension resistances of bolts connecting the analyzed beam to the column are verified to avoid brittle fracture.

11.2.7 Benchmark example

Inputs

Beam and column

- Steel S235
- Column HEB 200
- Beam IPE 330
- Column offset s = 200 mm

Weld

- Flange weld throat thickness a_f = 12 mm
- Web weld throat thickness a_w = 6 mm

End-plate

- Thickness t_p = 15 mm
- Height h_p = 450 mm
- Width b_p = 200 mm
- Bolts M27 10.9
- Bolts assembly in Fig. 11.2.7

Column stiffeners

- Thickness t_s = 15 mm
- Width b_s = 95 mm
- Related to beam flange, position upper and lower
- Weld throat thickness a_s = 12 mm

End-plate stiffener

- Thickness t_{st} = 10 mm
- Height h_{st} = 90 mm
- Weld throat thickness a_{st} = 7 mm

Outputs

- Design resistance by limit plastic strain ε = 15 % is $M_{j,Rd}$ = 120 kNm
- Rotational capacity φ_{Cd} = 205,3 mrad

12 PREQUALIFIED JOINTS FOR SEISMIC APPLICATIONS

12.1 EQUALJOINTS project

The European research project EQUALJOINTS provides prequalification criteria of steel joints for the next version of EN 1998-1. The research activity covered the standardization of design and manufacturing procedures for a set of bolted joint types and a welded reduced beam section with heavy profiles designed to meet different performance levels. There was also the development of a new loading protocol for European prequalification, representative of European seismic demand. The experimental campaign devoted to the cyclic characterization of both European mild carbon steel and high strength bolts achieved the required behavior for four types of pre-qualified joints: haunched bolted joints, unstiffened extended end plate bolted joints, stiffened extended end plate bolted joints, and welded reduced beam section joints; see Fig. 12.1.1. The results experimentally reached within the EQUALJOINJTS project are summarised in (Stratan et al. 2017) and (Tartaglia and D'Aniello, 2017).

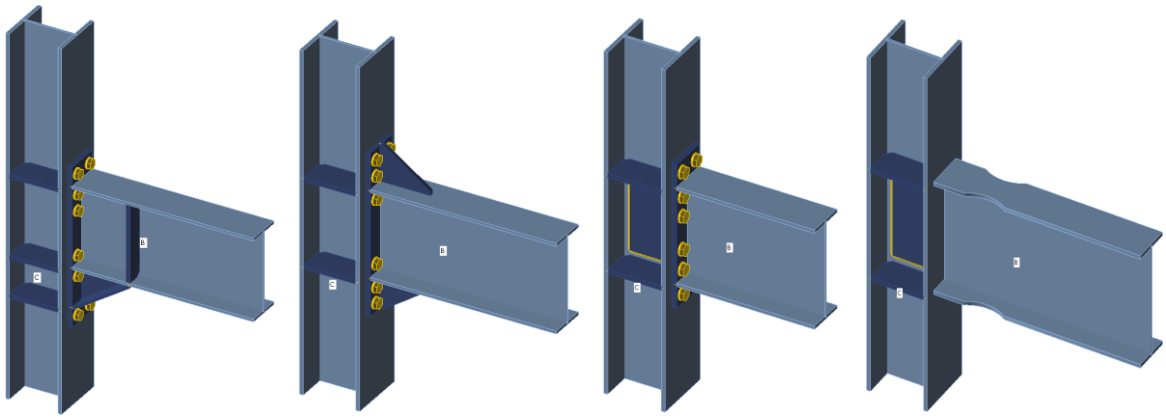

Fig. 12.1.1 Structural joints prequalified in EQUALJOINTS project

12.2 End plate joints

The extended stiffened end plate bolted connections are most common among European steel fabricating industries and are widely used in European practice as moment-resistant joints in low and medium-rise steel frames thanks to the simplicity and the economy of fabrication and erection. The design criteria and related requirements for bolted extended stiffened end plate beam-to-column joints are deeply investigated and critically discussed and currently codified in EN 1998-1:2005 based on a parametric study based on finite element analyses. Unfortunately, capacity design procedure was developed only in the framework of component method. It also accounts for the presence of ribs and is able to control the joint response for different performance levels.

Unstiffened extended end plate joints are commonly used in steel construction to connect steel I or H beam to steel I or H column in the case where significant bending moments have to be transferred. This configuration allows an easy erection by bolting while welding the end plate to the beam is automated in shop. The bending resistance of the connection is mostly lower than the bending resistance of the connected members. Therefore, such joints are considered as partial strength. Reaching an equal strength situation, in which the plastic resistance of the joint is roughly equal to the plastic resistance of the beam section, may be achieved through appropriate design. Their ductility in bending depends highly on the detailing of the joints, which influences the failure mode (Jaspart, 1997). If the joint component governing the failure is a ductile one, and if the resistance of the brittle active components is significantly higher, a ductile joint response may be reached. In the opposite case, no reliance should be made on the capacity of the joint to form plastic hinges and redistribute internal forces to absorb energy in a seismic area.

For the welded reduced beam section moment resisting connections, also referred to as dog-bone, two main strategies were adopted by strengthening the connection or weakening the beam. Among these two options for the profile of section reduction, the radius cut tends to exhibit a relatively more ductile behavior, delaying the ultimate fracture (Jones et al. 2002). However, the work showed that reduced beam section members are more prone to lateral-torsional buckling due to the decreased area of their flanges. Further experimental and analytical research focusing on the application of deep columns (Zhang and Ricles, 2006) indicated that the presence of a composite floor slab may greatly reduce the amount of twisting developing in the column, as it offers bracing to the beam and reduces the lateral displacement of the bottom flange.

According to the design procedure developed within the project EQUALJOINTS, the joint comprises three macro-components: the column web panel, the connection zone, and the beam zone; see Fig. 12.2.1. Each macro-component is individually designed according to specific assumptions, and then capacity design criteria are applied in order to obtain three different design

objectives defined to assess the joint: full strength, equal strength, and partial strength joints. Full strength joints are designed to guarantee the formation of all plastic deformations into the beam, which is consistent with EN 1998-1:2005 strong column – weak beam capacity design rules. Equal strength joints are theoretically characterized by the contemporary yielding of all macro-components, i.e. connection, web panel, and beam. Partial strength joints are designed to develop the plastic deformation only in the connection or column web panel. According to the resistance of the connection and column web panel macro-components for both equal and partial strength joints, an additional classification can be introduced. For strong web panel, the plastic demand is concentrated in the connection for partial strength joint or in the connection and in the beam for equal strength joint. In balanced web panel, the plastic demand is distributed between the connection and the column web panel for partial strength joint and in the connection, web panel, and the beam for equal strength joint. For weak web panel, the plastic demand is concentrated in the column web panel for partial strength joint or in the web panel and in the beam for equal strength joint.

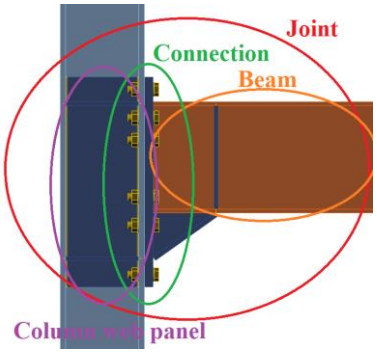

Fig. 12.2.1 Division of joint into macro components

The joint ductility depends on the type of failure mode and the corresponding plastic deformation capacity of the activated component. Deformation capacity may be roughly predicted by satisfying the developed criteria for CM or more precisely calculated by CBFEM. The examples of design of two prequalified joint configurations described in EQUALJOINJTS project materials and in ANSI/AISC358-16 standard are presented below considering the behavior of macro components separately.

12.2.2 Validation

The CBFEM models of rigidity, load-bearing capacity, and deformation capacity of pre-qualified joints were validated by Montenegro (2017) on a set of experiments available from EQUALJOINT project. The examples of structural solutions are in Fig. 12.2.2. The results of validation of the failure mode are shown in Fig. 12.2.3. The summary of validation of resistance and deformation capacity for 15 % strain are shown in Figs 12.2.4 and 12.2.5.

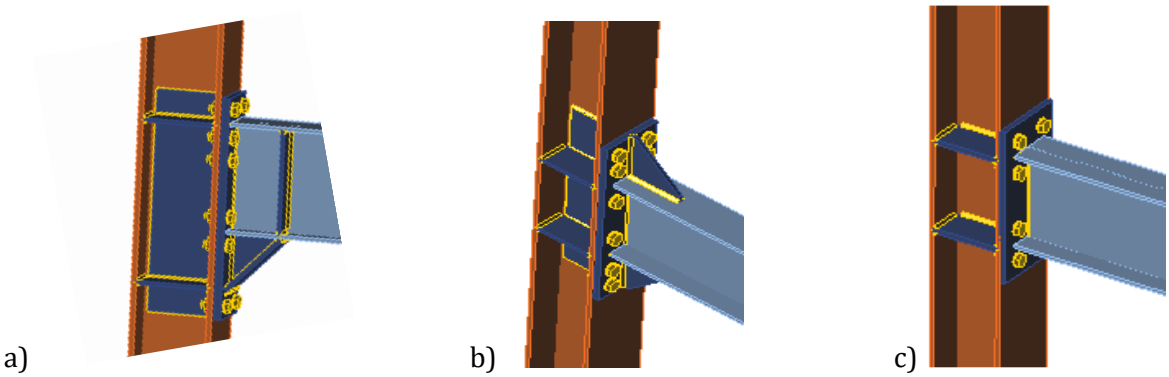

Fig 12.2.2 Joints used for validation and verification a) EH2- TS-35-M and EH2-TS-45-M, b) ES1-TS-F-M and ES3-TS-F-M, c) E1-TS-E-M and E2-TS-E-M

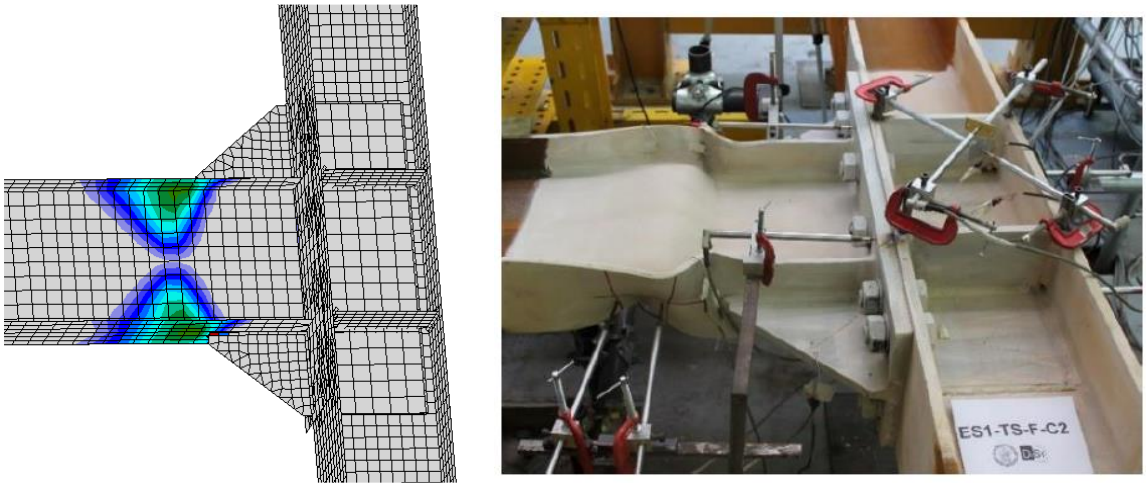

Fig. 12.2.3 Validation of failure mode of CBFEM on the extended end plate joints with haunch E1-TS-F-C2 (Tartaglia and D'Aniello, 2017)

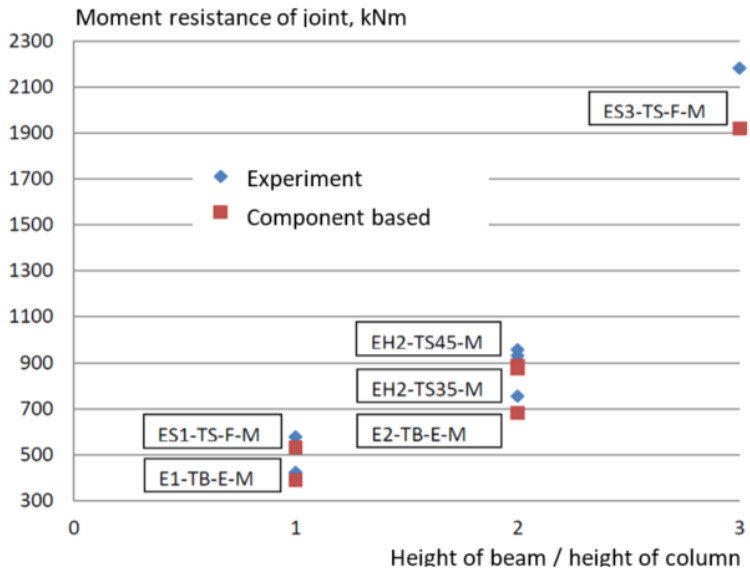

Fig.12.2.4 Validation of resistance of CBFEM on experiments from EQUALJOINTS project

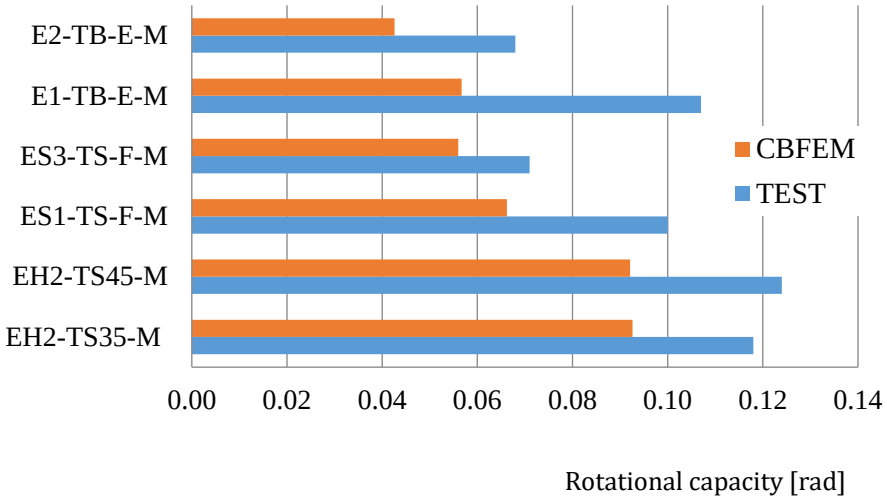

Fig. 12.2.5 Validation of rotational capacity of CBFEM on experiments from EQUALJOINTS project

12.2.3 Verification

The CBFEM model was verified to CM according to Ch. 6 in EN 1993-1-8:2006. The selection of results is presented in Tab.12.2.1 and Fig 12.2.6. The results show the loss of accuracy of CM for larger joints, where the rough assumption of lever arm is guiding the accuracy.

Tab. 12.2.1 Verification of CBFEM to CM

Typology #	Resistance			
	CM M_R [kNm]	CBFEM M_R [kNm]	CBFEM/CM%	Decisive component
Haunched joint				
EH2-TS35-M	901,2	889	1	Endplate in bending
EH2-TS45-M	959,3	875	10	Endplate in bending
4.2	876,1	1 016	−16	Column flange in bending
264	545,4	573	−5	Column flange in bending
267	1 998,9	2 100	−5	Endplate in bending
Extended stiffened joint				
ES1-TS-F-M	547,5	533	3	Column flange in bending
ES3-TS-F-M	1389	1 920	−27	Column flange in bending
Extended unstiffened joint				
E1-TB-E-M	347,8	389	−11	Endplate in bending
E2-TB-E-M	577,0	681	−15	Endplate in bending

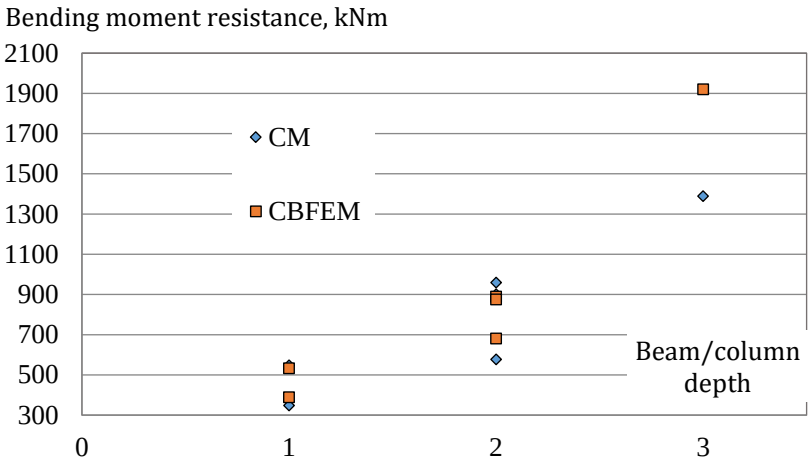

Fig. 12.2.6 Verification of resistance of CBFEM to CM

Three one-sided haunched joints are described in more detail in (Landolfo et al. 2017) and (Equaljoints application). The joints are loaded by both sagging and hogging bending moments and corresponding shear load. The column webs are reinforced by doublers, so the decisive components are T-stubs of either end plate or column flange. The axes of rotation are assumed at the center of the upper beam flange for sagging bending moment and in the middle of the haunch for hogging bending moment. The position of plastic hinge is assumed at the face of the stiffening plate at the end of the haunch. The bending moment at the column face used for check of the connection is increased by the corresponding shear load; see Fig. 12.2.7.

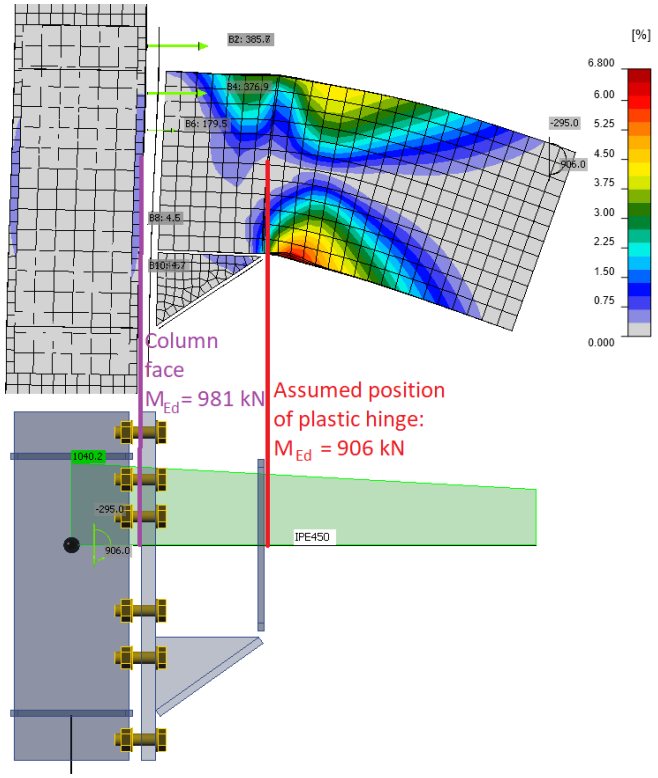

Fig. 12.2.7 Position of plastic hinge, course of bending moment in the haunched joint

Tab. 12.2.2 Resistance of components by CM for haunched joints

Resistance of components by CM	#4.2 (IPE450 to HEB340)	#264 (IPE360 to HEB280)	#267 (IPE600 to HEB500)
Moment at plastic hinge [kNm]	906	543	1869
Shear load [kN]	295	148	561
Moment at column face [kNm]	981	573	2105
Haunch resistance [kNm]	**956**	**582**	**1903**
Shear acting on column web [kN]	1581	1035	2447
Column web in shear resistance [kN]	**1632**	**1203**	**2774**
T-stub - end plate - hogging moment [kNm]	**1019**	**573**	**1999**
T-stub - end plate - sagging moment [kNm]	**1081**	**697**	**2318**
T-stub - column flange - hogging moment [kNm]	**876**	**545**	**2015**
T-stub - column flange - sagging moment [kNm]	**929**	**580**	**2107**

The strain-hardening factor was chosen 1,2 as suggested by EN 1993-1-8:2006 and Equaljoints project final report (EN 1998-1:2005 suggests value 1,1). Overstrength factor was assumed 1,25 (Landolfo et al. 2017). All steel was grade S355. The resistances of individual components are summarized in Tab. 12.2.2. Green colour is used for passing checks, red colour for failed checks. Note that haunch resistance is the plastic resistance of the beam section with the haunch at end plate. The strength of the beam is assumed increased by overstrength factor at the location of plastic hinge but not at the end plate. If the overstrength factor was used at the end plate as well, this resistance would be higher. Therefore, the next lowest resistance, the T-stub – end plate, was assumed to govern the joint resistance of joint No. 267. None of the investigated joints meets the requirement for full-strength joint. However, the resistance is very close, and the joints are equal-strength. The column web panel is in all cases strong.

The governing failure mode by CBFEM is failure of bolts with yielding of plates, mainly end plate, column flange, and haunch. According to CBFEM, joints No. 4.2 and No. 264 are full-strength and joint No. 267 equal-strength. Column web panels are strong in all cases.

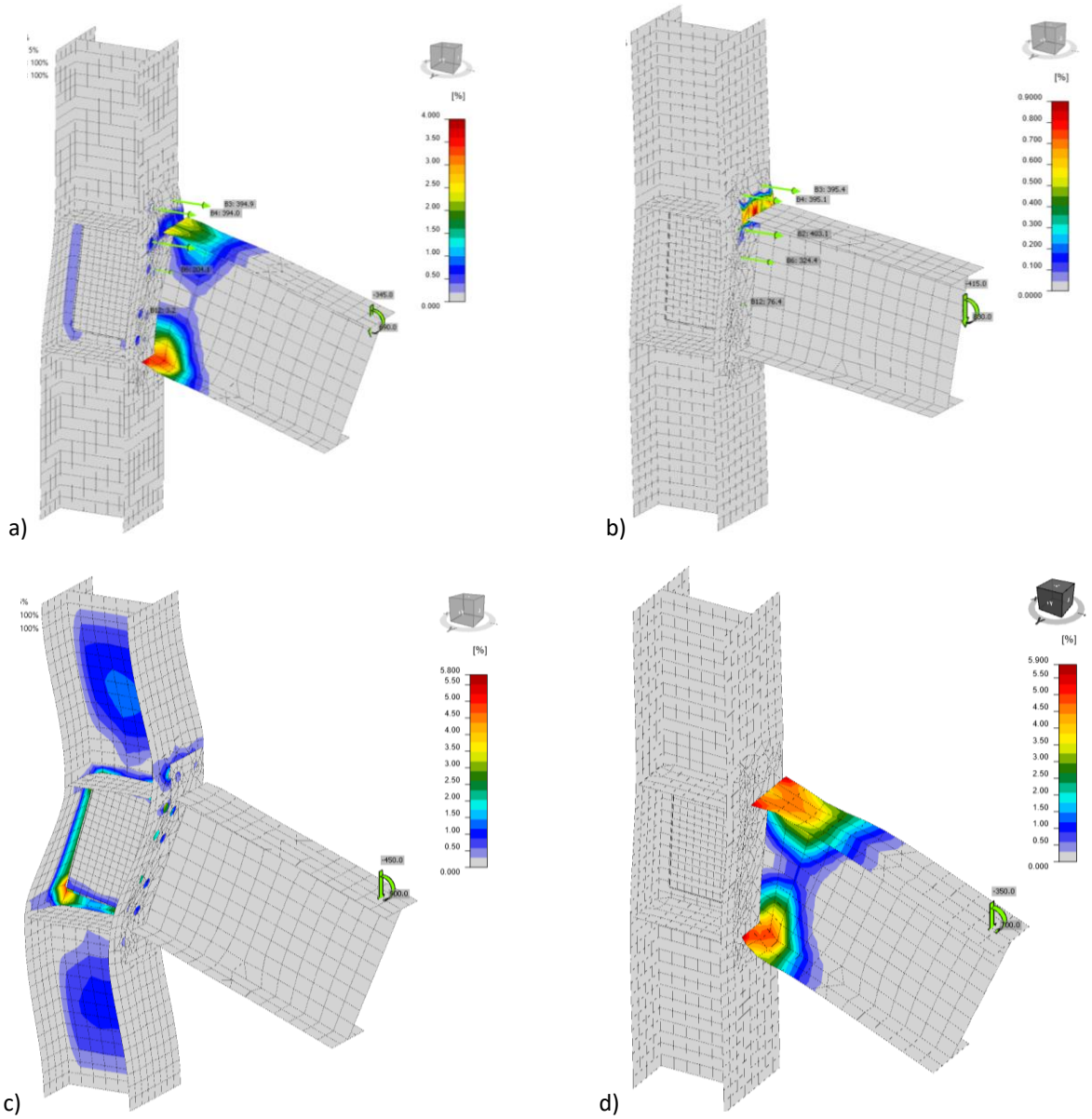

Fig. 12.2.8 The strains at resistance for a) the whole joint,
b) the macro-component bolted end-plate connection only c) the macro-component column web panel in shear with web doublers only, d) the macro-component beam only

12.2.4 Unstiffened extended end-plate joints

For sensitivity study, a prequalified unstiffened extended end-plate joint was selected. The beam IPE 450 is connected to column HEB 300 by an extended end plate 25 mm thick with twelve M30 10.9 bolts, with and without web doubler 10 mm thick. Steel grade S 355 was used for all plates. To determine the contribution of each macro component separately, the material diagram of the selected macro component was elastoplastic, while the rest of the joint was with only elastic material diagram. The strains at the resistance of the whole joint, the column web panel in shear with web doublers only, and the bolted end-plate connection only are compared to the beam macro-component only in Fig. 12.2.8. The influence of each macro-component on the behavior of

the joint is presented in Fig. 12.2.9, where column web panel with and without web doublers is shown. The joint behavior shows higher resistance of the connection macro-component.

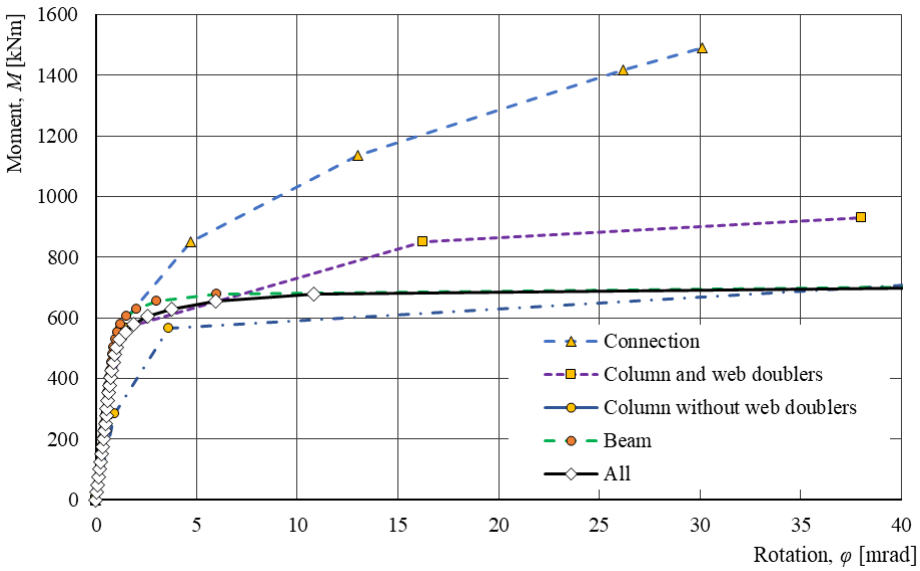

Fig. 12.2.9 Influence of macro-components, the column web panel with doublers in shear, the bolted end-plate connection and beam to the behavior of the whole joint

12.2.5 Location of compression center

For end-plate joints, EN 1993-1-8:2006 specifies that the compression center is located in the middle of the thickness of beam flange, or at the tip of the haunch in case of haunched joints. Experimental and numerical results showed that the location of compression center depends on both the joint type and the rotation demand due to the formation of plastic modes with different engagement of each joint component (Landolfo et al. 2017). According to the proposed CM design procedure and based on both experimental and numerical results, contact at about the centroid of the section made by the beam flange and the rib stiffeners is expected, for the stiffened endplate joints or at about 0,5 the haunch height in case of haunched joints. This rough assumption is précised by CBFEM procedure, which gives correct values during loading and initial yielding of parts of a joint.

The presented results show the good accuracy of CBFEM verified to ROFEM validated to EQUALIJOINTS experiments and CM. It brings the possibility to consider the behavior of macro-components separately and the position of neutral axes accurately according to the loading/plastification.

12.3 Welded reduced beam section joint

A prequalified welded reduced beam section joint according to ANSI/AISC 358-16 was selected for this study. The beam IPE 450 is connected to column HEB 300 by butt welds at flanges and fin plate 12 mm thick with three preloaded M30 10.9 bolts, with and without web doubler 10 mm thick; see Fig. 12.3.1. All used steel is grade S355.

The strains at the ultimate resistance of the whole joint and macro component column web panel in shear with web doublers only are shown in Fig. 12.3.2. The influence of each macro-component to the behavior of the joint is presented in Fig. 12.3.3, where column web panel with and without web doublers is shown. The joint shows that the resistances of the joint macro-components are well-optimized.

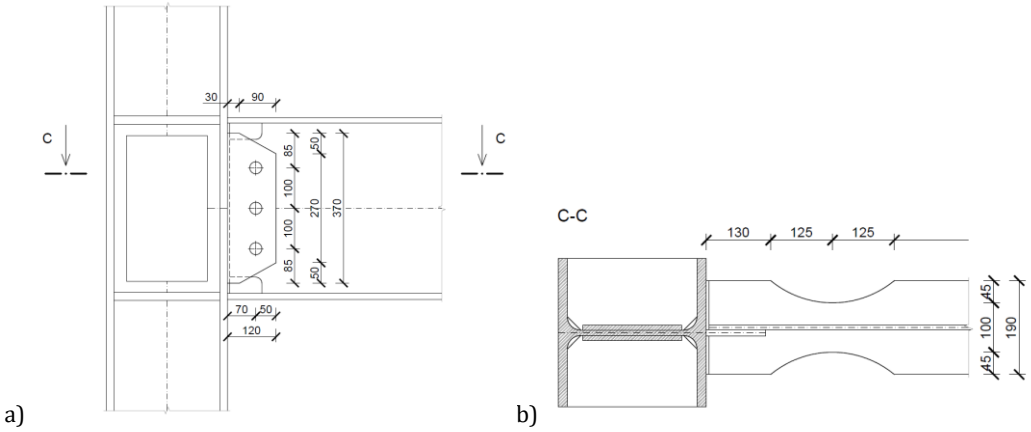

Fig. 12.3.1 Reduced beam section joint, a) beam with reduced section,
b) the column web panel with doublers in shear, the bolted end plate connection,

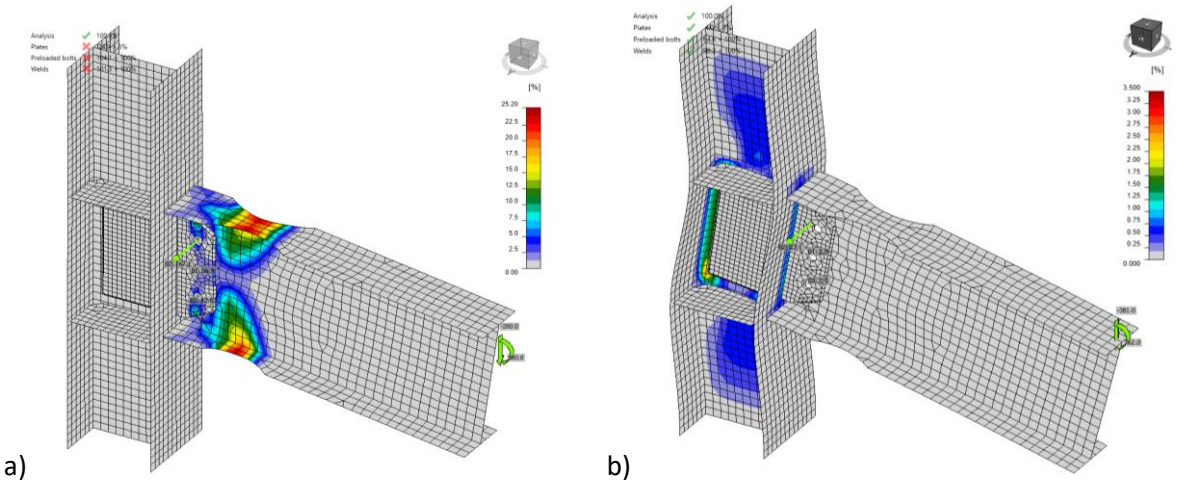

Fig. 12.3.2 The strains at resistance for
a) the whole joint and b) the macro component column web panel with doublers in shear only

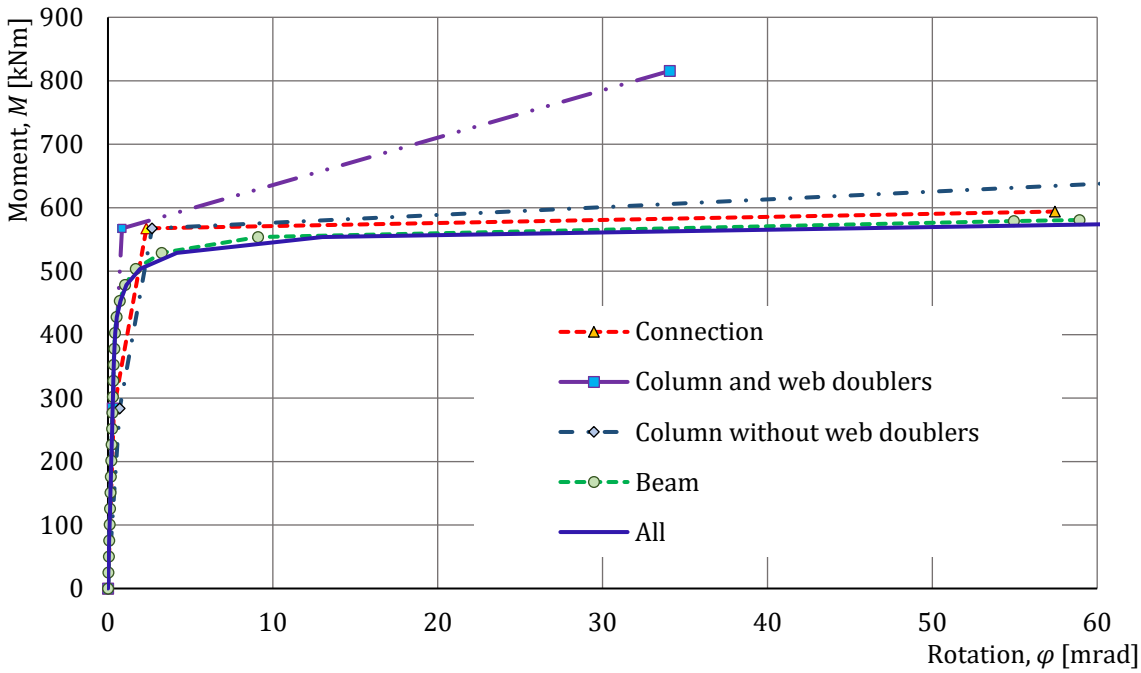

Fig. 12.3.3 Influence of macro-components on the behavior of the whole joint on *M*-*φ* diagram

REFERENCES

Agerskov H. High-strength bolted connections subject to prying, *Journal of Structural Division*, ASCE, 102 (1), 1976, 161-175.

AIAA. *Guide for the Verification and Validation of Computational Fluid Dynamics Simulations*, American Institute of Aeronautics and Astronautics, AIAA-G-077-1998, Reston, VA, 1998.

AISC 360-16:2016, *Specification for Structural Steel Buildings*, AISC, Chicago, 2016.

ANSI/AISC 358-16:2016, Prequalified Connections for Special and Intermediate Steel Moment Frames for Seismic Applications, AISC, Chicago, 2016.

ASME. *Guide for Verification and Validation in Computational Solid Mechanics*, The American Society of Mechanical Engineers, 2006, ISBN 079183042X.

Babuska I., Oden J.T. Verification and validation in computational engineering and science: Basic concepts, *Computer Methods in Applied Mechanics and Engineering,* 193 (36-38), 2004, 4057-4066.

Bajer M., Vild M., Barnat J., Holomek J. Influence of Selected Parameters on Design Optimisation of Anchor Joint, in *Steel, Space and Composite Structures,* Singapore, 2014,149–158.

Beg D., Zupančič E., Vayas I. On the rotation capacity of moment connections, *Journal of Constructional Steel Research*, 60 (3–5), 2004, 601–620.

Block F.M., Davison J.B., Burgess I.W., Plank R.J. Deformation-reversal in component-based connection elements for analysis of steel frames in fire, *Journal of Constructional Steel Research*, 86, 2013, 54-65.

Braun B. *Stability of steel plates under combined loading*, Institut für Konstruktion und Entwurf, Stuttgart, 2010.

Brito P. H., Rocha C.R., Filho F.C., Martins E., Rubira C.M.F. *A Method for Modeling and Testing Exceptions in Component-Based Software Development*, Dependable Computing, Lecture Notes in Computer Science, 3747, 2005, 61-79.

Bursi O.S., Jaspart J.P. Calibration of a Finite Element Model for Isolated Bolted End-Plate Steel Connections, *Journal of Constructional Steel Research,* 44, 3, 1997, 225-262.

Bursi O.S., Jaspart J.P. Benchmarks for finite element modelling of bolted steel connections, *Journal of Constructional Steel Research*, 43, 1-3, 1997, 17-42.

Červenka V., Jendele L., Červenka J. *ATENA Program Documentation Part 1: Theory*, Červenka Consulting s.r.o., http://www.cervenka.cz/downloads.

Chen, W.F., Abdalla K.M. Expanded database of semi-rigid steel connections, *Computers and Structures*, 56, (4), 1995, 553-564.

CSA S16-14:2016, *Steel Frame Design Manual*, Computers & Structures, Inc, 2016.

Da Silva L., Lima L., Vellasco P., Andrade S. *Experimental behaviour of end-plate beam-to-column joints under bending and axial force*, Database reporting and discussion of results, Report on ECCS-TC10 Meeting in Ljubljana, 2002.

Da Silva Simoes L. Towards a consistent design approach for steel joints under generalized loading, *Journal of Constructional Steel Research*, 64, 2008, 1059-1075.

Dlubal RFEM 5.0 - FEM Structural Analysis Software, Prague, https://www.dlubal.com/en

Driver, R.G., Grondin, Y.G., Kulak, G.L. *Unified block shear equation for achieving consistent reliability*, Department of Civil and Environmental Engineering, University of Alberta, 2005.

Dubina D., Iványi M. *Stability and Ductility of Steel Structures, SDSS'99*, 1st edition, Budapest, 1999.

Dvorkin E. N., Bathe K. J., Continue A. Mechanics Based Four Node Shell Element for General Nonlinear Analysis, *Engineering Computations*, 1, 1984.

EN 1998-1, Eurocode 8: *Design of structures for earthquake resistance* – Part 1: General rules, seismic actions and rules for buildings, Assessment and retrofitting of buildings. CEN, Brussels, 2006.

EN 1992-1-1, Eurocode 2, Design of concrete structures – Part 1-1: *General rules and rules for buildings,* CEN, Brussels, 2005.

EN 1992-4:2018, Eurocode 2: Design of concrete structures – Part 4: *Design of fastenings for use in concrete*, Brussels, 2018.

EN 1993-1-5, Eurocode 3, Design of steel structures – Part 1-5: *Plated Structural Elements*, CEN, Brussels, 2005.

EN 1993-1-8, Eurocode 3, Design of steel structures – Part 1-8: *Design of joints*, CEN, Brussels, 2005.

EN 1994-1-1, Eurocode 4, Design of composite steel and concrete structures – Part 1-1: *General rules and rules for buildings*, CEN, 2010.

EN 1998-1, Eurocode 8, Design of structures for earthquake resistance – Part 1: General rules, *Seismic actions and rules for buildings*, CEN, Brussels, 2004.

Equaljoints application, https://itunes.apple.com/us/app/equal-joints/id1406825195?mt=8

ETAG 001, *Guideline for European Technical Approval of Metal Anchors for Use in Concrete – Annex C: Design Methods for Anchorages,* Brussels, EOTA, 2010.

Faella C, Piluso V, Rizzano G., Plastic deformation capacity of bolted T-stubs: theoretical analysis and testing, in *Moment resistant connections of steel frames in seismic area, design and reliability*, E&FN Spoon, 2000.

Foley C.M., Vinnakota S. Toward design office moment–rotation curves for end-plate beam-to-column connections, *Journal of Constructional Steel Research*, 35, 1995, 217–53.

Gioncu V., Mazzolani F. *Ductility of seismic resistant steel structures*, Spon Press; 2002.

Girao A.M.C., Bijlaard F.S.K., da Silva L.S. Experimental assessment of the ductility of extended end plate connections, *Journal of Engineering Structures,* 26, 2004, 1185–1206.

Gödrich L., Wald F., Sokol Z. To Advanced modelling of end plate joints, *Connection and Joints in Steel and Composite Structures*, Rzeszow, 2013.

Gödrich L., Wald F., Kabeláč J., Kuříková M. Design finite element model of a bolted T-stub connection component, *Journal of Constructional Steel Research*. 2019, (157), 198-206.

Gödrich L., Kurejková M., Wald F., Sokol, Z. The bolts and compressed plates modelling, in *Steel, Space and Composite Structures*, Singapore, 2014, 215-224.

Gödrich L., Wald F., Sokol Z. Advanced modelling of end plate, in *Eurosteel 2014*, Brussels, ECCS, 2014, 287-288.

Grecea D., Stratan A., Ciutina A., Dubina D. Rotation capacity of the beam-to-column joints under cyclic loading, in *Connections in Steel Structures V*, Amsterdam, 2004.

Gresnight N., Romeijn A., Wald F., Steenhuis M. Column Bases in Shear and Normal Force, *HERON,* 53, 1/2, 2008, 87-108, ISSN 0046-7316.

Holdren J. P. *Increasing Access to the Results of Federally Funded Scientific Research, Memorandum for the Heads of Executive Departments and Agencies*, Office of Science and Technology Policy, Washington, D.C, 2013.

Huns, B.B.S, Grondin, G., Driver, R.G. *Block shear behaviour of bolted gusset plates*, University of Alberta, 2002.

Ibrahimbegovic A., Taylor R.L., Wilson E.L. A robust quadrilateral membrane element with drilling degrees of freedom, *International Journal for Numerical Methods in Engineering*, 30/3, 1990, 445-457.

IDEA StatiCa: *Product documentation*, www.ideastatica.com, 2020.

IIW XV-1439-13 ISO/FDIS 14346, *Static Design Procedure for Welded Hollow Section Joints – Recommendations*, ISO, 2012.

ISO 898-1, Mechanical properties of fasteners made of carbon steel and alloy steel, Part 1, *Bolts, screws and studs with specified, property classes*, Coarse thread and fine pitch thread, Geneva, 2009.

ISO, Guide to the Expression of Uncertainty in Measurement, ISO Geneva, 1993.

Jaspart J. P., Demonceau J. F., Weynand K., Müller C. Application of Eurocode 3 to steel connections with four bolts per horizontal row, SDSS'Rio 2010 *Stability and ductility of steel structures*, conference proceedings, Rio de Janeiro, 2010.

Jaspart J.P. Design of structural joints in building frames, *Prog. Struct. Engng Mater.*, 4, 2002, 18–34.

Jaspart J.P., Wald F., Weynand K., Gresnight N. Steel Column Base Classification, *Heron*, 2015, 53, 1/2, 69-86.

Jaspart J.P., Weynand K. Design of hollow section joints using the component method, *Tubular Structures XV,* 2015, 403-410.

Jaspart J.P. *Contributions to recent advances in the field of steel joints. Column bases and further configurations for beam-to-column joints and column bases.* These aggregation, University of Liege, Belgium, 1997.

Jetteur P., Cescotto S. A mixed finite element for the analysis of large inelastic strains, *International Journal for Numerical Methods in Engineering*, 31, 1991, 229-239.

Jones S.L., Fry GT., Engelhardt M.D. Experimental evaluation of cyclically loaded reduced beam section moment connections. *Journal of Structural Engineering.* 128 (4), 441–451, 2002.

Khoo X.E., Perera M., Albermani F. Design of eccentrically connected cleat plates in compression; In: *Advanced Steel Construction*; 2009, (6) 2. 678–687

Krishnamurthy N. *Analytical investigation of bolted stiffened tee stubs*, Report No. CE-MBMA-1902, Van-derbilt University, Nashville, 1978.

Krishnamurthy N. Fresh Look at Bolted End-Plate Behavior and Design, *Engineering Journal*, 15 (2), 1978, 39-49.

Kuhlmann U., Kuhnemund F. Rotation capacity of steel joints, *Verification Procedure and Component Tests*, 2000.

Kurejková M., Wald F., Kabeláč J., Šabatka L. Slender Compressed Plate in Component Based Finite Element Model, in *2nd International Conference on Innovative Materials, Structures and Technologies*, Riga, Latvia, 2015.

Kurejková M., Wald F. Compressed Stiffeners in Structural Connections, in *Eurosteel 2014*, Brussels, ECCS, 2014, 317-318.

Kuříková M., Wald F., Kabeláč J. Design of slender compressed plates in structural steel joints by component based finite element method, in *SDSS 2019: International Colloquium on Stability and Ductility of Steel Structures*, Prague, 2019.

Kwaśniewski L. Nonlinear dynamic simulations of progressive collapse for a multistorey

building, *Engineering Structures*, 32 (5), 2010, 1223-1235.

Kwaśniewski L. Numerical verification of post-critical Beck's column behavior, *International Journal of Non-Linear Mechanics,* 45 (3), 2010, 242-255.

Kwaśniewski L., Bojanowski, C. Principles of verification and validation, *Journal of Structural Fire Engineering*, 6, 1, 2015, 29-40.

Kwaśniewski L. On practical problems with verification and validation of computational models, *Archives of Civil Engineering*, 55, 3, 2009, 323-346

Landolfo R. et al. Design of Steel Structures for Buildings in Seismic Areas, ECCS Eurocode Design Manual. Wiley, 2017.

de Lima L.R.O., de F. Freire J.L., Vellasco P.C.G., de Andrade S.A.L., da Silva J.G.S. Structural assessment of minor axis steel joints using photoelasticity and finite elements, *Journal of Constructional Steel Research*, 65, 2009, 466-478.

Montenegro J.S. *Design of prequalified European beam-to-column connections for moment resistant frames with component based finite element method*, M.Sc. Theses, CTU in Prague, 2017.

NAFEMS, National Agency for Finite Element Methods, http://www.nafems.org/, 2013.

Neumann, N. Design model for combined in-plane and out-of-plane bending of steel joints connecting H or I sections, in *Eurosteel 2014*, Naples, 2014, 2050-2056.

Oberkampf W.L., Trucano T.G. Verification and validation benchmarks, *Nuclear Engineering and Design*, 238, 2008, 716–743.

prEN 1993-1-1:2019, Eurocode 3, Design of steel structures, Part 1-1, *General rules and rules for buildings*, CEN, Brussels, final draft, 2019.

prEN 1993-1-14:2020, Eurocode 3, Design of steel structures, Part 1-8, *Design assisted by finite element analysis*, CEN, Brussels, first draft, 2020.

prEN 1993-1-8:2020, Eurocode 3, Design of steel structures, Part 1-8, *Design of joints*, CEN, Brussels, sixth draft, 2020.

Roache P.J. Verification and validation in computational science and engineering, *Computing in Science Engineering*, Hermosa publishers, 1998, 8-9.

Šabatka L., Wald F., Kabeláč J., Kolaja D., Pospíšil M. Structural Analysis and Design of Steel Connections Using Component Based Finite Element Model, *Journal of Civil Engineering and Architecture*, 9 (9), 2015, 1-7. ,

Samaan R. A., El-Serwi A. A. I., El-Hadary R. A. Experimental and theoretical study of large capacity extended end-plate moment connection, *EUROSTEEL 2017*, conference proceedings, Copenhagen, 2017.

Sekal, D. *Analysis of Block Shear Failure*, diploma thesis, ČVUT, Prague, 2019.

Sherbourne A.N, Bahaari M.R. 3D simulation of bolted connections to unstiffened columns—II. Extended endplate connections, *Journal of Constructional Steel Research,* 40, 1996, 189–223.

Sherbourne A.N, Bahaari M.R. 3D simulation of end-plate bolted connections, *Journal of Structural Engineering,* 120, 1994, 3122–3136.

Sherbourne A.N., Bahaari M.R. Simulation of bolted connections to unstiffened columns T-stub connections, *Journal of Constructional Steel Research,* 40, 1996, 169–87.

SIMULIA, Abaqus 6.11, *Benchmarks Manual*, Dassault Systèmes, 2011.

Steenhuis M., Gresnigt N., Weynand K. Pre-Design of Semi-Rigid Joints in Steel Frames, in *Second state of the art workshop on semi-rigid behaviour of civil engineering structural connections*, COST C1, Prague, 1994, 131-140.

Steenhuis M., Jaspart J. P., Gomes F., Leino T. Application of the component method to steel joints, in *Control of the Semi-rigid Behaviour of Civil Engineering Structural Connections Conference*, COST C1, Liege, Belgium, 1998, 125-143.

Steenhuis M., Wald F., Sokol Z., Stark J.W.B. Concrete in Compression and Base Plate in Bending, *Heron*, 2008, 53, 1/2, 51-68.

Stratan A., Maris C, Dubina D, and Neagu C. *Experimental prequalification of bolted extended end plate beam to column connections with haunches.* ce/papers, 1(2–3), 414–423, 2017.

Stratan A., Maris C., Dubina D., Neagu C. Experimental prequalification of bolted extended end plate beam to column connections with haunches, Proceedings of Eurosteel 2017, 1 (2-3), 2017, 414-423.

Tartaglia R, D'Aniello M. Nonlinear performance of extended stiffened end-plate bolted beam-to-column joints subjected to column removal. *The Open Civil Engineering Journal* Vol 11, Issue Suppl-1, 369–383, 2017.

Topkaya C. A finite element parametric study on block shear failure of steel tension members, *Journal of Constructional Steel Research*, Ankara, 2004

VDI2230 *Systematic calculation of high duty bolted joints – Joints with one cylindrical bolt*, Association of German Engineers, Berlin, 2003.

Vesecký J., Cábová K., Jandera M., Tests of gusset plate connection under eccentric compression, in *SDSS 2019: International Colloquium on Stability and Ductility of Steel Structures*, Prague, 2019,

Vesecký J., Jandera M., Cábová K. Numerical modelling of gusset plate connections under eccentric compression, in *SDSS 2019: International Colloquium on Stability and Ductility of Steel Structures*, Prague, 2019.

Vesecký, J. *Buckling resistance of gusset plates*, diploma thesis, ČVUT, Prague, 2019.

Vild M., Kuříková M., Kabeláč J., Wald F. Design of gusset plate connection with single-sided splice member by component based finite element method, in *SDSS 2019: International Colloquium on Stability and Ductility of Steel Structures*, Prague, 2019.

Virdi K. S. et al. *Numerical Simulation of Semi Rigid Connections by the Finite Element Method*, Report of Working Group 6 Numerical, Simulation COST C1, Brussels Luxembourg, 1999.

Wald F., Burgess I., Kwasniewski L., Horová K, Caldová E. *Benchmark studies*, Experimental validation of numerical models in fire engineering, CTU Publishing House, 198 p., Prague, 2014.

Wald F., Burgess I., Kwasniewski L., Horová K., Caldová E. *Benchmark studies*, Verification of numerical models in fire engineering. CTU Publishing House, 328 p., Prague, 2014.

Wald F. *Column Bases*, CTU Publishing House, Prague, 1995.

Wald F., Gödrich L., Kurejková M., et al. Generally loaded connections by component based finite element method, in *Connections VIII*, Boston, May 24-26, 2016, 143-152.

Wald F., Gödrich L., Šabatka L., Kabeláč J., Navrátil J. Component Based Finite Element Model of Structural Connections, *in Steel, Space and Composite Structures*, Singapore, 2014, 337-344.

Wald F., Šabatka L., Bajer M., Barnat J., Gödrich L., Holomek J., Jehlička P., Kabeláč J. et al. *Benchmark cases for advanced design of structural steel connections*, Third extended edition, Prague, CTU, Czech Technical University Publishing House, 2019.

Wald F., Sokol Z., Moal M., Mazura V., Muzeau J. P. Stiffness of cover plate connections with slotted holes, in *Eurosteel 2002*, Coimbra, 2002, 1007-1016.

Wald F., Sokol Z., Steenhuis M., Jaspart, J.P. Component method for steel column bases, *Heron*, 53, 2008, 3-20.

Wald F., Sokol, Z., Jaspart J.P. Base plate in bending and anchor bolts in Tension, *Heron*, 2008, 53, 1/2, 21-50.

Wald F., Vild M., Kuříková M., Kabeláč J., Sekal D., Maier N. Finite-Element-Bemessung von Stahlverbindungen basierend auf der Komponentenmethode, *Stahlbau*, 5/2020, 482-495.

Wald F., Kurejková M., Gödrich L., Kočka M., Martínek K. Simple and advanced models for connection design in steel structures, in *International Conference on Advances in Civil and Environmental Engineering*, Universiti Teknologi Mara, 14-23, Pulau Pinang, 2015.

Wald F., Kwasniewski L. Gödrich L., Kurejková M. Validation and verification procedures for connection design in steel structures, in *Steel, Space and Composite Structures,* Singapore, 2014, 111-120.

Wald F., Šabatka L., Kabeláč J., Kolaja D., Pospíšil M. structural analysis and design of steel connections using component based finite element model (CBFEM), *Journal of Civil Engineering and Architecture*, 10, 2015.

Wald F., Šabatka L., Kabeláč J., Gödrich L., Kurejková M. Future design procedure for structural connections is component based finite element model, in *13th Nordic Steel Construction Conference (NSCC-2015)*, Tampere University of Technology, Tampere, 2015.

Wald, F.; Kabeláč J.; Kuříková M.; Perháč O., Ryjáček P., Minor García O., Flores Pazmino M. et al. Advanced procedures for design of bolted connections, In: *IOP Conference Series: Materials Science and Engineering*. Bristol: IOP Publishing Ltd., vol. 419, 2018.

Wang Z., Wang T. Experiment and finite element analysis for the end plate minor axis connection of semi-rigid steel frames, *Tumu Gongcheng Xuebao/China Civil Engineering Journal*, 45 (8), 2012, 83-89.

Wardenier J. *Hollow Sections Joints*, Delft University press, Delft, 1982.

Wardenier J., Packer J. A., Zhao X.-L., van der Vegte G. J. *Hollow Sections in Structural Applications*, CIDECT, Geneve, 2010.

Wu Z., Zhang S., Jiang S. Simulation of tensile bolts in finite element modelling of semi-rigid beam-to-column connections, *International Journal of Steel Structures* 12 (3), 2012, 339-350.

Zakouřil V. *End plate connection with four bolts in row,* Diploma thesis, ČVUT, Prague, 2019.

Zhang X., Ricles J.M. Experimental evaluation of reduced beam section connections to deep column*s. Journal of Structural Engineering*. 132 (3), 346-357, 2006.

Zoetemeijer P. *Bolted connections with flush end plates and haunched beams. tests and limit state design methods*, Report 6-81-15, Delft University of Technology, Stevin Laboratory, 1981.

Zoetemeijer P. *Summary of the researches on bolted beam-to-column connections*, Report 6-85-7, University of Technology, Delft 1985.

COMPONENT–BASED FINITE ELEMENT DESIGN OF STEEL CONNECTIONS

Wald F., Sabatka L., Bajer M.,
Jehlicka P., Kabelac J., Kozich M., Kurikova M., Vild M.

This publication introduces the Component-based Finite Element Method (CBFEM), which is a novel approach in the structural design of steel connections and joints. It allows engineers to analyze and assess generally loaded joints and connections with varying complexity of geometry. CBFEM is a synergy of the standard approach to connection design (component method) and finite elements. Implementation of the CBFEM for the structural steel design represents a qualitative leap for the whole structural engineering industry.

Following the CBFEM principles, this publication presents benchmark cases for its validation and verification for various structural steel joints and connections. The hierarchy of the system response quantity is prepared for welded and bolted connections as well as for column bases. Each benchmark case shows results from the analytical model according to design standards followed by references to laboratory experiments, validated models, and numerical experiments. Results from CBFEM calculations are thoroughly analyzed, taking into account the global behavior of the joint and verification of resistance.

Experiment

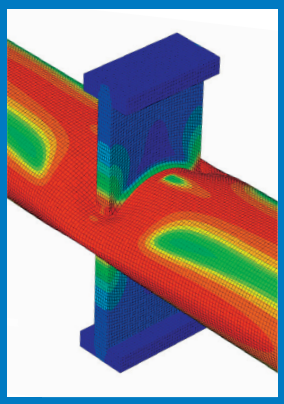

Stresses on research oriented model

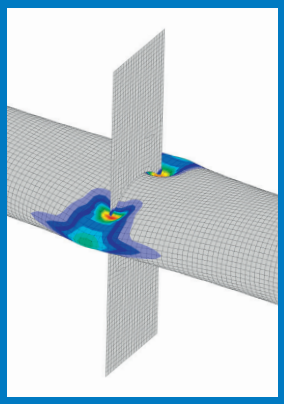

Strains on design oriented model

ISBN 978-80-01-06702-4

Published by the Czech Technical University in Prague
Prepared by Faculties of Civil Engineering of the Brno University of Technology and Czech Technical University in Prague
ISBN 978–80–01–06702–4 print
ISBN 978–80–01–06703–1 online

BRNO UNIVERSITY OF TECHNOLOGY

CTU CZECH TECHNICAL UNIVERSITY IN PRAGUE